# POTASSIUM CHANNEL KCSA AND ITS LIPID ENVIRONMENT

GARY STANLEY HOWARTH, II

Submitted in partial fulfillment of the requirements for the degree of

Doctor of Philosophy in the Graduate School of Arts and Sciences

COLUMBIA UNIVERSITY

2019

# ABSTRACT

---

Potassium Channel KcsA and Its Lipid Environment

Gary Stanley Howarth, II

There is a general lack of atomic resolution data of mobile regions of membrane proteins embedded in lipid bilayers. As an inherently complex system, few techniques can capture information about the mobile portions of an otherwise immobilized protein. The nature of crystallography and solid-state NMR relies on structural rigidity. Solution-state NMR relies on overall mobility of a protein for resolution. In the middle regime, there are few solutions to study these systems.

The inward-rectifying, pH-gated potassium channel KcsA from *Streptomyces lividans* makes an excellent model for the development of methods to study mobile regions of membrane proteins. Of its 160 residues, more than a third are in extracellular domains and are not typically captured by solid-state NMR or crystallographic techniques. These pages present evidence that KcsA's C-terminus is highly mobile and becomes increasingly dynamic when the protein is at low pH and high $K^+$ concentration, where the channel is known to be active. By applying proton-detected, high-resolution magic angle spinning NMR (HR-MAS) to fractionally deuterated KcsA,

previously unattainable correlations are collected and new resonance assignments are made, demonstrating the utility of the technique.

The lipid environment is well known to regulate the function of KcsA in particular and membrane proteins in general. It is generally assumed that reconstituting KcsA into a synthetic phospholipid membranes provides the protein a well-defined environment. Data is presented here which shows that KcsA co-purifies with phosphoglycerol lipids from the *Escherichia coli* membrane and that these molecules are $^{13}C$ enriched in the course of isotopically labeling KcsA. Further, significant hydrolysis of both co-purifying and synthetic lipids occurs under ordinary experimental conditions. These findings demand that routine analysis of samples must include verification of the chemical integrity of lipids.

Finally, the feasibility of applying dynamic nuclear polarization-enhanced NMR (DNP) to KcsA is investigated as a means of elucidating information about its termini. Although KcsA is known to enhance poorly by DNP, data presented here show that this is not an intrinsic property of the protein but rather an effect of the matrix in which KcsA is investigated. The use of a $^{15}N$-enriched free amino acid dissolved into buffers used for DNP is shown to be a powerful diagnostic internal standard.

# CONTENTS

# LIST OF FIGURES

# LIST OF TABLES



# LIST OF SEQUENCES

# ACKNOWLEDGEMENTS

Ann McDermott is a member of the New York Structural Biology Center (NYSBC). The NMR data were collected at the NYSBC with support from the Center on Macromolecular Dynamics by NMR Spectroscopy, a Biomedical Technology Research Resource supported by the National Institutes of Health (NIH) through Grant P41 GM-118302. The NYSBC is also enabled by a grant from the Empire State Division of Science Technology and Innovation and by Office of Research Infrastructure Programs/NIH Facility Improvement Grant CO6RR015495. The 600 MHz DNP/NMR spectrometer was purchased with funds from the NIH (S10RR029249). Data collected using the 750 MHz Avance I spectrometer is supported by the NIH (S10OD016432). The 900 MHz NMR spectrometers were purchased with funds from the NIH (P41GM066354), the Keck Foundation, New York State Assembly, and U.S. Dept. of Defense.

Electron micrographs in this thesis were collected at the Simons Electron Microscopy Center and National Resource for Automated Molecular Microscopy located at the New York Structural Biology Center, supported by grants from the Simons Foundation (SF349247), NYSTAR, and the NIH National Institute of General Medical Sciences (GM103310), and the NIH National Center for Research Resources (C06 RR017528-01-CEM).

This work was supported by NIH Grant R01 GM088724.

To Elise and Vivian for their patience.

And to Benedikt and Avalon for their friendship.

# Part I

# THE THESIS

# AN INTRODUCTION 1

## 1.1 STRUCTURE OF MEMBRANE PROTEINS

### 1.1.1 *Why Should We Care?*

Membranes are central to the very definition of life. For single cell organisms, membranes mark the boundary between one organism and its neighbor, between itself and its environment. By discriminating between what is outside and what is inside, from what is part of the organism and what is not, a membrane transforms an ensemble of biomolecules into a discrete living creature.

More often than not, proteins integrated into the membrane control what a cell uptakes. Nearly 30 % of proteins encoded by the human genome are membrane proteins, classified into 234 families with 3 major subcategories: receptors, transporters, and enzymes [1].

Membrane proteins perform many of the most interesting tasks of a cell, such as photosynthesis (and electron transport in general), cell signaling, and cell polarization. Channels and transporters traffic nutrients into the cell and waste out of the cell. Membrane embedded proteins such as G-protein coupled receptors sense the exterior environment and relay this information across the membrane. There is hardly any cellular process that does not directly involve a membrane protein.

The ubiquity of membrane proteins in the genome, the diversity of their function as well as their location at the cell surface, makes membrane proteins a central target for drugs. Given their accessibility, membrane proteins are the most important candidates for targeted drug design. Roughly 40 % of targets for drugs approved in the United States [16] are membrane proteins.

Consider the importance of a single membrane protein: the human-ether-a-go-go channel (hERG), an inward rectifying potassium channel common in mammalian muscle tissue. At least eight previously approved drugs have been shown to bind non-specifically to hERG causing prolonged cardiac QT symptoms, and leading in some cases to patient death [23]. The FDA now requires clinical screening for hERG inhibition symptoms. Most pre-clinical drug trails involve screening agents against hERG *in vitro*. Development of screening tools for hERG activity remains an important activity in biotech, an *in silico* screening tool has the potential to transform the drug screening landscape. However, we lack an atomic resolution structure of hERG, making modeling yet out of reach. Moreover, this is a general problem in the area of membrane proteins, and hERG is only a single example.

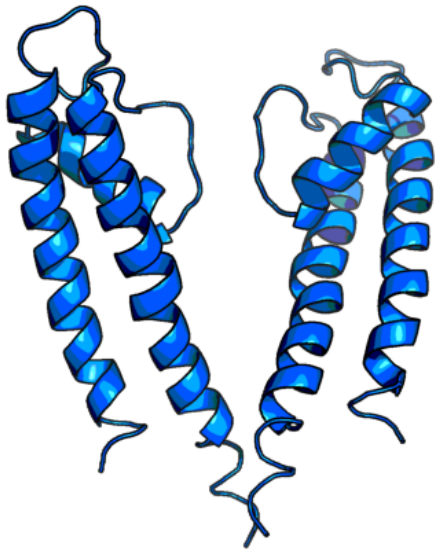

FIGURE 1.1: Structure of KcsA transmembrane domain, (PDB: 1BL8 [9].

The field of structural biology has made monumental progress since Perutz et al. and Kendrew et al. presented the first structures of proteins (hemoglobin and myoglobin, respectively) in 1960 [13, 21]. The RCSB Protein Data Bank [3] now contains 152 347 biomacromolecular entries as of May 2019. Yet, a mere 1.8 % of these are membrane proteins [32]. Due to the complex environment that membrane proteins occupy,

they pose special difficulties for the structural biologist. And since the structure and function of membrane proteins is dependent on their lipid surroundings, the task of drawing out useful structural data is made more complicated still.

The first atomic resolution structure (PDB: 1BL8) of an ion channel was collected over twenty years ago in 1998 [9], and with it Doyle et al. launched a new era of connecting membrane protein structure to function. This achievement earned Roderick MacKinnon a share of the 2003 Nobel Prize in Chemistry.

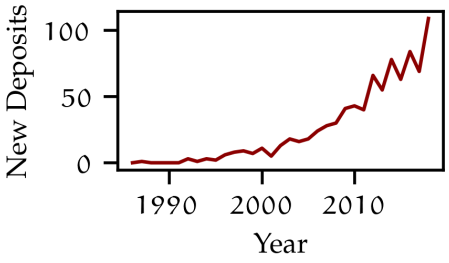


FIGURE 1.2: Annual deposits of unique membrane protein deposits made to the Protein Database [32].

From the more than 800 unique membrane protein entries in the PDB (Figure 1.2), we have gained transformative insight into the structural basis of membrane protein function. An open secret within the structural biology community is that only a handful of membrane proteins structures feature the full-length protein, and fewer still are in a lipid bilayer.

The majority of structures solve by both crystallography and solution NMR have relied on detergent solubilized proteins. A through study of the structural states of mitochondrial carriers (a integral membrane protein) in dodecylphosphocholine (DPC) micelles, a lipid-like detergent, shows that those structures cannot correlate to functional states, and the protein can no longer discriminate between it two ligands ATP and GTP [17]. Of more relevance to the studies at hand, the structure of KcsA at neutral pH in dodecylmatoside micelles [26] and neutral pH in asolectin bilayers [8] that there are considerable changes to the secondary and tertiary structure of KcsA. For example, in the lipid study, H25 a key pH sensor, is located along a transmembrane domain -helix, whereas in the micelle study, H25 no

longer appears in a helical structure. These are just one example of many that justify the need to conduct structural studied of membrane proteins in lipid bilayers.

The following chapters present improvements to the tools available to structural biologists in investigating the structure of membrane proteins embedded into lipid environments.

## 1.2 MISSING INFORMATION ON MOBILE REGIONS OF MEMBRANE PROTEINS

Early studies of KcsA were only able to crystallize KcsA with N- and C-terminal truncation [9]. While later studies made progress in the ability to crystallize more complete KcsA constructs [27], the termini regions could not be refined. This lead to the assumption that the termini are relatively mobile region, and which may remain quite dynamic even in the crystal. The large B-factors of the loop regions and the residues proximal to the termini in crystal refinement support this hypothesis [27].

The difficulty of resolving extramembrane portions of integral membrane proteins is by no means limited to KcsA or indeed other ion channels. Loops and cytosolic segments and other extracellular regions pose intense experimental challenges (see Kjaergaard and Kragelund [15] for a review of this topic), and are generally lacking in structural data. There have been monumental gains in our understanding of G-coupled protein receptors (GPCRs) fuled by a host of crystal structures. Many of those structure have relied on cleaving the mobile portions of the protein [29, 30], replacing mobile portions with more rigid, well folded domain (such as lysozyme)[20, 22]. In both these cases the native dynamics of the protein are lost.

Solution state NMR has provided extensive assignment of KcsA in detergent micelles [2, 6, 7, 11, 12, 14, 25], yet when removed from the lipid membrane KcsA is not a functional channel. The solid-state NMR community has provided detailed assign-

ments of full-length KcsA in liposomes for most of the residues in the transmembrane domain [4, 18, 19, 31, 33, 34], but loop regions and the termini remain largely unresolved. To understand the difficulty, we must examine the strengths and weaknesses of solid- and solution-state NMR.

## 1.3 SOME NMR BASICS

### 1.3.1 *What Are We Measuring Anyway?*

Many nuclei have an intrinsic nuclear magnetic moment ($\mu$), which is quantized and can assume integer multiples of ½. The nuclear magnetic moment and the nuclear angular momentum are directly proportional:

$$\mu \propto \gamma \frac{I}{\hbar} \tag{1.1}$$

where $\gamma$ is the gyromagnetic ratio characteristic of a nuclide, and $\hbar$ is the reduced Plank's constant. In an external magnetic field that we will specify is along the $z$-axis, the nuclear angular momentum ($m$) can assume the values of $m_z\hbar$ with $-I \leqslant m_z \leqslant I$ in integer steps.

From experience with everyday magnets, we know that one magnetic moment applies force to others in a distance dependent manner and that the forces involved are orientation specific. By the correspondence principal there is a direct analogy between the energy of a classical magnetic moment ($\mu$) placed in an external field ($B_0$) oriented in a direction ($z$) with a quantized system:

$$E = -\mu B_0 = -\gamma B_0 m_z \hbar \tag{1.2}$$

Selection rules dictate that transitions of $m_z$ must be in integer steps. So for a spin-½ nucleus the allowed energies are given by:

$$E = -\left( \pm \frac{1}{2} \right) \gamma B_0 \tag{1.3}$$

So given that for a particular spin-$^1/_2$ nuclide, there are only two energy levels and that all nuclides of a particular type have the identical gyromagnetic ratio, spin-$^1/_2$ NMR seems like it ought to be very boring. However in an NMR sample there is a vast continuum of states that are actually observed because of variations in the local magnetic environment experienced by an individual nucleus.

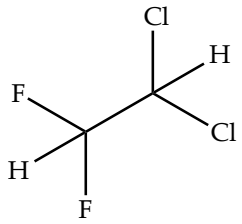


FIGURE 1.3: 1,1-dichloro-2,2-difluoroethane

Consider the molecule 1,1-dichloro-2,2-difluoroethane (Figure 1.3). The variations in the local electronic environment of the two non-equivalent hydrogen nuclei give rise to slightly different local magnetic field strengths, and as such create small differences in the energy transitions. These two hydrogens are easily resolved by NMR into discrete signals.

This still is not what we actually measure in NMR. In 0.5 mL of 10 mM solution of sucrose (the volume and concentration typical in solution NMR), there are about $3 \times 10^{21}$ sucrose molecules. These molecules add up to a considerable macroscopic magnetic moment ($M$). When an a perpendicular force is applied to this magnetic moment (when it's in an external field, like a big magnet), the moment is perturbed and presences around a the $z$-axis. This motion is analogous to a spinning top under a uniform field (gravity) that precesses around the normal when torqued out of the $z$-axis.

The procession of the magnetic moment around the $z$-axis means that a component of the magnetization is moving in a circular fashion through the $x-y$ plane of our

coordinate system. This so-called "transverse plane" magnetization can be detected by orienting a coil in such away as to generate a current through induction. The circular polarization of oscillation is transformed into linear oscillation as the coil must be oriented along a particular direction of the $x-y$-plane, and whatever direction this is is arbitrary called the x-axis. So in NMR we are only measuring the current induced by magnetic oscillation in the transverse plane in a direction arbitrarily called the x-axis.

### 1.3.2 *NMR is Insensitive*

Nuclear magnetic resonance is the most well-developed and powerful spectroscopic technique invented by humans. NMR can provide extensive insight into structure, dynamics, kinetics, thermodynamics and much more.Despite its power, NMR is an inherently insensitive technique.

In a simple case we can represent a system of nuclear spins as a set of eigenstates $|S\rangle$ with eigenvalues corresponding to the possible energies of the system $a_i$, which are related by the Hamiltonian operator. If there are only two eigenvalues for $|S\rangle$ in our basis set we can write:

$$\hat{H}|S\rangle = \sum_{0}^{i} a_i|S\rangle = a_\alpha|S\rangle + a_\beta|S\rangle \tag{1.4}$$

This is precisely the sort of system found when a set of identical spin-½ nuclei are placed in a static magnetic field. And in this scenario the energy of the two states are given by:

$$a_\beta = \hbar\frac{1}{2}\gamma B_0 \tag{1.5}$$

$$a_\alpha = -\hbar\frac{1}{2}\gamma B_0 \tag{1.6}$$

Where $\hbar$ the reduced Planck constant, $\gamma$ is the characteristic gyromagnetic ratio of the nuclear spin ($2.675 \times 10^8\,rads/T$ in the case of a proton), and $B_0$ is the external magnetic field strength. These of course are the solutions to Equation 1.2.

When a two state system is at thermal equilibrium the the Boltzmann distribution of the populations can be represented as:

$$\frac{N_\beta}{N_\alpha} = exp\left(\frac{-\Delta E}{kT}\right) \tag{1.7}$$

Where $N$ is the number of spins in the state, $\Delta E$ is the difference in energy between the states, $k$ is the Boltzmann constant and $T$ the temperature.

For proton spins in a 14 T magnet at 300 K, combining Equations 1.5 through 1.7:

$$\Delta E = 6 \times 10^{-8}\,s^{-1}$$

thus a 14 T magnet corresponds to a 600 MHz proton Larmour frequency, and:

$$\frac{N_\beta}{N_\alpha} \approx 0.99995$$

that is, the difference in population between the two states is 1 in 20 000, which is a very small amount of state polarization.

The sensitivity of an experiment is proportional to the changes in energy involved in the transitions. This only makes sense: bigger energies can obviously induce larger

| Transition | frequency (Hz) |
|---|---|
| Nuclear fluorescence | $10^{16} - 10^{18}$ |
| Electron orbital | $10^{14} - 10^{16}$ |
| Vibrational/Rotational | $10^{12} - 10^{14}$ |
| Electron spin* | $10^{9} - 10^{13}$ |
| Nuclear spin* | $10^{5} - 10^{9}$ |

TABLE 1.1: Typical transition frequencies of common energy transitions used in spectroscopy (*At practical magnetic fields).

changes, which in turn means their transitions are easier to observe, requiring less sensitive equipment. According to Planck's equation:

$$\Delta E = \nu h \tag{1.8}$$

the energy transitions are equal to the frequency of the transition multiplied by Plank's constant ($6.626 \times 10^{-34}$ J s). Table 1.1 compare the typical frequencies used in the most commonly employed forms of spectroscopy.

Yet, despite being the least sensitive of the major spectroscopic techniques, NMR has the potential to provide exquisitely detailed information. No other technique can report so many different types of information at so many sites within an ensemble of molecules.

NMR allows us to probe the local magnetic field of every nuclear spin in a molecule. Those local fields are affected by electron localization, nearby nuclear spins, local chemical environments, orientations within molecules, orientations between molecules, dynamics within the molecule. Nuclear magnetic resonance can be used to transfer magnetization in myriad ways, probing homogenous and complex samples. There is no end of experiments that NMR can perform. Nuclear spin dynamics are such are a robust reporter of so many different phenomena because nuclear spins are so easily

influenced. Nuclear spins are sensitive because they are influenced by weak forces, and as such they can only exert weak forces.

### 1.3.3 *Signal-to-Noise*

Signal-to-noise is a constant source of frustration in NMR, and the technique's insensitivity plagues practically every NMR experiment. Consider the most basic NMR experiment: an ensemble of identical spin-$1/2$ nuclei subjected to a an ideal $90°$ pulse. For such an experiment the major signal-to-noise is:

$$\frac{S}{N} = NK\eta M_0 \left( \frac{\mu_0 Q \omega_0 V_c}{4FkT_c \Delta f} \right)^{\frac{1}{2}} \tag{1.9}$$

where $N$ is the number of nuclei, $K$ is a numerical factor relating to coil geometry, $\eta$ is the fraction of coil volume occupied by the sample (filling factor), $M_0$ is the nuclear magnetization ($\propto B_0$), $\mu_0$ is the permeability free space, $Q$ is the quality factor of the coil, $\omega_0$ is the Larmour frequency of the nucleus of interest, $V_c$ is the volume of the coil, $F$ is the preamplifer noise figure, $k$ is Boltzmann's constant, $T_c$ is the probe temperature, and $Deltaf$ is the receiver bandwidth [10].

Over the past 80 years of practical NMR there have been incremental gains to improve each of these factors. Filling factors are approaching theoretical limits. Clever coil designs and geometries boost signal-to-noise ratio of modern instruments. Cryogenically cooled coils are now common place. Magnets of $23.5\,T$ ($1\,GHz$ $^1H$ field) are now in commercial production. It's worth noting, higher $B_0$ fields not only increase the signal to noise, but also increase resolution of the individual signals.

### 1.3.4 *Anisotropic Interactions*

The local magnetic environment of a nucleus is affected by neighboring charges. This gives rise to chemical shift phenomena that are the basis of NMR's utility. Dipolar interactions have a large effect on the local magnetic environment and therefore affect chemical shift in an orientation-dependent manner. The change of frequency ($\Delta\nu$) that results by directly coupled dipoles ($i$ and $s$) in an external magnetic field ($B_0$) is:

$$\Delta\nu \propto \frac{3\mu_i\mu_s}{\hbar r_{is}^3} 3\cos^2\theta_{is} - 1 \tag{1.10}$$

where $\hbar$ is Planck's constant, $r_{is}$ is the distance between the dipoles and $\theta_{is}$ is the vector angle away from the $B_0$ field. For nuclei in a solid-state NMR experiment, this can lead spans of shift of more than 100 kHz, effectively destroying the ability to resolve individual sites.

For small molecules, and small enough proteins, the dipolar contributions are negligible as the they are averaged to a limit approaching zero by rapid molecular tumbling. The rotational correlation time of, for example, $\alpha$-chymotrypsin at 20 °C in water is 83 MHz (12 ns) [24], and therefore more than 2 orders of magnitude greater than the dipolar coupling. Rotational correlation times for globular proteins can be estimated from Stokes' law as provided by Cavanagh and Palmer [5, p. 21]:

$$\tau_c = \frac{4\pi\eta r_H^3}{3k_B T} \tag{1.11}$$

where $\eta$ is the viscosity of the solvent, $k_B$ is Boltzmann's constant, and $T$ is temperature. The hydrodynamic radius, $r_H$ is generally proportional to the cube root of the volume of an individual protein. Hence, $\tau_c$ is proportional to the volume and therefore the molecular weight of a protein.

The KcsA tetramer has a molecular weight of 54 kDa, whereas α-chymotrypsin is less than half that at 25 kDa. More importantly though, in order for KcsA to be soluble in water it requires the presence of detergent (or other amphipaths) more than doubling its effective moleular weight [6]. In liposomes or cells, the protein membrane complex maybe hundreds of times larger still, leading to substantial anisotopic contributions to NMR signal.

### 1.3.5 *Magic Angle Spinning*

As shown in Equation 1.10, in a magnetic field (e.g. an NMR magnet), the dipolar (and CSA) contributions of the local magnetic field affected by spin $i$ on spin $s$ varies according to the angle, $\theta_{ij}$, formed between the vector $\vec{is}$ and the main magnetic field, $B_0$. The orientation-dependence of frequency shift caused by the dipolar and CSA contributions to the nuclear-spin Hamiltonian is related by:

$$\Delta\nu \propto \ 3\cos^2\theta_{is} - 1 \tag{1.12}$$

The angle at which Equation 1.12 evaluates to 0 (≈54.74°), is known as the *magic angle*. Mechanical spinning of samples about this angle (magic angle spinning or MAS) averages the dipolar and CSA in a spinning-speed-dependent fashion. This causes normally broad resonances of solid-state spectra to become sharp, isotropic-like lines as the MAS rate exceeds the dipolar and CSA couplings. For modern equipment typical spinning speeds range from 5 kHz in large sample rotors (4–7 mm) to 120 kHz or greater for small sample rotors (0.9 mm).

The principal catalog of solid-state MAS NMR experiments exploits the large, persistent dipolar couplings present in slow tumbling proteins. The most common ex-

periment in solid-state NMR, cross-polarization (CP), transfers polarization from one nucleus to neighboring nuclei. Even in molecules that have little or no amount of tumbling, such as proteins embedded in a bilayer at low temperature, may have domains that remain mobile relative to the rest of the protein. Since CP-MAS relies on persistent dipolar interactions, the technique tends to capture more information from rigid protein regions, such as transmembrane domains. Loop regions, or extra-membrane domains in the case of membrane proteins, are often not resolved by CP-MAS NMR.

Solution NMR tends to rely on J-couplings (also called scalar couplings). These couplings are typically small (5–200 Hz), and are not dependent on the orientation of the molecule with respect to the $B_0$ field. The fast tumbling of small molecules effectively averages out the dipolar coupling, rending CP experiments useless in solutions. J-couplings, however, are present in solid-samples but almost never used as a means to transfer polarization. Why not?

Consider one of the most important building blocks of solution state NMR, the heteronuclear single quantum coherence experiment (HSQC) [28]. The coherence transfer function ($\Gamma(t)$) of a decoupled, refocused HSQC experiment is given by: [5]:

$$\Gamma(t) = \sin(\pi J_{is} t)\cos(\pi J_{is} t) \tag{1.13}$$

where $t$ is the coherence transfer time, $J_{is}$ is the scalar coupling between the two spins.

From Equation 1.13 the optimal magnetization transfer time for a protein $^{1}H$-$^{15}N$ bond ($J \approx 90$ Hz) is 6 ms. For typical solid sample, the inhomogenous local environment for the various spins in an ensemble lead to a loss of coherence in the magnetization (in a process called spin-spin or $T_2$ relaxation). In solid protein samples, the $T_2$ relaxation time constants are often only a few milliseconds long.

### 1.3.6 *Relaxation*

The basic NMR experiment is where the bulk magnetic vector M begins parallel to the $B_0$ field (the *z*-axis) is rotated down to the $x-y$ plane following a 90° pulse. The M processes in the $x-y$ plane. Over time the bulk magnetization returns to equilibrium. The rate at which magnetization returns entirely to $M_z$ is the spin-lattice relaxation time or $T_1$. However, the $M_{x-y}$ component of the bulk vector in (virtually) all cases decays more quickly than $M_z$ is restored. This is because the individual spins the comprise $M_{x-y}$ have slightly different frequencies from varitions in their local magnetic environment and thus $M_{x-y}$ 'dephases' over time in a process called spin-spin or $T_2$ relaxation:

$$M_{x-y} \propto exp\left(\frac{-t}{T_2}\right) \tag{1.14}$$

The line width of an NMR resonance is linked to the lifetime of the resonance. By the Heisenberg uncertainty principal:

$$\Delta E\, \Delta t \approx \hbar \tag{1.15}$$

The the larger the linewidth ($\Delta\nu$), the shorter the lifetime ($T_2$) must be to meet the conditions of the uncertainty principal:

$$\Delta\nu \approx \frac{1}{\Delta t} \tag{1.16}$$

As stated earlier, the linewidths of solid samples, can span than 100 kHz. Even with MAS and modern decoupling routines, NMR linewidths of slow tumbling propor-

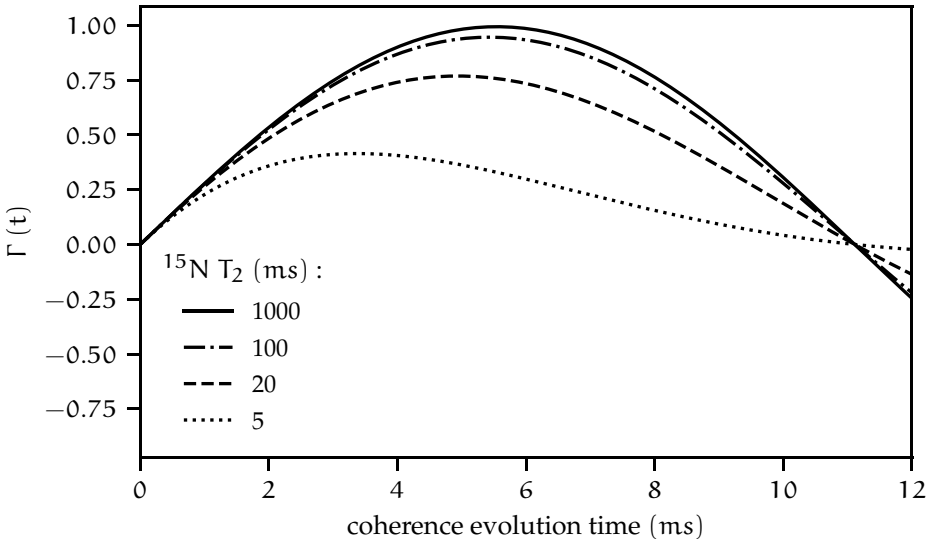


FIGURE 1.4: Efficiency of HSQC $^{1}$H-$^{15}$N amide ($J_{is}$ = 90 Hz) coherence transfer with various $^{15}$N $T_2$ spin-spin relaxation values plotted from Equation 1.13.

tions are still on the order of 200 Hz or larger meaning, $T_2$ values that are on the order of 5 ms.

Returning to why J-couplings are not utilized as transfer pathways for solid samples, Figure 1.4 shows a set of solutions for Equation 1.13 at various $^{15}$N $T_2$ values. As demonstrated, when the amide has a short $T_2$ value, the transfer by J-coupling becomes inefficient. This is worse still when the J-coupling is even smaller, such as for a transfer of coherence from $^{13}$C to amide $^{15}$N (J 11 Hz). This problem of short $T_2$ values is compounded when multiple coherence transfers occur in a pulse sequence, as utilized in, for example, a protein backbone experiment.

## 1.4 CONCLUSION

Mobile regions of membrane proteins are difficult to study by solid-state NMR because their motions are in a regime that makes them poor candidates for solid-state NMR studies, as they have weak average dipolar couplings. For solution NMR they

are poor canidates for the inverse reason, the residual dipolar couplings cause coherent manetization to relax too quickly for efficient transfer by J-coupling mechanisms.

In the chapters ahead two strategies are pursued. The first seeks to increase the effective $T_2$ times by elevating the sample temperature, substituting protons for deuterons and applying magic angle spinning. This set of strategies shows real promise by collecting the first 3D backbone correlations of KcsA's C-terminus while the channel is embedded in liposomes.

The second strategy seeks to limit the conformational motion of KcsA by investigating the protein at 100 K and to increase the signal by applying dynamic nuclear polarization.

[1] M. S. Almén, K. J. V. Nordström, R. Fredriksson, and H. B. Schiöth. "Mapping the human membrane proteome: a majority of the human membrane proteins can be classified according to function and evolutionary origin." In: *BMC biology* 7 (Aug. 2009), p. 50. DOI: 10.1186/1741-7007-7-50.

[2] K. A. Baker, C. Tzitzilonis, W. Kwiatkowski, S. Choe, and R. Riek. "Conformational dynamics of the KcsA potassium channel governs gating properties." In: *Nature Structural and Molecular Biology* 14.11 (2007), pp. 1089–1095. DOI: 10.1038/nsmb1311.

[3] H. M. Berman. "The Protein Data Bank." In: *Nucleic Acids Research* 28.1 (Jan. 2000), pp. 235–242. DOI: 10.1093/nar/28.1.235.

[4] M. P. Bhate, B. J. Wylie, L. Tian, and A. E. McDermott. "Conformational dynamics in the selectivity filter of KcsA in response to potassium ion concentration." In: *Journal of molecular biology* 401.2 (Aug. 2010), pp. 155–66. DOI: 10.1016/j.jmb.2010.06.031.

[5] J. Cavanagh and A. Palmer. *Protein NMR spectroscopy : principles and practice*. Second. Academic Press, 2007, p. 885.

[6] J. H. Chill, J. M. Louis, C. Miller, and A. Bax. "NMR study of the tetrameric KcsA potassium channel in detergent micelles." In: *Protein science : a publication of the Protein Society* 15.4 (Apr. 2006), pp. 684–98. DOI: 10.1110/ps.051954706.

[7] J. Chill, J. Louis, J. Baber, and A. Bax. "Measurement of 15N relaxation in the detergent-solubilized tetrameric KcsA potassium channel." In: *Journal of Biomolecular NMR* 36.2 (Oct. 2006), pp. 123–136. DOI: 10.1007/s10858-006-9071-4.

[8] D. M. Cortes, L. G. Cuello, and E. Perozo. "Molecular Architecture of Full-Length KcsA." In: *The Journal of General Physiology* 117.2 (Feb. 2001), pp. 165–180. DOI: 10.1085/jgp.117.2.165.

[9] D. A. Doyle et al. "The structure of the potassium channel: molecular basis of K+ conduction and selectivity." In: *Science (New York, N.Y.)* 280.5360 (Apr. 1998), pp. 69–77. DOI: 10.1126/science.280.5360.69.

[10] D. Hoult and R. Richards. "The signal-to-noise ratio of the nuclear magnetic resonance experiment." In: *Journal of Magnetic Resonance (1969)* 24.1 (Oct. 1976), pp. 71–85. DOI: 10.1016/0022-2364(76)90233-X.

[11] S. Imai, M. Osawa, K. Takeuchi, and I. Shimada. "Structural basis underlying the dual gate properties of KcsA." In: *Proceedings of the National Academy of Sciences of the United States of America* 107.14 (Apr. 2010), pp. 6216–21. DOI: 10.1073/pnas.0911270107.

[12] G. Kamnesky, H. Shaked, and J. H. Chill. "The Distal C-Terminal Region of the KcsA Potassium Channel Is a pH-Dependent Tetramerization Domain." In: *Journal of Molecular Biology* 418.3-4 (May 2012), pp. 237–247. DOI: 10.1016/j.jmb.2012.02.023.

[13] J. Kendrew, R. Dickerson, B. Strandberg, R. Hart, and D. Davies. "Structure of Myoglobin." In: *Nature* 185 (1960), pp. 422–427.

[14] D. M. Kim et al. "Conformational heterogeneity in closed and open states of the KcsA potassium channel in lipid bicelles." In: *The Journal of General Physiology* 148.2 (Aug. 2016), pp. 119–132. DOI: 10.1085/jgp.201611602.

[15] M. Kjaergaard and B. B. Kragelund. "Functions of intrinsic disorder in transmembrane proteins." In: *Cellular and Molecular Life Sciences* 74.17 (July 2017), pp. 3205–3224. DOI: 10.1007/s00018-017-2562-5.

[16] M. Kotlyar, K. Fortney, and I. Jurisica. "Network-based characterization of drug-regulated genes, drug targets, and toxicity." In: *Methods* 57.4 (Aug. 2012), pp. 499–507. DOI: 10.1016/J.YMETH.2012.06.003.

[17] V. Kurauskas et al. "How Detergent Impacts Membrane Proteins: Atomic-Level Views of Mitochondrial Carriers in Dodecylphosphocholine." In: *Journal of Physical Chemistry Letters* 9.5 (2018), pp. 933–938. DOI: 10.1021/acs.jpclett.8b00269.

[18] A. Lange et al. "Toxin-induced conformational changes in a potassium channel revealed by solid-state NMR." In: *Nature* 440.7086 (Apr. 2006), pp. 959–962. DOI: 10.1038/nature04649.

[19] D. Mance et al. "An Efficient Labelling Approach to Harness Backbone and Side-Chain Protons in 1 H-Detected Solid-State NMR Spectroscopy." In: *Angewandte Chemie* 127.52 (Dec. 2015), pp. 16025–16029. DOI: 10.1002/ange.201509170.

[20] G. Manley et al. "High Resolution Crystal Structure of an Engineered Human β2 - Adrenergic G protein-Coupled Receptor." In: *Science* 318.5854 (2017), pp. 1258–1265. DOI: 10.1371/journal.pone.0178059.

[21] M. F. Perutz et al. "Structure of Hæmoglobin: A Three-Dimensional Fourier Synthesis at 5.5-Å. Resolution, Obtained by X-Ray Analysis." In: *Nature* 185.4711 (Feb. 1960), pp. 416–422. DOI: 10.1038/185416a0.

[22] D. M. Rosenbaum et al. "GPCR engineering yields high-resolution structural insights into β2-adrenergic receptor function." In: *Science* 318.5854 (2007), pp. 1266–1273. DOI: 10.1126/science.1150609.

[23] R. R. Shah and P. D. Stonier. "Withdrawal of prenylamine: perspectives on pharmacological, clinical and regulatory outcomes following the first QT-related casualty." In: *Therapeutic Advances in Drug Safety* 9.8 (Aug. 2018), pp. 475–493. DOI: 10.1177/2042098618780854.

[24] E. J. Shimshick and H. M. McConnell. "Rotational correlation time of spin-labeled α-chymotrypsin." In: *Biochemical and Biophysical Research Communications* 46.1 (Jan. 1972), pp. 321–327. DOI: 10.1016/0006-291X(72)90665-1.

[25] K. Takeuchi, H. Takahashi, S. Kawano, and I. Shimada. "Identification and characterization of the slowly exchanging pH-dependent conformational rearrangement in KcsA." en. In: *The Journal of biological chemistry* 282.20 (May 2007), pp. 15179–86. DOI: 10.1074/jbc.M608264200.

[26] S. Uysal et al. "Crystal structure of full-length KcsA in its closed conformation." In: *Proceedings of the National Academy of Sciences* 106.16 (Apr. 2009), pp. 6644–6649. DOI: 10.1073/pnas.0810663106.

[27] F. I. Valiyaveetil, M. Leonetti, T. W. Muir, and R. Mackinnon. "Ion selectivity in a semisynthetic K+ channel locked in the conductive conformation." In: *Science (New York, N.Y.)* 314.5801 (Nov. 2006), pp. 1004–7. DOI: 10.1126/science.1133415.

[28] G. Wagner. "Heteronuclear nuclear magnetic resonance experiments for studies of protein conformation." In: vol. 176. 1976. 1989, pp. 93–113. DOI: 10.1016/0076-6879(89)76007-9.

[29] T. Warne, M. J. Serrano-Vega, C. G. Tate, and G. F. Schertler. "Development and crystallization of a minimal thermostabilised G protein-coupled receptor." In: *Protein Expression and Purification* 65.2 (2009), pp. 204–213. DOI: 10.1016/j.pep.2009.01.014.

[30] T. Warne et al. "UKPMC Funders Group β 1 -adrenergic receptor." In: 469.7329 (2011), pp. 241–244. DOI: 10.1038/nature09746.The.

[31] M. Weingarth et al. "Quantitative Analysis of the Water Occupancy around the Selectivity Filter of a K + Channel in Different Gating Modes." In: *Journal of the American Chemical Society* 136.5 (Feb. 2014), pp. 2000–2007. DOI: 10.1021/ja411450y.

[32] S. White. *Membrane Proteins of Known 3D Structure*. DOI: 10.1016/j.ymeth.2012.06.003.

[33] B. J. Wylie, M. P. Bhate, and A. E. McDermott. "Transmembrane allosteric coupling of the gates in a potassium channel." In: *Proceedings of the National Academy of Sciences of the United States of America* 111.1 (Jan. 2014), pp. 185–90. DOI: 10.1073/pnas.1319577110.

[34] Y. Xu, M. P. Bhate, and A. E. McDermott. "Transmembrane allosteric energetics characterization for strong coupling between proton and potassium ion binding in the KcsA channel." In: *Proceedings of the National Academy of Sciences of the United States of America* 114.33 (Aug. 2017), pp. 8788–8793. DOI: 10.1073/pnas.1701330114.

# 2 INVESTIGATIONS OF KCSA BY HIGH-RESOLUTION MAGIC ANGLE SPINNING

## 2.1 ABSTRACT

The structure of the transmembrane domain of bacterial potassium channel KcsA has been extensively characterized, yet little structural data exist on its cytosolic N- and C-termini. This study presents high-resolution magic angle spinning (HR-MAS) and fractional deuteration as tools to study these poorly resolved regions when KcsA is embedded in liposomes. We show, by recombinantly truncating the C-terminus of KcsA, that HR-MAS NMR can detect this region of KcsA when the channel is embedded into liposomes. We show that full-length KcsA in liposomes at neutral pH $^{15}$N-HSQC data shows 15 broad resonances, whereas at pH 4, that experiment reveals 30 sharp resonances in a markedly different chemical shift dispersion. We interpret this as the C-terminus transitioning from a rigid structure at neutral pH (where the channel is inactive) to highly mobile conformation at pH 4 (conditions where the channel is active). The resonances reported here are the first experiments where the C-terminus of full-length KcsA are resolved in native-like liposome structures. Using

fractionally deuterated KcsA, the first J-based backbone NMR experiments of KcsA in liposomes are presented.

## 2.2 INTRODUCTION

KcsA is perhaps the most studied membrane channel, having been investigated in hundreds of studies including more than 50 unique structures of KcsA (or portions of it) deposited in the Protein Data Bank [4] and the Biological Magnetic Resonance Data Bank [68]. The wealth of structural, biochemical, eletrophysiological, and biophysical data on KcsA has made it a favorite pet protein to investigate allosteric coupling [15, 74], activation and inactivation mechanism and kinetics [23, 27], lipid-protein interaction [29, 45], and virtually any other question concerning ion channels specifically or membrane proteins in general.

One reason KcsA continues to capture attention is its homology with other potassium channels in general and in particular the Human ether-a-go-go channel (hERG) [62], a potassium channel that binds promiscuously to drugs and plays a critical role in regulating cardiac rhythm.

Another reason that KcsA is a commonly used model protein is that it is both easy to produce and difficult to study. All membrane channels are difficult, because by nature they are complex system of proteins and lipids. Studies of KcsA in a lipid bilayer are essential for investigating KcsA's complex behavior, structure, and function. After all, KcsA cannot sensibly be called a channel unless it is conducting ions across a

membrane. Yet despite the membrane environment being essential for KcsA function and structure, and even though we have more structural data on KcsA than any other ion channel, we do not yet have a full-length, atomic-resolution structure of KcsA in a lipid membrane. This is because the most mobile portions of KcsA, its extracellular termini in particular, show characteristics that make it excessively challenging to resolve while in the membrane.

Here we show that HR-MAS can be utilized to capture information from the C-terminus of full length KcsA in the lipid membrane.

### 2.2.1 *Meet KcsA*

KcsA is an inward-rectifying potassium channel from the gram-positive soil bacterium *Streptomyces lividans*. KcsA is composed of four identical subunits of 160 amino acids, each with two transmembrane spanning domains. It is perhaps the most extensively investigated of all membrane proteins. There are, for example, 69 unique deposits (including fragments and mutants) in the PDB as of December 2018. Of those structures 65 were determined by x-ray diffraction, 3 by solution NMR and 1 by electron spin resonance.

Cortes, Cuello, and Perozo [14] performed sequential cysteine mutagenesis on KcsA. Using solvent accessibility probes and electron spin resonance of those constructs in liposomes at pH 4 (where electrophysiology measurements reveal KcsA is active) they developed a model where the C-terminus formed an $\alpha$-helix oriented perpendicular

to the membrane surface and the N-terminus also as a helix oriented along the normal of the membrane (Figure 2.1). A study by neutron and x-ray small angle scattering of full-length KcsA at pH 7.5 presented a similar model for the C-terminus where a bundle extending out from the membrane narrowed near residue 140 and then expanded outward [78]. This general model is supported by NMR chemical shift analysis of tetrameric KcsA in detergent micelles at pH 6 and 323 K that showed the shifts conforming to helical structure from residues [11].

From these structural studies, we see KcsA has three primary domains: Residues 1–20 form an amphipathic- -helix that is oriented toward the cytosol. Residues 21–125 form four transmembrane spanning -helices which form the channel's potassium selectivity filter (T75, V76 G77, Y78, G79, D80). Residues 125–160 form a cytosolic region whose function and structure are debated and will be discussed at length.

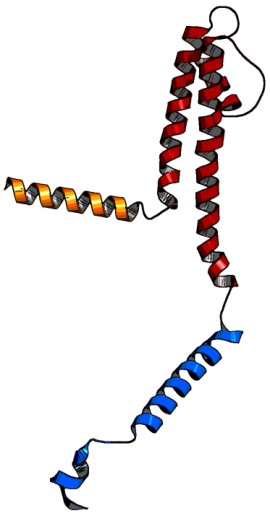

FIGURE 2.1: KcsA structure from spin-labeled electron spin resonance PDB: 1F6G [14] , with residues 1–25 in orange, and 125–160 in blue.

Functionally, the channel displays three well-established electrophysiological states: a) *deactivated state* or *resting state* with neutral pH at the cytosolic gate and where no $K^+$ flow occurs; b) an *activate state* where $K^+$ conduction through the channel follows a drop of intracellular pH below 5; and c) an *inactivated state* where spontaneous exponential decay to virtually no conduction $K^+$ follows activa-

tion and lasts for milliseconds to seconds [10, 23]. Following inactivation, the channel will spontaneously re-open returning to state (b) if the pH remains low or it will enter the resting state (a) should the cytosolic pH be neutral.

KcsA shares many similarities with eukaryotic potassium channels. For example, *Homo sapien* human-ether-a-go-go (hERG), *Drosophila melanogaster* Shaker channel, and *Mus musculus* Kv1.2, are all homotetrameric $K^+$ channels with highly conserved selectivity filters [62, 75]. All of these channels also contain long extracellular C-terminal domains. Despite hundreds of structural studies on these various channels, little such information is known about their C-terminal domains.

### 2.2.2 *Functional Significance of KcsA*

KcsA channel is a proton-gated channel that allows $K^+$ to flow into the cell at low pH. Yet, why an organism might need this function is not clear. Potassium channels are ubiquitous in bacteria, archaea, and monocellular fungi. Some organisms have many genes for potassium channels. *Paramecium tetraurelia*, for example has a whopping 298 genes encoding putative potassium channels [38]. The yeast species *Schizosaccharomyces pombe* contains no recognizable potassium channel genes [38]. Others, such as *E. coli* has only a single potassium channel [35, 43].

Knockouts of the sole *E. coli* channel (Kch) do not even lead to changes in growth rates of the organism *in vitro* in a variety of culture media. Yet, a general consensus is that the Kch in *E. coli* forms an important part of maintaining the potential across the

cell membrane [35, 38]. Since pH og both the exterior and the interior ($H^+$ concentration), plays a major role in the cell potential, one could imagine that $K^+$ influx might play a role in stabilizing with a high $H^+$ concentration, such as activating a signaling pathway. The fact of the matter is that the role of inward rectifying potassium channels in prokaryotes remains an open area of investigation. An exotic alternative hypothesis of KcsA's role *in vivo* is that it forms supramolecular complexes with the common cellular polymers oligo-(R)-3-hydroxybutyrates (OHBs) and inorganic polyphosphate (polyP) [46], for which there is some evidence [77]. In *E. coli* OHB (130–140 units) and polyP (60 65 units) have the curious property of forming complexes that create ion channels that selectively allow $Ca^{2+}$ to pass through the membrane [16], and these channels are both temperature and pH sensitive [17]. Negoda, Negoda, and Reusch found that the presence of OHB and polyP in KcsA when purified and caused the channel to open at neutral pH. rather than the low pH ( 4) normally required. Mutating residues S102G and S129G lead to a loss of OHB and polyP from KcsA channels and a subsequent return to the typical, low pH function [46]. Using this as evidence, Negoda, Negoda, and Reusch proposed that the C-terminus stabilizes OHB and polyB by acting a cradle for the chains. Despite these data, the theory that KcsA forms supramolecular complexes *in vivo* or that it might have gating modes that are not pH-dependent, has not found traction in the larger research community.

### 2.2.3 *Significance of the N-Terminus*

Although there is limited structural data on KcsA's termini, there is a wealth of functional information. The N-terminus (residues 1 to about 25), is located at the cytosolic side of the membrane and plays a role in maintaining channel stability, stabilizing the open structure of KcsA, and sensing the lipid environment [1, 30, 56]. Cortes, Cuello, and Perozo [14] published a full-length structure of KcsA using a set of electron spin resonance (ESR) experiments from sequential spin-labeled KcsA cysteine mutants. That structure indicated that N-terminus was likely a helix with its long axis 14 degrees offset from parallel to the lipid membrane.

KcsA is highly thermostable and remains a tetramer in lipids upto 90 °C [56]. The N-terminus plays a key role in KcsA's thermostability. For example, trifluoroethanol (TFE) incorporates into lipid membranes and causes dissociation of KcsA tetramers in neutral liposomes. However when the liposome headgroup composition is 30 % phosphoglycerol (PG) or phophoatidic acid (PA), which are negatively charged headgroups, KcsA retains its tetrameric structure at room temperature in the presence of TFE [71]. However, N-terminal truncation constructs ($\Delta 1 - 18$) are no longer thermostable when subjected to TFE regardless of lipid composition [55].

Iwamoto and Oiki showed that mutations to either of the charged residues on the N-terminus (R11 and K14) significantly decreased the open-probability of KcsA and also presented evidence that the N-terminus has a pH pH dependent conformation (Figure 2.3), an arrangement they call an amphipathic antenna [29]. That study also

showed that only the lipid composition of the inner leaflet of the membrane (the side on which the N-terminus is located) affects the channel open-probability.

### 2.2.4 *Significance of the C-Terminus*

Early studies suggested that the C-terminus plays a role in pH gating. The first hints of the mechanism by which KcsA senses pH came from Cortes, Cuello, and Perozo, who found that that sequential deletions of portions the C-terminus (Δ140, Δ125, Δ120) showed a progressive decrease in pH dependence of the channel [14]. The C-terminus is rich in charged residues, having a net theoretical charge of 2, and a calculated pI of 10. The tight bundle of charged helices suggested to the authors that the bundling might be involved in gating, perhaps serving as a mechanism to block potassium from entering the cytosol. However, they found that truncating the C-terminus did not change the rate of ion conduction during activation events, showing that the C-terminus is not blocking $K^+$ access to the pore during activation, at least not at low pH.

Through various truncation constructs, Molina et al. found that KcsA residues 120–124 were the most critical for channel tetramer stability and assembly [44]. Applying molecular dynamics, the authors described contacts between residues at the end of the final transmembrane segments with residues in the region where the N-terminus meets the first transmembrane segment (e.g. T112-H25-D118, R121-A23, S22-H124).

Pau et al. found the deletion of the C-terminus ($\Delta 112-160$) enhanced tetramer thermal stability at acidic pH and weakened stability at basic pH [48]. Then studying the a C-terminal fragment ($KcsA_1 12-160$) by solution NMR, the authors found the fragments oligomerizes as pH increases with an aggregation profile similar to the pH activation profile of the full-length channel in membranes.

In a clever application of phase display, Uysal et al. [69] identified multiple fragment antigen binding antibody (Fab) that bind to KcsA's C-terminus when the channel was solubilized in dodecyl-maltoside detergent. This approach yielded a crystal structure that resolved the C-termnius and transmembrane domains of the channel. The structure featured a closed $K^+$ gate and revealed the C-terminus of each monomer as an $\alpha$-helix, forming a tight bundle protruding perpendicular to the membrane normal with various charged residues (H145, A147, A149, G152) coordinating across subunits. The study also resolved a structure of truncated KcsA construct ($\Delta 126$) showing that residues 110–124 assume a much different conformation than the full-length structure. Finally, the study observed that the same conformation of the C-terminus was found for two different Fab antibodies.The similarity of two structures at two different conditions with two different Fab antibodies suggests that the study captures a low-energy structure. However, since the C-terminus is resolves in crystal structure using this method of stabilization, the behavior of the termini must be fundamentally altered by this procedure.

Considering that the C-terminus might regulate tetramer stability, Yuchi, Pau, and Yang found that replacing the KcsA C-terminal domain with an artificial domain

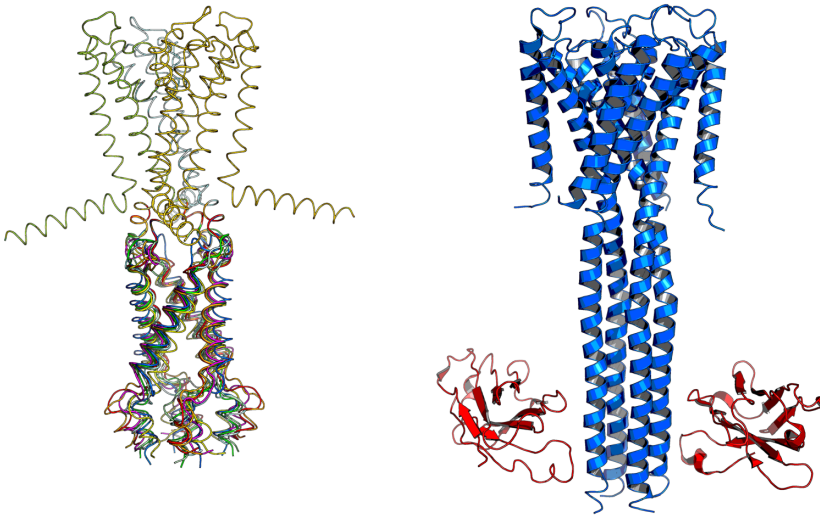

(A) PDB 1F6G structures of KcsA in liposomes at pH 4 by EPR with various low-energy structures displayed in differing colors [14].

(B) PDB 3EFF structure of KcsA in detergent micelles at pH 4 (blue) by x-ray with portions of two of four FAB antibody fragments (red) [69] .

FIGURE 2.2: Structural models of KcsA at pH 4.

(GNC4-LI) with known tetramerization function yielded a tetrameric channel with similar thermostability to wild-type channels but that was completely insensitive to changes in pH [76]. It was also noted that KcsA does not express without the C-terminus ( 120), but inclusion of GNC4-LI in its place restored expression. This lead to the authors to hypothesize that the C-terminal domain was essential for assembly or localization into the membrane and reinforced the notion that the C-terminus if not sensing pH directly is involved in activation.

The models presented in Figure 2.2 were both collected in a buffer at pH 4. The ESR is of KcsA embedded into liposomes and that preparation was shown to conduct ions [14], whereas the X-ray structure was collected in the absence of a lipid bilayer and the selectivity filter of from that structure is shown to be in the closed state [69].

Truncations of the C-terminus of KcsA have been shown to increase the flow of ions at neutral pH [14], to negatively impact the channel's thermostability [14, 44, 48, 54], and alter (though not destroy) the channels pH dependence on gating [14]. All demonstrating that the C-terminus is functionally significant.

Pau et al. [48] found using analytical ultracentrifugation that peptide fragment $KcsA_{112-160}$ ran as a monomer at pH 4, but oligomerized into larger structures of uncertain oligomerization number at neutral pH. Kamnesky, Shaked, and Chill [31] performed a series of solution NMR experiments NMR experiments on the free C-terminal fragment of $KcsA_{128-160}$. The studies showed that the C-terminal fragment was a monomer in solution at low concentration at neutral pH that chemical shift analysis predicted was of helical character. With increasing concentration of the peptide, the fragments aggregate and undergo significant rearrangement to form a tetramer with chemical shifts characteristic of an $\alpha$-helix. Tetramerization is disrupted, returning the fragments to monomers, as the buffer is lowered below pH 5. Specifically, they found that dissociation of the tetramer is correlated with protonation of H145. Following up this finding, Kamnesky et al. performed alanine screening and sedimentation equilibrium analysis on the C-terminal domain fragment investigated in their prior study [31, 32]. These new data conform with the other observations [26] that mutations of D149, E152, and R147 disrupt tetramer stability. Mutations in R147 in particular lead to much greater stability that WT. By examining constructs with solution NMR, the authors found that the point mutation E152A or L151A decreased proton linewidths by roughly half and the mutant R147A yielded a powder pattern rather

than the resolved J-couplings of the wild-type fragment. All of these data portray a picture of the C-terminus that has an extensive network of cross-subunit hydrogen bonds at neutral pH that are disrupted at low pH.

Recently, this model of KcsA C-terminus behavior has been shown to be valid for full-length KcsA in lipid nanodisks. Lipid-protein nanodisks are of considerable interest to the NMR community for study of membrane proteins as they can vastly decrease sample anisotropy (See [8, 42] for reviews on this topic). Protein nanodisk systems provide lipid protein units of 1–50 nm (with ~10 nm being typical) in diameter and are soluble in solution. This provides a relatively isotropic systems often suitable for solution NMR, often incorporating a single protein and about 100 lipid molecules [3, 24] such that the protein-lipid nanodisk is tumbling in solution. Thus, the rotational correlation times of nanodisk systems are vastly decreased compared to liposome systems, decreasing anisotropic interactions. Lipid nanodisks can have a wide variety of lipid compositions and there are even applications that utilize the native lipid bilayer of organisms used as the protein expression system [19]. Nanodisk systems must be optimized empirically to provide the best results.

Qasim et al. presented a series of NMR spectra of KcsA embedded in lipid nanodisks [53]. Specifically, MSP1D1 was used as an amphipathic belt-protein surrounding KcsA embedded into short-chained, unsaturated lipid 1,2-dimyristoyl-sn-glycero-3-phosphocholine (DMPC), incorporating single tetrameric channels into a disk. Using $^{1}$H-$^{15}$N and $^{1}$H-$^{13}$C TROSY data of $^{15}$N and methyl labeled KcsA in an otherwise deuterated background, the authors identified two major states: a low pH state with

35 sharp amide resonances; and a second state at neutral pH that revolves only six broad resonances. The work in nanodisks follows directly from the work of Kamnesky et al. [32] of $KcsA_{128-160}$ fragments in solution. Specifically, Qasim et al. applied the resonance assignments made from backbone NMR experiments performed by [32] to assign the chemical shifts of the full-length KcsA in the nanodisk system. Qasim et al. presents an argument where the C-terminus is relatively flexible at low pH and become more rigid upon the deprotonation of certain residues, in particular F148. This study shows for the first time that the C-terminus of full-length KcsA in lipids does have a pH dependent conformation. That study states it was unable to collect 3D correlations of perdeuterated full-length KcsA with protonated amides, which is why it relied on previous assignments.

### 2.2.5 *Interactions of the C-terminus with the Transmembrane Domain*

The KcsA point mutation E71A leads to channels that are inactivation resistant, having a much higher open probability and no exponential decay of signal as observed in wild type channels [13]. This mutation is frequently used as a background for studies as it simplifies the overall gating model and makes data collection much more efficient (especially for electrophysiologic studies.) Constructing a chimera where the calcium gated potassium channel MthK had its C-terminal domain substituted for KcsA's C-terminal domain, Hirano et al. showed the MthK-KcsA chimera showed pH sensitive gating with an open-probability profile similar to that of inactivation

resistant KcsA (E71A). Through site-directed mutagenesis, substituting neutral, polar residues for charged residues in the chimera, the authors established that D156, D157, and particularly E146 and D149, play a role in pH-dependent gating of the chimera.

A study of methyl labeled full-length KcsA in DDM detergent micelles by solution NMR Imai et al. resolving two slowly exchanging confirmations corresponding to neutral pH and low pH both in the presence of 50 mM $K^+$. Using site-directed mutagenesis, NOE measurements and exchange-edited HMQC spectra, the authors assigned 41 methyl labeled residues in the high pH condition and 41 in the low pH condition with 32 residues in common, spanning from L5 to L155 That study found the differences between states were substantial enough that completely independent assignments had to be made for each condition. In addition to identifying two major states, the study correlated the states to protonation of H25, again supporting its role as a pH sensor. A recombinant truncation of KcsA (δ126) finds that the two spectra states are still observed as a function of pH. The study also shows there are two distinct pH transition points, one at $pH_{1/2} = 5.0$ for the transmembrane domain resonances and the second at $pH_{1/2} = 6.4$ for the C-terminal domain. Takeuchi et al. had the first success in identifying KcsA's pH sensor definitively [66]. Using recombinant KcsA truncated by chymotrypsin (Δ126), a series of TROSY spectra at varying pH found that H25, which is at the interface between the N-terminal and first transmembrane spanning domain, had the largest pH dependent conformational rearrangement and the mutation H25A of full-length KcsA destroyed pH-dependent gating. Further

work has definitely characterized H25 as being essential for pH sensing, leading the authors to conjecture that the C-terminus did not play a significant role in pH sensing.

However, [51] showed that both mutations to both H25 and E118, which is located at the interface of the C-terminus and the cytosolic domain, were required to abolish pH sensing entirely. These residues are located close in space within the assembled KcsA tetramer, and using electrophysiology measurements that study showed that the mutation H25 has a much larger pKa difference between the open and closed conformation than E118 leading to the authors proposing the former as a 'strong' pH sensor and the latter a 'weak' pH sensor.

### 2.2.6 *A Synthesis of KcsA's C-terminal Functional Role.*

We currently understand KcsA's function to be an inward rectifying potassium channel that activates upon drop of the intracelluar pH. The main pH sensor, H25, is located close in space to residues in the near-membrane portion of the C-terminus where a hydrogen-bonding network exists when H25 is not protonated. The protonation of H25 disrupts the hydrogen-bonding network of T112-H25-D118, S22-H124, and A23-R121. The C-terminus of KcsA forms a bundle of helices at neutral pH, when the channel is closed, and which is stabilized by L144, F148, L151, M154, and L155 through a complex system of interactions. F148 is a key residue, however, as mutations to it (e.g. F148A) cause a major conformational shift in the C-terminus that appears, by NMR, to be the same conformation the C-terminus assumes at low pH.

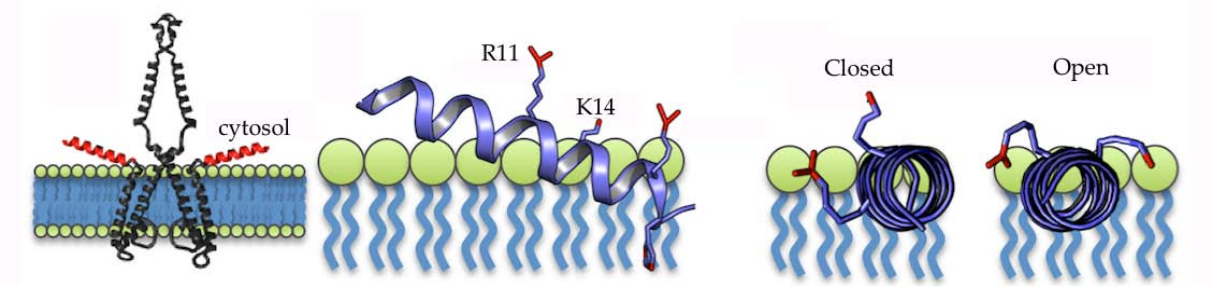


FIGURE 2.3: Model of mechanism proposed by Iwamoto and Oiki by which the KcsA N-terminus stabilizes the open confirmation by sensing lipid headgroups adapted from [29].

### 2.2.7 *Lipid Sensing Sites*

Seelig, MacDonald, and Scherer proposed a bilayer model in which individual lipids behave as "molecular electromers" [60], where lipids respond to the species within the bilayer environment (e.g. lipid compositions, and peptides, sterols, etc.) the dipolar fields arising from lipid headgroup and fatty acid chain packing, and to the total electrical environment of the bilayer and its interface with the surrounding aqueous medium. Further, the aqueous environment at the interface of the bilayer varies from that of the bulk solution due to surface effects, such as the concentration of metal and hydronium ions. Through various truncation constructs, Molina et al. found that KcsA residues 120–124 were the most critical for channel tetramer stability and assembly [44]. Applying molecular dynamics simulations, the authors described contacts between residues at the end of the final transmembrane segments with residues in the region where the N-terminus meets the first transmembrane segment (e.g. T112-H25-D118, R121-A23).

### 2.2.8 *Progress on KcsA by NMR*

Figure 2.4 shows the backbone atoms of KcsA in liposomes that are definitely identified in solid-state NMR data sets made by the McDermott group ([6, 73, 74]) and the group of Marc Baldus ([36, 40, 72]), which represented the two most concerted efforts to assign and report NMR chemical shifts of KcsA in a lipid environment. The data represented in the figure is compiled from the assignment tables provided in the supplementary data tables. These data were collected using various 3- and 4-dimensional datasets designed to transfer magnetization along the protein backbone.

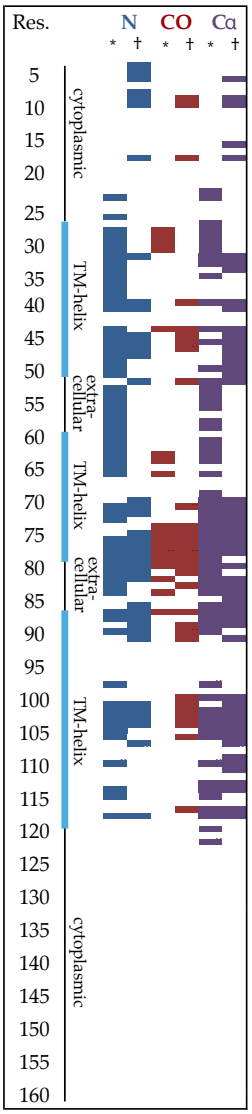


FIGURE 2.4: Solid-state NMR backbone assignments of KcsA in liposomes as described by the McDermott Group (*)[6, 73, 74] or Baldus Group (†)[36, 40, 72].

Several efforts [2, 28, 31, 34, 66], most notably by Chill et al. [11], have provided near complete assignments for KcsA in detergent micelles. The solution studies are often truncation mutants and at high temperature (e.g. > 45 °C). Solution studies have provided remarkable information about the dynamics [12] and secondary structure [11], and they have identified the major [67] and minor pH [48] sensors. Yet, in the absence of the structural data

in the actual membrane environment, we have an incomplete picture.

Solid-state NMR has proven to be a worthy tool to investigate the structural and functional properties of KcsA in a native-like environment and under physiologic-like conditions. For example, solid-state NMR can collect structural information in the same environment where electrophysiology data are collected, thereby directly connecting structure to function.

## 2.3 RESULTS

As established above, the C-terminus of KcsA is functionally important. The desire to study KcsA in a biologically relevant, native-like environment pushes us to investigate methods of measuring aspects of the C-terminus's function and structure in native-like lipid bilayer. Since the C-terminus of KcsA is not detected by CP-MAS or crystallography, which require rigid structures, one way to detect these signals would be by J-based NMR measurements which work well on isototropic systems, as seen in the work of KcsA in nanodisks [53]. The liposome environment increases the tumbling time of embedded molecules and thus increases the anisotropy. Proton-detected, J-based, high-resolution magic angle spinning NMR (HR-MAS) has unique potential to be useful for just such a system where portions of a sample (e.g. the termini) are mobile but anchored to a relatively immobile domain.

U-$^{13}$C,$^{15}$N-KcsA was reconstituted into a 1 : 1 mass ratio with a binary mixture of mono-unsaturated, diacyl phospholipids, 1,2-dioleoyl-sn-glycero-3-phospho-ethanolamine (DOPE) and 1,2-dioleoyl-sn-glycero-3-phospho-L-serine (DOPS) (9 : 1 mass ratio). This lipid system is well established as being suitable for detecting state changes by electrophysiology and conformational changes by NMR [5, 6, 73]. $^{1}$H-$^{13}$C and $^{1}$H-$^{15}$N HSQC correlations were collected by HR-MAS at 5 kHz MAS, and 308 K probe set temperature, resolving numerous protein peaks in both sets of correlations.

### 2.3.1 *HR-MAS Selectively Detects Signal from KcsA C-Terminus*

The $^{1}$H-$^{13}$C HSQC spectrum of full-length KcsA in liposomes was compared to a C-terminal instruction construct (KcsA-Δ125) in liposomes and 9 : 1 DOPE-DOPS lipids prepared without protein Figure 2.6. and reconstituted into 9 : 1 DOPE-DOPS lipids. Pure DOPE-DOPS (9 : 1 liposomes were also examined to quickly identify the resonances arising from lipids.

The terminal 34 residues of KcsA were first truncated by chymotrypsin as described previously [14, 44, 49]. The completion of the cleavage reaction was confirmed using SDS-PAGE gel (Figure 2.5a) and the product of the reaction was confirmed to be the C-terminal cleavage product by liquid chromatography tandem mass spectrometry-mass spectrometry (LC-MS/MS) (Table 2.1). The peptide fragments detected in the LC-MS/MS were compared to the full-length sequence of KcsA with a 80 % peptide probability cut-off. The peptide fragments captured by LC-MS/MS of full-length sam-

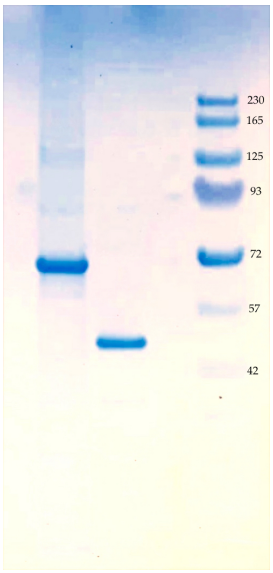


(A) Full-length (left), following reaction with chymotrypsin (center), and protein ladder (right). Full length tetramer = 70.8 kDa, expected clevage product = 53.5 kDa.

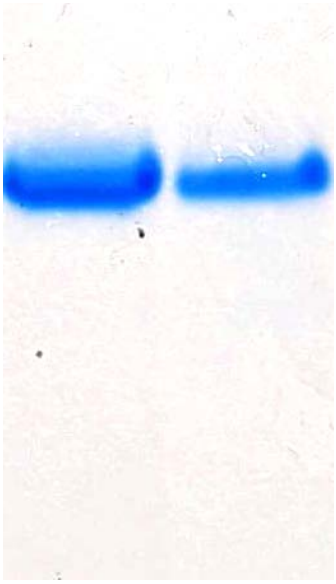

(B) KcsA- 125 in detergent (left) and following incorporation into liposomes (right). Samples had the same theoretical protein concentration.

FIGURE 2.5: SDS-PAGE gels of KcsA stained with coomassie brilliant blue

ple and the chymotrypsin cleaved sample represent 34 % and 27 % of the full-length sequence, respectively. It is common, especially for membrane proteins, for certain fragments to go undetected by this technique [39]. Both samples display consistently strong sensitivity for the fragments captured, as indicated by the total number of spectra that count a particular fragment. Whereas the full-length construct has several fragments from the C-terminus, not a single similar fragment is detected from the chymotrypsin treated sample, providing strong evidence that the C-terminus has been successfully cleaved. A more detailed presentation of the results is provided in Appendix B.

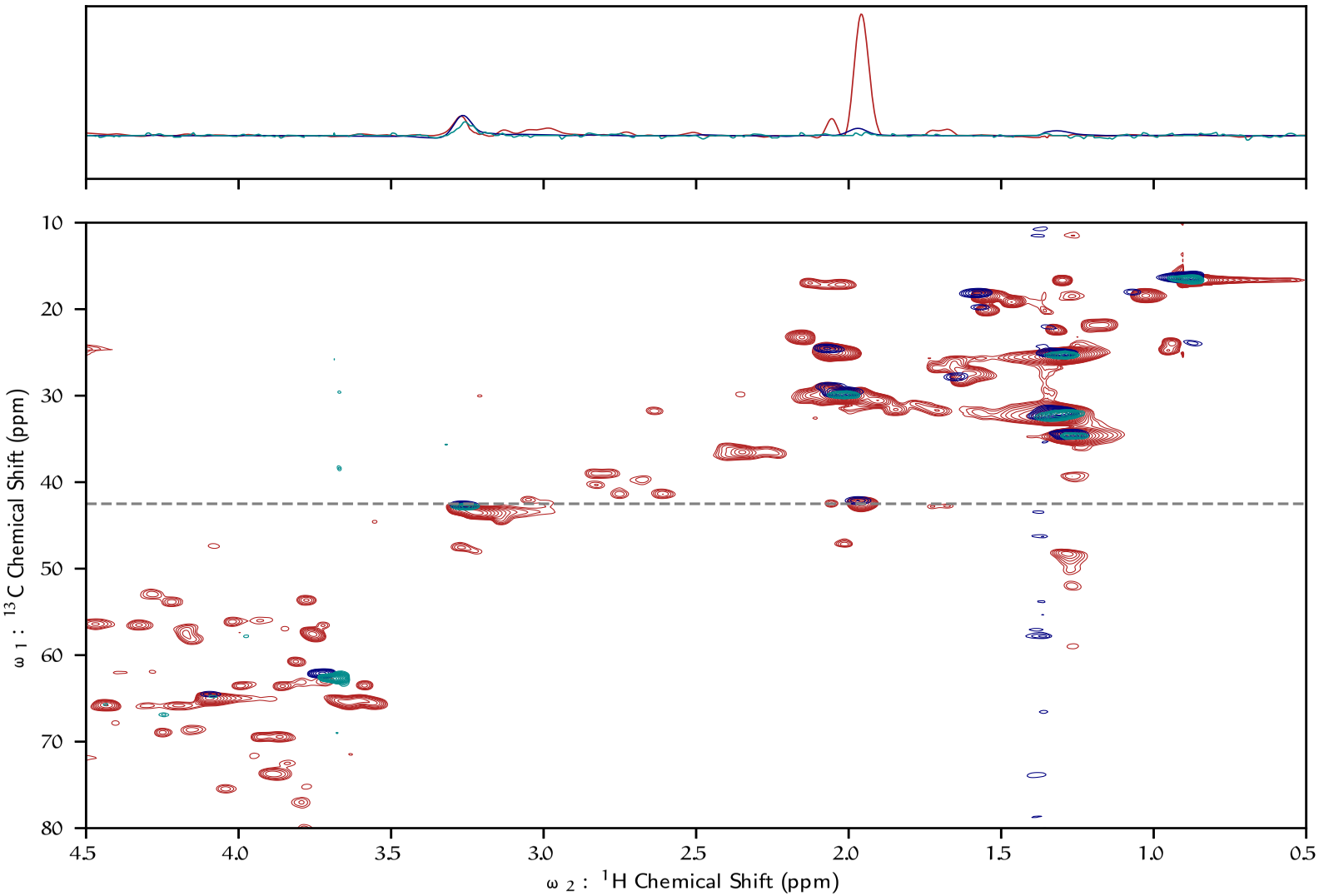


FIGURE 2.6: Superimposed $^{1}H$–$^{13}C$ HSQC by HR-MAS of: full-length KcsA in DOPE-DOPS liposomes (red), KcsA-Δ125 in DOPE-DOPS liposomes (navy), and DOPE-DOPS liposomes (cyan), showing that most resonances in full-length KcsA originate from residues 125-160. Slice of data at dash line displayed at top, showing PE-β ($^{1}H$: 3.25) signal intensity is similar for all three samples. All samples: pH 7.25, 50 mM $K^{+}$ 308 K, 5 kHz MAS.

| Sample | Res. start | Res. end | Peptide sequence | I.D. probability | Count |
|---|---|---|---|---|---|
| ΔC | 1 | 17 | MHHHHHHPPMLSGLLAR | 99.7% | 218 |
| FL | 1 | 17 | MHHHHHHPPMLSGLLAR | 99.7% | 369 |
| ΔC | 26 | 33 | HGSALHWR | 99% | 218 |
| FL | 26 | 33 | HGSALHWR | 99% | 369 |
| ΔC | 59 | 70 | GAPGAQLITYPR | 99.7% | 218 |
| FL | 59 | 70 | GAPGAQLITYPR | 99.7% | 369 |
| FL | 134 | 145 | HSEKAAEEAYTR | 99.7% | 369 |
| FL | 138 | 145 | AAEEAYTR | 99% | 369 |
| FL | 138 | 148 | AAEEAYTRTTR | 89% | 369 |
| FL | 160 | 166 | MLDDNRR | 90% | 369 |

TABLE 2.1: Peptide fragments identified by LC-MS/MS from full-length KcsA (FL) and the chymotrpsin digestion product (ΔC).

Comparing $^{1}$H-$^{13}$C spectra (Figure 2.6) of full-length KcsA to KcsA-Δ125, and to empty 9 : 1 DOPE-DOPS liposomes shows that the C-terminus is responsible for the vast majority of the protein signal in the full-length construct in that correlation. The synthetic phospholipids into which the samples are reconstituted are the primary source of signal in the KcsA-Δ125 sample as revealed by comparison to spectrum of the protein-free liposomes sample.

To confirm there the presence of isotopically enriched protein in the KcsA-Δ125 $^{1}$H-$^{15}$N HSQC spectrum (Figure 2.8) at 308 K and a CP-MAS $^{13}$C–$^{13}$C proton driven spin diffusion (DARR) spectrum at 265 K (Figure 2.7) were collected of the sample and compared to spectra of the full-length construct.

The $^{1}$H-$^{15}$N spectrum shows that most (though not all) resonances are eliminated when the C-terminus is truncated. indicating that HR-MAS signal of KcsA principally

arises from the C-terminus. Previous work shows the $^{13}C$–$^{13}C$ spectrum of full-length KcsA in liposomes records resonances arising from KcsA's transmembrane domain [73], therefore the Figure 2.7 shows that the transmembrane domain of KcsA-Δ125 is well-folded and $^{13}C$ enriched.

Figure 2.7 compares the CP-MAS $^{13}C$-$^{13}C$ spectra of a full-length construct of KcsA and the C-terminal truncated KcsA construct (Δ125) in liposomes at neutral pH. The slice of the data indicates that the two samples have similar signal-to-noise ratios at that particular section. Although the number, intensity, and distribution of the two samples is very similar there are some important differences. In particular, the KcsA-FL sample has several additional resonances that KcsA-Δ125 sample is missing. Assignments from previous studies in our group ([7, 73]) were used to assign the resonances that are present in KcsA-FL but absent in KcsA-Δ125. Many of the differing resonances are ambiguous or unassigned from the previous studies, and hence are not labeled in Figure 2.7. A fascinating pattern emerges from the differing resonances that can be emerged. Specifically, the resonances near the interface of the selectivity filter and the loop regions appear to be systematically missing. Many of these resonances are used in previous studies as indicators of KcsA in its bond-potassium state. Previous work in our group has proven T74CA-CB chemical shift to be an indicator of the $K^+$ apo and bound states of the channel [6, 74]. Importantly, these previous studies show *changes* in the chemical shifts, not absence of resonances. The first crystal structure of KcsA was of a KcsA-Δ125 construct [20] . The resonances that are present in KcsA-FL and absent in KcsA-Δ125 are mapped onto that structure in Figure 2.9. That

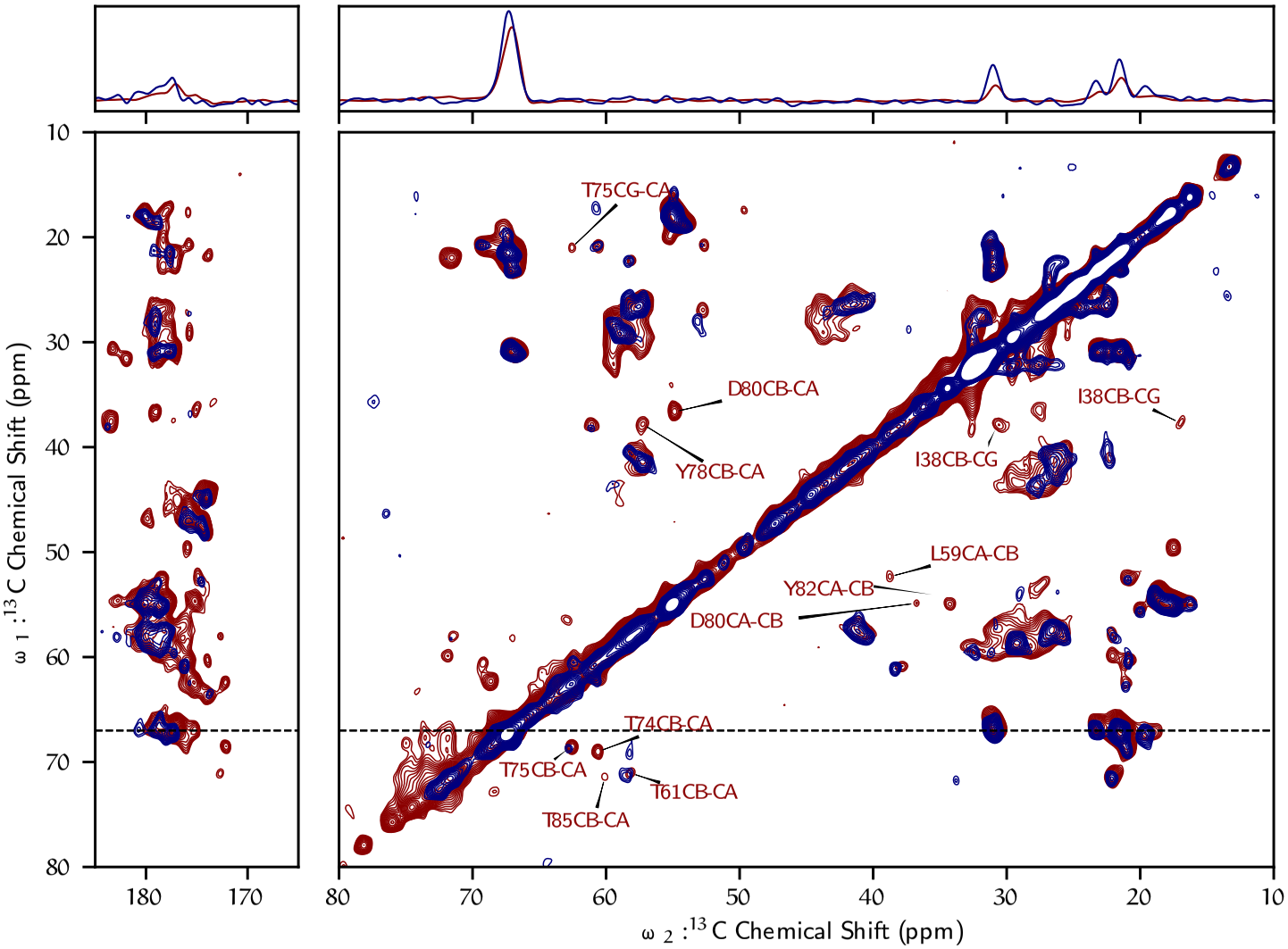


FIGURE 2.7: Superimposed $^{13}C$–$^{13}C$ proton-driven spin diffusion (DARR) CP-MAS full-length WT KcsA in DOPE-DOPS liposomes (red), KcsA-Δ125 in DOPE-DOPS liposomes (navy), showing the transmembrane domain of KcsA-Δ125 is folded and $^{13}C$ enriched. Assignments displayed propagated to full-length construct from previous studies [5, 73] from samples at similar conditions. Slice of data at dashed line displayed on top. 50 ms DARR mixing period, pH 7.25, 50 mM $K^+$, 270 K, 16.6 kHz MAS.

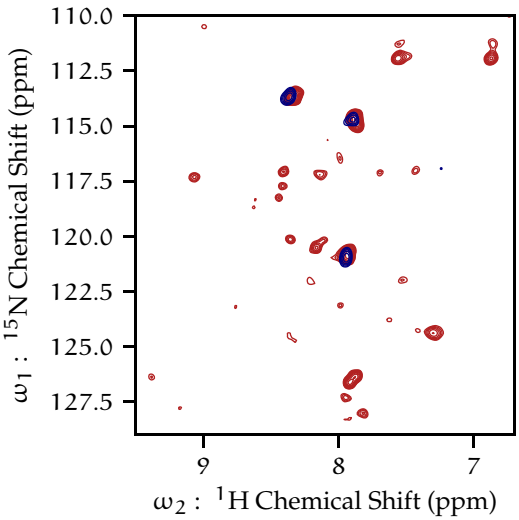


FIGURE 2.8: $^{1}$H–$^{15}$N HSQC by HR-MAS of full-length wild-type KcsA (red), and KcsA- 125 (navy). pH 7.25, 50 mM $K^+$ 308 K, 5 kHz MAS.

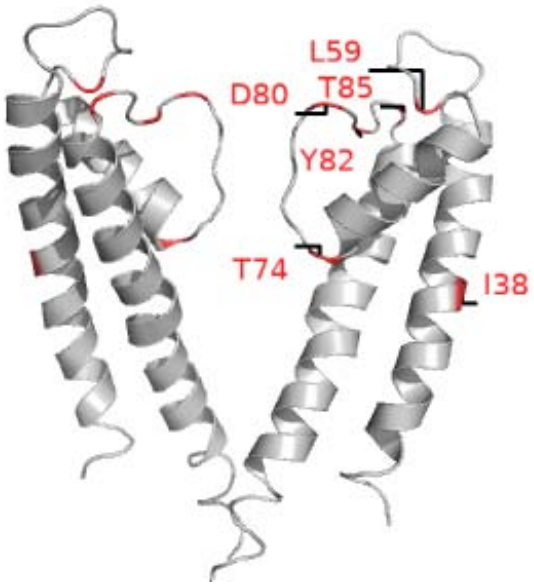


FIGURE 2.9: Resonances missing KcsA- 125 CP-MAS $^{13}$C-$^{13}$C spectrum from mapped onto PDB: 1BL8 [20].

crystal structure was able to resolve the entire selectivity region, the connecting loop regions and the resonances in between, supporting the notion (at least in detergent once crystallized), that the regions are relatively rigid. The most likely explanation of these NMR data, however, is that the C-terminal truncation leads to much greater dynamics, or much greater heterogeneity, of the regions at the interface between KcsA's loop regions and selectivity filter.

The KcsA-Δ125 sample (Figure 2.6) shows a number of additional peaks that are consistent with amino acid side chain resonances (e.g. 1.6 ppm/20–30 ppm) and consistent with a number of different amino acids, and therefore cannot be readily type-assigned.

### 2.3.2 *Transverse Relaxation of* $^{1}$H,$^{13}$C,$^{15}$N-*KcsA*

The protein resonances in the protein $^{1}$H-$^{13}$C and $^{1}$H-$^{15}$N HSQC data of uniformly-enriched (U) $^{1}$H,$^{13}$C,$^{15}$N KcsA provided vanishingly small signal on heteronuclear backbone experiments (e.g. HNCO, HNCA) normally used to establish atom assignments. This style of backbone experiment (diagrammed at Figure 2.13) requires polarization to be transferred between sites by using atom pair J-couplings, and short $T_2$ values of backbone resonances lead to loss of signal before significant polarization transfer can occur (Figure 1.4). Site-specific $^{13}$C $T_2$ (see Figure C.4 for pulse sequence details) values were measured to establish if transverse relaxation was leading to loss of signal during polarization transfer (Table 2.2). The average putative $^{13}C\alpha$ $T_2$ of

| Site | Type | $^{1}$H (ppm) | $^{13}$C (ppm) | $^{13}$C $T_2$ (ms) |
|---|---|---|---|---|
| | protein | 4.04 | 51.4 | 3.6 |
| | protein | 3.98 | 54.6 | 3.4 |
| Arg-α | protein | 4.03 | 55.2 | 2.8 |
| Met-α | protein | 4.30 | 55.8 | 3.9 |
| | protein | 4.16 | 56.9 | 2.7 |
| Lys-α | protein | 3.72 | 56.9 | 2.8 |
| | protein | 4.37 | 61.6 | 2.2 |
| Thrβ | protein | 4.19 | 69.0 | 2.4 |
| PE-β | lipid | 3.24 | 43.9 | 6.5 |
| PE-α | lipid | 4.05 | 64.2 | 5.9 |
| PG-γ | lipid | 3.56 | 64.7 | 3.7 |
| PG-γ | lipid | 3.63 | 64.7 | 3.8 |
| PG-α | lipid | 3.82 | 68.9 | 4.3 |
| PG-α | lipid | 3.88 | 68.9 | 4.4 |
| PG-β | lipid | 3.80 | 73.1 | 7.2 |

TABLE 2.2: $^{13}$C α $T_2$ U-$^{1}$H,$^{13}$C,$^{15}$N-KcsA in 9:1 DOPE-DOPS liposomes, pH 4.0, 50 mM $K^+$, 308K, 5 kHz MAS. Lipids assigned from chemical shifts, other resonances assumed to be protein H-Cα resonances

KcsA was found to be 2.9 ms and the average for lipid headgroup $^{13}$C to be 5.2 ms. The optimal transfer for Cα-N polarization transfer (in the absence of relaxation) is approximately 23 ms ($\frac{1}{4J} \approx 23$ ms). Applying Equation 1.13 using the average protein $^{13}$C $T_2$ finds much less than 1 % of magnetization remains during a carbon-nitrogen coherence transfer period, showing that transverse relaxation is simply too fast in this system to use J-based $^{13}$C-$^{15}$N transfers efficiently.

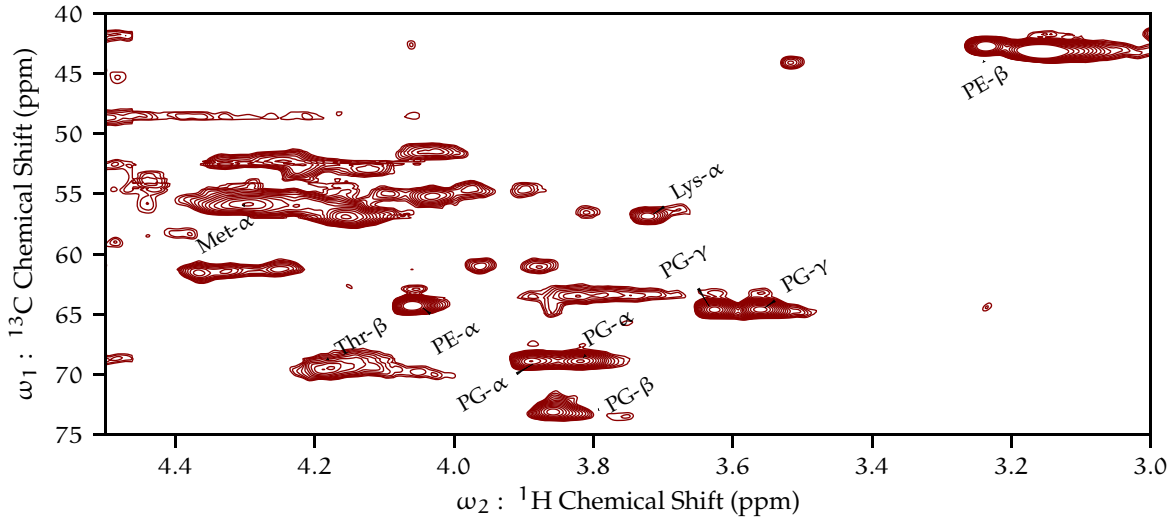


FIGURE 2.10: $^{1}$H-$^{13}$C HSQC by HR-MAS of KcsA in 9 : 1 DOPE-DOPS lipids at pH 4.0, 50 mM $K^{+}$. 5 kHz MAS, 308 K. Including labels associated with Table 2.2.

### 2.3.3 *Fractional Deuteration*

Anisotropic interactions lead to shorter $T_2$ relaxation values for proteins. Residual dipolar couplings with $^{1}$H can vastly attenuate J-based cohenrence transfer in backbone experiments. Replacing $^{1}$H with $^{2}$H in proteins is a well established method of reducing these dipolar couplings, thus increasing $T_2$ times, imporving resolution and coherence transfer efficiency [33, 37].

Although several examples of highly-[28, 52, 66] and perdeuterated [11] KcsA exist in the literature, several attempts by this author and other members of the McDermott group to perdeuterated KcsA lead to incomplete expression or the failure of the protein to form a tetramer. However, two different fractional deuteration schemes were successful.

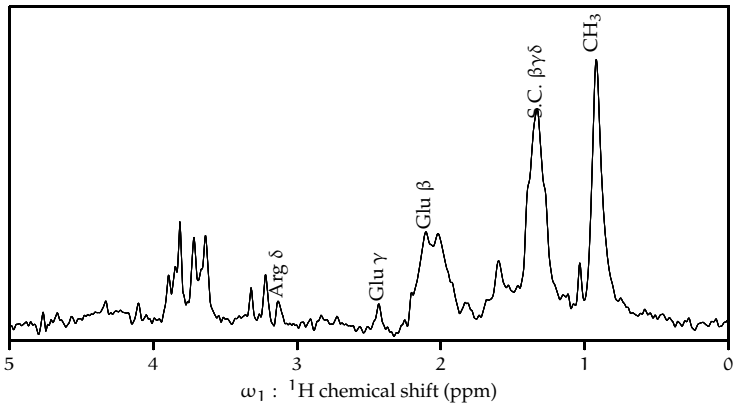


FIGURE 2.11: $^{1}$H-$^{13}$C back-INEPT spectrum of U-$^{1}$H,$^{13}$C,$^{15}$N-KcsA in proteoliposomes (9 : 1 DOPE-DOPS) at pH 4.0, 50 mM $K^{+}$, with peak annotations. Assignments made from 2D and 3D data. 9 kHz MAS, 308 K.

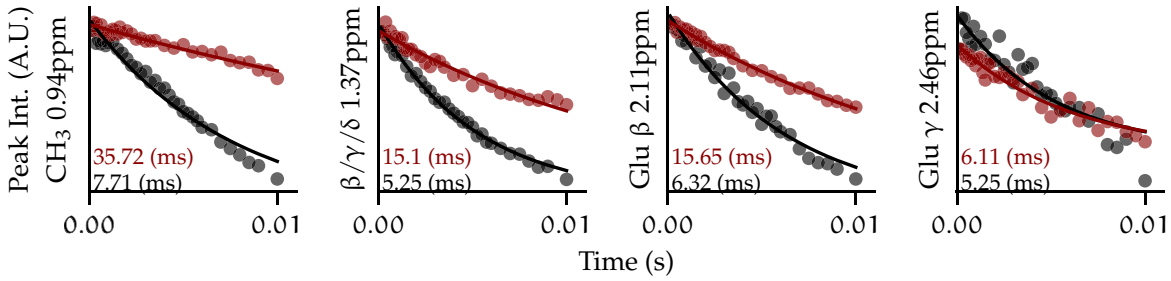


FIGURE 2.12: $^{13}$C spin-spin relaxation of selected peaks from 1D back-INEPT experiment and T2 fits for U-$^{1}$H,$^{13}$C,$^{15}$N-KcsA (black) and Fractional-$^{2}$H-U-$^{13}$C,$^{15}$N-KcsA (red) samples at pH 4, 50 mM $K^{+}$.

Previous work has found that expressing proteins in $D_2O$ minimal media supplemented with U-$^{1}$H,$^{13}$C-glucose and $^{15}$N-ammonium chloride leads to proteins that have very high levels of deuteration at the H-C$\alpha$ position and fractional deuteration in the side chains that vary by amino acid [63]. Here, we expressed KcsA in this manner, and incorporated it into 9 : 1 DOPE-DOPS liposomes. $^{13}$C relaxation profiles were determined using a 1D back-INEPT experiment with a dephasing period time, ($^{1}$H $\xrightarrow{\text{INEPT}}$ $^{13}$C $\xrightarrow{\text{dephasing}}$ $\xrightarrow{\text{INEPT}}$ $^{1}$H), to build $^{13}$C $T_2$ relaxation profiles of the fractional-$^{2}$H-KcsA (F-$^{2}$H) and U-$^{1}$H-KcsA, both with a U-$^{13}$C,$^{15}$N background. In addition to profiles for the methyl region and the aliphatic region, Glu-$^{13}$C $\beta$ and Glu-$^{13}$C $\gamma$ profiles are displayed because they are easily identifiable on the 1D spectrum of both samples. The results show that the relaxation profile is vastly improved of the F-$^{2}$H sample over the uniformly $^{1}$H labelled sample. The Glu-C$\gamma$ profiles are similar for both samples, whie agrees well with previous observations that both glutamate $\gamma$ protons tend to remain protonated in this labeling scheme and a portion of the Glu-H$\beta$ remain protonated in this labeling scheme [40].

The real testament to the effectiveness of this fractional deuteration protocol is that previously untenable 3D correlations are now possible. With the fully protonated sample, there was not enough signal to collect even the 2D plane of the canonical HNCA or HNCO correlations experiments. Whereas with F-$^{2}$H-KcsA, full 3D datasets were obtained showing a host of well resolved resonances (Figure 2.17, Figure 2.18. This pair of 'out-and-back' style experiments (diagrammed in Figure 2.13) provide an intra-residue correlation (HNCA) and an inter-residue (i to i-1) correlation (HNCO).

Unfortunately, there was not enough signal to justify collection of spectra that further facilitate assignment such as the HNCACB (either the forward or out-and-back), HCB-CANH, HNCOCANH, and other similar sequences. Transverse relaxation remains a major barrier in these experiments.

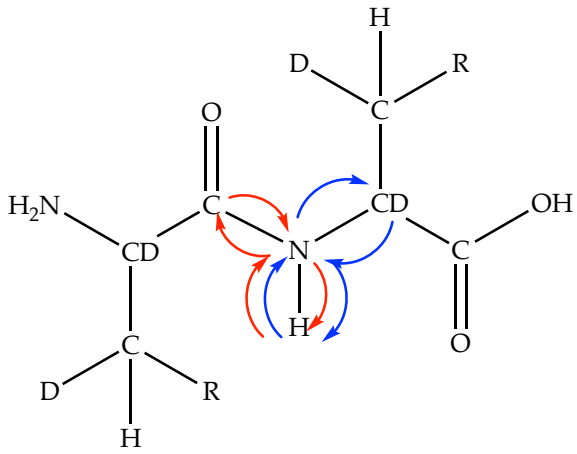


FIGURE 2.13: Schematic of HNCA (blue) and HNCO (red) polarization transfer pathway on a fractionally deuterated model peptide.

The HNCA (i) and HNCO (i-1) are linked back to the same root H-N amide resonance, forming a sequential pair in the protein (see diagram Figure 2.13). An H-N resonance that appears in both the HNCA and the HNCO spectrum is a link between two residues, and thirteen such links were identified. Chemical shift values are often characteristic of particular residue type. The PLUQ algorithm uses a database of chemical shifts deposited in the BMRB to predict the liklihood of a chemical shift arising from an amino acid type [22]. Using PLUQ, each CO peak from the HNCO experiment was scored for the probability of arising from each of the 20 amino acids types. Each H-N-C$\alpha$ correlation from the HNCA experiment was scored for the probability of its chemical shifts arising for each of the 20 amino acids types. Amino acids with less than 0.1 % probability arising from the given shift are discarded as candidates. Sequential pairs of KcsA were then evaluated. For example, the amide H-N resonance at 8.13 ppm-126.4 ppm appears in both the HNCO spectrum and HNCA spectrum, indicating the CO resonance is con-

nected to the i-1 residue of the amide. The first sequential pair of KcsA is Met-His, so based on the chemical shifts, the probability that the H-N-CA set of resonance is from a histidine is determined and the probability the connecting CO is from a methionine is determined. The joint probability is constructed as $P_{CO} \times P_{HNCA}$. This process is repeated for each sequential pair of KcsA. This process is then repeated for each set of connected HNCO and HNCA correlations. This creates a probability matrix for the likelihood of each resonance arising from each sequential pair. The matrix is not easily displayed on a printed page, it is organized in HTML format (Probability Table (links to external website)).

### 2.3.4 *Predicting Residue Types and Secondary Structure*

Amino acid-side chain shifts are characteristic of residue type. To type-assign the correlations in the $^{1}H$-$^{13}C$ HSQC, HcCH-TOCSY and hCCH-TOCSY 3D correlations were collected on KcsA in 9 : 1 DOPE-DOPS liposomes at pH 7.25, 50 mM using the DIPSI-2 sequence [58]. This experiment performs isotropic mixing of spin polarization through $^{13}C$-$^{13}C$ bonds and allows for the connectivity of a network of $^{13}C$ spins. This experiment is particularly useful in assigning side-chain resonances as it establishes each of the $^{13}C$ shifts in an unbroken bond network at a particular $^{1}H$ frequency (examples displayed in Figure 2.14). The hCCH-TOCSY is particularly powerful as it encodes $^{13}C$-$^{13}C$ which can be an excellent predictor of protein secondary structure (in particular from $^{13}C$ $\alpha$-$^{13}C$ $\beta$ correlations) [9, 64]. PLUQ software was used exten-

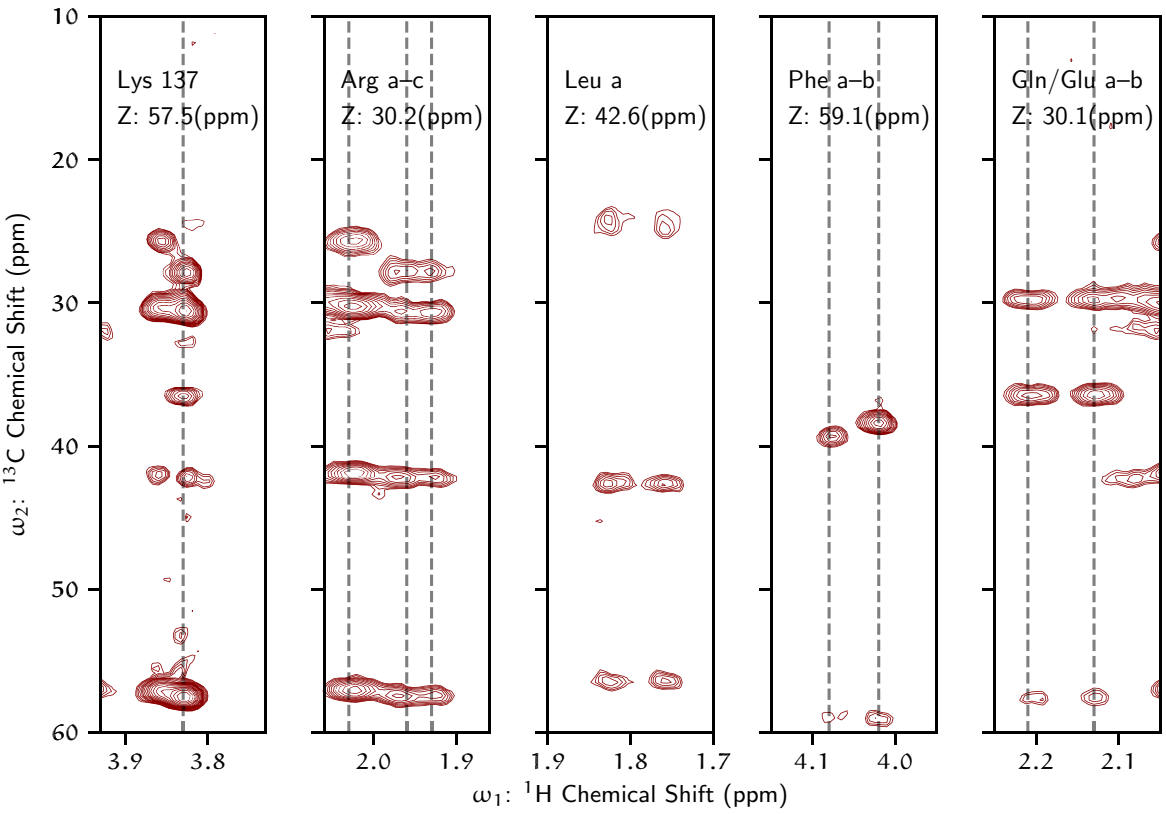


FIGURE 2.14: Strips plots of hCCH-TOCSY experiments showing $^{1}$H-$^{13}$C plane with $^{13}$C ( $_{2}$) shift specified. Annotations provide the given residue type/assignment for each strip shown. KcsA in 9 : 1 DOPE-DOPS, pH 7.25, 50 mM $K^{+}$, 9 kHz MAS, 309 K, 90 % $D_2O$ buffer.

sively to guide assignment of the residues and was used to predict the secondary structure probability from various residue types using $^{13}$C -$^{13}$C $\tau$ correlations (Table 2.3). Based on the number of amino acids spin systems collected it is unlikely the majority of these systems arise from individual sites. It is more likely an aggregation of similar populations of residue types. For example, three sets of arginine resonances can be observed. However there are 17 arginine residues in KcsA with 10 in the C-terminus alone. K129 can be positively identified, as lysine has a distinctive TOCSY pattern; there are only two lysines in KcsA (K14, K129) and the corresponding lysine resonance is missing upon cleavage of the C-terminus.

| Residue | P Helix | P Coil | P Sheet | Cα | Cβ | Cγ | Cδ | Cδ.1 | Cϵ | Hα | Hβ1 | Hβ2 | Hγ | Hδ |
|---|---|---|---|---|---|---|---|---|---|---|---|---|---|---|
| Lys 129 | 41.8 | 42.6 | 15.6 | 57.5 | 32.6 | | | | 42.1 | 3.83 | | | | |
| Arg a | 33.7 | 48.9 | 17.4 | 57.1 | 30.4 | 25.6 | 41.8 | | | 3.86 | 2.09 | | 1.63 | 3.15 |
| Arg b | 30.7 | 50.4 | 18.9 | 57.0 | 30.2 | 25.6 | 41.8 | | | 3.83 | 2.06 | | 1.63 | 3.14 |
| Arg c | 41.1 | 44.6 | 14.3 | 57.4 | 30.6 | 27.8 | 42.1 | | | 3.77 | 1.96 | | 1.62 | 3.14 |
| Leu a | 30.8 | 47.8 | 21.3 | 56.3 | 42.7 | | 23.7 | 24.9 | | 3.81 | 1.82 | 1.76 | | |
| Leu b | 33.5 | 46.5 | 20.0 | 56.3 | 42.6 | | 23.8 | 24.8 | | 3.81 | 1.82 | 1.76 | 1.82 | |
| Phe a | 45.1 | 43.6 | 11.3 | 58.9 | 38.3 | | | | | 4.01 | 3.28 | | | |
| Phe b | 44.9 | 43.7 | 11.3 | 58.9 | 38.4 | | | | | 4.02 | 3.13 | | | |
| Gln /Glu a | 27.1 | 60.5 | 12.4 | 57.5 | 29.7 | 36.4 | | | | 3.83 | 2.12 | | 2.44 | |
| Gln/Glu b | 26.9 | 60.1 | 13.0 | 57.1 | 29.6 | 36.4 | | | | 4.08 | 2.20 | | 2.44 | |

TABLE 2.3: Amino acid types identified in hCCH-TOCSY experiment of KcsA in 9 : 1 DOPE-DOPS at pH 7.2, with probability (in %) of secondary structure as predicted from PLUQ [22] based on Cα and Cβ shifts.

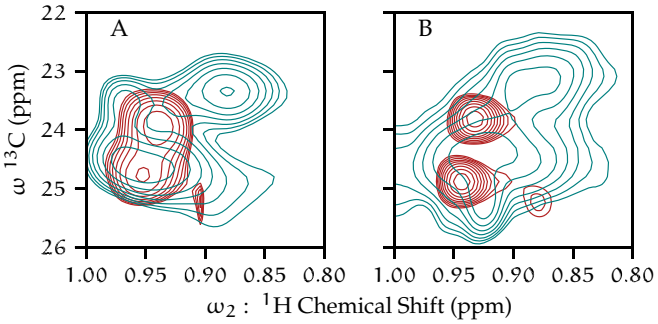


FIGURE 2.15: pH induced conformational changes in leucine $^{1}$H-$^{13}$C shifts. pH 7.25 (red contours) and pH 4.0 (blue contours) for fully protonated KcsA (A) and fractionally deuterated KcsA (B) in liposomes.

### 2.3.5 *Leucine as a C-terminal Conformational Indicator*

One reliable identifier of pH was identified from the spectra: a set of leucine $^{1}$H-$^{13}$C correlations (as identified from TOCSY data) show reliable shifts when pH drops from 7.25 to 4.0 in KcsA embedded in 9:1 DOPE-DOPS liposomes (Figure 2.15). Specifically, in both fractionally deuterated samples and in fully protonated samples, there is a reliable shift from a sharp set of resonances arising from two different leucine residues to more disperse, right-shifted peaks. These particular resonances are not present in the C-terminal truncation construct, confirming they are in that region. The difference in the shift dispersion is a strong indication that at low pH the conformation of the C-terminus is more heterogeneous than the conformation at neutral pH where the channel is expected to be in the closed conformation. Also, these data show that fractional deuteration can be a strategy that retains enough information to draw information from side chain correlations while still slowing transverse magnetization relaxation.

These data also show that for these particular indicators, fractional deuteration is not strictly necessary and that $^{13}C$ labeling is sufficient.

### 2.3.6 *TROSY*

Transverse relaxation-optimized spectroscopy (TROSY) [50] has become an indispensable technique for deuterated macromolecule NMR. As discussed above, CSA and dipole-dipole interactions lead to fast transverse relaxation of slow tumbling molecules. In the case of an amide nitrogen, the most important interactions leading to relaxation is the dipole interaction with the amide proton and the CSA of the protons. These two contributions cause different rates of relaxation for each element of the $^{1}H$-$^{15}N$ resonance multiplet. The CSA is dependent on magnetic field strength, but the dipolar coupling is not, so at certain magnetic fields (around 900 MHz to 1 GHz $^{1}H$ frequency [50, 65]) for the amide proton, these two relaxation effects can lead to near complete cancellation of three of the four multiplet peaks leaving only the sharpest resonance. This effect tends to be improved by extensive deuteration of the protein [21, 65]. Typically, amide proton linewidths can be decreased by a factor of two, with a attenuation of total signal of a factor of $\sqrt{2}$ [21, 50]. The narrower lines often lead to improved overall signal-to-noise even with the attenuation of signal from selection a signal component of the multiplet.

TROSY $^{1}H$-$^{15}N$ spectrum was collected of the fractionally deuterated KcsA sample (Figure 2.19. The linewidth is indeed narrower, but with a substantial sacrifice in total

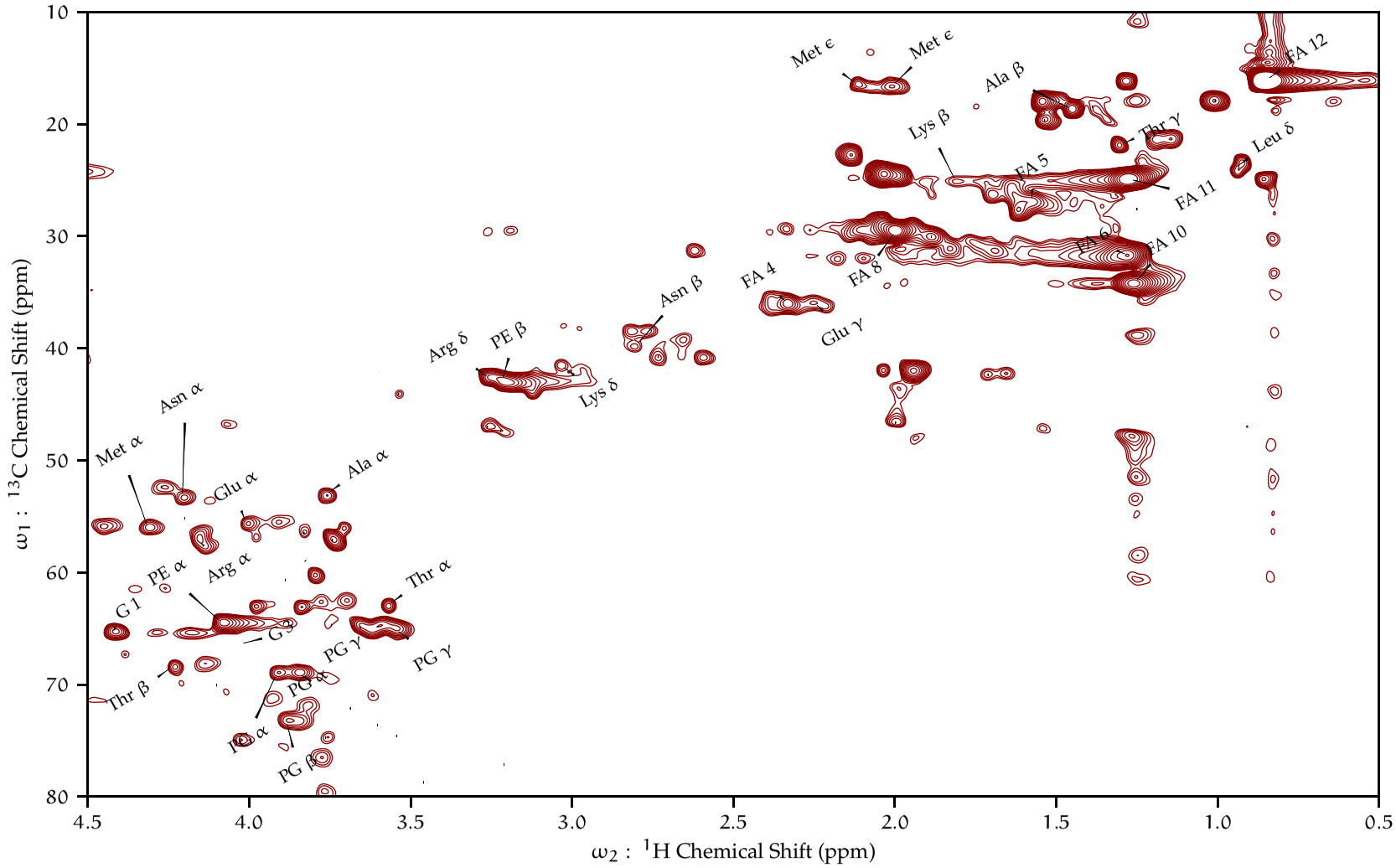


FIGURE 2.16: $^{1}$H-$^{13}$C HSQC by HR-MAS of U-$^{1}$H,$^{13}$C,$^{15}$N-KcsA in 9 : 1 DOPE-DOPS. With annotations as assigned by HcCH-TOCSY. 5 kHz MAS, 308 K.

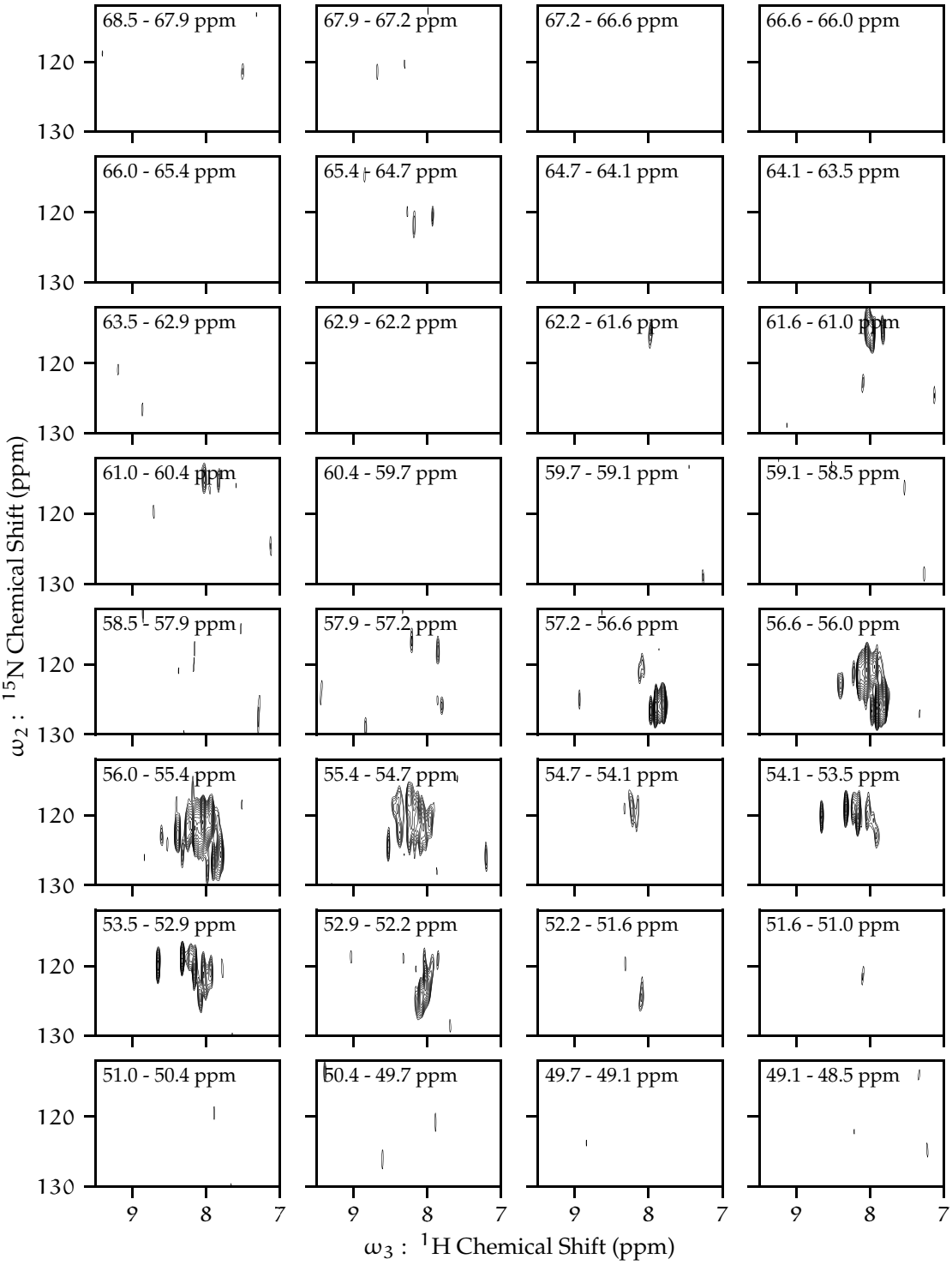


FIGURE 2.17: Planes Inter-residue HNCA 3D correlation of fractionally deuterated U-$^{13}$C,$^{15}$N-KcsA at pH 4.0, 50 mM $K^+$. Z-axis ($^{13}$C (ppm)) range is annotated on each plane. 9 kHz MAS, 308 K

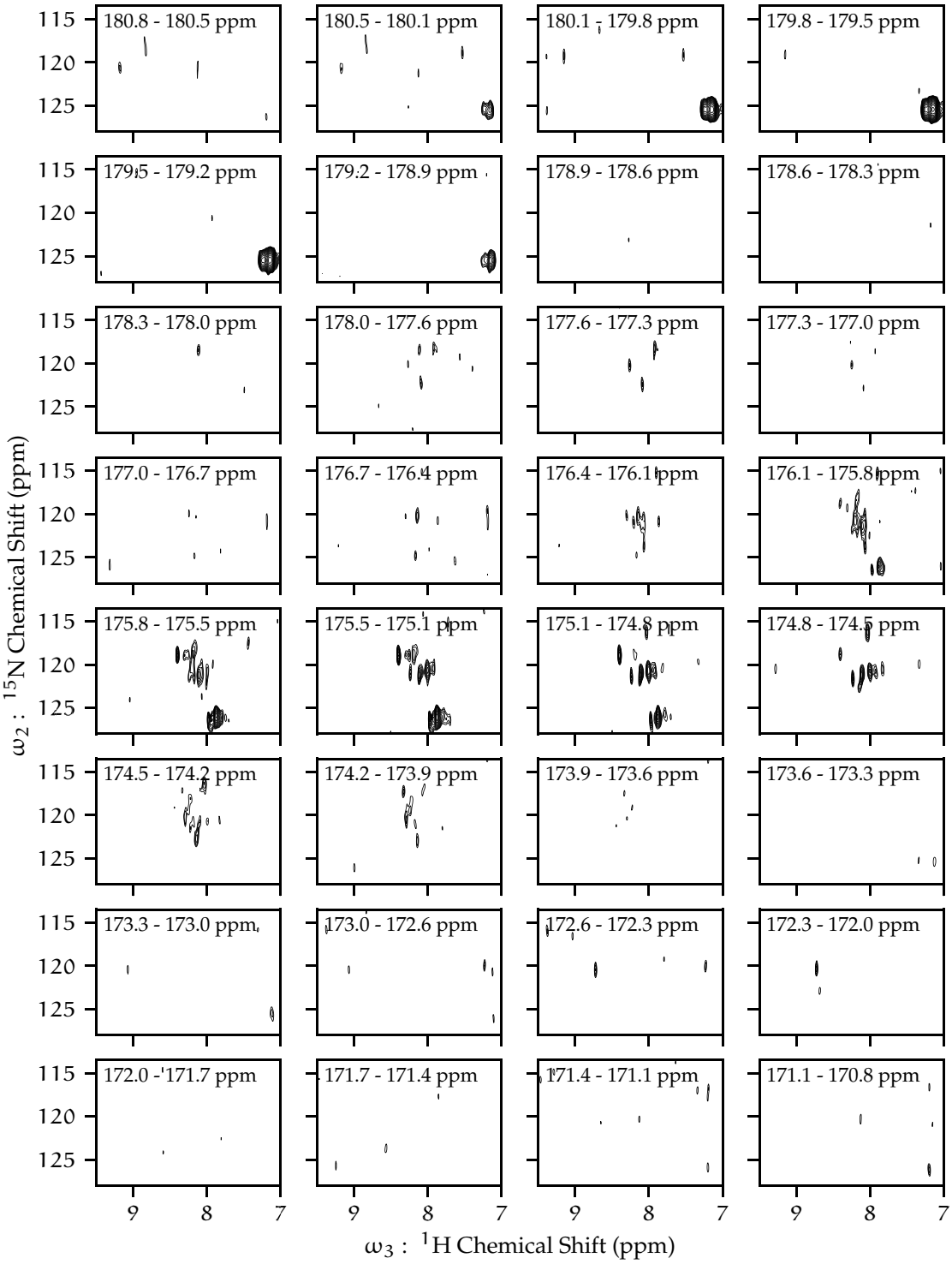


FIGURE 2.18: Intra-residue (i+1) HNCO backbone strips of fractionally deuterated U-$^{13}$C,$^{15}$N-KcsA at pH 4.0, 50 mM $K^+$. Z-axis ($^{13}$C (ppm)) range is annotated on each plane. 9 kHz MAS, 308 K

signal. Linewidth gains, as demonstrated by the slice, vary based on resonance. But overall, the signal-to-noise is much lower on the TROSY based experiment.

The first point of the TROSY HNCO was also collected and compared with the HSQC HNCO Figure 2.20. Here, the loss of signal is shown to be substantial for the TROSY HNCO, and given the only modest increase in linewidth demonstrated by the $^{1}$H-$^{15}$N TROSY 2D experiment, the collection of a 3D dataset was not justified.

This experiment was performed on a 750 MHz magnet, and moving to a higher field may improve the gains.

## 2.4 DISCUSSION

Here we present data that KcsA in model liposomes assumes distinct conformations at pH 7.25, where the channel is inactive, and at ph 4.0, under which conditions the channels is able to activate. The specific lipid model we have selected here has been shown to allow past studies to collect detailed structural information collapse inactivation [5] and allosteric coupling between sites within KcsA [73, 74], and thus connect structure to channel function.

The conformational dynamics presented here support previous structural models in a number of ways. A sequential spin-labeled, ESR structure of KcsA in bilayers at pH 4 recorded significant probe mobility of the C-terminus [14]. Full-length KcsA

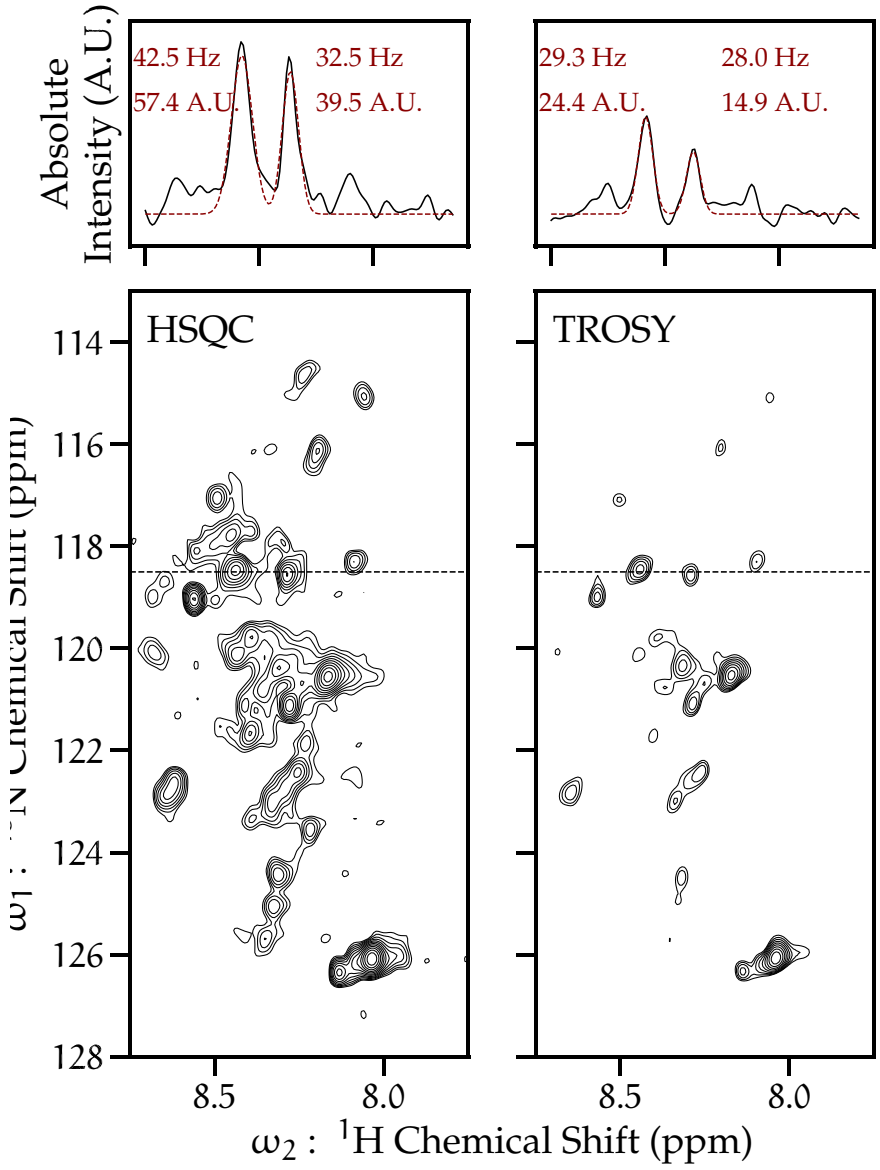


FIGURE 2.19: $^{1}$H-$^{15}$N HSQC (left) and TROSY (right) of F-$^{2}$H,U-$^{13}$C,$^{15}$N-KcsA pH 4, 50 mM $K^{+}$, 308 K, 9 kHz MAS, 128 scans, 1024 160 complex points. Contours begin at 5 noise. Slice of data at dotted line shown above with linewidths and integrals of Gaussian fits shown.

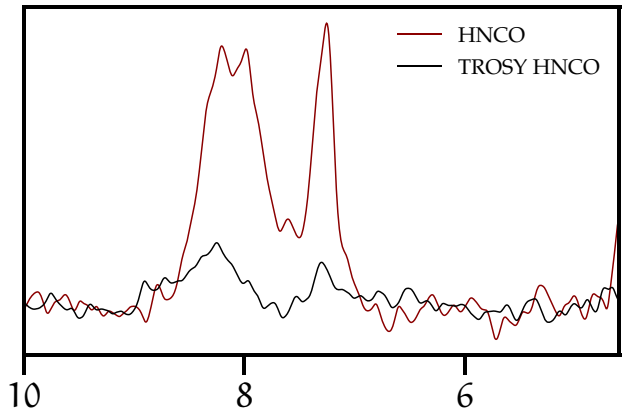


FIGURE 2.20: $^{1}$H-$^{15}$N HSQC NCO (black) and TROSY NCO (red) of F-$^{2}$H,U-$^{13}$C,$^{15}$N-KcsA pH 4, 50 mM $K^{+}$, 308 K, 9 kHz MAS, 400 scans, 1024 complex points.

with its C-terminus stabilized by Fab antibodies at neutral pH was rigid enough to capture by x-ray crystallography [69].

This work expands on those previous observations and shows a proof of concept that the increased dynamics of the C-terminus can be leveraged to provide the first backbone correlations of KcsA termini in lipids and makes initial resonance assignments within that region.

Similar to [32, 52], this study observes two distinct conformations of the KcsA C-terminus as a function of pH. Dramatic changes can be observed in the $^{1}$H-$^{15}$N HSQC data (Figure 2.21), with many more peaks with much narrower linewidths at low pH than compared to pH. This is the case when comparing both fractionally deuterated samples and fully protonated samples, showing that it is not an effect merely of the labeling scheme. This does suggest that as the pH is lowered the KcsA C-terminus moves more freely.

For $^{1}$H-$^{15}$N data, the number and the distribution of KcsA at low pH are similar for both fully protonated protein, and the fractionally deuterated samples (data not displayed). Yet, they the low pH differ dramatically in dispersion, linewidth and number of resonances comparing low pH KcsA (pH 4) to neutral pH KcsA. Using DSS as an internal reference, resonances of low pH align well with other low pH samples, and resonances from neutral pH (ranging from pH 7.5 to 6.3), align precisely with all other samples. For $^{1}$H-$^{13}$C data, the vast majority of peaks (with exceptions, such as the previously noted leucine $\delta$ resonances), all peaks align well when referenced to DSS as an internal standard. This supports that the referencing is correct and the amide protons shifts are showing a significant change in conformation caused by the change in pH. Resonances assignments of the $^{1}$H-$^{15}$N data cannot be meaningfully propagated from low pH to high pH samples because of the dramatic differences observed between these two states the occur.

This work also shows leucine $^{1}$H-$^{13}$C$\delta$ resonances in HSQC data that provide a markers of the low and high pH state. Further, the change from sharp peaks at neutral pH, to broader more disperse peaks at acid pH reiterates that the change in conformation goes from relatively ordered to more conformationally heterogeneous as suggested by structural data. [52] also found that leucine residues provided a convenient marker to distinguish the two states in methyl labeled KcsA by solution NMR. Here, we show that these markers are present in both U-$^{1}$H, $^{13}$C, $^{15}$N-KcsA as well as F-$^{2}$H, U-$^{13}$C $^{15}$N-KcsA.

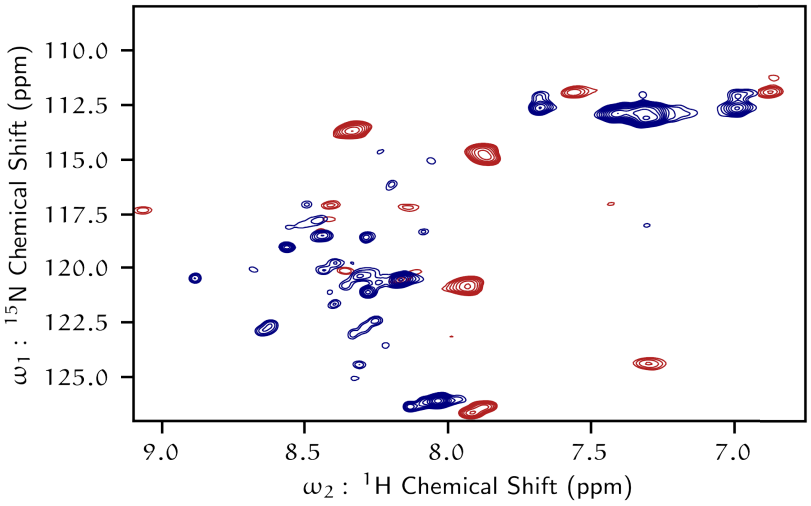


FIGURE 2.21: $^{1}$H-$^{15}$N HSQC of KcsA at pH 7.25 (red), and F-$^{2}$H-KcsA at pH 4.0 (blue) by HR-MAS. 5 kHz MAS, 308 K, 50 mM $K^{+}$

The hCCH-TOCSY data showed ten resolved groups of amino acid resonances (summarized in Table 2.3). This data alone established the an additional assignment (Lys 129) that has not been previously made in solid-state NMR data. There are three resolved sets of arginine resonances in those data. However, KcsA contains 17 arginine residues, with 1 in the N-terminus, 6 in the transmembrane domain, and the remaining 11 in the C-terminus. All of the characteristic arginine spins in HR-MAS data are absent in the spectrum of KcsA-Delta128. So the three resonances are in almost certainly from the C-terminus. The three resonances could represent various 'pools' of more than one arginine sharing a similar magnetic environment. Alternatively, they could be the most mobile three resonances within the C-terminus, which would likely be those at the end (e.g. R153, M154, L155, D156, D157, N158, R159, R160). These end resonances closely mirror the composition of the resonances identified by type show in Table 2.3. Work in KcsA nanodisks assigned the few resonances appearing in the

$^{1}$H-$^{15}$N HSQC at neutral pH to D157, N158, R159, R160, with others being remaining unassigned [52]. It should be noted that the chemical shifts from that study do not align with those from this study, and as such cannot be propagated across the studies.

Crystal studies of Fab stabilized KcsA and sequential-spin labeled KcsA structures agree that at high pH, that the C-terminus of each monomer of KcsA forms an $\alpha$-helix [14, 69]. NMR chemical shifts are highly predictive of secondary structure, with the C$\alpha$-C$\beta$ correlation being particularly strong indicator [22]. In the hCCH-TOCSY data the secondary structure predicted on the shifts of type-assigned resonances agree with the hypothesis that KcsA's C-terminus forms an alpha helix, with all of the resonances giving the highest probability of being in helical conformation.

Previous studies show that as a soluble fragment KcsA$_{128-160}$ oligomerizes into a tetramer at netural pH and dissociates into monomers at low pH [31, 32, 48]. These two states of the KcsA$_{128-160}$, monomer and tetramer, are easily distinguished by the number and position of amide resonances in $^{1}$H-$^{15}$N HSQC data from those studies. Lipid nanodisks DMPC containing tetrameric full-length KcsA at low pH show a near identical $^{1}$H-$^{15}$N spectrum to monomeric C-terminal domain fragment in solution NMR [53]. The peak lists for both the monomeric and the tetrameric states of the C-terminal fragment were published by Kamnesky, Shaked, and Chill [31] and formed the basis for the assignment of the data of KcsA in nanodisks by Qasim et al. Using the peak lists provided by Kamnesky, Shaked, and Chill [31], synthetic $^{1}$H-$^{15}$N spectra were constructed with NMRPipe [18] software. Those synthetic spectra are plotted with data from this study of KcsA in $9:1$ DOPE-DOPS liposomes by HR-MAS in

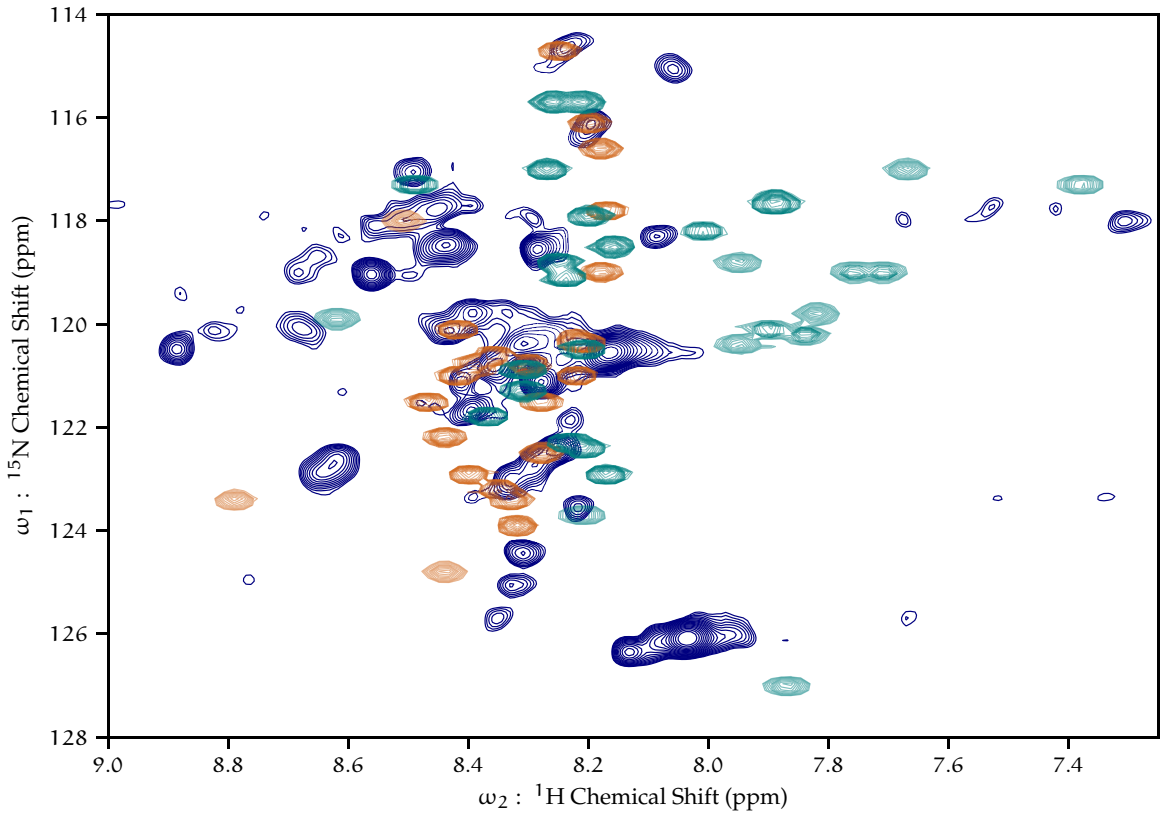


FIGURE 2.22: $^{1}$H-$^{15}$N HSQC data showing previously reported conformations of KcsA (teal and orange), vary from that reported in this study (blue). Data from fractionally deuterated KcsA at pH 4, 50 mM $K^+$ in 9 : 1 DOPE-DOPS liposomes by HR-MAS (blue). Simulated spectra from peak lists published by Kamnesky et al. [32] of $KcsA_{126\ \ 160}$ peptide in monomeric state (orange), and tetrameric state (teal) in solution. The tetrameric state(teal) is nearly identical to FL-KcsA in DMPC nanodisks by solution NMR presented by Qasim et al. [53], whose peak table is not published.

Figure 2.22. Both the original data presented here and the Kamnesky, Shaked, and Chill data used the same same referencing system of 4,4-dimethyl-4-silapentane-1-sulfonic acid (DSS) as an internal standard for $^{1}H$ and indirect referencing to DSS on $^{15}N$. This plot reveals that the KcsA in liposomes at pH 4, under which conditions it is known to be a functional channel, is distinct from both monomeric and tetrameric $KcsA_{128-140}$ fragment. The lipid composition of the nanodisk sample and the data presented in this chapter vary considerably. Specifically, the nanodisks have DMPC as the only lipid component, a short-chained (14), saturated lipid with a zwitterionic headgroup. From electrophysiology studies we know a fraction of lipid headgroups must be anionic for KcsA to activate [25, 70] and that KcsA fails to open at any pH when incorporated into single component 1-palmitoyl-2-oleoyl phosphatidylcholine (POPC) lipids [29, 41].

The data presented here in this work are not of "active" or "open" channels. The wild-type KcsA open-probability is quite low due to its inactivation characteristics [10, 13]. However, we do have strong evidence that this system of KcsA and liposomes can be used to detect changes of protonation state, can be used to measure a host of structural phenomena such as the allosteric coupling between the selectivity filter and the extracellular potassium gate [73, 74], and selectivity-filter opening and closing upon protonation of key residues [5]. The data presented here show that HR-MAS is a viable method to investigate the structure of KcsA's C-terminal domain.

There are several interesting functional questions that could be addressed with this system. For example, our group has demonstrated that depleting the system of $K^{+}$

in the low pH state leads to structural changes and subsequently to the inactivation of KcsA, showing a strong allosteric connection between binding of potassium at the selectivity filter and protonation of pH sensors at E118 and E120 [74]. HR-MAS could detect if the C-terminus also has an allostericity induced conformational change, perhaps reverting to the more rigid structure upon depletion of $K^+$ from the selectivity filter.

Fractional deuteration of KcsA was essential to collecting 3D correlations. Preparations of fully protonated KcsA at pH 4 (data not show), showed a similar number and distribution of $^{1}H$-$^{15}N$ shifts on the HSQC as the fractionally-deuterated sample. However, the backbone correlation experiments failed to provide enough signal to justify collecting full data sets. The $^{13}C$ $T_2$ relaxation profiles that compare fully protonated KcsA with F-$^{2}H$-KcsA at pH 4.0 (Figure 2.12) show that for a dramatic increase in $T_2$ from deuteration. Those data do not show the effect on C$\alpha$ relaxation as th C$\alpha$ positions are not protonated in the fractional deuterated sample. Despite the increases in spin-spin relaxation times, it was still not possible to correlate CO or C$\alpha$ resonances to C$\beta$ resonances, which would be key to making assignments. As the assignment probability matrix shows (Probability Table (links to external website)), the correlations collected are not enough to type-assign any of backbone 3D correlations with confidence. These data rank each set set of resonances as their probability from arising from each pair. By this method, no individual pair has more than a 20 % chance of being correctly assigned using these resonances.The extension of these resonances

to include Cβ resonances would over this difficulty and allow for many assignments to be made.

## 2.5 LIPID SELECTION

The motivation to use the mixture of lipids in these studies, 9:1 DOPE-DOPS, arose from the previous success of characterizing functional states of KcsA in this particular mixture [6, 73, 74]. The PE moiety is zwitterionic and the PS moiety carries a net −1 charge under the conditions used in these pages. Numerous studies have established that lipids with anionic headgroups are required for channel activation [25, 41, 70], with the presence of those lipids required specifically on the inner leaflet of the membrane [29]. This justifies the use of PS headgroup in a PE background. Yet there is an entire lipid space that has not been explored in terms of increasing mobility for J-based experiments. It is worth considering alternative lipid schemes.

Lipid-protein nanodisks have show particular promise for the study of KcsA. Work of KcsA in PC nanodisks showed that the C-terminus has a pH dependent conformation, which this work supports in 9:1 DOPE-DOPS liposomes [52]. This suggests that the lipid milieu does not determine the C-terminal helix bundle dissociation at low pH. One suggested function of the C-terminus helix bundling is that the contacts made across monomers may aid the stabilization of the KcsA tetramer at neutral pH [32]. Those data were collected on a solution-NMR instrument, and found that resonances were too broad and the $T_2$ values too short to conduct 3D backbone

experiments. Here, we have demonstrated the ability to conduct 3D experiments in liposomes, and we might see significant increases in resolution and improvements in T2 relaxation by combining both nanodisks and and HR-MAS. The spinning speed would need to be judiciously selected to prevent sedimentation of the nanodisks, which would likely negate the faster rate of tumbling that nanodisks undergo compared to liposomes.

In studies presented in this thesis, the proteoliposomes are not expected by be rapidly tumbling. Instead, the protein diffusion through the lipid bilayer is the largest source of translational motion for the entire protein, and then individual domains such as the C-terminus, are likely to undergo further localized movement that can decrease anisotropic interactions. Lipid composition varies the rate at which lipids and proteins diffuse through the membrane surface. The lipid composition and the protein-to-lipid ratio could be tuned to produce more rapid diffusion and which might lead to improved relaxation and resolution characteristics. Lateral diffusion of lipid probes is inversely proportional to bilayer thickness [57]. Lipid hydration is very important in determining diffusion, with maximum diffusion rates occurring above 40 % water by mass [**Lindblom2009**]. Lipid acyl chain composition changes the diffusion rates, with DPPC (saturated lipid with 16 carbon chain), diffusing at more than two times the rate of DOPC (single cis-double bond per chain and 18 carbon chains) [**Oradd2005**]. Headgroup plays a dramatic role as well, with DOPG diffusing at twice the rate of DOPC [**bibid**]. Most of these studies named here are examining a lipid probe in a single component bilayer. The rate of protein diffusion is not only lipid dependent but

also protein dependent [57], and there is no good frame work, of which this author is aware, to predict the rate of diffusion of a particular protein in a mixture of lipids. So, in all likelihood a large lipid screen would need to be conducted to optimize the rate of diffusion of KcsA in the membrane. Even, then, it is not clear to what extent this would improve resolution and relaxation.

## 2.6 METHODS

### 2.6.1 *Protein Expression and Purification*

See Appendix A for more detailed information on constructs, protein expression, and purification. Brief notes and deviations from the methods described in Appendix A follow. The fully protonated KcsA data presented in this chapter is from protein that was uniformly $^{13}C$ and $^{15}N$ enriched by expressing KcsA in *Escherichia coli* JM83 cells. The JM83 cell line is a proline auxotrophic, so natural abundance proline was added to cultures.

Fractionally deuterated protein was produced as described in Section A.3

### 2.6.2 *KcsA Reconstitution*

Liposomes were formed from a fixed ratio of lipid by mass with a $9:1$ ratio of 1,2-dioleoyl-sn-glycero-3-phosphoethanolamine (DOPE) to 1,2-dioleoyl-sn-glycero-3-

phospho-L-serine (DOPS)), which were obtained as a chloroform solution (Avanti), dried as a thin film under $N_2$ gas, resolubilized in n-hexane (Sigma), dried again under $N_2$ gas and solubilized by bath sonication in 10 mM DM, 50 mM Tris, 100 mM KCl, pH 7.5. Lipids were mixed in mass ratio with KcsA of 1 : 1, diluted to 2 mM DM and dialyzed in 30 kDa MWCO tubing (Spectrum Chemical) with three exchanges of 4 L of buffer at 12–18 h intervals at room temperature. Proteoliposomes were harvested by centrifugation at 5700 RCF for 30 min and then stored at −80 °C. The presence of KcsA as a tetramer in the liposomes was verified by SDS-PAGE. Pellets were stored at −80 °C until ready for further experimentation.

### 2.6.3 *NMR*

J-coupled based experiments were performed on a Bruker magnet with a proton field of 750 MHz using a 4 mm high-resolution magic angle spinning probe (HR-MAS) with $^{1}H/^{13}C/^{15}N/^{2}H$ channels with a 40 G/cm gradient coil oriented along the magic angle. Experiments were generally performed between 4–5 kHz MAS and 308 K. Typical hard-pulses were 31kHz for $^{1}H$, 33 kHz for $^{13}C$, and 20kHz for $^{15}N$. Decoupling fields and spinlocks were typically 10 kHz. Heteronuclear decoupling was accomplished using WALTZ16 [61]. TOCSY spinlocks were full-rotor period synchronized; as failure to do so caused unpredictable spectral artifacts. HSQCs were phase sensitive [47] using double inept transfer, trim pulses (100 µs), with Echo/Antiecho-TPPI gradient selection [59] and decoupling during acquisition. Site specific $T_2$ measurements were

collected by adding a rotor-synchronized $^{13}C$ spin-echo between the two inept transfers and increasing the delay over at least five steps until magnetization had decayed to at least 90 %.

Cross polarization MAS was performed on either the Bruker 750 or a Bruker 900 on 3.2 mm $^{1}H/^{13}C/^{15}N$ e-free probes at 17 kHz and 19 kHz MAS, respectively and 275 K. Typical field strengths were 100 kHz for $^{1}H$ and 50 kHz for $^{13}C$. Acquisition times in the direct dimension were approximately 20 ms collected in 2048 points and indirect dimension were typically 4 ms in 128 points. All $^{13}C$-acquired data was zero-filled to 2× the number of points acquired and were multiplied by Lorentzian-to-Gaussian function with 10–40 Hz of line broadening and 0.3–0.01 Gaussian factors applied empirically in the direct dimension and indirect dimension data were multiplied by $sin^2$ function of pure $cosine$ phase.

Solution NMR was performed on a Bruker 500 Ascend instrument using a H/C/N (H) probe. Sample temperatures were 300 K. Typical field strengths were 18 kHz for $^{1}H$ and 8 kHz for $^{13}C$ for hard pulses, and 2 kHz for $^{13}C$ heteronuclear decoupling using WALTZ16. Homo-soil gradients were accomplished with 7.6 T $m^{-1}$ of 1 ms duration. HSQCs were phase sensitive and multiplicity edited using double inept transfer, trim pulses (1 ms), used shaped pulses for inversion on $^{13}C$ (500 µs) with Echo/Antiecho-TPPI gradient selection and decoupling during acquisition (Bruker sequence: hsqcedetgpsp.3). Direct dimensions were acquired for 50 ms in 2048 points and indirect dimensions were acquired for approximately 10 ms in 512 points. The 3D TOCSY data was acquired for 7.5 ms in 128 points in the $^{1}H$ dimension and the $^{13}C$

dimension acquired for 2.5 ms in 64 points. All proton acquired data was zero-filled to 2× the number of points, rounding up to the nearest perfect-square. FIDs and were multiplied by $sin^2$ function of pure cosine phase.

### 2.6.4 *KcsA Cleavage Preparation*

N-terminal His-tagged KcsA was expressed and purified as described in Appendix A. To cleave the C-terminus, 1 mg mL$^{-1}$ KcsA in 5 mM decyl-β-maltopyranoside (Anatrace) detergent (DM) was incubated with 20 µg mL$^{-1}$ of bovine α-chymotrypsin (Sigma) for 3 h at 35 °C. KcsA was isolated using His-Select nickle-affinity gel (Fisher), washing with five volumes of buffer 35 mM imidazole and eluting with two volumes of buffer containing 300 mM imidazole. An aliquot of the full-length construct and the post-reaction purified KcsA were analyzed by SDS-PAGE using a 4–12 % Bis-Tris mini gel (Thermo Fisher) at 200 V for 35 min. BLUeye protein ladder (Sigma) was used as a standard. The gel was then stained with PageBlue (Thermo Fisher) coomassie brilliant blue stain according to manufacturer direction. Individual bands were then cut from the gel and placed into new centrifuge tubes and delivered within two hours, on ice, to the proteomics core for mass spectrometry

The process was repeated using uniform isotopic enrichment protocol (Appendix A) for the NMR sample and incorporated into liposomes as described above.

[1] S. J. Alvis, I. M. Williamson, J. M. East, and A. G. Lee. "Interactions of Anionic Phospholipids and Phosphatidylethanolamine with the Potassium Channel KcsA." In: *Biophysical Journal* 85.6 (2003), pp. 3828–3838. DOI: 10.1016/S0006-3495(03)74797-3.

[2] K. A. Baker, C. Tzitzilonis, W. Kwiatkowski, S. Choe, and R. Riek. "Conformational dynamics of the KcsA potassium channel governs gating properties." In: *Nature Structural and Molecular Biology* 14.11 (2007), pp. 1089–1095. DOI: 10.1038/nsmb1311.

[3] T. H. Bayburt and S. G. Sligar. "Membrane protein assembly into Nanodiscs." In: *FEBS letters* 584.9 (2010), pp. 1721–7. DOI: 10.1016/j.febslet.2009.10.024.

[4] H. M. Berman. "The Protein Data Bank." In: *Nucleic Acids Research* 28.1 (Jan. 2000), pp. 235–242. DOI: 10.1093/nar/28.1.235.

[5] M. P. Bhate and A. E. McDermott. "Protonation state of E71 in KcsA and its role for channel collapse and inactivation." In: *Proceedings of the National Academy of Sciences of the United States of America* 109.38 (Sept. 2012), pp. 15265–70. DOI: 10.1073/pnas.1211900109.

[6] M. P. Bhate, B. J. Wylie, L. Tian, and A. E. McDermott. "Conformational dynamics in the selectivity filter of KcsA in response to potassium ion concentration." In: *Journal of molecular biology* 401.2 (Aug. 2010), pp. 155–66. DOI: 10.1016/j.jmb.2010.06.031.

[7] M. P. M. Bhate. "Mechanistic studies of ion binding and inactivation in the potassium channel KcsA by solid state NMR." PhD thesis. Columbia University, 2012. DOI: 10.7916/D8V12BWP.

[8] B. B. Bonev. *High-Resolution Solid-State NMR of Lipid Membranes*. 1st ed. Vol. 17. Copyright © 2013 Elsevier Inc. All rights reserved., 2013, pp. 299–329. DOI: 10.1016/B978-0-12-411516-3.00011-5.

[9] A. Cavalli, X. Salvatella, C. M. Dobson, and M. Vendruscolo. "Protein structure determination from NMR chemical shifts." In: *Proceedings of the National Academy of Sciences* 104.23 (2007), pp. 9615–9620. DOI: 10.1073/pnas.0610313104.

[10] S. Chakrapani, J. F. Cordero-Morales, and E. Perozo. "A Quantitative Description of KcsA Gating I: Macroscopic Currents." In: *The Journal of General Physiology* 130.5 (2007), pp. 465–478. DOI: 10.1085/jgp.200709843.

[11] J. H. Chill, J. M. Louis, C. Miller, and A. Bax. "NMR study of the tetrameric KcsA potassium channel in detergent micelles." In: *Protein science : a publication of the Protein Society* 15.4 (Apr. 2006), pp. 684–98. DOI: 10.1110/ps.051954706.

[12] J. Chill, J. Louis, J. Baber, and A. Bax. "Measurement of 15N relaxation in the detergent-solubilized tetrameric KcsA potassium channel." In: *Journal of Biomolecular NMR* 36.2 (Oct. 2006), pp. 123–136. DOI: 10.1007/s10858-006-9071-4.

[13] J. F. Cordero-Morales, L. G. Cuello, and E. Perozo. "Voltage-dependent gating at the KcsA selectivity filter." In: *Nature structural & molecular biology* 13.4 (Apr. 2006), pp. 319–22. DOI: 10.1038/nsmb1070.

[14] D. M. Cortes, L. G. Cuello, and E. Perozo. "Molecular Architecture of Full-Length KcsA." In: *The Journal of General Physiology* 117.2 (Feb. 2001), pp. 165–180. DOI: 10.1085/jgp.117.2.165.

[15] L. G. Cuello et al. "Structural basis for the coupling between activation and inactivation gates in K(+) channels." In: *Nature* 466.7303 (July 2010), pp. 272–5. DOI: 10.1038/nature09136.

[16] S. Das, U. D. Lengweiler, D. Seebach, and R. N. Reusch. "Proof for a nonproteinaceous calcium-selective channel in Escherichia coli by total synthesis from (R)-3-hydroxybutanoic acid and inorganic polyphosphate." In: *Proceedings of the National Academy of Sciences* 94.17 (1997), pp. 9075–9079. DOI: 10.1073/pnas.94.17.9075.

[17] S. Das, D. Seebach, and R. N. Reusch. "Differential effects of temperature on E. coli and synthetic polyhydroxybutyrate/polyphosphate channels." In: *Biochemistry* 41.16 (2002), pp. 5307–5312. DOI: 10.1021/bi025520g.

[18] F. Delaglio et al. "NMRPipe: A multidimensional spectral processing system based on UNIX pipes." In: *Journal of Biomolecular NMR* 6.3 (1995), pp. 277–293. DOI: 10.1007/BF00197809.

[19] J. M. Dörr et al. "Detergent-free isolation, characterization, and functional reconstitution of a tetrameric K+ channel: the power of native nanodiscs." In: *Proceedings of the National Academy of Sciences of the United States of America* 111.52 (Dec. 2014), pp. 18607–12. DOI: 10.1073/pnas.1416205112.

[20] D. A. Doyle et al. "The structure of the potassium channel: molecular basis of K+ conduction and selectivity." In: *Science (New York, N.Y.)* 280.5360 (Apr. 1998), pp. 69–77. DOI: 10.1126/science.280.5360.69.

[21] C. Fernández and G. Wider. "TROSY in NMR studies of the structure and function of large biological macromolecules." In: *Current Opinion in Structural Biology* 13.5 (2003), pp. 570–580. DOI: 10.1016/j.sbi.2003.09.009.

[22] K. J. Fritzsching, M. Hong, and K. Schmidt-Rohr. "Conformationally selective multidimensional chemical shift ranges in proteins from a PACSY database purged using intrinsic quality criteria." In: *Journal of Biomolecular NMR* 64.2 (Feb. 2016), pp. 115–130. DOI: 10.1007/s10858-016-0013-5.

[23] L. Gao, X. Mi, V. Paajanen, K. Wang, and Z. Fan. "Activation-coupled inactivation in the bacterial potassium channel KcsA." In: *Proceedings of the National Academy of Sciences of the United States of America* 102.49 (Dec. 2005), pp. 17630–5. DOI: 10.1073/pnas.0505158102.

[24] F. Hagn, M. Etzkorn, T. Raschle, and G. Wagner. "Optimized phospholipid bilayer nanodiscs facilitate high-resolution structure determination of membrane proteins." In: *Journal of the American Chemical Society* 135.5 (2013), pp. 1919–1925. DOI: 10.1021/ja310901f.

[25] L. Heginbotham, L. Kolmakova-Partensky, and C. Miller. "Functional Reconstitution of a Prokaryotic K + Channel." In: *The Journal of General Physiology* 111.6 (June 1998), pp. 741–749. DOI: 10.1085/jgp.111.6.741.

[26] M. Hirano, Y. Onishi, T. Yanagida, and T. Ide. "Role of the KcsA channel cytoplasmic domain in pH-dependent gating." In: *Biophysical Journal* 101.9 (2011), pp. 2157–2162. DOI: 10.1016/j.bpj.2011.09.024.

[27] S. Imai, M. Osawa, K. Takeuchi, and I. Shimada. "Structural basis underlying the dual gate properties of KcsA." In: *Proceedings of the National Academy of Sciences* 107.14 (2010), pp. 6216–6221. DOI: 10.1073/pnas.0911270107.

[28] S. Imai, M. Osawa, K. Takeuchi, and I. Shimada. "Structural basis underlying the dual gate properties of KcsA." In: *Proceedings of the National Academy of Sciences of the United States of America* 107.14 (Apr. 2010), pp. 6216–21. DOI: 10.1073/pnas.0911270107.

[29] M. Iwamoto and S. Oiki. "Amphipathic antenna of an inward rectifier K+ channel responds to changes in the inner membrane leaflet." In: *Proceedings of the National Academy of Sciences of the United States of America* 110.2 (Jan. 2013), pp. 749–54. DOI: 10.1073/pnas.1217323110.

[30] M. Iwamoto et al. "Surface structure and its dynamic rearrangements of the KcsA potassium channel upon gating and tetrabutylammonium blocking." In: *The Journal of biological chemistry* 281.38 (Sept. 2006), pp. 28379–86. DOI: 10.1074/jbc.M602018200.

[31] G. Kamnesky, H. Shaked, and J. H. Chill. "The Distal C-Terminal Region of the KcsA Potassium Channel Is a pH-Dependent Tetramerization Domain." In: *Journal of Molecular Biology* 418.3-4 (May 2012), pp. 237–247. DOI: 10.1016/j.jmb.2012.02.023.

[32] G. Kamnesky et al. “Molecular determinants of tetramerization in the KcsA cytoplasmic domain.” In: *Protein Science* 23.10 (2014), pp. 1403–1416. DOI: 10.1002/pro.2525.

[33] L. E. Kay et al. “Selective Methyl Group Protonation of Perdeuterated Proteins.” In: *Journal of Molecular Biology* 263.5 (2002), pp. 627–636. DOI: 10.1006/jmbi.1996.0603.

[34] D. M. Kim et al. “Conformational heterogeneity in closed and open states of the KcsA potassium channel in lipid bicelles.” In: *The Journal of General Physiology* 148.2 (Aug. 2016), pp. 119–132. DOI: 10.1085/jgp.201611602.

[35] M. M. C. Kuo, W. J. Haynes, S. H. Loukin, C. Kung, and Y. Saimi. “Prokaryotic K+ channels: From crystal structures to diversity.” In: *FEMS Microbiology Reviews* 29.5 (2005), pp. 961–985. DOI: 10.1016/j.femsre.2005.03.003.

[36] A. Lange et al. “Toxin-induced conformational changes in a potassium channel revealed by solid-state NMR.” In: *Nature* 440.7086 (Apr. 2006), pp. 959–962. DOI: 10.1038/nature04649.

[37] D. M. Lemaster. “Deuteration in of Proteins.” In: *Molecular Biology* 1957.60 (1990).

[38] S. H. Loukin et al. “Microbial K+ channels.” In: *Journal of General Physiology* 125.6 (2005), pp. 521–527. DOI: 10.1085/jgp.200509261.

[39] B. Lu, D. B. McClatchy, Y. K. Jin, and J. R. Yates. “Strategies for shotgun identification of integral membrane proteins by tandem mass spectrometry.” In: *Proteomics* 8.19 (2008), pp. 3947–3955. DOI: 10.1002/pmic.200800120.

[40] D. Mance et al. “An Efficient Labelling Approach to Harness Backbone and Side-Chain Protons in 1 H-Detected Solid-State NMR Spectroscopy.” In: *Angewandte Chemie* 127.52 (Dec. 2015), pp. 16025–16029. DOI: 10.1002/ange.201509170.

[41] P. Marius et al. “Binding of anionic lipids to at least three nonannular sites on the potassium channel KcsA is required for channel opening.” In: *Biophysical journal* 94.5 (Mar. 2008), pp. 1689–98. DOI: 10.1529/biophysj.107.117507.

[42] I. Maslennikov and S. Choe. “Advances in NMR structures of integral membrane proteins.” In: *Current opinion in structural biology* 23.4 (Aug. 2013), pp. 555–62. DOI: 10.1016/j.sbi.2013.05.002.

[43] R. Milkman. “oo VV4 P.” In: 91.April (1994), pp. 3510–3514.

[44] M. L. Molina et al. “Influence of C-terminal protein domains and protein-lipid interactions on tetramerization and stability of the potassium channel KcsA.” In: *Biochemistry* 43.47 (2004), pp. 14924–14931. DOI: 10.1021/bi048889+.

[45] M. L. Molina et al. "Competing lipid-protein and protein-protein interactions determine clustering and gating patterns in the potassium channel from streptomyces lividans (KcsA)." In: *Journal of Biological Chemistry* 290.42 (2015), pp. 25745–25755. DOI: 10.1074/jbc.M115.669598.

[46] A. Negoda, E. Negoda, and R. N. Reusch. "Importance of oligo-(R)-3-hydroxybutyrates to S. lividans KcsA channel structure and function." In: *Molecular BioSystems* 6.11 (2010), pp. 2249–2255. DOI: 10.1039/c0mb00092b.

[47] A. G. Palmer, J. Cavanagh, R. A. Byrd, and M. Rance. "Sensitivity improvement in three-dimensional heteronuclear correlation NMR spectroscopy." In: *Journal of Magnetic Resonance (1969)* 96.2 (1992), pp. 416–424. DOI: 10.1016/0022-2364(92)90097-Q.

[48] V. P. Pau, Y. Zhu, Z. Yuchi, Q. Q. Hoang, and D. S. Yang. "Characterization of the C-terminal domain of a potassium channel from Streptomyces lividans (KcsA)." In: *Journal of Biological Chemistry* 282.40 (2007), pp. 29163–29169. DOI: 10.1074/jbc.M703277200.

[49] E. Perozo, D. M. Cortes, and L. G. Cuello. "Structural rearrangements underlying K+-channel activation gating." en. In: *Science (New York, N.Y.)* 285.5424 (July 1999), pp. 73–8. DOI: 10.1126/science.285.5424.73.

[50] K. Pervushin, R. Riek, G. Wider, and K. Wüthrich. "Attenuated T2 relaxation by mutual cancellation of dipole–dipole coupling and chemical shift anisotropy.pdf." In: *Proceedings of the National Academy of Sciences of the United States of America* 94.November (1997), pp. 12366–12371.

[51] D. J. Posson, A. N. Thompson, J. G. McCoy, and C. M. Nimigean. "Molecular interactions involved in proton-dependent gating in KcsA potassium channels." In: *The Journal of general physiology* 142.6 (Dec. 2013), pp. 613–24. DOI: 10.1085/jgp.201311057.

[52] A. Qasim et al. "Investigation of a KcsA Cytoplasmic pH Gate in Lipoprotein Nanodiscs." In: *ChemBioChem* 20.6 (Mar. 2019), pp. 813–821. DOI: 10.1002/cbic.201800627.

[53] A. Qasim et al. "Investigation of a KcsA Cytoplasmic pH Gate in Lipoprotein Nanodiscs." In: *ChemBioChem* 52900 (2019), pp. 813–821. DOI: 10.1002/cbic.201800627.

[54] M. Raja. "The role of extramembranous cytoplasmic termini in assembly and stability of the tetrameric K(+)-channel KcsA." In: *The Journal of membrane biology* 235.1 (May 2010), pp. 51–61. DOI: 10.1007/s00232-010-9255-4.

[55] M. Raja. "The role of phosphatidic acid and cardiolipin in stability of the tetrameric assembly of potassium channel KcsA." In: *The Journal of membrane biology* 234.3 (Apr. 2010), pp. 235–40. DOI: 10.1007/s00232-010-9251-8.

[56] M. Raja, R. E. Spelbrink, B. de Kruijff, and J. A. Killian. "Phosphatidic acid plays a special role in stabilizing and folding of the tetrameric potassium channel KcsA." In: *FEBS Letters* 581.29 (2007), pp. 5715–5722. DOI: 10.1016/j.febslet.2007.11.039.

[57] S. Ramadurai, R. Duurkens, V. V. Krasnikov, and B. Poolman. "Lateral diffusion of membrane proteins: Consequences of hydrophobic mismatch and lipid composition." In: *Biophysical Journal* 99.5 (2010), pp. 1482–1489. DOI: 10.1016/j.bpj.2010.06.036.

[58] S. P. Rucker and A. J. Shaka. "Broadband homonuclear cross polarization in 2D N.M.R. using DIPSI-2." In: *Molecular Physics* 68.2 (1989), pp. 509–517. DOI: 10.1080/00268978900102331.

[59] J. Schleucher et al. "A general enhancement scheme in heteronuclear multidimensional NMR employing pulsed field gradients." In: *Journal of Biomolecular NMR* 4.2 (Mar. 1994), pp. 301–306. DOI: 10.1007/BF00175254.

[60] J. Seelig, P. M. MacDonald, and P. G. Scherer. "Phospholipid head groups as sensors of electric charge in membranes." In: *Biochemistry* 26.24 (Dec. 1987), pp. 7535–7541. DOI: 10.1021/bi00398a001.

[61] A. Shaka, J. Keeler, and R. Freeman. "Evaluation of a new broadband decoupling sequence: WALTZ-16." In: *Journal of Magnetic Resonance (1969)* 53.2 (June 1983), pp. 313–340. DOI: 10.1016/0022-2364(83)90035-5.

[62] R. T. Shealy, A. D. Murphy, R. Ramarathnam, E. Jakobsson, and S. Subramaniam. "Sequence-function analysis of the K + -selective family of ion channels using a comprehensive alignment and the KcsA channel structure." In: *Biophysical Journal* 84.5 (2003), pp. 2929–2942. DOI: 10.1016/S0006-3495(03)70020-4.

[63] A. Shekhtman, R. Ghose, M. Goger, and D. Cowburn. "NMR structure determination and investigation using a reduced proton (REDPRO) labeling strategy for proteins." In: *FEBS Letters* 524.1-3 (July 2002), pp. 177–182. DOI: 10.1016/S0014-5793(02)03051-X.

[64] Y. Shen, F. Delaglio, G. Cornilescu, and A. Bax. "TALOS+: a hybrid method for predicting protein backbone torsion angles from NMR chemical shifts." In: *Journal of Biomolecular NMR* 44.4 (Aug. 2009), pp. 213–223. DOI: 10.1007/s10858-009-9333-z. arXiv: NIHMS150003.

[65] K. Takeuchi, H. Arthanari, and G. Wagner. "Perspective: revisiting the field dependence of TROSY sensitivity." In: *Journal of Biomolecular NMR* 66.4 (Dec. 2016), pp. 221–225. DOI: 10.1007/s10858-016-0075-4.

[66] K. Takeuchi, H. Takahashi, S. Kawano, and I. Shimada. "Identification and characterization of the slowly exchanging pH-dependent conformational rearrangement in KcsA." en. In: *The Journal of biological chemistry* 282.20 (May 2007), pp. 15179–86. DOI: 10.1074/jbc.M608264200.

[67] A. N. Thompson, D. J. Posson, P. V. Parsa, and C. M. Nimigean. "Molecular mechanism of pH sensing in KcsA potassium channels." In: *Proceedings of the National Academy of Sciences* 105.19 (2008), pp. 6900–6905. DOI: 10.1073/pnas.0800873105.

[68] E. L. Ulrich et al. "BioMagResBank." In: *Nucleic Acids Research* 36.Database (Dec. 2007), pp. D402–D408. DOI: 10.1093/nar/gkm957.

[69] S. Uysal et al. "Crystal structure of full-length KcsA in its closed conformation." In: *Proceedings of the National Academy of Sciences* 106.16 (Apr. 2009), pp. 6644–6649. DOI: 10.1073/pnas.0810663106.

[70] F. I. Valiyaveetil, Y. Zhou, and R. MacKinnon. "Lipids in the structure, folding, and function of the KcsA K+ channel." In: *Biochemistry* 41.35 (2002), pp. 10771–10777. DOI: 10.1021/bi026215y.

[71] E. van den Brink-van der Laan, V. Chupin, J. A. Killian, and B. de Kruijff. "Stability of KcsA Tetramer Depends on Membrane Lateral Pressure †." In: *Biochemistry* 43.14 (Apr. 2004), pp. 4240–4250. DOI: 10.1021/bi036129d.

[72] M. Weingarth et al. "Quantitative Analysis of the Water Occupancy around the Selectivity Filter of a K + Channel in Different Gating Modes." In: *Journal of the American Chemical Society* 136.5 (Feb. 2014), pp. 2000–2007. DOI: 10.1021/ja411450y.

[73] B. J. Wylie, M. P. Bhate, and A. E. McDermott. "Transmembrane allosteric coupling of the gates in a potassium channel." In: *Proceedings of the National Academy of Sciences of the United States of America* 111.1 (Jan. 2014), pp. 185–90. DOI: 10.1073/pnas.1319577110.

[74] Y. Xu, M. P. Bhate, and A. E. McDermott. "Transmembrane allosteric energetics characterization for strong coupling between proton and potassium ion binding in the KcsA channel." In: *Proceedings of the National Academy of Sciences of the United States of America* 114.33 (Aug. 2017), pp. 8788–8793. DOI: 10.1073/pnas.1701330114.

[75] L. Yu et al. "Nuclear magnetic resonance structural studies of a potassium channel-charybdotoxin complex." In: *Biochemistry* 44.48 (2005), pp. 15834–15841. DOI: 10.1021/bi051656d.

[76] Z. Yuchi, V. P. Pau, and D. S. Yang. "GCN4 enhances the stability of the pore domain of potassium channel KcsA." In: *FEBS Journal* 275.24 (2008), pp. 6228–6236. DOI: 10.1111/j.1742-4658.2008.06747.x.

[77] E. Zakharian and R. N. Reusch. "Functional evidence for a supramolecular structure for the Streptomyces lividans potassium channel KcsA." In: *Biochemical and Biophysical Research Communications* 322.3 (2004), pp. 1059–1065. DOI: 10.1016/j.bbrc.2004.08.027.

[78] J. Zimmer, D. A. Doyle, and J. Günter Grossmann. "Structural characterization and pH-induced conformational transition of full-length KcsA." In: *Biophysical Journal* 90.5 (2006), pp. 1752–1766. DOI: 10.1529/biophysj.105.071175.

# INVESTIGATIONS OF LIPIDS CO-PURIFYING WITH KCSA 3

## 3.1 ABSTRACT

The inward rectifying potassium channel KcsA is regulated by the lipids in which it is embedded. This study shows that KcsA expressed in *E. coli* consistently co-purifies with lipids possessing a phosphoglycerol head group, supporting previous observations. When KcsA is isotopically enriched during over-expression in *E. coli*, we show that co-purifying lipids are also enriched. Degradation of proteoliposomes used in structural studies has not been well examined. We show here that fatty acid ester hydrolysis of model dioleoylglycerolethanolamine (DOPE)-dioleoylgycerophosphoserine (DOPS) liposomes approximates first-order kinetics with a rate constant of $0.03\,d^{-1}$, where the lipid head group shows no measurable hydrolysis. A subset of actual samples of KcsA-liposomes, however, are shown by HR-MAS NMR to experience extensive hydrolysis of lipid group within a matter of days. These data demonstrate the need for measurements of lipid stability as a matter of routine course for structural studies utilizing model phospholipids.

Membrane lipids have extensive structural and functional diversity, serving as structural components [49], signaling molecules [26], energy sources [32], and a host of other functions. The bilayer has a particularly important role in modulating membrane protein structure and function through both specific [38, 55], and non-specific interactions [58]. Lipids mediate insertion [25], folding [62], stabilization [30], and function of proteins [58] in the membrane.

Potassium channel KcsA is a homotetramer *in vivo*, and the lipid composition of the membrane is known to play an important role in stabilizing the KcsA tetramer [74, 76], in facilitating successful incorporation into the membrane [15, 57], and modulating channel function [31, 35].

As an ion channel, the function and structure of KcsA cannot be meaningfully separated from its membrane composition. Thus, the most relevant studies of ion channels in general and KcsA in particular are conducted of channel embedded in lipid bilayers. An understanding of the composition of such a bilayer is essential for results to be meaningfully interpreted. The following studies challenge the notion that synthetic phospholipid bilayers used for structural studies are well-defined and unreactive. Instead we find that the lipid composition is augmented by the presence of co-purifying lipids and is subject to reactions that change the chemical composition over time.

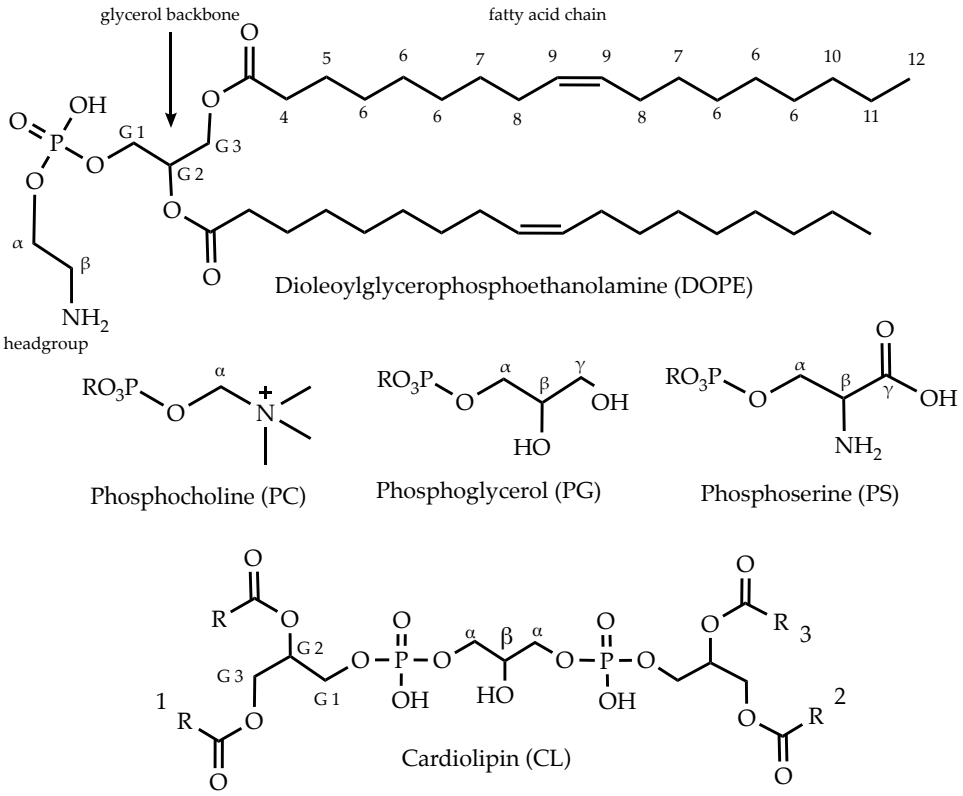


FIGURE 3.1: Anatomy of phospholipids with three head groups relevant to these studies and indicating the nomenclature used throughout this thesis. Atoms with duplicate numbers (e.g. 6), are degenerate in NMR spectra

### 3.2.1 *Lipids, Bound and Unbound*

Membrane-protein interactions with lipids fall into two major categories: transient interactions with bulk lipids and persistent interactions with bound lipids. The membrane surrounds a membrane protein with a complex, ever-changing mixture of lipids. Some protein lipid interactions are characterized by one or more lipids binding non-covalently to a membrane protein. In the Protein Data Bank (PDB) [4], there are more than 100 membrane protein structures that also resolve bound lipids, supporting the growing consensus that specific lipid binding interactions are typical for membrane proteins *in vivo*. See [28, 80] for reviews on this topic.

Structural understanding of KcsA is better than any other membrane channel with both the first crystal structure of an ion channel [20], as well as more structures published than any other channel. An early crystal structure of KcsA revealed an electron density that resolved as a non-covalently bound diacyl chain situated between each pair of monomers of KcsA channels (Figure 3.2) [85], and it was assumed that this density corresponded to a co-purifying lipid. To date, more than 20 structures of KcsA have been published containing similar diacyl densities (Section 3.7 provides an exhaustive list of KcsA crystal structures containing putative lipid signals). Using thin layer chromatography, Valiyaveetil, Zhou, and MacKinnon found phopsphotidylglycerol (PG), a negatively charged head group, was present in KcsA samples purified from *E. coli* [74] by nickel chromatography, leading to the conclusion that the diacyl chain was likely from a lipid molecule with a PG head group, finding that PG was present in a $0.7 : 1$ molar ratio with KcsA. Although the diacyl chain is captured in more than two dozen KcsA crystal structures, electron densities corresponding to the head group are not resolved. This is generally interpreted as the head group having a high degree of conformational heterogeneity or undergoing rapid conformational exchange within the crystal. Either case would suggest that the lipid head group is not engaging in long-lived, persistent interactions KcsA.

The lipids revealed by crystallography are located close in space to two tryptophan residues, W67 and W68 [45]. Exploiting this feature, Marius et al. used tryptophan florescence quenching and electrophysiological measurements to established a binding constant of $0.42 \pm 0.06$ moles of PG to moles of KcsA, and that the fraction of

dioleoylglycerolphosphoglycerol (DOPG) in dioleoylglycerolphosphocholine (DOPC) membranes increased channel open probability from 0 % (0 % PG) to 60 % (100 % PG). Since the PG (opposed to some other head group) is consistently observed with KcsA the identify of the head group binding is important. In particular R89 has been implicated as a hydrogen binding partner for one of the hydroxyl groups of the glycerol head group [20, 72, 74].

In order to establish the molecular determinants of KcsA-lipid affinity, Deol et al. used the first PDB structure of KcsA that includes diacyl chain (PDB 1K4C), to perform a set molecular dynamics simulations of KcsA in PC membranes with a fraction of either PA, PE, or PG lipids included as well. All three sets of trials found lipids bind at protein subunit interfaces and that the head group and phosphate moieties participate in hydrogen bonding with R64 of one subunit and R89 of the adjacent subunit (Figure 3.2) [18]. [44] established through mutagenesis of R64 and R89 and observing changes to electrophysiology signal and $^{31}$P–NMR lineshape that removing the positive charge from those residues acts synergisticly to reduce channel open probability and to reduce the extent to which membrane PG is bound (as measured by $^{31}$P shift change).

From these various data a model emerges where a lipid with a negatively charged head group sits between pairs of KcsA subunits, and this interactions specifically stabilizes the tetramer against dissociation, and plays a role in allowing the channel to active at low pH. Neither the molecular dynamics simulation nor the crystallography establishes how the channel is sensing the head group of the lipid. The coordination

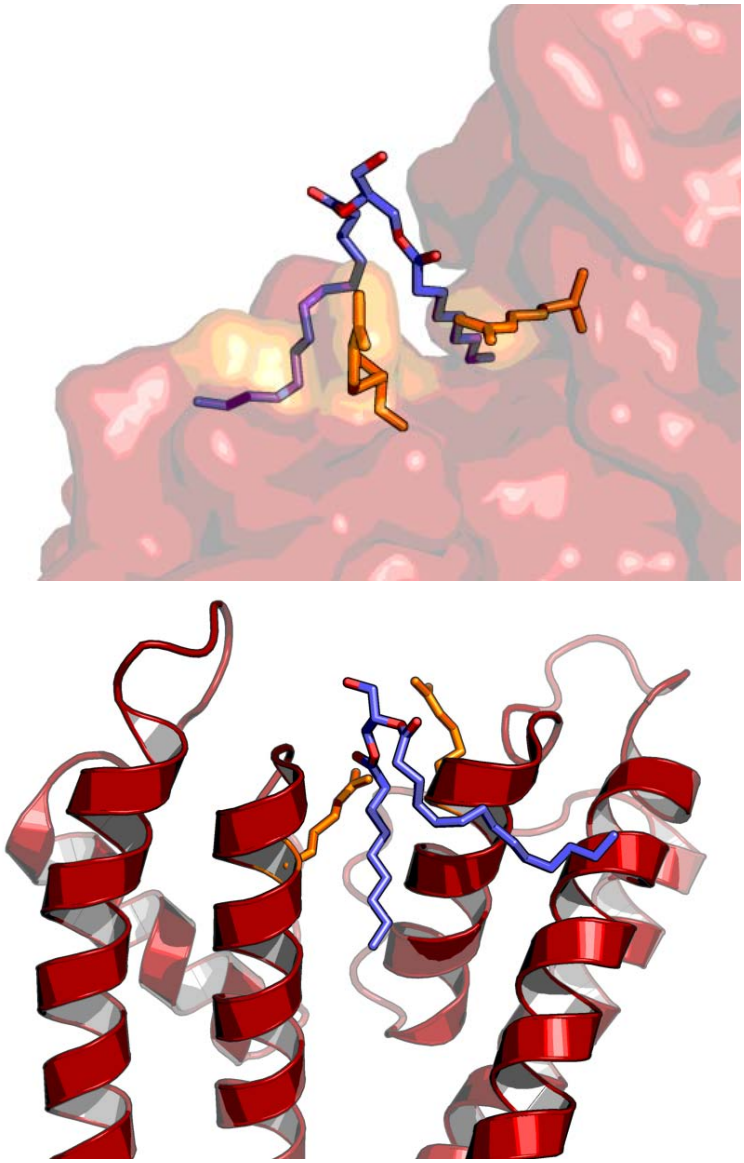

FIGURE 3.2: Two views of KcsA crystal structure (PDB: 1K4C[85] showing diacylglycerol small molecule between two subunits (two hidden for clarity) with R64 and R89 highlighted.

| PC/PG(1 : 1) | PC/PG(5 : 1) | PC/PA(1 : 1) | PE/PG(1 : 1) | PE/PA(1 : 1) | PC/PE(1 : 1) |
|---|---|---|---|---|---|
| 1 : 100 | 2 : 3 | 1 : 100 | 1 : 9 | 1 : 1 | 3 : 7 |

TABLE 3.1: Ratio of lipids co-detected with KcsA from binary mixtures as analyzed by ESI-MS from Demmers et al.[17], demonstrating KcsA has high preference for binding to lipids with negatively charged headgroups

of the lipid by R64 and R89 (Figure 3.2) suggests those residues are involved with hydrogen bonding with the carboxyl group of the fatty-acid ester of the side chain and potentially the headgroup as well.

### 3.2.2 *KcsA Lipid Affinity*

As suggested above, KcsA has affinity for specific lipids. In order to determine the affinity that KcsA has for various lipid head groups Demmers et al. reconstituted KcsA into binary lipid mixtures and used mass spectrometry to establish which lipids are co-detected following electrospray [17]. The results of that experiment are summarized in Table 3.1. The study reveals a portrait of KcsA maintaining a high affinity for the net-negatively charged lipids (PA, PE, and PG), with PG affinity being highest of all.

Some observations suggest that individual KcsA channels affect the concentration lipid head group types in their vicinity *in vivo*. For example, SMALPS (styrene maleic acid lipid polymer system)[36, 39] is a method of adding a short styrene maleic acid copolymer to lysed cells to form protein-lipid nanodisks. The SMA polymer than acts as a detergent and amphipathic belt to effectively excise portions of a cell membrane

into lipid nanodisks, capturing the native lipids and any embedded proteins. His-tagged proteins, for example, can then be purified by affinity chromatography to obtain a membrane protein in a "native"-lipid nanodisk. Dörr et al. [19] used the SMALPS system to isolate over-expressed KcsA from the *E. coli* membrane. Using mass spectrometry, that study showed the purified nanodisks were enriched in both PG and cardiolipin (CL) (a minor component of *E. coli* membrane), lipids as compared with the total membrane lipid composition. The enrichment of the local environment of KcsA with CL is interesting in the light that CL increases the open-probability of the channel [27]. Using tryptophan fluorescence quenching, Alvis et al. [2] proposed a two-site model where diacyl-lipids (particularly DOPG) have a high affinity for one site, and cardiolipin has a high affinity for the second site, and whose selectivity is mutually exclusive.

These biophysical studies operate on the assumption that the lipid membrane of the model systems is well-defined and does not change over the course of an experiment. These following studies question the validity of the assumption that the synthetic phospholipid membrane environment is well defined and chemically inert.

## 3.3 RESULTS

Extensive progress on KcsA has been made by the McDermott group using KcsA embedded into 9 : 1 DOPE-DOPS lipids in a 1 : 1 protein-lipid mass ratio (LPR=1) [5–7, 68, 78, 79]. Samples are prepared by over-expressing KcsA in *E. coli*, purifying by

affinity chromatography, and reconstituting the protein with synthetic phospholipids in detergent and dialyzing against a given buffer. The samples are packed into MAS rotors as a hydrated pellet.

To analyze lipid composition of these pellets, high-resolution magic angle spinning NMR (HR-MAS) was applied at 308 K. HR-MAS allows for $^{1}H$ detection of relatively isotropic components of heterogeneous or solid-like samples. Magic angle spinning speeds used for HR-MAS ($\leqslant$10 kHz) has a limited ability to attenuate strong dipolar couplings of static or very slow-tumbling molecules, but it can reduce remaining anisotropic interactions of small molecules in solids [69], and improves $B_0$ and $B_1$ field homogeneity [10]. HR-MAS is able to utilize solution-like pulse sequences and exploit the high gamma and high natural abundance of $^{1}H$ spins while resolving small molecule and fast moving macromolecule resonances into relatively sharp lines. For these reasons, HR-MAS is particularly well adept for studying the lipids in a membrane environment above the lipid crystalline melting point.

The HR-MAS $^{1}H$-$^{13}C$ HSQC of uniformly (U) enriched $^{1}H$, $^{13}C$, $^{15}N$-KcsA in natural abundance liposomes is able to resolve nearly every site of the synthetic phospholipids into which KcsA is reconstituted with the exception of some degenerate $CH_2$ groups. Since the spectra contain signal from relatively fast-relaxing, $^{13}C$ enriched protein, a $T_2$ filtered $^{1}H$-$^{13}C$ HSQC were also aquired (see Figure C.4 for pulse program). Assignments were made based on literature values of lipid shifts [23, 67], and using solution spectra of lipid-standards. The lipid chemical shifts are summarized in Table 3.2.

| Peak | $^{1}H$ | (ppm) | $^{13}C$ | (ppm) |
|---|---|---|---|---|
| F.A. 12 ($\omega$) | 0.88 | $\pm$0.018 | 16.6 | $\pm$0.12 |
| F.A. 11 ($\omega - 1$) | 1.3 | $\pm$0.017 | 25.3 | $\pm$0.06 |
| F.A. 8 ($\underline{CH_2}$–HC=C) | 2.02 | $\pm$0.038 | 29.9 | $\pm$0.19 |
| F.A. 6 ($CH_2$) | 1.29 | $\pm$0.022 | 32.1 | $\pm$0.1 |
| F.A. 10 ($\omega - 2$) | 1.27 | $\pm$0.02 | 34.6 | $\pm$0.08 |
| F.A. 4 ($\alpha$-$CH_2$) | 2.33 | $\pm$0.033 | 36.6 | $\pm$0.24 |
| PE $\beta$ | 3.24 | $\pm$0.037 | 43.3 | $\pm$0.37 |
| PE $\alpha$ | 4.11 | $\pm$0.027 | 64.6 | $\pm$0.48 |
| PG $\gamma$ + glycerol a | 3.67 | $\pm$0.025 | 65.4 | $\pm$0.1 |
| PG $\gamma$ + glycerol b | 3.61 | $\pm$0.044 | 65.4 | $\pm$0.09 |
| G3 a | 4.23 | $\pm$0.028 | 67 | $\pm$2.2 |
| G3 b | 4.46 | $\pm$0.027 | 67 | $\pm$2.3 |
| G1 | 4.3 | $\pm$0.23 | 67.5 | $\pm$3.4 |
| PG $\alpha$ a | 3.94 | $\pm$0.022 | 70 | $\pm$1.8 |
| PG $\alpha$ b | 3.88 | $\pm$0.025 | 70 | $\pm$1.8 |
| PG $\beta$ | 3.93 | $\pm$0.028 | 72 | $\pm$2.2 |
| G2 | 5.26 | $\pm$0.012 | 73.3 | $\pm$0.15 |
| glycerol ($CH_1$) | 3.83 | $\pm$0.035 | 74 | $\pm$2.4 |
| F.A. 9 (HC=C) | 5.31 | $\pm$0.027 | 132.2 | $\pm$0.12 |
| Mystery (HC=C) | 5.09 | $\pm$0.026 | 127 | $\pm$0.1 |

TABLE 3.2: Lipid chemical shifts

Average $^{1}H$–$^{13}C$ HSQC lipid and related chemical shifts of KcsA proteoliposome (9 : 1 DOPE-DOPS) samples by HR-MAS with standard error given from samples described in Table 3.4.

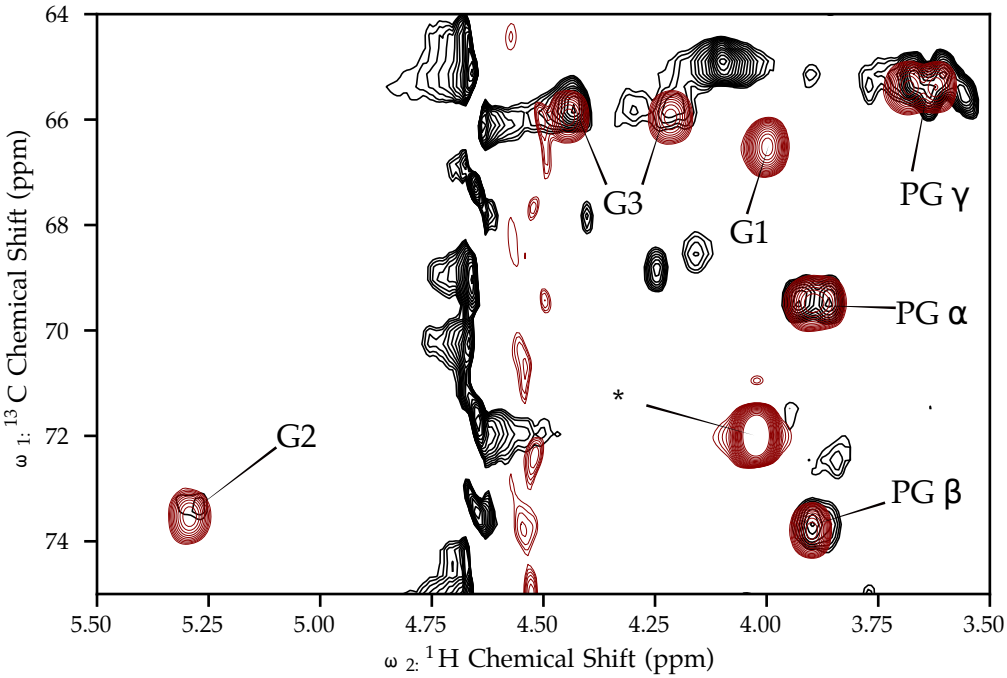


FIGURE 3.3: Head group and glycerol backbone region from $^{1}$H-$^{13}$C HSQC data of U-$^{13}$C, $^{15}$N-KcsA in 9:1 DOPE-DOPS proteoliposomes by HR-MAS (black) and DOPG liposomes by solution NMR (red), showing the PG signal is present in KcsA proteoliposome samples. HR-MAS spectrum collected at 5 kHz MAS, 308 K and solution spectrum collected at 325 K. Contaminant (likely 4-dioxane) indicated by '*'.

### 3.3.1 *KcsA Co-Purifies with Phosphoglycerol Lipid*

There are a set of resonances consistent with the synthetic phospholipids into which KcsA is reconstituted. There are an additional set of resonances consistent with PG that are immediately obvious, having characteristic chemical shifts that are distinct from protein shifts or those of DOPE and DOPS. The chemical shifts of the glycerol head group moiety in KcsA proteoliposome spectra by HR-MAS agree with the shifts collected of DOPG in detergent by solution NMR (Figure 3.3 A). The HcCH-TOCSY 3D correlation, which established through-bond $^{1}$H-$^{13}$C-$^{1}$H spin networks (Figure 3.4),

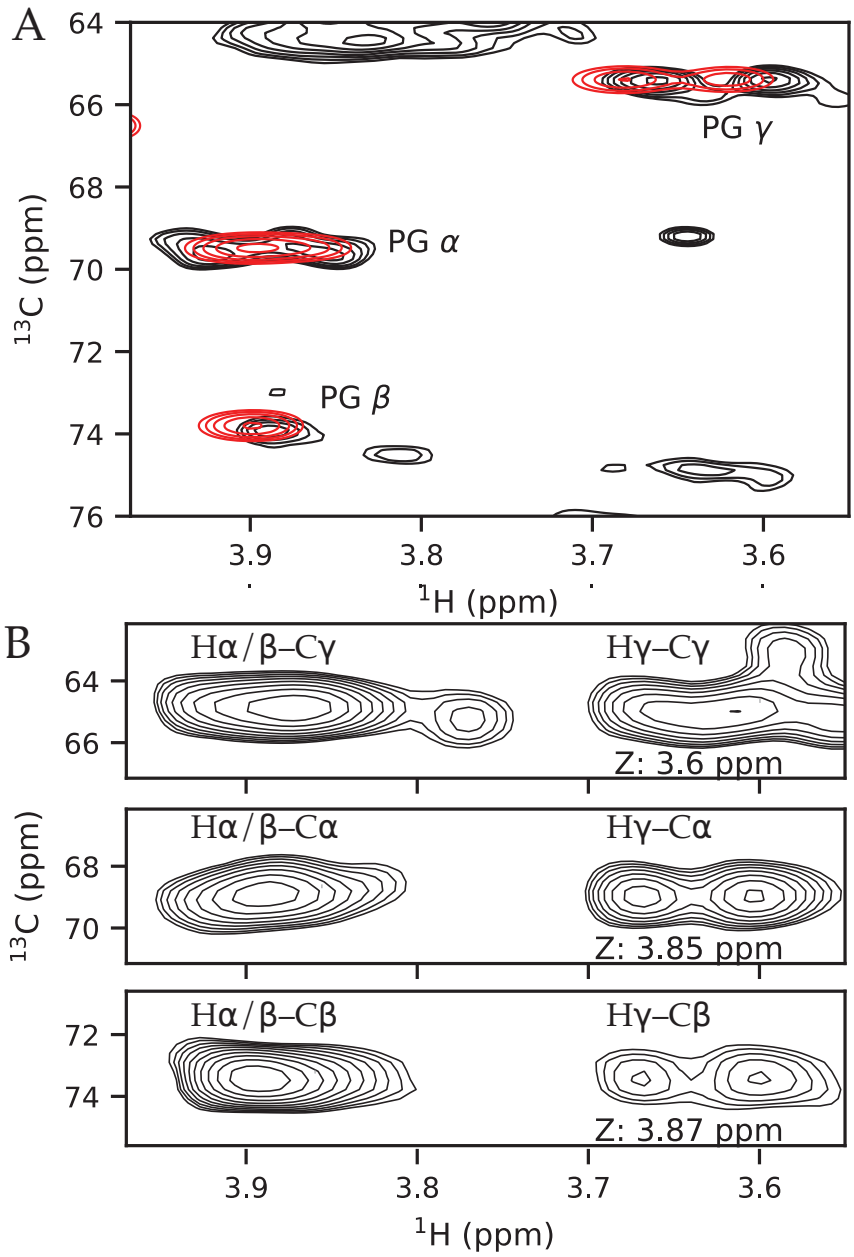


FIGURE 3.4: $^{1}$H-$^{13}$C HSQC by HR-MAS of PG in KcsA liposomes (black) and DOPG in SDS detergent by solution NMR (red) (A), strip plots of HcCH-TOCSY 3D correlation of PG connectivity in KcsA liposomes (B).

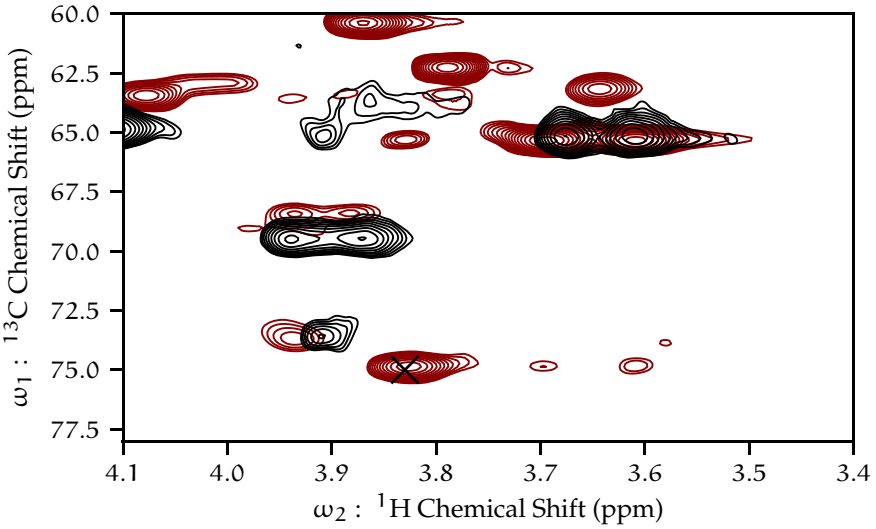


FIGURE 3.5: Overlay of HSQC of two KcsA proteoliposome: one with no degredation of PG at pH 7.25 (black), one with free glycerol and pH 6.3(red). Free glycerol resonance marked. Both samples in 9 : 1 DOPE-DOPS.

establishing the resonances are structurally connected. In the $^{1}$H-$^{13}$C HSQC of PG in detergent (Figure 3.3) the most intense peak is from a resonance that is not part of a larger spin network as determined by the TOCSY-HSQC experiment, suggesting a very simple molecule. The shift is consistent with 4-dioxane which is frequently used a chloroform stabilizer. The DOPG used in this experiment was obtained from the vendor in a chloroform, dried over nitrogen and hydrated in buffer.

The presence of PG in samples in summarized in Table 3.3, and sample details in Table 3.4. The presence of PG was detected in every KcsA sample examined by HR-MAS with the exception of a recombinant KcsA sample with a C-terminal deletion, KcsA- 126. Some of the samples also display the presence of a strong signal from free glycerol. Figure 3.5 compares two samples of KcsA reconstituted into 9 : 1 DOPE-DOPS, differing only in pH (7.25 versus 6.5), one of which shows the five PG

resonances, the other sample shows an additional resonance which arises from glycerol H-Cβ position as confirmed by the hCCH-TOCSY experiment (Figure 3.9a).

Four samples reveal the presence of two resonances in the alkene region $^{1}$H-$^{13}$C HSQC data. One resonance (5.31 ppm-132 ppm) conforms to the shifts for the C-C double bond of singly unsaturated oleic fatty acid (18:1 cis-9) of DOPE/DOPS into which KcsA is reconstituted. There exists a second, unexpected shift (5.09 ppm-127 ppm) which is also a CH group as determined by multiplicity editing, that suggests a second, different alkene species is present in the data. Although more than 30 crystal structures of KcsA reveal the presence of a diacyl chain corresponding to a lipid (Section 3.7), the high B-factor of lipid signal [42] in those structures, does not allow for the acyl chain to be well characterized in terms of bond saturation. The unidentified alkene resonance is compatible with several different lipids. Notably, since there is only one resonance besides the double bond from oleoyl fatty fatty, it suggest a mono-unsaturated fatty acid, as multiple unsaturated acids tend to have several non-equivalent shifts for double-bonded carbons and their respective protons [1]. This leaves the most likely candidate for the unassigned resonances as arising from a $\omega - 3$ position of a fatty acid which typically have resonance at 5.1 ppm- 127 ppm. However, the chemical shift analysis is not enough to definitely assign the lipid as previous work characterizes the shifts of lipid dissolved in organic solvents, whereas here, a mixture of lipids formed into liposomes, we would expect perturbations arising from the interactions with other lipids or KcsA.

| ID | Protein | Lipid | pH | PG α<br>$^{1}$H (ppm) / $^{13}$C (ppm) | PG β | PG γ & Glycerol $CH_2$† | Glycerol CH | HC=C | PE-β (%) | EA-β (%) | PG-β (%) | gly-β (%) |
|---|---|---|---|---|---|---|---|---|---|---|---|---|
| A | (empty) | PE/PS | 7.3 | – | – | – | – | – | 100 | 0 | 0 | 0 |
| B | KcsA | PE/PS | 7.3 | 3.94/73.7 ; 3.88/68.4 | 3.94/68.5 | 3.69/65.4 ; 3.61/65.4 | 3.83/74.9 | 5.1/126.9 | 42 | 57 | 21 | 79 |
| D | KcsA | PE/PS | 6.3 | 3.92/69.4 ; 3.86/69.4 | 3.89/73.7 | 3.63/65.4 ; 3.61/65.3 | – | 5.09/127.1 | 100 | 0 | 100 | 0 |
| E | KcsA | PE/PS | 4 | 3.92/69.6 ; 3.85 / 69.6 | 3.89/73.8 | 3.66/65.2 ; 3.6/65.2 | – | – | 100 | 0 | 100 | 0 |
| F | $^{2}$H KcsA | PE/PS | 6.3 | – | – | 3.64/65.5 ; 3.55/65.5 | – | – | 100 | 0 | 100 | 0 |
| G | $^{2}$H KcsA | PE/PS | 4 | – | 3.95/73.6 | 3.71/65.4 | 3.8/74.5 | – | 26 | 74 | 27 | 73 |
| H | KcsA–ΔC | PE/PS | 7.3 | – | – | – | – | – | 100 | 0 | 0 | 0 |
| I | KcsA | PE/PS | 7.3 | 3.94/69.1 ; 3.89/69.1 | 3.93/73.5 | 3.67/65.4 ; 3.58/65.4 | o | – | 100 | 0 | – | – |
| J | KcsA | PE/PS | 7.3 | 3.95/69.4 ; 3.88/69.3 | 3.92/73.6 | o | o | – | 100 | 0 | – | – |
| K | KcsA | PE/PS | 7.3 | o | o | 3.66/65.4 ; 3.57/65.4 | o | – | 85 | 15 | – | – |
| L | KcsA | PE/PS | 6.3 | 3.98/69.3 ; 3.91/69.3 | 3.96/73.6 | 3.7/65.5 ; 3.61/65.4 | o | 5.11/126.9 | 100 | 0 | – | – |
| M | KcsA | PC | 4 | 3.92/73.8 | 3.96/69.5 | 3.7/65.3 ; 3.63/65.3 | – | 5.05/127 | 0 | 0 | 100 | 0 |

Table 3.3: $^{1}$H-$^{13}$C–HSQC chemical shifts of exogenous lipid signals in KcsA liposome samples by HR-MAS. "–" indicates no detected signal for given peak and "o" indicates the presence of grossly overlapping peaks in peak region. HC=C indicates shift of unknown alkene. Final four columns show relative ratio of PG to free glycerol (gly) and relative ratio of PE to free ethanolamine (EA) as measured by relative $^{1}$H-$^{13}$Cβ HSQC peak intensity. †: glycerol $CH_2$ is degenerate with PG γ signal, "–" indicates overlapping peak prevented quantification. All samples reconstituted in natural abundance phospholipids with dioleoyl fatty acids chains with lipid-to-protein ratio of 1 (w/w), 308 K, 5 kHz MAS, internally referenced to DSS, see Table 3.4 for more details.

| ID | Protein | Labeling | Lipid | pH | Sucrose (% w/w) | Buffer | $K^+$ (mM) | $Mg^{2+}$ (mM) | $D_2O$ (% vol.) |
|---|---|---|---|---|---|---|---|---|---|
| A | no protein | U-$C^{13}N^{15}$ | DOPE/DOPS | 7.3 | 0 | tris | 50 | 0 | 15 |
| B | KcsA | U-$C^{13}N^{15}$ | DOPE/DOPS | 7.3 | 0 | tris | 50 | 0 | ~ 90 |
| D | KcsA | U-$C^{13}N^{15}$ | DOPE/DOPS | 6.3 | 0 | pipes | 50 | 0 | 10 |
| E | KcsA | U-$C^{13}N^{15}$ | DOPE/DOPS | 4 | 0 | citrate | 50 | 0 | 10 |
| F | KcsA | F–$^2$H U-$C^{13}N^{15}$ | DOPE/DOPS | 6.3 | 0 | pipes | 50 | 0 | 7 |
| G | KcsA | F–$^2$H U-$C^{13}N^{15}$ | DOPE/DOPS | 4 | 0 | citrate | 50 | 0 | 7 |
| H | KcsA–$\Delta$C | U-$C^{13}N^{15}$ | DOPE/DOPS | 7.3 | 0 | tris | 50 | 0 | ~ 90 |
| I | KcsA | U-$C^{13}N^{15}$ | DOPE/DOPS | 7.3 | 38 | tris | 50 | 2 | 10 |
| J | KcsA | U-$C^{13}N^{15}$ | DOPE/DOPS | 7.3 | 42 | tris | 50 | 0 | 10 |
| K | KcsA | U-$C^{13}N^{15}$ | DOPE/DOPS | 7.3 | 44 | tris | 50 | 2 | 10 |
| L | KcsA | U-$C^{13}N^{15}$ | DOPE/DOPS | 6.3 | 45 | tris | 50 | 0 | 10 |
| M | KcsA | U-$C^{13}N^{15}$ | DOPC | 4 | 0 | citrate | 150 | 0 | ~ 20 |

Table 3.4: Description of various samples used in HR-MAS samples, providing details for Table 3.3

### 3.3.2 *Lipid Degradation in Model Liposomes*

In addition to serving as a convenient experimental model, liposomes are of major interest as vehicles for drug delivery. Lipids in liposomes undergo various chemical reactions over days and weeks, such as hydrolysis of the fatty acids and head groups, oxidation of double bonds, and any number of enzymatic reactions. Hydrolysis of the fatty acid ester of phosphocholine occurs on the hours time scales under certain conditions (e.g. $\approx$70 °C at greater than pH 9 or less than pH 4 [22]), first forming lyso-PC (with the fatty acid at the G2 position hydrolysing) followed by the formation of free phosphocholine (2-(trimethylammonio)ethyl hydrogen phosphate). Hydrolysis of the head group from the phosphate moiety can also occur [34]. Free fatty-acids and lyso-lipids destabilize bilayer structure, dramatically altering the bulk properties of liposomes [87], and can even form micellar structures under certain conditions [21].

To study the effects of hydrolysis on the most common lipid system our group employs for the study of KcsA (9 : 1 DOPE-DOPS), we prepared 50 mg of liposomes by detergent dialysis in 1 mL of 50 mM Tris, 50 mM KCl, pH 7.25, 0.02 % (w/v) sodium azide and left it to sit on the bench for two months, taking eight aliquots, then extracted the lipids into deuterated chloroform according to Bligh and Dyer [8] and analyzed by NMR for chemical changes. Over 65 day, several notable changes in the spectra occurred (Figure 3.7) in particular shift of the G2 and G3 protons as the lipids undergo hydrolysis. Also the first methylene ($\alpha$-position or FA 4 by Figure 3.1) of the fatty acid chain shifts from a multiplet to a triplet as it undergoes hydrolysis (Fig-

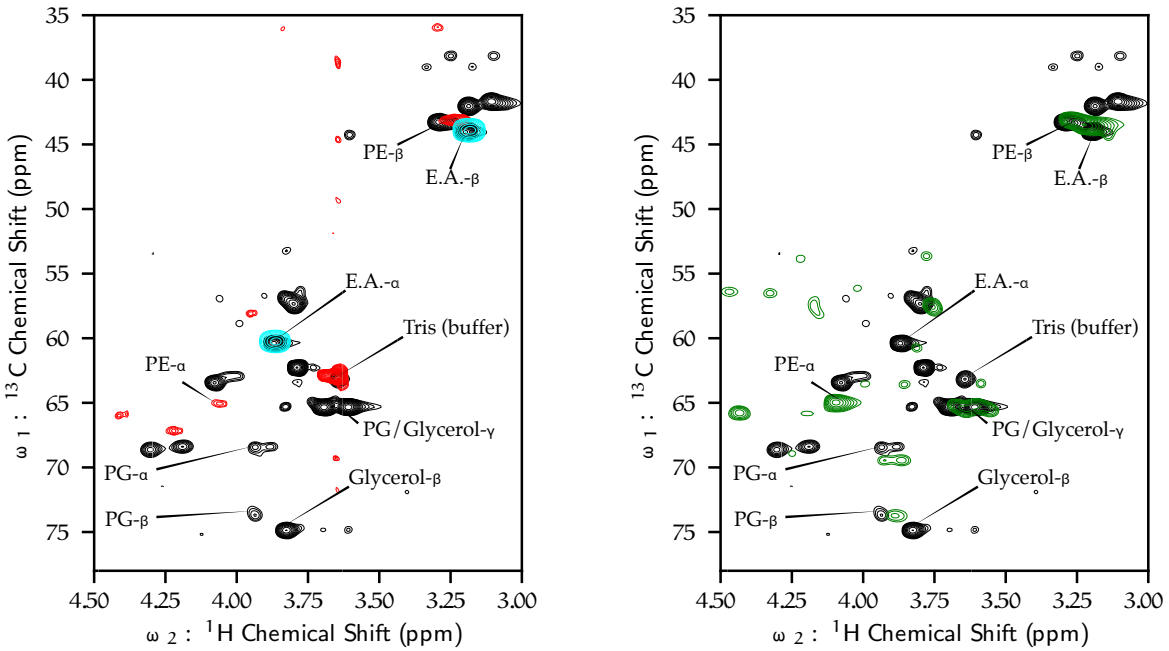


(A) Overlay $^{1}$H-$^{13}$C HSQC of KcsA in 9 : 1 DOPE-DOPS liposomes (black) is shown to contain ethanolamine and PE signal. 9 : 1 DOPE-DOPS liposomes (red), ethanolamine (data from [64]) (cyan) are shown for comparison.

(B) Overlay $^{1}$H-$^{13}$C HSQC of two KcsA samples with different degredation patterns: both contain PG and glycerol, one contains E.A. as well. Both samples reconsituted into 9 : 1 DOPE-DOPS in Tris Buffer

FIGURE 3.6: Degradation of lipid head groups in $^{1}$H-$^{13}$C HSQC.

ure 3.7) and thus serves as a convenient set of shifts to track the total hydrolysis of the fatty acid ester to free fatty acid. Modeling the decay using a monoexpoential decay function, the rate constant for the hydrolysis reaction at these conditions is found to be 0.03 $d^{-1}$ (Figure 3.8). There is no detectable hydrolysis of the PE head group over this same period as shown by the HSQC where no new peaks emerge nor does the intensity of the head group decrease. The PS-α resonance is degenerate in shift with the PE-α. Also, as a minority species (10 %) PS it is likely below the signal-to-noise limit in these spectra. The fatty acid ester multiplet shifts slightly as time progresses, likely reflecting the difference from hydrolysis of a neighboring fatty acid. The shift of

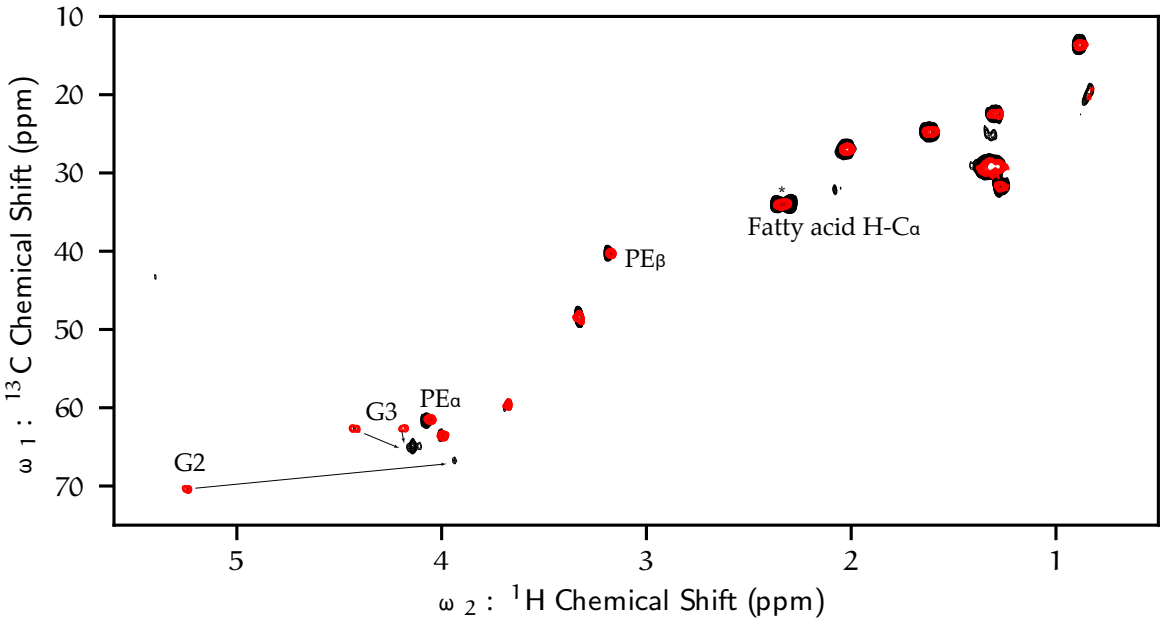


FIGURE 3.7: Effects on chemical shifts of hydrolysis of liposomes. Superimposed $^{1}H$–$^{13}C$ HSQC of 9 : 1 DOPE-DOPS liposomes extracted after 3 d incubating on the bench (black) and 65 d of incubating on the bench (red) with shifts indicated as determined by COSY, TOCSY, and multiplicity edited experiments (not shown). 300 K in $CDCL_3$.

both the G2 and G3 resonances support a model in which both fatty acid groups undergo hydrolysis simultaneously. There is not enough resolution in the time sampling to justify a multiple-exponential decay which might elucidate the individual rates for each of the fatty acid chains.

### 3.3.3 *Degradation of Lipids in Samples*

Solid-state NMR samples routinely spend a week or more in the probe. Although the set temperature is typically around 260 K, work in our group has established friction from magic angle spinning and radiofrequency radiation both elevate temperature by 20 K or more for short periods of time [83]. To investigate if any significant degradation

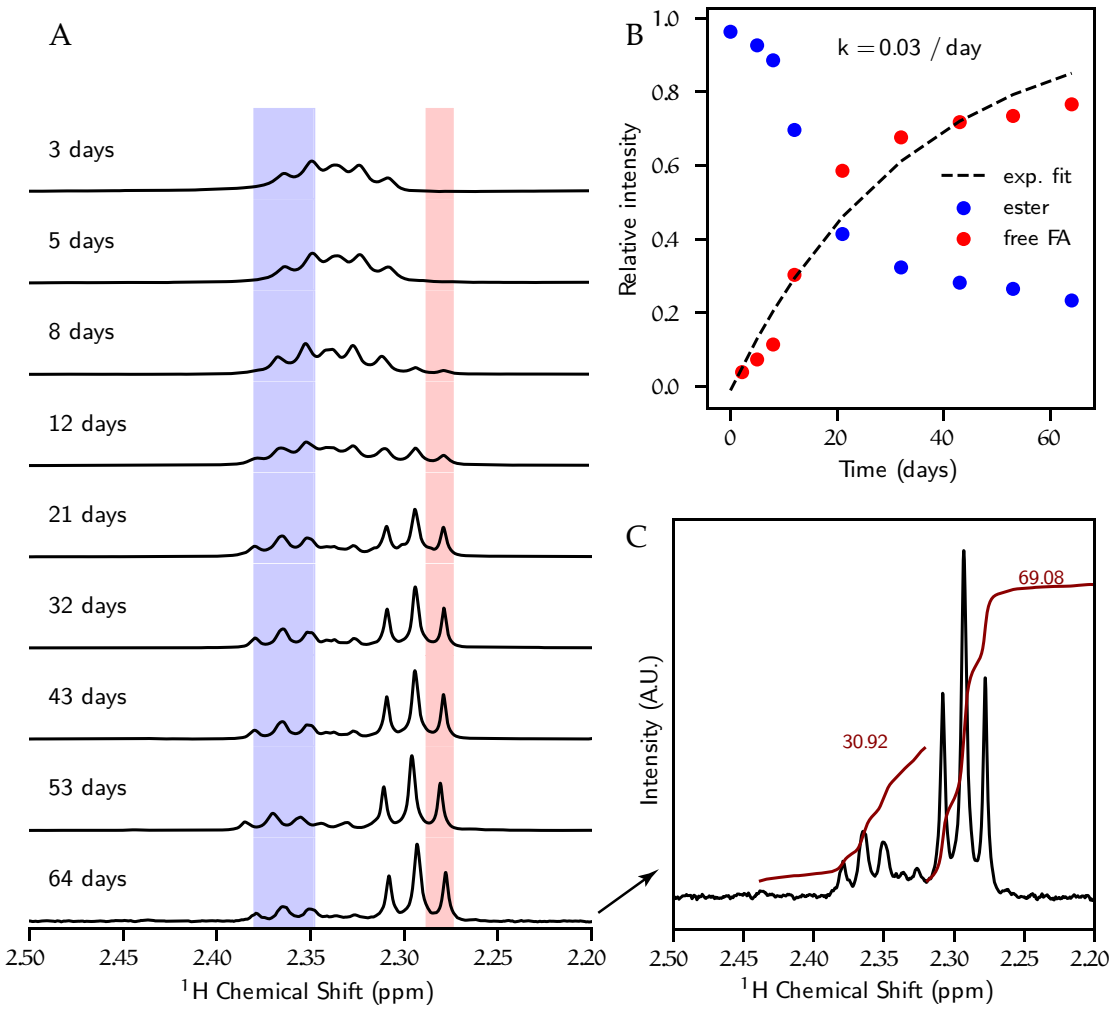


FIGURE 3.8: Hydrolysis of the fatty acid ester. Time series of quantitative $^1$H NMR of aliquots of aqueous liposome solutions extracted into $CDCl_3$ (A). Intensity of highest intensity peak of fatty acid ester (within blue area) and intensity of highest peak of free fatty acid (within red area) against total (blue and red peak) (B). Integral of the fatty acid ester and free fatty acid area (C). Lia Parkin assisted in the collection of this data.

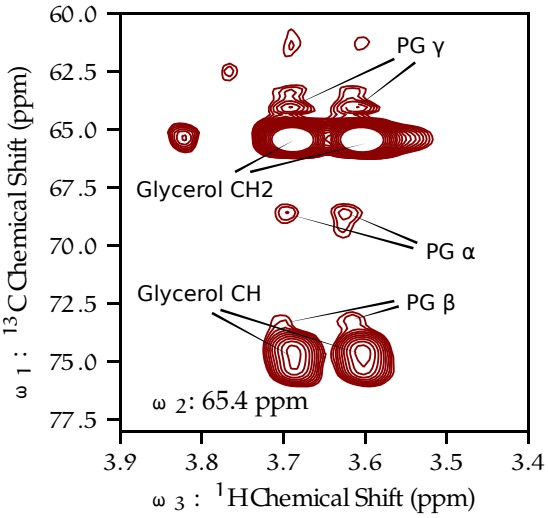


(A) Slice of hCCH-TOCSY 3D correlation at 65.4 ppm. With minor resonances from PG and major from free glycerol labelled.

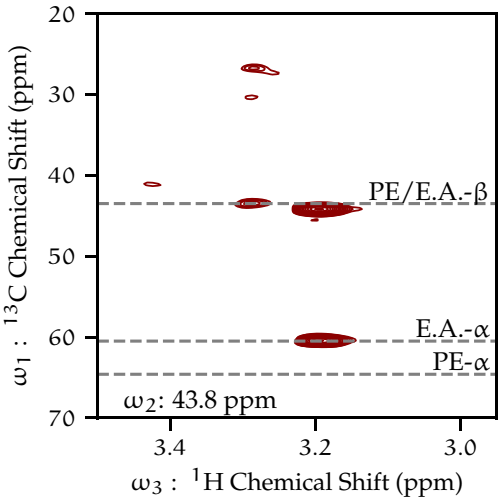


(B) Slice of hCCH-TOCSY 3D correlation at 43.8 ppm. Expected $^{13}$C shifts for phosphoethanol amine related species indicated.

FIGURE 3.9: hCCH-TOCSY-3D slices showing lipid degradation products

of lipids in actual samples had occurred, various KcsA-liposomes data sets collected by HR-MAS were re-examined for signs of hydrolysis.

In samples of KcsA proteoliposomes, the strong protein background signal did not allow for the analysis of fatty acid hydrolysis by 1D nor 2D NMR as gross overlapping peaks did not permit the analysis of subtle changes in shift as in the previous section. However, in several HR-MAS spectra, there are several, sharp, intense, previously unassigned peaks which we assign to the free glycerol and free ethanolamine in the sample. To support these assignments, a hCCH-TOCSY experiment (Figure 3.9a), reveals spin systems that correspond to the literature values of free glycerol [65] and free ethanolamine [64]. The hCCH-TOCSY experiment has a $^{13}$C-$^{13}$C mixing phase that relies on $^{13}$C enrichment of a molecule for efficient transfer [33]. $^{13}$C's natural abundance is about 1 %, so naturally occurring $^{13}$C-$^{13}$C bonds are about 1 in 10 000.

The intensity of the ethanolamine, presumably from natural abundance PE into which KcsA is reconstituted, is much less than that of the free glycerol, which we conclude must be from hydrolyzed PG. Based on sample composition, DOPE and DOPS constitutes half the sample by mass, with DOPE being 9 times more concentrated than DOPS, so nearly half of the sample is DOPE, whereas we expect that co-purifying PG must be two or more orders of magnitude smaller. The methelyene groups adjacent to the amine in PE (β position) and the ethanolamine have very similar the $^{1}H/\ ^{13}C$ chemical shifts in neutral aqueous solution (PE: 3.3/43 ppm; ethanolamine: 3.2/44 ppm), so the same slice of the TOCSY experiment shown in Figure 3.9b would be expected to contain both amine adjacent methylenes, possibly overlapping. The other methylene group of PE (α position) and ethanol amine have distinct shifts (PE: 4.1/65 ppm, ethanolamine: 3.9/61 ppm). We would expect then (should be species exist in the same solution) for the TOCSY experiment to resolve two resonances at the 'β'-proton frequency, one each for the PE and the ethanolamine. Yet, there is only a single spin system, one corresponding to the free ethanolamine.

The $^{1}H$-$^{13}C$ HSQC data have well resolved peaks that distingish between PG $^{1}H$-$^{13}C\beta$ and the glycerol $^{1}H$-$^{13}C\beta$ (the methine group in each species) and that spectrum also resolves the PE $^{1}H$-$^{13}C\beta$ and ethanolamine $^{1}H$-$^{13}C\beta$ (methelyene adjacent to the amine). By integrating these four peaks a ratio of free glyerol to PG and a ratio of free ethanol amine to PE was determined for each of the samples analyzed and those data are presented as the final columns of Table 3.3.

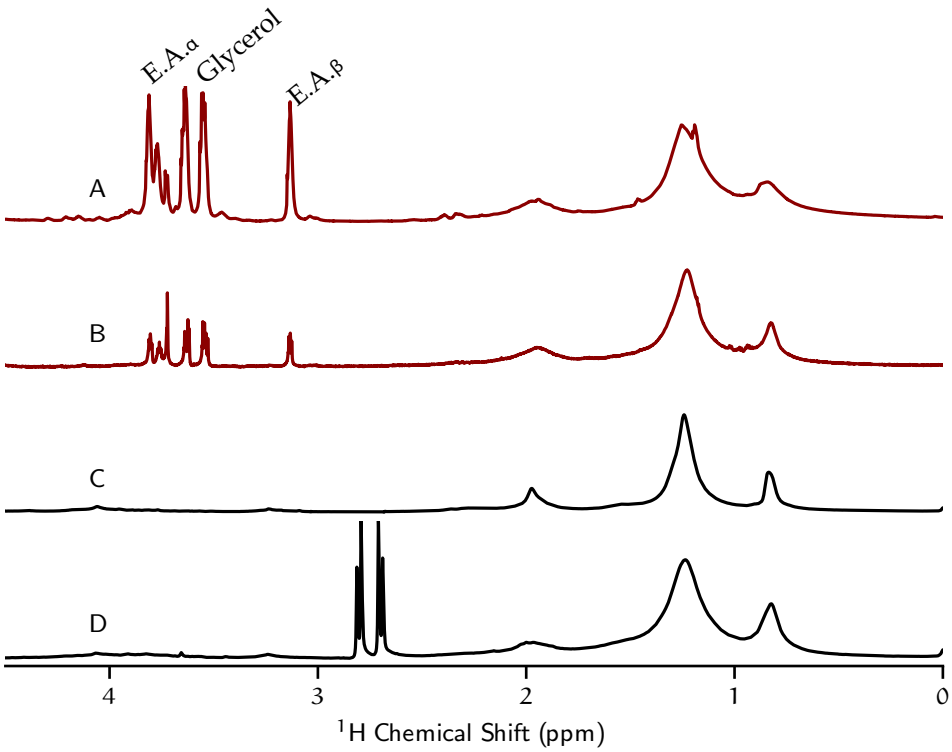


FIGURE 3.10: Utility of 1D $^{1}$H spectrum to diagnose hydrolysis. $^{1}$H spectra with presaturation by HR-MAS of four KcsA proteoliposomes samples. Samples that contained free ethanolamine signal are displayed in red. The samples that contain only PE and no ethanolamine are displayed in black. All samples spectra collected at 308 K, 5 kHz MAS. Spectra are normalized to the bulk $CH_2$ signal (~1.2 ppm). All samples are of U-$^{1}$H-$^{13}$C-$^{15}$N-KcsA in 9 : 1 DOPE liposomes, LPR = 1. Sample A is at pH 7.25, 50 mM tris, 50 mM KCl, 10 % $D_2O$. Sample C is the same composition as Sample A plus 2 mM MgCl. Sample B has the same composition as sample A save it contains ≈90 % $D_2O$. Sample D is pH 4.0, 40 mM citrate (responsible for doublet of doublets at 2.8 ppm), 50 mM KCl, 10 % $D_2O$. Free glycerol and ethanolamine (E.A.) peaks are labeled.

The HSQC of fresh, pure, 9 : 1 DOPE-DOPS liposomes, ethanol amine, and a pellet showing hydrolysis are shown in Figure 3.6 (note the liposome and proteoliposomes were prepared in 50 mM Tris-base as buffer), and the ethanolamine spectrum was produced from data from [64]. This spectrum again clearly shows that a pattern of shifts matching free ethanol amine, but not PE-lipid. These data suggest than that the vast majority of PE and PG head groups have been hydrolyzed. Both of the samples shown in Figure 3.6 were prepared fresh and their HSQC collected immediately after

preparation. The sample displayed in black was re-suspended in 9 : 1 $D_2O$-$H_2O$ buffer, green in 9 : 1 $H_2O$-$D_2O$ buffer. They were prepared by the same protocol by the same person. The $D_2O$ sample was prepared in order to observe $^{1}H$-$^{13}C$ signals near the water signal that are lost in the other sample. The only way in which this sample should differ from the standard samples is the use of $D_2O$ in the buffer. The cause of the rapid degradation of the lipid head groups is not known, but is discussed below in Section 3.4.2.

### 3.3.4 S. lividans *Lipid Analysis*

The membrane composition of *E. coli* varies according to growth temperature [13, 46], culture density [3], media composition, the presence of exogenous chemicals [29], growth phase[12], and other factors. Despite these variables reports agree that the primary lipid content is from phospholipid species dominated by three major head groups: (75–90 %), phosphoglycerol (4–17 %), and diphosphoglycerol (cardiolipin) (2–16 %).

Since KcsA co-purifies with a lipid containing the PG head group, we ask if this particular lipid is present in its native organism, the gram-positive bacterium *Streptomyces lividans*. Gram-positive bacteria all share a common trait of a relatively thick peptidoglycan-rich cell envelope that readily absorbs crystal violet stain. The lipids of gram-positive bacteria vary considerably amongst organisms, though phospholipids

tend to form the majority of the membrane with PG, PE, CL, and PI (phosphoinistitol) representing the most common head groups [53].

*S. lividans* total lipids were extracted by homogenizing the a wet cell pellet with methanol and then vortexed for an hour in methyl t-butyl ether (which has been shown to produce excellent recovery of total lipids including unusual and minor components such as sphingomyelins and excludes peptidoglycans [48]). A side-by-side comparison was made using *E. coli* cells.

Thin layer chromatography (TLC) was used as a coarse-grained analysis identifying the major head groups present in the lipids. TLC was conducted by spotting DOPA, DOPC, DOPE, DOPG, DOPS as standards and the *E. coli* and *S. lividans* extracts onto silica plates plate containing an inorganic fluorescent indicator with a peak absorbance at 254 nm and run with chloroform-isopropanol-triethylamine-methanol-100 mM KCl as the mobile phase in a procedure shown to give good selection of head group regardless of acyl chain composition [71]. The plate was assayed using short wave UV light (254 nm) which detects species that quench florescence of the inorganic indicator, long wave UV-light which detects species that fluoresce, developed in 1 % ninhydrin in methanol solution which detects primary and secondary amines, then subsequently developed in 0.5 % $(NH_4)_2MoO_4$ in methanol which detects phosphate containing compounds. The results of these assays are displayed in Figure 3.12 and summarized

FIGURE 3.11: NMR tube containing *S. lividans* total lipid extract. Note the aqueous layer at the top from the two-phase system used in this experiment.

in Table 3.5. The TLC of *E. coli* shows that PE is the major component and PG a minor component, corresponding to the expected ratio. The *S. lividans* sample while showing both PG and PE displays those two species in a similar ratio. It is especially evident in the UV images that *S. lividans* has far more components in the lipid membrane with some notable species fluorescing under long wavelength UV. These florescent species are likely responsible for the striking color of the *S. lividans* total lipid extract. Although PG and PE are the dominant species suggested by the TLC of *S. lividans*, it is clear that many other unidentified species are present in significant quantities.

The multiplicity-edited, gradient-selected, $^{1}$H-$^{13}$C HSQC of the *E. coli* lipids (Figure 3.15) and of the *S. lividans* lipids (Figure 3.14) reiterate the data from the TLC. The *E. coli* spectrum displays two major head group components identifiable from standard chemical shifts [23] as PG and PE with a weak signal arising from a small fraction of CL. The presence of PE and PG are also confirmed in the *S. lividans* HSQC data. Further, the complexity of the lipids are also underscored by the number and diversity of resonances throughout the *S. lividans* spectra. Most notably, there is a constellation of methyl groups (as indicated by shift and multiplicity) between $^{1}$H: 0.6–1.7 ppm and $^{13}$C: 10–30 ppm. There are also a number of unassigned resonances in the head group region $^{1}$H: 3–5.5 ppm and $^{13}$C: 38–75 ppm, showing again that the *S. lividans* lipid head groups are much more diverse than than those of *E. coli*. The *S. lividans* lipids show a number of resonances consistent with aromatic compounds, $^{1}$H: 6.2–8.45 ppm and $^{13}$C: 110–150 ppm.

| Species | PA | PC | PE | PG | PS |
|---|---|---|---|---|---|
| *E. coli* | ? | − | + | + | − |
| *S. lividans* | ? | − | + | + | ? |

TABLE 3.5: Lipid TLC results, where '+' indicates present and ' ' indicates absent.

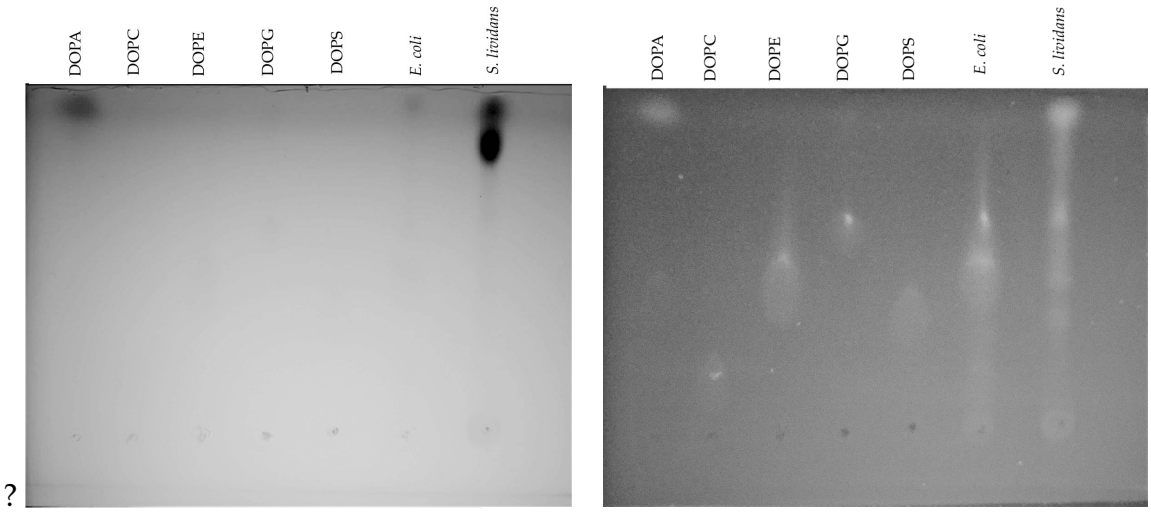


(A) Short wave UV (254 nm)

(B) Long wave UV (365 nm)

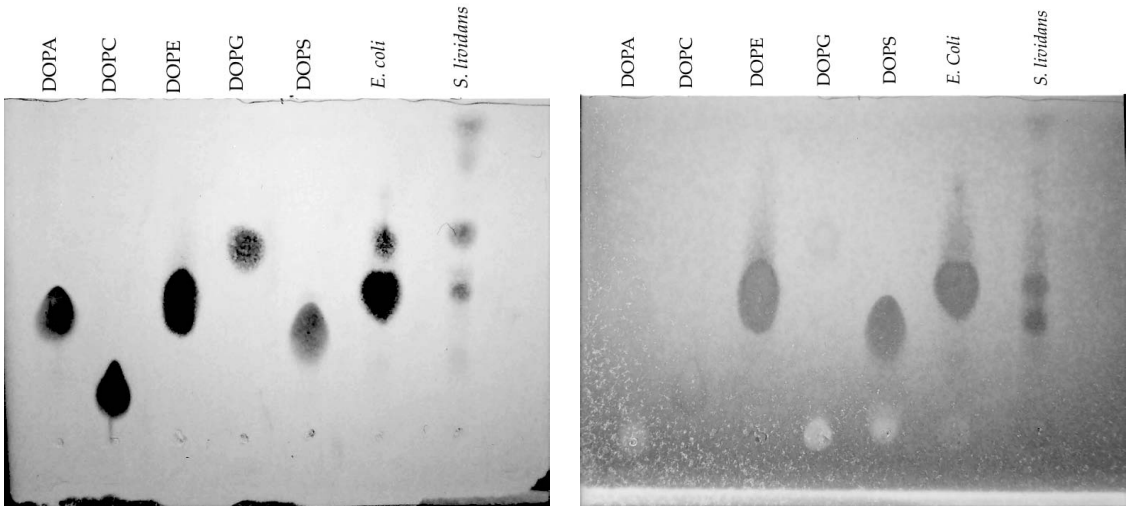


(C) $(NH_4)_2MoO_4$ stain

(D) Ninhydrin stain

FIGURE 3.12: Thin layer chromatography of *E. coli* and *S. lividans* total lipids and various di-oleoyl phospholipids run in 30 : 25 : 18 : 7 : 6 chloroform-isopropanol-triethylamine-methanol-100 mM KCl on plates with 254 nm inorganic indicator

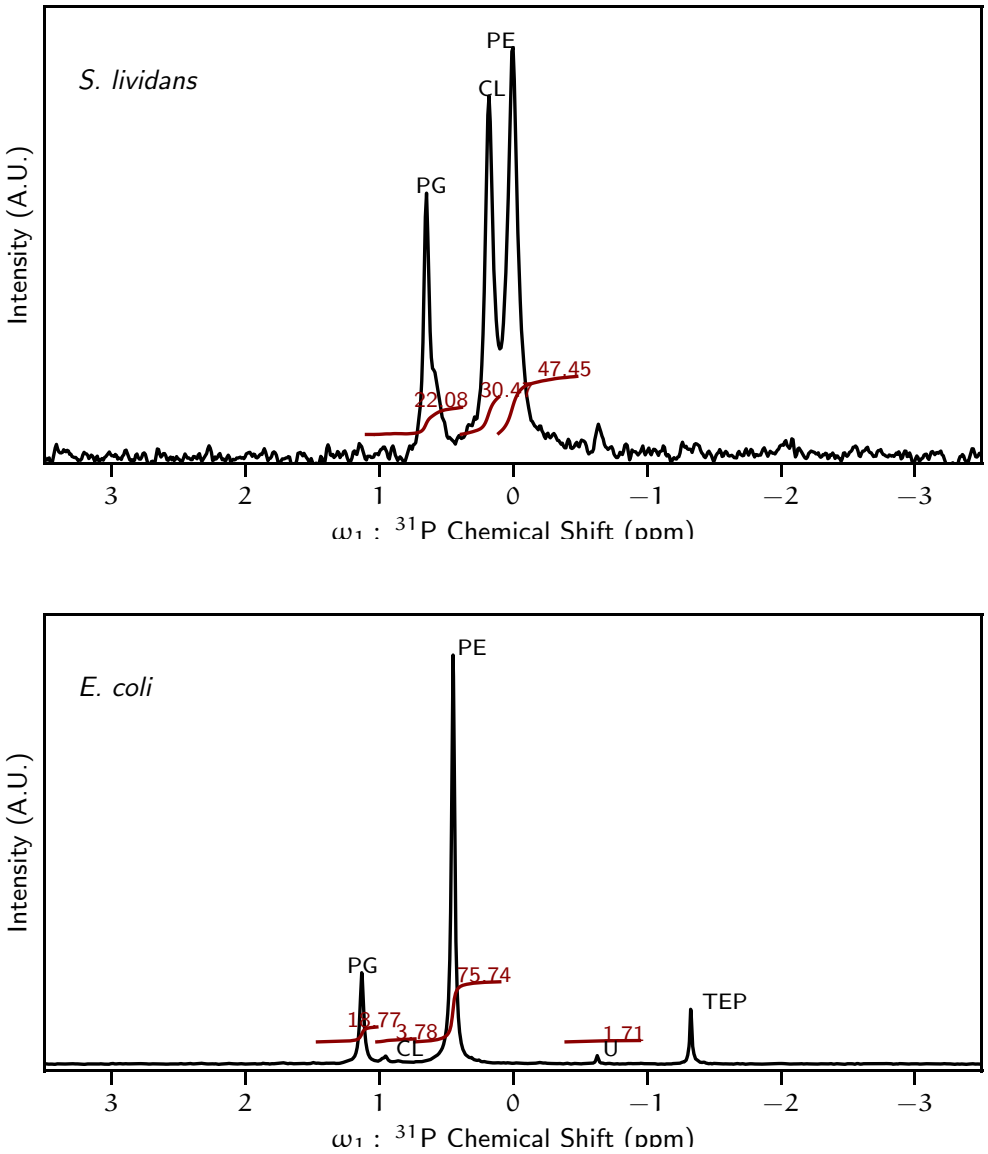


FIGURE 3.13: Quantitative $^{31}$P NMR of lipids extracted from *S. lividans* (top) in 9:4:1 $CDCl_3$-MeOD-200 mM CsEDTA, and *E. coli* in 2:1 $CDCl_3$-MeOD (bottom), with integrals relative to 100 indicated. Triethylphosphate (TEP) was added to the *E. coli* sample as an internal standard.

| | PE | | | PG | | | CL | | | Unknown | | |
|---|---|---|---|---|---|---|---|---|---|---|---|---|
| | shift (ppm) | FWHM (Hz) | Int. (%) | shift | *FWHM* | Int. | shift | FWHM | Int. | *shift* | FWHM | Int. |
| S. lividans | −0.021 | 14.1 | 47.45 | 0.61 | 12.3 | 22.1 | 0.21 | 13.3 | 30.4 | | | |
| E. coli | 0.463 | 6.58 | 75.7 | 1.13 | 8.3 | 18.8 | 0.96 | 8 | 3.78 | −0.62 | 6.7 | 1.7 |

TABLE 3.6: $^{31}$P chemical shifts, full-width half maximum line widths, and integral of total phosphorous signal for lipid extracts of bacteria

For quantitative analysis of phospholipid head groups, Aliquots of both extracts *E. coli* and *S. lividans* were dried and re-suspended into 2 : 1 $CDCl_3$-MeOD a solvent system that generally resolves the major phospholipid head groups [63] and examined by $^{31}$P NMR. While the *E. coli* sample give very sharp lines, the *S. lividans* sample had broad, grossly overlapping peaks (not shown), so it was dried and re-dissolved into an alternative solvent system shown to give better dispersion [50] consisting of 9:4:1 $CDCl_3$-MeOD-(200 mM CsEDTA in $D_2O$). This gives a two phase solution that tends to provide excellent peak dispersion and reliable chemical shifts of the major phospholipids. The chemical shifts provided in the literature [50] give good agreement with the HSQC data that PG, PE, and CL are present in the sample. Whereas CL only makes up a small fraction of the total lipid extract for *E. coli*, agreeing with literature values that report CL as generally less than 10 % of the *E. coli* membrane. The cell membrane of organisms of the Actinobacteria phylum have a diverse range of cardiolipin content with some organisms having none, while for others cardiolipin comprises nearly half of the membrane content (e.g. *Micrococcus clyophilus* membrane is 45 % CL) [9].

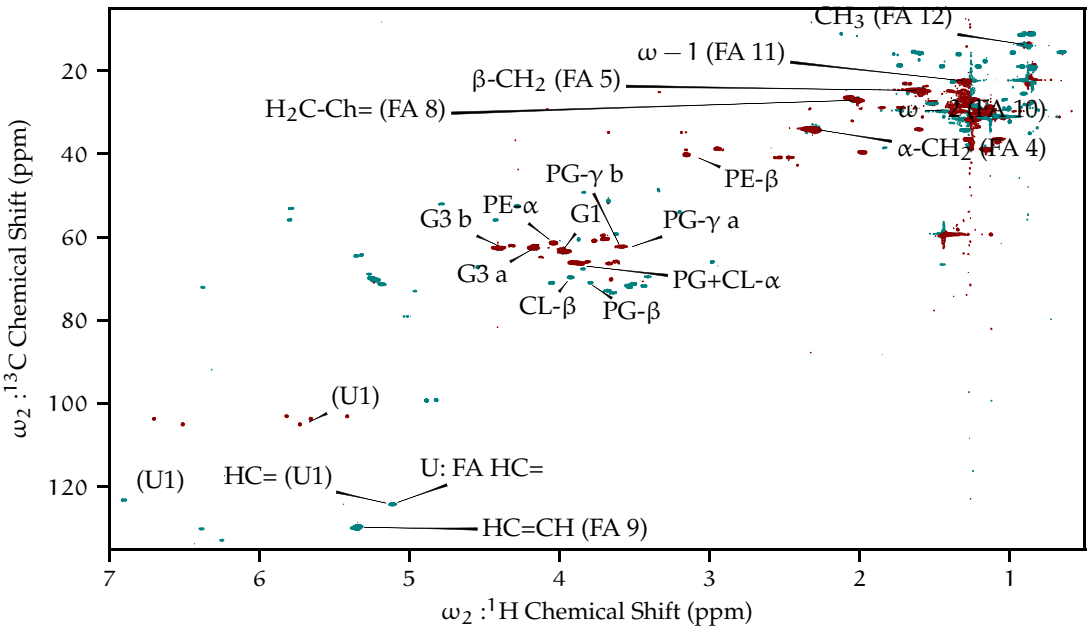


FIGURE 3.14: Multiplicity-edited (CH and $CH_3$ purple, $CH_2$ red) gradient-selected, $^1H$–$^{13}C$ HSQC of *S. lividans* total lipid extract with assignments.

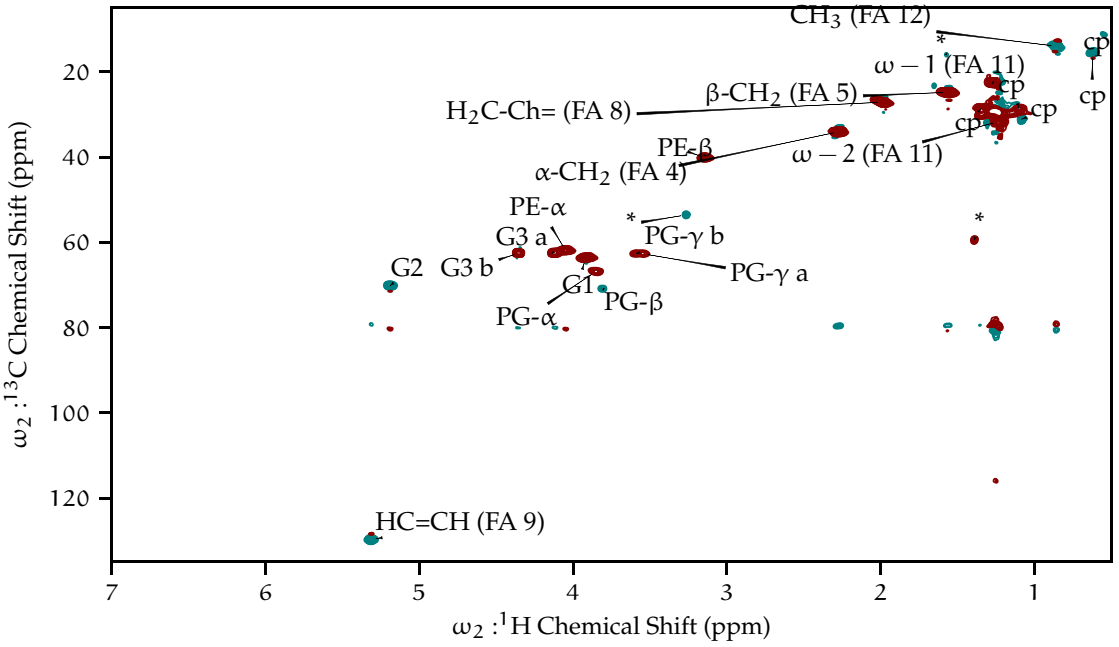


FIGURE 3.15: Multiplicity-edited (CH and $CH_3$ organge, $CH_2$ red) gradient-selected $^1H$–$^{13}C$ HSQC of *E. coli* total lipid extract.

## 3.4 DISCUSSION

### 3.4.1 *Phosphoglycerol in KcsA Proteoliposomes*

This study provides the best evidence and characterization to date of PG co-purifying with KcsA channels when expressed in and purified from *E. coli*. These lipids are isotopically enriched from the growth protocol and undergo hydrolysis in ordinary conditions.

The crystal structures listed in Section 3.7 all contain diacyl chain moieties believed to belong to lipids, but none resolve the headgroup. This study shows it is possible that some do not have a headgroup at all or merely a part of one.

In Chapter 2 the KcsA-Δ125 construct was presented showing the majority of HR-MAS signal of KcsA proteoliposomes arises from from C-terminal residues. Characterization by solid-state NMR showed that it was still a well folded protein. The KcsA-Δ125 sample is the *only* KcsA proteoliposome sample examined by HR-MAS that did not show the presence of an exogenous lipid, only revealing signal from the lipids into with the protein was reconstituted.

The diacyl chain revealed by crystallography appears alongside KcsA's transmembrane domain with the head group near to the extracellular side of the channel. The C- and N-termini are oriented on the cytosolic side of the membrane, placing them at the distal end of the KcsA with respect to the PG head group. Therefore, it seems unlikely that C-terminus has any direct contact with lipids bound between KcsA sub-

units. KcsA-Δ125 has very low open probability at low pH and is less thetarmostable than the full-length channel [51, 57, 73]. It has also been shown that, when stripped of its lipids [56], in the absence of lipids with negatively charged head groups [73], or when residues near the diacyl chain are mutated [44], KcsA exhibits similar behavior: low open probability and poor thermostability. It seems likely then that the C-terminus and the bound lipid are involved in a larger allosteric network that works to stabilize the KcsA in its low pH, open conformation. When the C-terminus is cleaved, the lipid is no longer present, suggesting that this change leads KcsA to bind with less affinity to PG.

### 3.4.2 *Lipid Degradation of KcsA-Proteoliposomes*

Work in model liposomes support previous findings, that the fatty-ester acids are readily hydrolyzed but the head groups of the DOPE-DOPS lipid system remained unreacted after two months of incubation on the bench top. It is shocking to find then that in actual proteoliposome samples not only experience hydrolysis of fatty acid chains but also of lipid headgroups. In one case, in fact, the lipid head groups appear to be entirely hydrolyzed. As demonstrated from the model liposome study, headgroup hydrolysis is negligible for months at room temperature. The catalytic agent leading to significant hydrolysis of actual proteoliposome samples ]has not yet been identified.

The free glycerol peaks of the $^{1}H$ spectra of hydrolyzed samples are of the same magnitude as the free ethanolamine, suggesting that the glycerol peaks are not arising from only co-purifying lipids. The most likely cause of the intense signal from glycerol in the $^{1}H$ spectra is that the lipid glycerol backbone is hydrolyzed from the phosphate and the fatty acid chains. Since, however, many of the samples do not show any amount of free glycerol, but only signal consistent with phosphoglycerol lipid, we can conclude that $^{13}C$ enriched PG co-purifies with KcsA.

This study demonstrates that proteopliposome samples demand routine quality measurements. This is especially true in cases where studies make claims regarding the effect of lipid composition. HR-MAS requires specialized equipment and the data acquisition time for an $^{1}H$-$^{13}C$ HSQC is at least 3 hours. However, here we show that a 1D proton spectrum is adequate to diagnosis the presence of hydrolyzed head groups, which requires no, or very little, change to a CP-MAS experimental setup and can be collected in a matter of minutes.

### 3.4.3 *Alternative Lipids*

The hydrolysis of model DOPE-DOPS liposomes reflects earlier findings: the fatty acid esters are labile and subject to measurable hydrolysis even at neutral pH in the absence of catalysts. Even over a period of months, no measurable amount hydrolysis of the headgroup or glycerol backbone occurred.

Curiously, many actual proteoliposome samples show clear evidence of hydrolysis of the headgroup and likely the glycerol backbone. This poses a serious challenge to studies that rely on a well define lipid composition.

Ether lipids where the fatty acid chain is linked by an ether group to the glycerol backbone rather though an ester linkage (see [16] for a review of these), have a much lower propensity to experience fatty acid hydrolysis. Since the ether linkage is much more stable than the ester, ether lipid have been shown to be much more chemically stable [77]. Ether ester lipids with PC headgroups have been shown by $^{2}$H NMR to have very similar dynamics to that of their ester lipid counterparts [60], meaning that they would likely be good substitutes in biophysical studies for ester fatty acid lipids.

Yet, these studies also show that the headgroup is liberate from the phosphate group in some subset of samples and that likely the glycerol backbone is also completely hydrolyzed. There is not obvious alternative to phospholipids that would bring the same physiologic relevance to these studies. As the most largest component of lipid membrane in bacteria, phospholipids are indispensable. Rather than selecting alternative lipids, ensuring the chemical integrity of biologically relevant lipids (using $^{1}$H NMR, for example) and seeking the catalysts leading to accelerated hydrolysis should be viewed as a priority.

### 3.4.4 *S. lividans Lipids*

Several interesting observations emerge upon comparing *E. coli* lipids and *S. lividans* lipids. The first is the *S. lividans* has an much more complex lipid composition that defies simple analysis. The visible appearance of *S. lividans* grown on agar plates is of bright pink-orange colonies. The visible appearance of the *S. lividans* total lipid extract was a bright pink solution. *E. coli* colonies yield pale off-white colonies and their extracts have a slight yellow hue.

KcsA co-purifies with the PG head group from *E. coli*. This author made several attempts to transform *S. lividans* cells with a plasmid carrying a KcsA gene, but none of the cells proved viable and or had the correct selection traits. So, it remains an open question as to what sort of lipid binds to KcsA *in vivo* in its native host organism.

The diversity of functional groups present in *S. lividans* offers a tantalizing questions. As a gram-positive soil bacterium, *S. lividans* has a dramatically different characteristics than the gram-negative bacterium *E. coli*. Specifically, *S. lividans* have many more observable components in their membrane. Also, *S. lividans* shows a very high content of cardiolipin-type phospholipid, which is in a small minority in the *E. coli* membrane. As mentioned in the introduction, the presence of anionic lipid head groups, such as PA or PS, has a thermostabalizing effect on KcsA as a tetramer [15], and trunction of the N-terminus disrupts the ability of PA to thermostabilize the channel [57]. It has also been observed that cardiolipin also improves KcsA tetramer thermostability [56] in a manner that does not depend on the N-terminus. Dörr et al. [19] used

the SMALPS system [39], where styrene-maleic polymer creates nanodisks of "native" lipids and overexpressed protein, to isloate KcsA from the *E. coli* membrane. That study showed the purified nanodisks were enriched in both CL and PG, suggesting that the composition of the *E. coli* membrane near KcsA is enriched in the same components that are present in KcsA's host organism, *S. lividans*.

It was critical to the accuracy of the lipid characterization of *S. lividans* that the extract was used fresh. A previous attempt characterized *S. lividans* lipid extract that had for two months and those results yielded dramatically different results. Specifically, no PG head group was detected in the stored solution. No visible precipitation was observed in the sample, and the presence of PE and other constituents were still readily detected. This again underscores the need to for routine quality metric of lipid samples.

### 3.4.5 *Possible Presence of Carotenoids*

*S. lividans* belongs to the family Actinobacteria who have attracted considerable interest because of a host of unusual molecules they synthesize. Carotenoids, tetra-terpene pigments, have been identified in a number of antinobacteria and in members of the *Streptomyces* genus in particular. The best known example of this class of molecule is β-carotene with its characteristic bright orange color when dissolved in solution. Carotenoids have extensive π-conjugations systems and frequently incorporate cy-

loalkene, aromatic, and heterocycle moieties, and have remarkable structural diversity in nature [9].

There are a number of peculiar and unassigned resonances in the spectra of *S. lividans* lipids. For example, the strong resonance in the *S. lividans* total lipid HSQC at $^{1}$H: 5.11 ppm $^{13}$C: 124.3 ppm, is a CH group as shown by multiplicity edited experiments. This frequency corresponds to an alkene functional group, but the specific shift does not match any common lipid double-bonds [1]. COSY, TOCSY-COSY, and TOCSY-HSQC experiments (Figure D.1) reveal a network of spins connecting alkene resonances to some of the unidentified resonances in the aromatic region ($^{1}$H: 6.5–9.5 ppm, $^{13}$C:110–140 ppm) and a region typical for cyclo- and terminal-alkenes ($^{1}$H: 4.5–7 ppm, $^{13}$C: 90–110 ppm) as well as to the methyl region ($^{1}$H: 0.5–1.5 ppm, 10–20 ppm). This type of spin system suggests the alkene is part of a conjugated spin network that is common to carotenoids.( Figure 3.16 shows an example of two carotenoids that have been found in *Streptomyces* strains.) There are hundreds of known carotenoids [9] and they play important roles in redox-chemistry in particular in electron-transport for photosynthetic bacteria (See Stange [66] for an extensive review of this topic). The particular way in which bacterial carotenoids have branched methyl groups also may explain the profusion of signal in the methyl region of the HSQC. Further, the presence of carotenoids would also explain the brilliant orange-pink color of the *S. lividans* extract. Some NMR studies have been conduced on microbial carotenoids (e.g. [24, 43]). The chemical shift patterns they report are very similar to the unidentified resonances in the *S. lividans* HSQC (See Figure D.4 for a simulated spectra of microbial

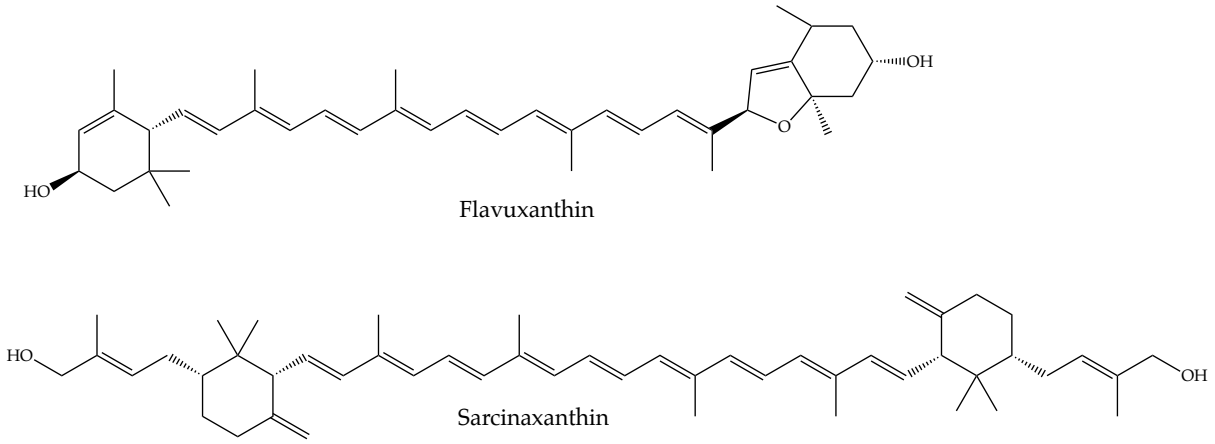


FIGURE 3.16: Examples of structures of carotenoids identified in *Steptomyces* bacteria.

carotenoid shifts). The intensity of the signal arising from putative carotenoids are approximately 25 % of that arising from individual lipid species, suggesting that they are a minority component but an important part of the *S. lividans* bilayer, whatever they are.

## 3.5 CONCLUSION

Many studies have shown that KcsA is more stable when reconstituted into lipids with anionic head groups and with CL. We find here that the composition of KcsA's host organism is rich in PG, a net negatively charged head group, and CL. The lipid composition of *S. lividans* is complex and contains many components that defy easy identification. Until now, the lipid composition of *S. lividans* has been undocumented, and there has been no reason to examine how KcsA might interact with more peculiar lipid and lipoid species. Yet, the analysis of *S. lividans* demonstrates that *in vivo* in its host organism, KcsA might have strikingly different binding partners.

In its native lipid milieu, how might KcsA's gating characteristics be different? KcsA has been a champion performer for biophysical studies seeking to understand channel-ligand binding, allostery, gating kinetics, and a host of other processes. KcsA has proven its worth as a model organism time and again and continues to be a valuable system. KcsA in lipids is often presented as a system whose function can directly inform our understanding of channels with direct relevance to human health such as the human potassium channel hERG. Several authors have suggested, however, that our basic assumptions about KcsA's functional role are incorrect. Zakharian and Reusch [82], for example, has presented evidence that KcsA in *S. lividans* forms a supramolecular complex with poly-(R)-3-hydroxybutyrate and inorganic polyphosphates to form a channel which is temperature activated rather than pH activated. Molina et al. [52] have presented evidence that KcsA channels cooperate in supermolecular gating clusters with important lipid dependence on the cooperativity. By studying KcsA expressed (and hence co-purifying) with non-native lipids (i.e. from the gram-negative bacterium *E. coli*), then reconstituted again in synthetic phospholipids whose composition is in doubt due to reactivity, we must ask what important characteristics of this channel are we missing? And if KcsA in a non-native environment is a sound model for membrane channels in general, how much better might this model system be if studied as part of a yet more native environment?

## 3.6 METHODS

### 3.6.1 *Bacterial Culture fo Lipid Analysis*

As a comparison *E. coli* from BL21 cells (New England Biolabs) containing a the PASK90 plasmid carrying a gene for resistance to ampicillin and KcsA was grown in the typical manner for preparation of a KcsA sample: grown in LB-Miller broth supplemented with 100 µL ampicillin at 37 °C and 250 RPM shaking to a cell density of $OD_{600} = 0.9$. The lipids from this sample were then extracted following the same procedure used to extract the *S. lividans* lipids.

*S. lividans* cells, ATCC 35287 containing PJ702 plasmid which contains a thistrepton resistance gene, were plated on R2YE (Section A.3.1.1) media at 30 °C, 20 % agar thiostrepton selection plates overnight and a single colony was selected and grown in R2YE-thiostrepton media for 15 h at 30 °C until the culture reached $OD_{600} = 0.83$. The cells were harvested by centrifuge and stored at −80 °C until their lipids were extracted.

### 3.6.2 *Lipid Extraction*

Lipids were extracted according to a procedure described by Matyash et al. [48], which finds better recovery (especially of minor components) and better reproducible than the more widely used procedure described by Bligh and Dyer [8]. Briefly, cells (1 g) are

vortexed first in methanol (7.5 mL) until suspended, then shaken in methyl-tert butyl ethanol (MTBE) (25 mL) for 1 h at room temperature. Phase seperation was initiated by the addition of 7.5 mL of deionized water. The organic layer was collected using a separatory funnel. The aqueous layer was treated with an additional 10 mL of 10:4:3.5 MTBE-MeOH-$H_2O$ and shaken for another hour. An additional 5 mL of water was added and the organic layer collected and combined with the previous collection. The lipids were then dried over $N_2$ gas and stored at $-20\,^{\circ}C$ until further analysis was conducted.

### 3.6.3 *Protein Expression and Purification*

See Appendix A for more detailed information on constructs, protein expression, and purification. Brief notes and deviations from the methods describe in Appendix A follow.

The fully protonated KcsA data presented in this chapter is from protein that was uniformly $^{13}C$ and $^{15}N$ enriched by expressing KcsA in *E. coli* JM83 cells. The JM83 cell line is a proline auxotrophic, so natural abundance proline was added to cultures.

Fractionally deuterated protein was produced as described in Section A.3

### 3.6.4 *KcsA Reconstitution*

Liposomes were formed from a fixed ratio of lipid by mass (most samples $9:1$ ratio of 1,2-dioleoyl-sn-glycero-3-phosphoethanolamine (DOPE) to 1,2-dioleoyl-sn-glycero-3-phospho-L-serine (DOPS)), which were obtained as a chloroform solution (Avanti), dried as a thin film over $N_2$ gas, resolubilized in n-hexane (Sigma), dried again over $N_2$ gas and solubilized by bath sonication in 10 mM DM, 50 mM Tris, 100 mM KCl, pH 7.5. Lipids were mixed in a known mass ratio with KcsA (typically $1:1$), diluted to 2 mM DM and dialyzed in 30 kDa MWCO tubing (Spectrum) with three exchanges of 4 L of buffer at 12–18 h intervals at room temperature. Proteoliposomes were harvested by centrifugation at 5700 RCF for 30 min and then stored at $-80\,^{\circ}\mathrm{C}$. The presence of KcsA as a tetramer in the liposomes was verified by SDS-PAGE. Pellets were stored at $-80\,^{\circ}\mathrm{C}$ until ready for further experimentation.

### 3.6.5 *Liposome Preparation*

The liposome hydrolysis study was conducted in part by Lia Parkin as a summer undergraduate research project. This author thanks L. Parkin for her assistance. Liposomes for the hydrolysis study were obtained as pure chloroform solutions (Avanti). 50 mg of $9:1$ DOPE-DOPS were dried under $N_2$ gas for 1 h and then suspended in a 10 mL solution of 50 mM Tris, 50 mM KCl, 10 mM β-D-maltose-pyranoside (Anatrace), pH 7.25 by bath sonication. The solutions were dialyzed against 4 L of 50 mM

Tris, 50 mM KCl, pH 7.25 in reconstituted cellulose membranes (Spectra) with a molecular-weight-cut-off of 5 kDa with three exchanges. The final exchange contained (in addition to aforementioned components) 0.02 % (w/v) sodium azide to control microbial growth. Following dialysis, the liposomes were pelleted by centrifuge and suspended in 1 mL of their buffer and left on the bench top to age. 100 µL aliquot were collected by briefly vortexing the solution and collecting by 1 mL pipette with a tip whose entrance had been roughly doubled in diameter by a razor blade. Lipids were extracted from solution using a chloroform-methanol solution as described in [8] and dried using a flow of nitrogen. The samples were then suspended in $CDCl_3$ "100 %" (Sigma) and were referenced using the residual protonated chloroform resonance in the $^1H$ spectrum (7.260 ppm).

### 3.6.6 *NMR Sample Preparation*

Synthetic phospholipids standards (DOPA, DOPC, DOPE, DOPG, DOPS) were obtained in chloroform (Avanti) and dried under a flow of $N_2$ gas before use. Before further use, lipid films were first redissolved in n-hexanes (Sigma) then dried under a flow of $N_2$ gas then placed under vacuum for at least 30 min.

To hydrate lipids for aqueous liposome studies, the respective buffer (see text) was added to the tube containing the lipid film and bath sonicated for 10–30 min. To form unilamellar liposomes, the suspensions were extruded using a syringe extrusion device (Avanti) holding two 0.1 µm polycarbonate membranes 21 times with the final

pass ending on the opposite side of the membrane from the beginning of the procedure. $D_2O$ (>98 % Cambridge) containing DSS (Sigma) was added to the sample to a final concentration of 10 % and 10 mM, respectively.

For studies in organic solvent, lipid films were solvated in $CDCl_3$ ( >95 %, Sigma) and re-dried under $N_2$ gas twice, and placed under vacuum for at least 30 min to reduce residual solvent signals. The samples were then solvated in either $CDCl_3$ ("100 % + 0.03 % TMS", Cambridge Isotopes) or 2 : 1 (v/v) $CDCl_3$–MeOD (MeOD: "100 %", Cambridge Isotopes) as specified in the text.

Typically, 0.5–0.6 mL of solution was placed into a 5 mm NMR tube (Wilmad) rated for use at fields of ⩽600 MHz.

For $^{31}P$ quantification of the *S. lividans* sample, a three-solvent, two-phase system was employed to improve resolution of peaks as adapted from [50]. Following experiments with 2 : 1 $CDCl_3$-MeOD solvent system, teh sample was dried under nitrogen gas flow. The sample was then reconstituted into 9:4:1 $CDCl_3$-MeOD-20 mM Cs-EDTA. This system provides exceptionally sharp lines and reproducible chemical shifts, easily distinguishing various phospholipid head groups.

### 3.6.7 *NMR*

J-couple-based experiments were performed on a Bruker magnet with a proton field of 750 MHz using a 4 mm high-resolution magic angle spinning probe (HR-MAS) with

$^{1}H/^{13}C/^{15}N/^{2}H$ channels with a 40 G/cm gradient coil oriented along the magic angle. Experiments were generally performed between 4–5 kHz MAS and 308 K. Typical hard-pulses were 31 kHz for $^{1}H$, 33 kHz for $^{13}C$, and 20 kHz for $^{15}N$. Decoupling fields and spinlocks were typically 10 kHz. Heteronuclear decoupling was accomplished using WALTZ-16 [61]. TOCSY spinlocks used the DIPSI-2 [59] sequence and were full-rotor period synchronized as failing to do so caused unpredictable spectral artifacts.

HSQCs were collected using double inept transfer, trim pulses (100 µs), with Echo/Antiecho-TPPI gradient selection and decoupling during acquisition. Site specific $T_2$ measurements were collected by adding a rotor-synchronized $^{13}C$ spin-echo during the $^{1}H$-$^{13}C$ coherence transfer period increasing the delay over at least five steps until magnetization had decayed to at least 90 %.

Solution NMR was performed on a Bruker 500 Ascend instrument using a H/C/N (H) probe. Sample temperatures were 300 K unless otherwise stated. Typical field strengths were 18 kHz for $^{1}H$ and 8 kHz for $^{13}C$ for hard pulses, and 2 kHz for $^{13}C$ heteronuclear decoupling using WALTZ-16. Homo-spoil gradients were accomplished with 7.6 T $m^{-1}$ of 1 ms duration. HSQCs were phase sensitive and multiplicity edited using double inept transfer, trim pulses (1 ms), used shaped pulses for inversion on $^{13}C$ (1 ms) with Echo/Antiecho-TPPI gradient selection and decoupling during acquisition (Bruker sequence: hsqcedetgpsp.3). Direct dimensions were acquired for 50 ms in 2048 points and indirect dimensions were acquired for approximately 10 ms in 512 points. The 3D TOCSY data was acquired for 7.5 ms in 128 points in the $^{1}H$ dimension and the $^{13}C$ dimension acquired for 2.5 ms in 64 points. All proton acquired data was

zero-filled to 2× the number of points acquired and were multiplied by $sin^2$ function of pure cosin phase.

Lipid head group quantification was performed on a Bruker 400SL spectrometer equipped with an inverse-detected TBO probe with a phosphorous frequency of 161.975 30 MHz. Spectra were acquired using a 90° one-pulse experiment, collecting 129 862 complex points over 1.00 s with WALTZ-16 decoupling during acquisition. The typical $^{31}P$ pulse-length was 17 µs. The recycle delay was set to 6.2 s, which was $6 \times T_1$ the longest relaxing peak (PE) of the *E. coli* sample, where $T_1$ was measured with the T1ir experiment. The experiments were signal averaged until the signal-to-noise ratio of the least intense peak of interest was at least 20, which was 2560 scans for the *S. lividans* sample and 512 for the *E. coli* sample. The FID was zero-filled with an equal number of points as acquired and an exponential window function applied with 5 Hz of line broadening. The temperature was maintained at 300 K sample temperature as calibrated using a 5 % MeOH in $CDCl_3$ standard by facility staff.

For all solution experiments, shimming was preformed to achieve a FWHM linewidth on the DSS or TMS line of the $^1H$ methyl signal of >1.1 Hz with a Lorentzian lineshape and clear carbon satellite peaks visible.

### 3.6.8 *Solid-State NMR*

Figure 4.10 was collected by Dongyu "Allison" Zhang from the McDermott group and this author is grateful for her sharing the data. The data was collected on a

900 MHz Avance II spectrometer at 267 K set temperature, with a spinning rate of 16.66 kHz. Hard pulses for $^{1}H$ and $^{13}C$ were 90 kHz and 54 kHz respectively, with 90 kHz of proton-coupling using the SPINAL64 sequence applied during aquisition. The direct dimension was digitized in 2670 complex points over 19.4 ms and the direct dimension aquired in 13.3 ms over 1200 complex points using States-TPPI collection. The recycle delay was 2.5 s.

### 3.6.9 *Thin Layer Chromatography*

The procedure for TLC was adapted from Touchstone, Chen, and Beaver [71]. Briefly, prepared (Sigma) 10 $cm^2$ glass plates with 250 µm silica containing an inorganic fluorophore with peak absorbance at 254 nm were pre-treated by placing in a sealed tank containing $30:25:18:7:6$ chloroform-isopropanol-triethylamine-methanol-100 mM KCl (by volume), where the solvent front was allowed to run to approximately 90 % of the plate height. The plate was then dried for an hour in a fume hood. 10 µL of lipids solutions (chloroform for the standards and MTBE for the extracts) were spotted onto the plate and allowed to dry for 20 min minutes in a fume hood. The plate was then placed in the tank and the solvent front allowed to run to approximately 80 % of the plate height. The plate was allowed to dry for 1 h in a fume hood then dried on a warm (≈100 °C) hotplate for 20 min. The plates were then imaged under single wavelength UV lights at 254 and 365 nm. The plate was then treated with 1 % ninhydrin in methanol (w/v) solution (Sigma) using a spray applicator and until vis-

ibly wetted, then allowed to dry in a fume hood for 20 min. The plate was developed by placing on a ≈100 °C hotplate until blue spots developed (about 1 min). The image has a high background due to some reactivity with residual triethylamine. The plate was then allowed to cool for 1 h. Then a solution of 0.5 % (w/v) $(NH_4)_2MoO_4$ solution in 2 : 1 water-methanol (v/v) was painted onto the plate by hand with a horse hair paint brush. The plate was allowed to dry for 1 h. The plate was developed by placing on a ≈100 °C hotplate until purple spots developed (about 2 min). All solvent used were from Sigma and of HPLC grade. Synthetic phospholipids were obtained as 10 mg $mL^{-1}$ chloroform solutions from Avanti and used without further purification.

## 3.7 PUTATIVE LIPIDS IN KCSA CRYSTAL STRUCTURES

The following is a list of KcsA crystal structures deposited in the Protein Data Bank (PDB) [4] featuring diacyl chains of putative lipid molecules.

1K4C, 1K4D[85]; 1R3I, 1R3J, 1R3K, 1R3L [86]; 1S5H [84]; 2BOB, 2BOC [41]; 1ZWI, 2ATK [11]; 2IH1, 2IH3 [75]; 2DWD, 2DWE, 2HVJ, 2HVK [81]; 2NLJ [42]; 3GB7, 3IGA [70]; 4LBE, 4LCU [54]; 2P7T, 2JK5, 2W0F, 4UUJ [40]; 4MSW, 5EBL, 5EBM, 5EBW, 5EC2 [47]; 5VKE, 5VKH [14]; 6BY2, 6BY3 [37].

[1] E. Alexandri et al. "High resolution NMR spectroscopy as a structural and analytical tool for unsaturated lipids in solution." In: *Molecules* 22.10 (2017), pp. 1–71. DOI: 10.1016/B978-0-12-374984-0.01275-4.

[2] S. J. Alvis, I. M. Williamson, J. M. East, and A. G. Lee. "Interactions of Anionic Phospholipids and Phosphatidylethanolamine with the Potassium Channel KcsA." In: *Biophysical Journal* 85.6 (2003), pp. 3828–3838. DOI: 10.1016/S0006-3495(03)74797-3.

[3] N. Arneborg, A. Salskov-Iversen, and T. Mathiasen. "The effect of growth rate and other growth conditions on the lipid composition of Escherichia coli." In: *Applied Microbiology and Biotechnology* 39.3 (June 1993), pp. 353–357. DOI: 10.1007/BF00192091.

[4] H. M. Berman. "The Protein Data Bank." In: *Nucleic Acids Research* 28.1 (Jan. 2000), pp. 235–242. DOI: 10.1093/nar/28.1.235.

[5] M. P. Bhate et al. "Preparation of uniformly isotope labeled KcsA for solid state NMR: Expression, purification, reconstitution into liposomes and functional assay." In: *Protein Expression and Purification* (2013). DOI: 10.1016/j.pep.2013.07.013.

[6] M. P. Bhate and A. E. McDermott. "Protonation state of E71 in KcsA and its role for channel collapse and inactivation." In: *Proceedings of the National Academy of Sciences of the United States of America* 109.38 (Sept. 2012), pp. 15265–70. DOI: 10.1073/pnas.1211900109.

[7] M. P. Bhate, B. J. Wylie, L. Tian, and A. E. McDermott. "Conformational dynamics in the selectivity filter of KcsA in response to potassium ion concentration." In: *Journal of molecular biology* 401.2 (Aug. 2010), pp. 155–66. DOI: 10.1016/j.jmb.2010.06.031.

[8] E. G. Bligh and W. J. Dyer. "A rapid method of total lipid extraction and purification." In: *Canadian journal of biochemistry and physiology* 37.8 (Aug. 1959), pp. 911–7. DOI: 10.1139/o59-099.

[9] P. J. Brennan. "Mycobacterium and other actinomycetes." In: *Microbial Lipids Volume 1s*. Ed. by C. Ratledge and S. Wilkinson. US Ed. San Diego: Academic Press, 1988, pp. 203–298.

[10] J.-h. Chen and S. Singer. *High-Resolution Magic Angle Spinning NMR Spectroscopy*. Elsevier BV., 2007, pp. 113–147. DOI: 10.1016/B978-0-444-52841-4.50005-9.

[11] J. F. Cordero-Morales et al. "Molecular determinants of gating at the potassium-channel selectivity filter." en. In: *Nature structural & molecular biology* 13.4 (Apr. 2006), pp. 311–8. DOI: 10.1038/nsmb1069.

[12] J. E. Cronan. "Phospholipid alterations during growth of Escherichia coli." In: *Journal of bacteriology* 95.6 (June 1968), pp. 2054–61.

[13] J. E. Cronan. "Thermal Regulation of the Membrane Lipid Composition of Escherichia coli." In: *The Journal of Biological Chemistry* 250.17 (1975), pp. 7074–7077.

[14] L. G. Cuello, D. M. Cortes, and E. Perozo. "The gating cycle of a K+channel at atomic resolution." In: *eLife* 6 (2017), pp. 1–18. DOI: 10.7554/eLife.28032.

[15] A. van Dalen, S. Hegger, J. Killian, and B. de Kruijff. "Influence of lipids on membrane assembly and stability of the potassium channel KcsA." In: *FEBS Letters* 525.1-3 (Aug. 2002), pp. 33–38. DOI: 10.1016/S0014-5793(02)03061-2.

[16] J. M. Dean and I. J. Lodhi. "Structural and functional roles of ether lipids." In: *Protein & cell* 9.2 (2018), pp. 196–206. DOI: 10.1007/s13238-017-0423-5.

[17] J. A. Demmers, A. Van Dalen, B. De Kruijff, A. J. Heck, and J. A. Killian. "Interaction of the K+ channel KcsA with membrane phospholipids as studied by ESI mass spectrometry." In: *FEBS Letters* 541.1-3 (2003), pp. 28–32. DOI: 10.1016/S0014-5793(03)00282-5.

[18] S. S. Deol, C. Domene, P. J. Bond, and M. S. Sansom. "Anionic phospholipid interactions with the potassium channel KcsA: simulation studies." In: *Biophysical Journal* 90.3 (2006), pp. 822–830. DOI: 10.1529/biophysj.105.071407.

[19] J. M. Dörr et al. "Detergent-free isolation, characterization, and functional reconstitution of a tetrameric K+ channel: the power of native nanodiscs." In: *Proceedings of the National Academy of Sciences of the United States of America* 111.52 (Dec. 2014), pp. 18607–12. DOI: 10.1073/pnas.1416205112.

[20] D. A. Doyle et al. "The structure of the potassium channel: molecular basis of K+ conduction and selectivity." In: *Science (New York, N.Y.)* 280.5360 (Apr. 1998), pp. 69–77. DOI: 10.1126/science.280.5360.69.

[21] M. Grit and D. J. Crommelin. "Chemical stability of liposomes: implications for their physical stability." In: *Chemistry and Physics of Lipids* 64.1-3 (Sept. 1993), pp. 3–18. DOI: 10.1016/0009-3084(93)90053-6.

[22] M. Grit, J. H. de Smidt, A. Struijke, and D. J. Crommelin. "Hydrolysis of phosphatidylcholine in aqueous liposome dispersions." In: *International Journal of Pharmaceutics* 50.1 (Feb. 1989), pp. 1–6. DOI: 10.1016/0378-5173(89)90173-7.

[23] F. D. Gunstone, J. L. Harwood, and J. L. Harwood. *The Lipid Handbook with CD-ROM*. CRC Press, Mar. 2007. DOI: 10.1201/9781420009675.

[24] A. Guskov et al. "Cyanobacterial photosystem II at 2.9-Å resolution and the role of quinones, lipids, channels and chloride." In: *Nature Structural and Molecular Biology* 16.3 (2009), pp. 334–342. DOI: 10.1038/nsmb.1559.

[25] X. Han, J. H. Bushweller, D. S. Cafiso, and L. K. Tamm. "Membrane structure and fusion-triggering conformational change of the fusion domain from influenza hemagglutinin." In: *Nature Structural Biology* 8.8 (2001), pp. 715–720. DOI: 10.1038/90434.

[26] Y. A. Hannun and L. M. Obeid. "Principles of bioactive lipid signalling: lessons from sphingolipids." In: *Nature Reviews Molecular Cell Biology* 9.2 (Feb. 2008), pp. 139–150. DOI: 10.1038/nrm2329.

[27] L. Heginbotham, L. Kolmakova-Partensky, and C. Miller. "Functional Reconstitution of a Prokaryotic K + Channel." In: *The Journal of General Physiology* 111.6 (June 1998), pp. 741–749. DOI: 10.1085/jgp.111.6.741.

[28] C. Hunte and S. Richers. "Lipids and membrane protein structures." In: *Current Opinion in Structural Biology* 18.4 (2008), pp. 406–411. DOI: 10.1016/j.sbi.2008.03.008.

[29] L. O. Ingram. "Changes in lipid composition of Escherichia coli resulting from growth with organic solvents and with food additives." In: *Applied and environmental microbiology* 33.5 (May 1977), pp. 1233–6.

[30] G. Isenberg and V. Niggli. "Interaction of Cytoskeletal Proteins with Membrane Lipids." In: 178 (2008), pp. 73–125. DOI: 10.1016/s0074-7696(08)62136-1.

[31] M. Iwamoto and S. Oiki. "Amphipathic antenna of an inward rectifier K+ channel responds to changes in the inner membrane leaflet." In: *Proceedings of the National Academy of Sciences of the United States of America* 110.2 (Jan. 2013), pp. 749–54. DOI: 10.1073/pnas.1217323110.

[32] S. Jackowski. *Cell cycle regulation of membrane phospholipid metabolism*. 1996. DOI: 10.1074/jbc.271.34.20219.

[33] L. Kay, G. Xu, A. Singer, D. Muhandiram, and J. Formankay. "A Gradient-Enhanced HCCH-TOCSY Experiment for Recording Side-Chain 1H and 13C Correlations in H2O Samples of Proteins." In: *Journal of Magnetic Resonance, Series B* 101.3 (June 1993), pp. 333–337. DOI: 10.1006/jmrb.1993.1053.

[34] C. R. Kensil and E. A. Dennis. "Alkaline hydrolysis of phospholipids in model membranes and the dependence on their state of aggregation." In: *Biochemistry* 20.21 (Oct. 1981), pp. 6079–6085. DOI: 10.1021/bi00524a025.

[35] D. M. Kim et al. "Conformational heterogeneity in closed and open states of the KcsA potassium channel in lipid bicelles." In: *The Journal of General Physiology* 148.2 (Aug. 2016), pp. 119–132. DOI: 10.1085/jgp.201611602.

[36] T. J. Knowles et al. "Membrane Proteins Solubilized Intact in Lipid Containing Nanoparticles Bounded by Styrene Maleic Acid Copolymer." In: *Journal of the American Chemical Society* 131.22 (June 2009), pp. 7484–7485. DOI: 10.1021/ja810046q.

[37] A. J. Labro, D. M. Cortes, C. Tilegenova, and L. G. Cuello. "Inverted allosteric coupling between activation and inactivation gates in K <sup>+</sup> channels." In: *Proceedings of the National Academy of Sciences* 115.21 (2018), pp. 5426–5431. DOI: 10.1073/pnas.1800559115.

[38] A. Laganowsky et al. "Membrane proteins bind lipids selectively to modulate their structure and function." In: *Nature* 510.7503 (2014), pp. 172–175. DOI: 10.1038/nature13419.

[39] S. C. Lee et al. "A method for detergent-free isolation of membrane proteins in their local lipid environment." In: *Nature Protocols* (2016). DOI: 10.1038/nprot.2016.070.

[40] M. J. Lenaeus, D. Burdette, T. Wagner, P. J. Focia, and A. Gross. "Structures of KcsA in complex with symmetrical quaternary ammonium compounds reveal a hydrophobic binding site." In: *Biochemistry* 53.32 (2014), pp. 5365–5373. DOI: 10.1021/bi500525s.

[41] M. J. Lenaeus, M. Vamvouka, P. J. Focia, and A. Gross. "Structural basis of TEA blockade in a model potassium channel." In: *Nature Structural and Molecular Biology* 12.5 (2005), pp. 454–459. DOI: 10.1038/nsmb929.

[42] S. W. Lockless, M. Zhou, and R. MacKinnon. "Structural and thermodynamic properties of selective ion binding in a K+ channel." In: *PLoS biology* 5.5 (May 2007), e121. DOI: 10.1371/journal.pbio.0050121.

[43] T. Maoka, T. Etoh, A. Osawa, and K. Shindo. "Characterization and Singlet Oxygen Quenching Activity of (3R)-3-Hydroxy-4-Ketotorulene and (3R)-3-Hydroxy-4-Keto-ˆ|ˆgamma;- Carotene from the Yeast Xanthophyllomyces dendrorhrous." In: *Journal of Oleo Science* 61.7 (2012), pp. 401–406. DOI: 10.5650/jos.61.401.

[44] P. Marius, M. R. R. de Planque, and P. T. F. Williamson. "Probing the interaction of lipids with the non-annular binding sites of the potassium channel KcsA by magic-angle spinning NMR." In: *Biochimica et biophysica acta* 1818.1 (Jan. 2012), pp. 90–6. DOI: 10.1016/j.bbamem.2011.09.017.

[45] P. Marius et al. "Binding of anionic lipids to at least three nonannular sites on the potassium channel KcsA is required for channel opening." In: *Biophysical journal* 94.5 (Mar. 2008), pp. 1689–98. DOI: 10.1529/biophysj.107.117507.

[46] A. G. Marr and J. L. Ingraham. "Effect of temperature on teh composition of fatty acids in Escherichia coli." In: *Journal of bacteriology* 84.6 (Dec. 1962), pp. 1260–7.

[47] K. Matulef, A. W. Annen, J. C. Nix, and F. I. Valiyaveetil. "Individual Ion Binding Sites in the K+Channel Play Distinct Roles in C-type Inactivation and in Recovery from Inactivation." In: *Structure* 24.5 (2016), pp. 750–761. DOI: 10.1016/j.str.2016.02.021.

[48] V. Matyash, G. Liebisch, T. V. Kurzchalia, A. Shevchenko, and D. Schwudke. "Lipid extraction by methyl-tert-butyl ether for high-throughput lipidomics." In: *Journal of lipid research* 49.5 (May 2008), pp. 1137–46. DOI: 10.1194/jlr.D700041-JLR200.

[49] G. van Meer, D. R. Voelker, and G. W. Feigenson. "Membrane lipids: where they are and how they behave." In: *Nature Reviews Molecular Cell Biology* 9.2 (Feb. 2008), pp. 112–124. DOI: 10.1038/nrm2330.

[50] P. Meneses and T. Glonek. "High resolution 31P NMR of extracted phospholipids." In: *Journal of lipid research* 29.5 (1988), pp. 679–89.

[51] M. L. Molina et al. "Influence of C-terminal protein domains and protein-lipid interactions on tetramerization and stability of the potassium channel KcsA." In: *Biochemistry* 43.47 (2004), pp. 14924–14931. DOI: 10.1021/bi048889+.

[52] M. L. Molina et al. "Competing lipid-protein and protein-protein interactions determine clustering and gating patterns in the potassium channel from streptomyces lividans (KcsA)." In: *Journal of Biological Chemistry* 290.42 (2015), pp. 25745–25755. DOI: 10.1074/jbc.M115.669598.

[53] W. O'Leary and S. Wilkinson. "Gram positive lipids." In: *Microbial Lipids Volume 1*. Ed. by C. Ratledge and S. Wilkinson. London: Academic Press, 1989.

[54] D. J. Posson, A. N. Thompson, J. G. McCoy, and C. M. Nimigean. "Molecular interactions involved in proton-dependent gating in KcsA potassium channels." In: *The Journal of general physiology* 142.6 (Dec. 2013), pp. 613–24. DOI: 10.1085/jgp.201311057.

[55] J. Poveda et al. "Lipid modulation of ion channels through specific binding sites." In: *Biochimica et Biophysica Acta (BBA) - Biomembranes* 1838.6 (June 2014), pp. 1560–1567. DOI: 10.1016/j.bbamem.2013.10.023.

[56] M. Raja. "The role of phosphatidic acid and cardiolipin in stability of the tetrameric assembly of potassium channel KcsA." In: *The Journal of membrane biology* 234.3 (Apr. 2010), pp. 235–40. DOI: 10.1007/s00232-010-9251-8.

[57] M. Raja, R. E. Spelbrink, B. de Kruijff, and J. A. Killian. "Phosphatidic acid plays a special role in stabilizing and folding of the tetrameric potassium channel KcsA." In: *FEBS Letters* 581.29 (2007), pp. 5715–5722. DOI: 10.1016/j.febslet.2007.11.039.

[58] D. M. Rosenbaum, S. G. Rasmussen, and B. K. Kobilka. "The structure and function of G-protein-coupled receptors." In: *Nature* 459.7245 (2009), pp. 356–363. DOI: 10.1038/nature08144.

[59] S. P. Rucker and A. J. Shaka. "Broadband homonuclear cross polarization in 2D N.M.R. using DIPSI-2." In: *Molecular Physics* 68.2 (1989), pp. 509–517. DOI: 10.1080/00268978900102331.

[60] M. J. Ruocco, A. Makriyannis, D. J. Siminovitch, and R. G. Griffin. "Deuterium NMR investigation of ether- and ester-linked phosphatidylcholine bilayers." In: *Biochemistry* 24.18 (Aug. 1985), pp. 4844–4851. DOI: 10.1021/bi00339a018.

[61] A. Shaka, J. Keeler, and R. Freeman. "Evaluation of a new broadband decoupling sequence: WALTZ-16." In: *Journal of Magnetic Resonance (1969)* 53.2 (June 1983), pp. 313–340. DOI: 10.1016/0022-2364(83)90035-5.

[62] B. Shanmugavadivu, H. J. Apell, T. Meins, K. Zeth, and J. H. Kleinschmidt. "Correct Folding of the β-Barrel of the Human Membrane Protein VDAC Requires a Lipid Bilayer." In: *Journal of Molecular Biology* 368.1 (2007), pp. 66–78. DOI: 10.1016/j.jmb.2007.01.066.

[63] N. Sotirhos, B. Herslöf, and L. Kenne. "Quantitative analysis of phospholipids by 31P-NMR." In: *Journal of lipid research* 27.4 (1986), pp. 386–92.

[64] A. Souvorov et al. *Ethanolamine*. 2006. DOI: 10.13018/BMSE000276.

[65] A. Souvorov et al. *Glycerol*. 2011. DOI: 10.13018/BMSE000856.

[66] C. Stange, ed. *Carotenoids in Nature*. Vol. 79. Subcellular Biochemistry. Cham: Springer International Publishing, 2016. DOI: 10.1007/978-3-319-39126-7.

[67] R. E. Stark and H. C. Gaede. "NMR of a Phospholipid: Modules for Advanced Laboratory Courses." In: *Journal of Chemical Education* 78.9 (Sept. 2001), p. 1248. DOI: 10.1021/ed078p1248.

[68] Z. Sun, Y. Xu, D. Zhang, and A. E. McDermott. "Studies of Allosteric Coupling in KcsA Using a Constitutively Open Mutant." In: *Proceedings of the National Academy of Sciences* submitted, (2019), pp. 1–12. arXiv: 567024 [10.1101].

[69] J. L. Taylor et al. "High-resolution magic angle spinning proton NMR analysis of human prostate tissue with slow spinning rates." In: *Magnetic Resonance in Medicine* 50.3 (Sept. 2003), pp. 627–632. DOI: 10.1002/mrm.10562.

[70] A. N. Thompson et al. “Mechanism of potassium-channel selectivity revealed by Na+ and Li + binding sites within the KcsA pore.” In: *Nature Structural and Molecular Biology* 16.12 (2009), pp. 1317–1324. DOI: 10.1038/nsmb.1703.

[71] J. C. Touchstone, J. C. Chen, and K. M. Beaver. “Improved Separation of Phospholipids.” In: 5 (1979).

[72] I. Triano et al. “Occupancy of nonannular lipid binding sites on KcsA greatly increases the stability of the tetrameric protein.” In: *Biochemistry* 49.25 (2010), pp. 5397–5404. DOI: 10.1021/bi1003712.

[73] F. I. Valiyaveetil, R. MacKinnon, and T. W. Muir. “Semisynthesis and folding of the potassium channel KcsA.” In: *Journal of the American Chemical Society* 124.31 (2002), pp. 9113–9120. DOI: 10.1021/ja0266722.

[74] F. I. Valiyaveetil, Y. Zhou, and R. MacKinnon. “Lipids in the structure, folding, and function of the KcsA K+ channel.” In: *Biochemistry* 41.35 (2002), pp. 10771–10777. DOI: 10.1021/bi026215y.

[75] F. I. Valiyaveetil, M. Leonetti, T. W. Muir, and R. Mackinnon. “Ion selectivity in a semisynthetic K+ channel locked in the conductive conformation.” In: *Science (New York, N.Y.)* 314.5801 (Nov. 2006), pp. 1004–7. DOI: 10.1126/science.1133415.

[76] E. van den Brink-van der Laan, V. Chupin, J. A. Killian, and B. de Kruijff. “Stability of KcsA Tetramer Depends on Membrane Lateral Pressure †.” In: *Biochemistry* 43.14 (Apr. 2004), pp. 4240–4250. DOI: 10.1021/bi036129d.

[77] G. F. White, N. J. Russell, and E. C. Tidswell. “Bacterial scission of ether bonds.” In: *Microbiological Reviews* 60.1 (1996), pp. 216–232.

[78] B. J. Wylie, M. P. Bhate, and A. E. McDermott. “Transmembrane allosteric coupling of the gates in a potassium channel.” In: *Proceedings of the National Academy of Sciences of the United States of America* 111.1 (Jan. 2014), pp. 185–90. DOI: 10.1073/pnas.1319577110.

[79] Y. Xu, M. P. Bhate, and A. E. McDermott. “Transmembrane allosteric energetics characterization for strong coupling between proton and potassium ion binding in the KcsA channel.” In: *Proceedings of the National Academy of Sciences of the United States of America* 114.33 (Aug. 2017), pp. 8788–8793. DOI: 10.1073/pnas.1701330114.

[80] P. L. Yeagle. “Non-covalent binding of membrane lipids to membrane proteins.” In: *Biochimica et Biophysica Acta - Biomembranes* 1838.6 (2014), pp. 1548–1559. DOI: 10.1016/j.bbamem.2013.11.009.

[81] S. Yohannan, Y. Hu, and Y. Zhou. “Crystallographic Study of the Tetrabutylammonium Block to the KcsA K+Channel.” In: *Journal of Molecular Biology* 366.3 (2007), pp. 806–814. DOI: 10.1016/j.jmb.2006.11.081.

[82] E. Zakharian and R. N. Reusch. "Functional evidence for a supramolecular structure for the Streptomyces lividans potassium channel KcsA." In: *Biochemical and Biophysical Research Communications* 322.3 (2004), pp. 1059–1065. DOI: 10.1016/j.bbrc.2004.08.027.

[83] D. Zhang, B. Itin, and A. E. McDermott. "TmDOTP : An NMR- based Thermometer for Magic Angle Spinning NMR Experiments 2." In: *bioRxiv* (2019), pp. 1–10. DOI: 10.1101/566729..

[84] M. Zhou and R. MacKinnon. "A mutant KcsA K+channel with altered conduction properties and selectivity filter ion distribution." In: *Journal of Molecular Biology* 338.4 (2004), pp. 839–846. DOI: 10.1016/j.jmb.2004.03.020.

[85] Y. Zhou, J. H. Morais-Cabral, A. Kaufman, and R. MacKinnon. "Chemistry of ion coordination and hydration revealed by a K+ channel-Fab complex at 2.0 A resolution." In: *Nature* 414.6859 (Nov. 2001), pp. 43–8. DOI: 10.1038/35102009.

[86] Y. Zhou and R. MacKinnon. "The occupancy of ions in the K+selectivity filter: Charge balance and coupling of ion binding to a protein conformational change underlie high conduction rates." In: *Journal of Molecular Biology* 333.5 (2003), pp. 965–975. DOI: 10.1016/j.jmb.2003.09.022.

[87] N. J. Zuidam, H. E. Gouw, Y. Barenholz, and D. J. Crommelin. "Physical (in) stability of liposomes upon chemical hydrolysis: the role of lysophospholipids and fatty acids." In: *Biochimica et Biophysica Acta (BBA) - Biomembranes* 1240.1 (Nov. 1995), pp. 101–110. DOI: 10.1016/0005-2736(95)00180-5.

# INVESTIGATIONS OF DNP ENHANCEMENTS ON KCSA 4

## 4.1 ABSTRACT

NMR is an inherently insensitive technique and large, dilute molecules pose particular challenges. Dynamic nuclear polarization-enhanced magic angle spinning NMR (DNP) is able to enhance signal by more than two orders of magnitude by converting electron spin polarization to nuclear spin polarization. This technology enables spectroscopists to access much more dilute systems and dramatically reduce data acquisition time. However, membrane proteins have proven to be difficult targets for this technology with lower than typical DNP enhancements. Here several aspects of sample preparation for KcsA DNP are investigated on a 600 MHz / 395 GHz NMR spectrometer/ gyrotron system using the soluble biradical AMUPol. The data show that the poor enhancement is not intrinsic to KcsA and that large enhancements can be achieved in the absence of lipids. Fractional deuteration on KcsA provides modest improvements to DNP enhancement compared to fully protonated samples. Dissolved $^{15}$N-glycine is introduced as a powerful diagnostic internal standard.

As discussed at length in Chapter 1, NMR is an inherently insensitive technique. The problem of insensitivity is compounded when performing NMR on large molecules, such as proteins, as the sample concentration becomes increasingly dilute as the molecular weight of the compound increases. Proteins embedded in membranes suffer from an additional loss of sensitivity, as the sample is diluted by the presence of lipids. When a membrane is placed in an equal amount of lipid, for example, the effective concentration is halved, decreasing signal-to-noise by a factor of four (Equation 1.9).

A typical protein will have considerable degeneracy of resonances in a 1D spectrum and often even in 2D correlations, and this is particularly the case for solid-state spectra where peaks tend to be broader. This problem is made worse still with proteins that have extensive $\alpha$-helix domains, as is the case with many membrane proteins, as the similar environment for the residues with a helix leads to less chemical shift dispersion. Higher dimensional spectra are applied to resolve these crowed spectra, a the acquisition time required increases exponentially with the number of dimensions. A complete data set of a 3D spectrum can easily demand two weeks of spectrometer time. Most assignment strategies require at least two complimentary 3D spectra, and so the endeavor of protein NMR assignment can become costly in terms of instrument time.

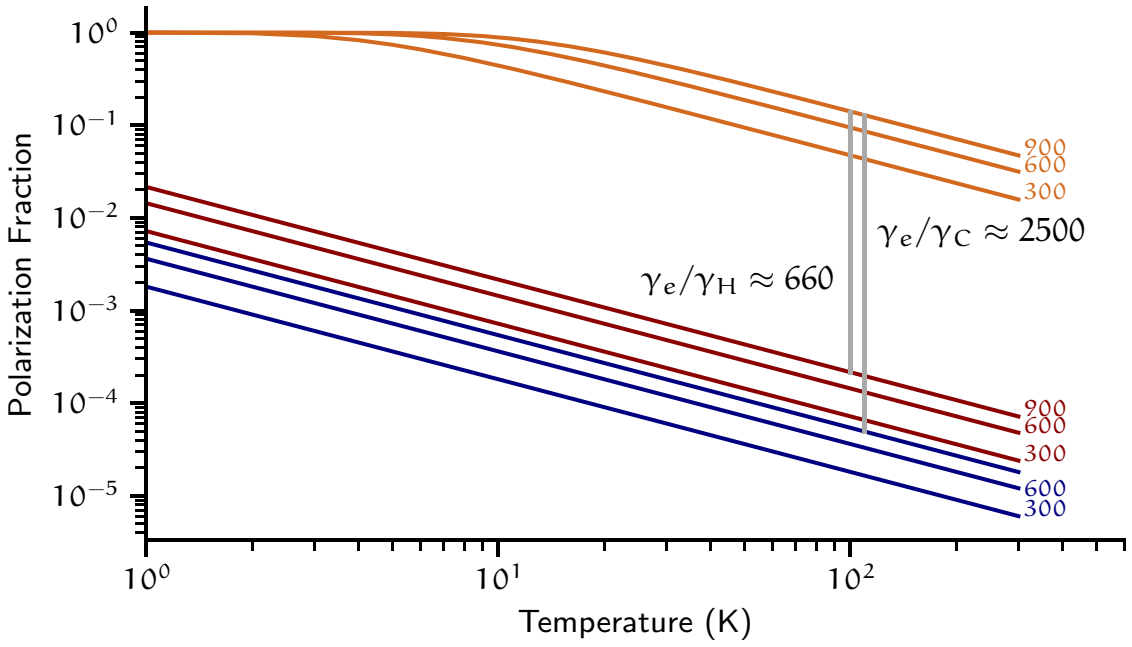


FIGURE 4.1: Polarization fraction of electron spins (orange), and $^1$H (red) and $^{13}$C (blue) nuclear spins at three magnetic fields (300, 600, and 900 MHz) over a range of temperatures.

In Chapter 2, proton detection by HR-MAS was shown to accelerate 3D data acquisition of mobile portions of KcsA when compared to carbon-detection. Dynamic nuclear polarization-enhanced NMR (DNP) provides another strategy to increase sensitivity through polarization enhancement. Further, the conditions under which DNP is performed is conducive to examining even highly mobile regions of proteins using solid-state techniques.

### 4.2.1 *Dynamic Nuclear Polarization*

DNP is a process by which electron spin polarization is converted into nuclear spin polarization. As a general principal, the transition energy between the spin-states in a

spin-$^1/_2$ system (e.g. $^1$H, $^{13}$C, $^{15}$N nuclei, or the electron) in an external magnetic field ($B_0$) is given by:

$$\Delta E = \hbar \gamma B_0 = h\nu \tag{4.1}$$

where $\Delta E$ is the energy difference between states (in this case the Zeeman energy), $h$ is Planck's constant, $\gamma$ is the gyromagnetic ratio of the nuclide (or electron), and $\nu$ is the Larmor frequency of the spin. The Boltzmann distribution describes the distribution of states of a population of spins, and the ratio of the two spin-states ($\alpha$ and $\beta$ is described by:

$$\frac{N_\beta}{N_\alpha} = exp\left(\frac{-\Delta E}{kT}\right) \tag{4.2}$$

where $N$ is the number of spins in the state, $\Delta E$ is the difference in energy between the states, $k$ is the Boltzmann constant and $T$ the temperature of the system.

Electrons and protons differ in their gyromagnetic ratio (2800 and 43 $MHz\,T^{-1}$, respectively). A set of solutions to Equation 4.1 and Equation 4.2 for an ensemble of electrons and for $^1$H and $^{13}$C nuclei is plotted for typical NMR conditions (Figure 4.1), specifically indicating that at commercially available magnetic fields for NMR at 100 K, the difference in polarization of unpaired electrons and free protons is approximately 660.

When a metal with spin-$\frac{1}{2}$ nuclei (e.g. such as $^{207}$Pb or $^{103}$Rh), for example, is placed into a static magnetic field, two set of Zeeman levels are observed: two levels each for the nucelei and for the conduction band electrons [32]. Overhauser [58] predicted (and Carver and Slichter [19] subsequently measured) that an alternating magnetic applied to a metal leads to a decrease in the population difference (i.e. polarization) between the electron states, which they termed "saturation." This saturation is caused by a resonance transition between the electron and nuclear spins, leading to a massive effective increase in nuclear spin polarization. Electron spin resonance (ESR) from unpaired electrons to protons was first demonstrated in the stable radical DPPH [12]. ESR saturation of sodium metal dissolved in liquid ammonium was then show to produce a nuclear spin signal enhancement of ammonia protons by more than 4000 % [20], the first example of dynamic nuclear polarization.

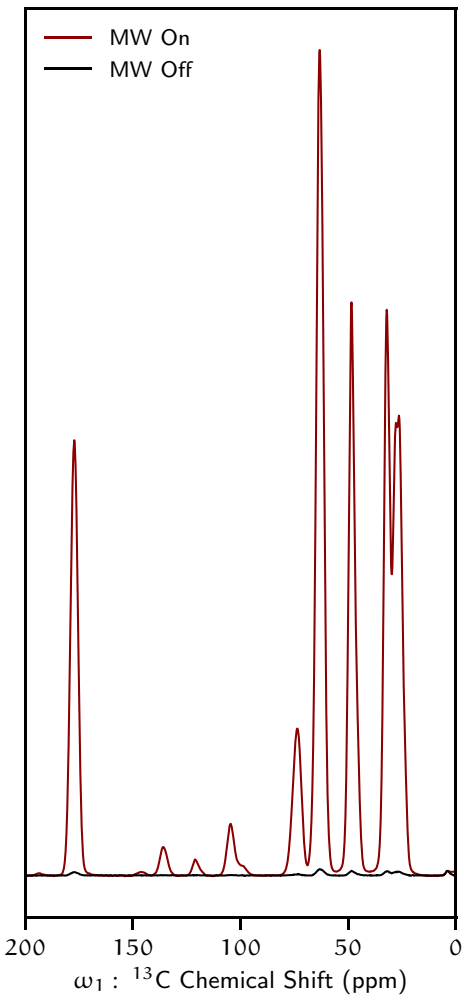


FIGURE 4.2: DNP-enhanced NMR. $^{13}$C CP-MAS NMR spectrum of $^{13}$C-proline at 105 K with 20 mM AMUpol, 3:2:1 $^{2}$H-glycerol-$D_2O$-$H_2O$ with microwave source off (black) and microwaves on (red). Enhancement is 125

### 4.2.2 *Dynamic Nuclear Polarization and Nuclear Magnetic Resonance*

The 1940s and 1950s were a breathless time in magnetic resonance. The discovery of NMR was made in 1946 by Purcell, Torrey, and Pound [62] and Bloch, Hansen, and Packard [17]. The observation that the chemical environment affects the energy levels, and hence frequency, of the nuclear magnetic moment in 1950 [24, 61] led to collection of spectra that resolved three distinct nuclear spins in ethanol [6], establishing NMR as an essential tool in organic chemistry for the rest of time in 1951. The observation of J-coupling [33] was presented that same year. The first double resonance NMR experiments were made by Royden [65] in 1954. In 1956 Bloch published his seminal theory of NMR relaxation, which is still taught today [16]. Abragam and Proctor [2] showed ESR could enhance NMR signal and then immediately published work applying that theory to practical enhancement of $^{13}C$ signal for coal samples [1] (an inspired choice of model system due to piqued interest in the subject, the abundance of free electrons in the system, and the chemical diversity).

From there, the use of NMR became indispensable to chemists, while DNP became a niche area of research employed by a subset of nuclear physicists. The use of DNP to enhance NMR signal was then largely abandoned for the next thirty years.

One central barrier to the application of DNP at modern NMR magnet frequencies (>2.3 T or 100 MHz $^1H$ field) was lack of sufficiently high-power, high frequency microwave sources needed to stimulate the ESR transition at these fields. At 5 T, for example, an electron resonance frequency is $1.4 \times 10^{11}$ Hz, which far exceed typical

microwave frequency sources. Also, there are few microwave sources that have a duty-cycle that can endure for many hours of continuous power output. The lab of Robert Griffin launched the modern DNP movement by overcoming this technical barrier, demonstrating purpose-built, high-power maser [11] and gyrotron [10] microwave sources that could be used to transfer polarization from unpaired electrons in stable nitroxide radicals while conducting NMR at 5 T. Shortly after, that same group demonstrated a DNP signal enhancement of nearly 100 on $^{15}$N-arginine labeled T4 lysozyme at 5 T [34] using the nitroxide radical TEMPO (Figure 4.3).

In the last 20 years, DNP for biological systems has exploded with over a hundred publications using the technique in 2018 alone. There have been considerable advances in gyrotron and radical, magic angle spinning, and NMR in general all converging to realizing the potential of dynamic nuclear polarization NMR.

### 4.2.3 *DNP Today*

Today, commercial DNP-NMR spectrometers are in production and the technique has found considerable use in the biological and material sciences.

Typically, solid-state NMR of biological samples is performed at temperatures near 250 K, which is easily reached easily by modern equipment, decreases dynamics, and yet maintains a liquid hydration layer around macromolecules [72]. Yet, DNP-enhanced NMR is typically performed at temperatures near 100 K [40] or below. Liquid helium driven systems routinely operate at 40 K [10] or as low as 4 K [39]. DNP

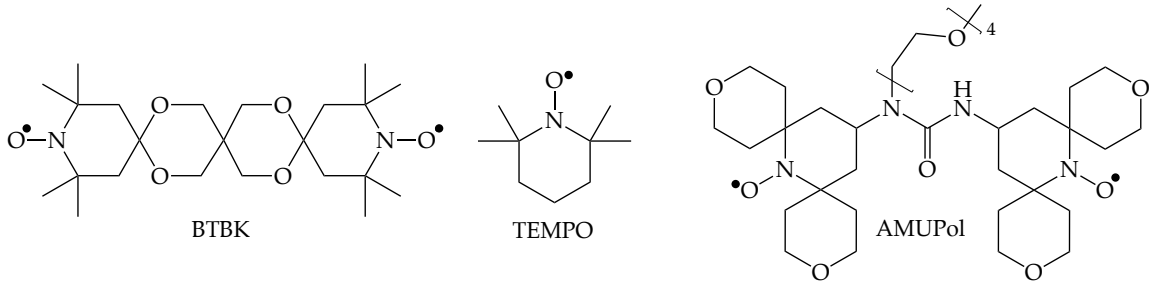


FIGURE 4.3: Nitroxide radicals commonly used in DNP.

NMR tends to use low temperatures because $T_1$ relaxation is increased, reducing leakage of proton polarization and increasing electron-electron cross relaxation efficiency [34]. Also, the low temperatures reduce damage to delicate samples being subjected to 20–200 $W$ of microwave radiation.

The typical unpaired electron source for DNP experiments have been nitroxide radical species. The compound AMUPol (4.3)[67] was used throughout the experiments described in this chapter. These studies were collected on a 14.1 T magnet equipped with a gyrotron operating at 395 GHz as source to stimulate the ESR transition.

The effectiveness of polarization transfer is generally measured as the factor ($\epsilon$) by which signal increases for the system when the microwave source is on versus when it is off:

$$\epsilon = \frac{\text{Max Signal}_{\text{MW ON}}}{\text{Max Signal}_{\text{MW OFF}}} \tag{4.3}$$

Biological DNP presents some especially difficult challenges, and perhaps none greater than sample inhomogeneity. At DNP temperatures, around 100 K, biological

samples become solid, with much of sample buffer forming a crystalline structure. Biomolecules such as proteins, lipids, and nucleic acids, however, have less well defined relationships to states of matter, and rarely form a crystalline network under these conditions. The hydration shell of those biomolecules, for example, is unlikely to be in a crystalline state [72] at 100 K.

Small molecules are often added to a sample matrix to prevent bulk ice formation. These cryoprotectant substances are generally uncharged, polar molecules dissolved into water in a requisite quantity to disrupt water hydrogen bonding patterns at 100 K. Such protective measures typically increase DNP enhancements by an order of magnitude [34]. Cryoprotetants have been used in the presence of membrane proteins to increase DNP enhancement. Lee and Hong in [47] examined the performance of various cryoprotectants on the transmembrane domain of the M2 protein in lipid bilayers and found that DMF, DMSO, and glycerol performed similarly well with glycerol having a slight (≈10 %) effect on enhancement, yielding enhancement of 100 on C$\alpha$ sites.

In order to maximize signal, samples must be optimized to transfer electron spin polarization to nuclear spin polarization. Diluting the sample with cryoprotectants sacrifices signal. Similarly, the spin polarization may transfer into the matrix constituents rather than targeting the sample. Deuteration of the buffer and matrix elements is a popular tool to concentration spin diffusion to analytes of interest [37]. Deuteration in particular must be done cautiously, as a bulk protein reservoir proves critical as a network to distribute polarization and as nuclear spin reservoir for cross-polarization

(CP) experiments, which are the backbone of solid-state spectroscopy. In a model membrane protein system, in fact, [50] showed that perdeuteration of lipids doubled the enhancement of an embedded protein, but that the effect on CP efficiency was decreased by nearly the same factor, providing little benefit.

On the system on which these studies were performed, at the New York Structural Biology Center, DNP often achieves enhancements of about 150 for model systems (e.g. $^{13}C$,$^{15}N$-proline with 20 mM AMUPol dissolved in $^{2}H$-50 % glycerol, 40 % $D_2O$, 10 % $H_2O$ by mass). Sample conditions have a major role in successful DNP enhancement. Sample temperature, polarizing agent, polarizing agent concentration, protein concentration, polarization buildup time, polarization agent/sample homogenization, ice/glass formation, concentration of protons and many other factors affect the efficiency of enhancement.

Because membrane protein systems have inherently poor sensitivity due to sample dilution, there is considerable interest in applying DNP to these systems. Some membrane protein systems give excellent enhancements under DNP such as bacteriorhodopsin by 90 [8], t4sscc membrane associated complex by 60 [42], and M2 (transmembrane domain) by 100 [50], and ROCKER peptide by 80 [50], with these measurements being made on 400 MHz/263 GHz, magnet/gyrotron frequencies. Many attempts in our group have been unable to enhance KcsA samples beyond 20, with enhancements of 5–15 more common. In fact, there is a notable lack of studies of ion channels by DNP in the literature.

In general, there are very few reports of membrane proteins studied by DNP-enhanced NMR. Despite several laboratories pursuing DNP-enhanced measurements of KcsA (personal communication), there are only two published reports of these efforts. Visscher et al. [79] describes dilute KcsA clustering in liposomes by 1D NMR achieving indirect DNP enhancements ($e^- \xrightarrow{\mu} {}^1H \xrightarrow{CP} {}^{15}N$) of 25–50 with AMUPol radical at 15 mM on a 400 MHz / 263 GHz DNP system. Van Der Cruijsen et al. [77] used soluble AMUPol and AMUPol-methylsilane derivative covalently linked to a KcsA mutant on both a 400 MHz/263 GHz and 800 MHz /527 GHz. The AMUPol experiment enhanced KcsA by 16 at 400 MHz, but enhancements were merely 4 the same sample at 800 MHz system. Site-directed tag performed similarly at both fields, achieving a maximum of ~18. These measurements agree with the field dependence on the performance of soluble AMUPol [67], but it is unclear why the tagged system has such similar behavior at two different fields.

### 4.2.4 *Polarization Buildup*

The transfer of electron polarization to nuclear polarization requires a buildup time and the rate of the buildup is dependent on the concentration and source of unpaired electrons, the concentration of the nuclei, the distance between the electrons and the target nuclei, magnetic field strength, microwave field strength and frequency, polarization pathway, and a number of more poorly understood factors [73].

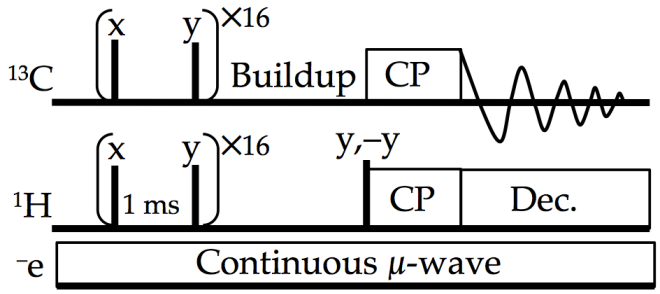


FIGURE 4.4: Diagram of NMR pulse sequence used to measure DNP polarization buildup rates on of $^{1}$H spins, where the 'buildup' period is varied over a range of times in a pseudo-2D experiment. The sequence uses cross polarization to detect on $^{13}$C (shown here) or $^{15}$N to improve resolution. Solid lines indicate 90°-hard pulses. $^{1}$H CP pulse is x phase; $^{13}$C CP phase cycle is x x -x -x y y -y -y; and receiver phase cycle is x -x -x x y -y -y y.

In this work, the $^{1}$H polarization buildup times are measured using the pulse sequence described in Figure 4.4, where transverse-plane magnetization is dephased by a series of pulses, polarization is allowed to build up for a period of time on $^{1}$H, magnetization is transferred to either $^{13}$C or $^{15}$N using cross polarization and then detected. The data acquired by varying the buildup period are fit monoexpoenential model, where measured signal (S) is predicted by the buildup time (t) and a buildup constant ( ):

$$S(t) = S_{max} \quad 1 \quad e^{-\frac{t}{}} \tag{4.4}$$

### 4.2.5 *It's Not All About Enhancement*

The experimental conditions demanded by DNP increase the line

widths of NMR resonances. Figure 4.5 demonstrates, as an example, the difference in the linewidth for the amide nitrogen in a CP-MAS experiment when the temperature is lowered from 300 K to 100 K. Although the overall signal of the sample at 100 K is improved with a 5-fold increase in signal intensity measured by integration, the linewidth increases 4-fold, thus only increasing the effective signal-to-noise of the peak by a factor of 1.6. The improved signal is likely due to an increase in cross polarization efficiency due to larger contribution of $^{1}$H-$^{13}$C dipolar coupling at the lower temperature [18].

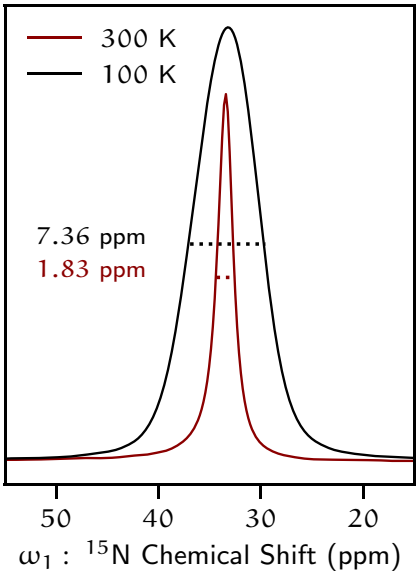


FIGURE 4.5: $^{15}$N CP-MAS spectrum of crystalline $^{13}$C,$^{15}$N-glycine collected at 300 K (red) and 100 K (black). FWHM indicated for each peak. Probe tuned and shimmed, and experiment optimized for each temperature. 10 kHz MAS.

The effect of lower temperature is more pronounced and more complicated in a protein. There exists a generally observed 'protein glass transition' that occurs between 160–230 K [26, 27, 69]. This transition leads to substantial inhomogeneous resonance linewidth broadening of proteins at low temperature [7, 80]

The addition of an exogenous radical can lead to increases of resonance linewidths. Specifically, the radicals at concentrations used for DNP have been shown to exhibit a large paramagnetic relaxation enhancement on spin-spin ($T_2$) relaxation of nearby species [23, 41, 49, 50].

## 4.3 RESULTS

### 4.3.1 *'Unlabeling' Aliphatic Residues in KcsA*

Previous work in the McDermott group (unpublished) showed that KcsA by typical DNP sample preparation methods leads to modest DNP enhancements of less than 20. Further, in KcsA samples at 250 K in the $^{13}C$-$^{13}C$ CP-MAS spectrum there are more than one hundred 100 resonances resolved, where with DNP only broad regions are resolved.

In order to reduce the number of correlations in DNP spectra of KcsA and to bias the remaining correlations toward the termini, a metabolic isotopic labeling scheme was developed.

Proteins for NMR study are typically isotopically enriched to improve signal-to-noise. Much of this work has focused on uniformly-$^{13}C/^{15}N$ enriched proteins. However, a common tool is to selectively enrich key amino acids to leave only a few correlations of interest. Another strategy is periodically employed with selectively unlabels (frequently called 'reverse labeling'), that targets particular sites for placement

of natural abundance atoms. (See Verardi et al. [78] for a review of the topic of selective isotopic and metabolic labeling in NMR.) Bellstedt et al. [13] performed a heroic study in which the protein GB1 was expressed in BL21(DE3) *E. coli* cells in M9 minimal media supplemented with U-$^{13}$C-glucose and $^{15}$N-ammonium chloride. Trials were conducted of supplementing growths with individual natural abundance amino acids and tracking which atom positions were successfully unlabeled. In some cases supplementing the growth with an excess of a particular natural abundance amino acid leads to the unlabeling of several residues in a process often called "scrambling".

This downstream metabolic labeling process is typically an inconvenience by silencing or labeling unintended resonances. However, here an unlabeling scheme was developed to express KcsA enriched with U-$^{13}$C-glucose and $^{15}$N-ammonium chloride and supplement the media with a variety of natural abundance amino acids to both directly unlabel particular amino acids and also lead to unlabeling of some downstream targets. The aim of the scheme was to deprive $^{13}$C and $^{15}$N enrichment to aliphatic residues. This would have the effect of reducing the total number of correlations and also target the transmembrane domain of KcsA in particular for unlabeling, biasing remaining correlations to the termini region. A map of the desired labeling scheme on the KcsA sequence can be found at Figure A.1. The specific scheme exploits pathways that leads to deprivation of enriched amino acids to both carbonyl and/or amide nitrogen such that very 2 N-CO pairs were expected to be labeled in the transmembrane domain (residues 25-116) and many 17 pairs would be labeled in the C-terminus (residues 118-140); and 5 in the N-terminus (residues 1-25).

| **Directly Unlabeled Residue** | | | **Scrambled Products** | | |
|---|---|---|---|---|---|
| | % N.A.-CO | % N.A.-N | | % N.A.-CO | % N.A.-N |
| Ala | 90 | 100 | | | |
| Gly | 70 | 100 | Trp | 70 | 50 |
| | | | Ser | >50 | 100 |
| Ile | 100 | 80 | | | |
| Leu | 100 | 80 | Ile | | 80 |
| Phe | 100 | 70 | Tyr | | 60 |
| Thr | 100 | 100 | Gly | 50 | |
| | | | Trp | | 50 |
| Tyr | 100 | 50 | Phe | | 50 |
| Val | 100 | 100 | | | |

TABLE 4.1: Proposed aliphatic unlabeling pattern. The left columns specify natural abundance amino acids supplemented directly to the M9 media and the expected extent to which the amide nitrogen and carbonyl carbon will be unlabeled (percent of amino acids natural abundance). The right columns shows which amino acids are expected to be unlabelled as downstream metabolic products from the amino acid supplemented to the material in the same row. Unlabeling predictions from [13, 44].

Aliphatic unlabeled KcsA was expressed and reconstituted into lipids with a 1 : 1 mass ratio using 9 : 1 DOPE-DOPS (w/w) lipids. Previous work has suggested that radical concentration for DNP samples must be empirically optimized with a typical range between 5–100 mM producing the best enhancements, [46, 50, 66], though 15–20 mM is the most common for nitroxides [4].

AMUPol radical was titrated with KcsA proteoliposome pellets in the presence of cyroprotectants by adding aliquots of 200 mM AMUpol in matched cryo-protectant/buffer over a range of 5–40 mM. The results of this radical titration experiment are summarized in Figure 4.6. The titration shows that there is little effect over that particular range, which 12 mM providing the best overall enhancement.

Each amino acid has characteristic shifts in the $^{13}C$-$^{13}C$ spectrum that can be used to identify the type of residue. Type-assignment in this case was accelerated as the majority of KcsA resonances in CP-MAS samples have previously been assigned [82]. The outcome of the aliphatic unlabeling scheme was evaluated using a DNP enhanced $^{13}C$-$^{13}C$ dipolar driven rotational resonance experience (DARR) with a 50 ms mixing time (Figure 4.7) and the findings of that analysis are summarized in Table 4.2. The scheme finds many of the residues expected to be unlabeled are in fact present. In particular, there are peaks in the alanine C$\alpha$-C$\beta$ region and in the valine C$\alpha$-C$\beta$ region although no apparent C$\beta$-C$\gamma$ correlations are found. The intensity of the aliphatic region in general is vastly attenuated and the unlabeled spectrum is much cleaner and better resolved (Figure 4.8). In fact, the uniformly labeled sample has essentially no individual sites which are discernible in the $^{13}C$-$^{13}C$ spectrum, whereas the aliphatic

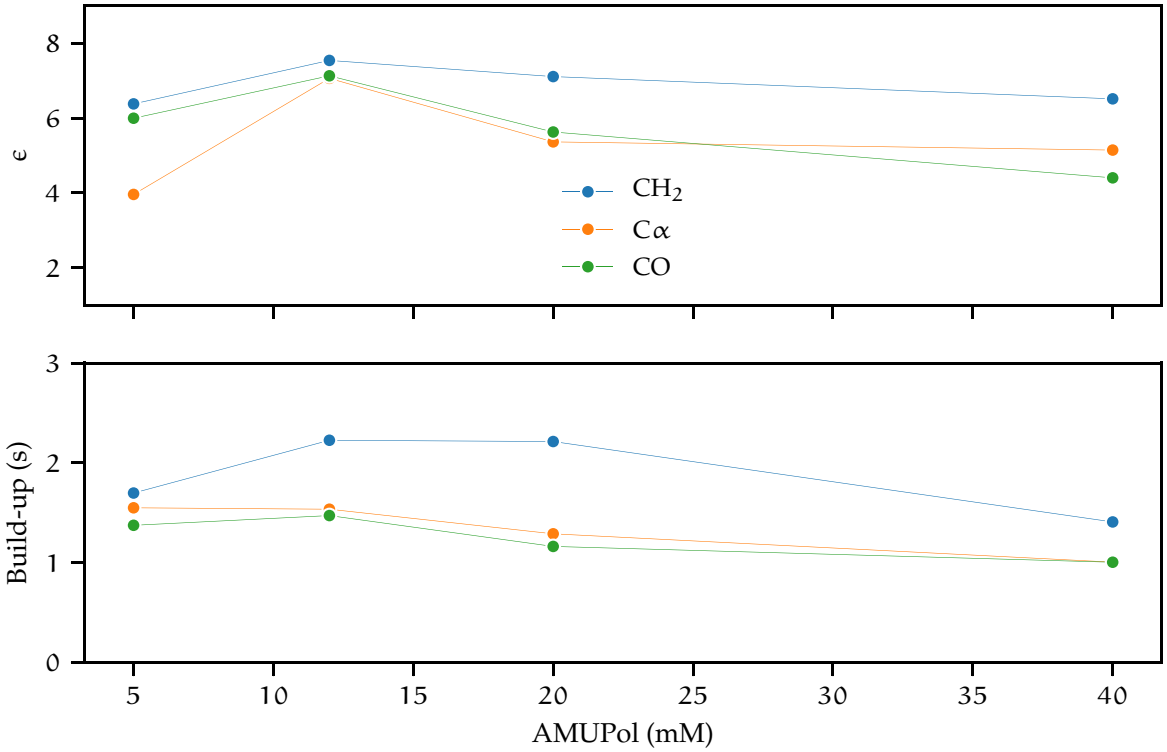


(A) Effect of AMUPol concentration on $^{13}C$ CP enhancement and polarization buildup constants. Peak regions are defined as specified in Figure 4.6b.

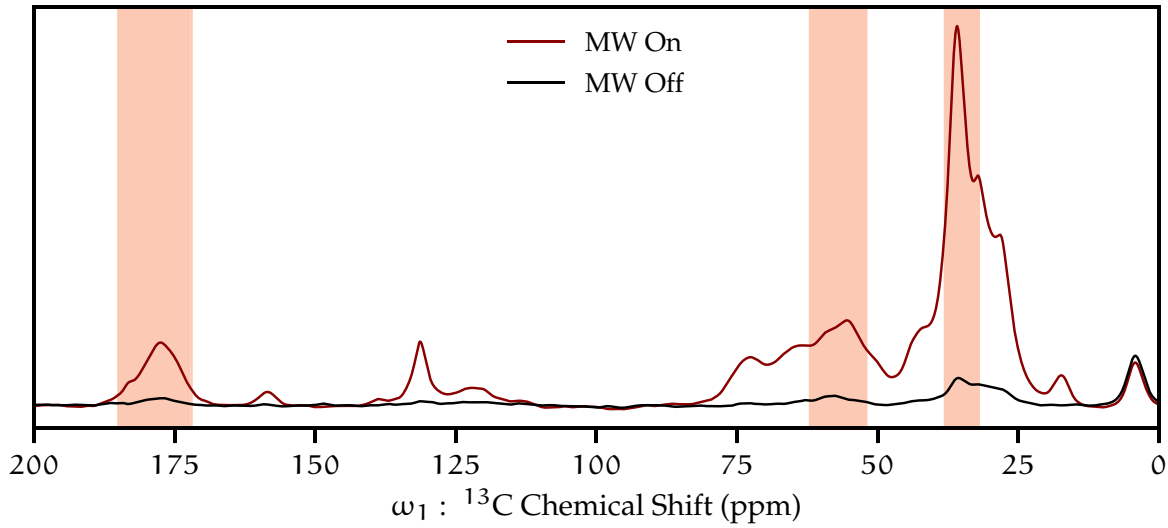


(B) $^{13}C$ CP-MAS spectra of KcsA enhanced by AMUPol. Shaded bands indicate regions used for $\pi$ and buildup time constants presented in Figure 4.6a. 12 mM AMUPol.

FIGURE 4.6: Effect of AMUPol on DNP Enhancement of 'Reverse-labeled'-KcsA in 9 : 1 DOPE-DOPS, LPR=1, pH 7.5, 105 K,11 kHz MAS 3 : 4 glycerol-$D_2O$.

| Residue | N.A. AA | Expectation | Outcome |
|---|---|---|---|
| Ala | Direct | – | Attenuated |
| Arg | | + | Yes (coil and helix) |
| Asn | | + | Degen. |
| Asp | | + | N.D. ($\beta - \gamma$) |
| Gln | | + | Degen. |
| Glu | | + | Degen. |
| Gly | Direct | – | Attenuated |
| His | | + | Present |
| Ile | Direct | – | N.D. ($\gamma - \delta$) |
| Leu | Direct | – | N.D. ($\alpha$-$\beta$) |
| Lys | | + | Degen. |
| Met | | + | Present |
| Phe | Direct | – | Degen. W |
| Pro | | + | Unclear |
| Ser | Metabolic | low | Degen. diag. |
| Thr | Direct | – | N.D. ($\alpha - \beta$) |
| Trp | Metabolic | low | Yes (coil and helix) |
| Tyr | Direct | – | N.D. ($\gamma - \zeta$) |
| Val | Direct | – | Attenuated |

TABLE 4.2: Amino acids detected in aliphatic unlabeled KcsA samples as measured by the presence of characteristic correlations in $^{13}C$-$^{13}C$ spectrum as measured by DNP NMR (Figure 4.7) with the method of unlabeling (directly supplied natural abundance amino acids (Direct) or downstream metabolic targets (metabolic)) compared to the expected outcome ('+' for present in spectrum '–' for absent in spectrum) based on design of labeling scheme. Comparison made to U-$^{13}C$,$^{15}N$-KcsA in 9:1 DOPE-DOPS prepared and collected by Rivkah Ragowski (see Figure 4.8).

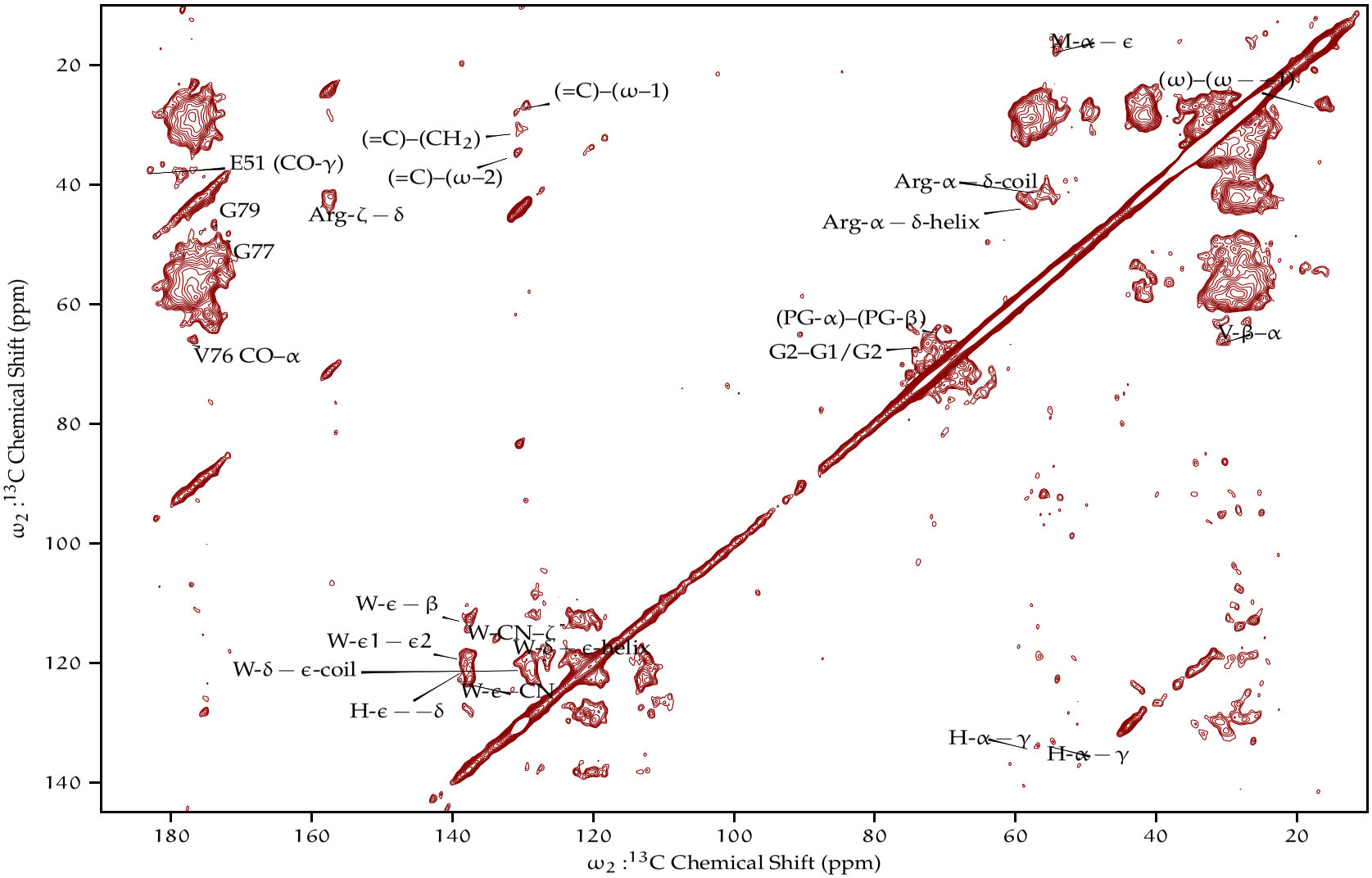


FIGURE 4.7: $^{13}$C-$^{13}$C DNP enhanced correlation (50 ms DARR) of aliphatic unlabeled KcsA. 105 K, 13.3 kHz MAS, 12 mM AMUPol with peaks labeled according to characteristic shifts. Tentative assignments of V76 and Gly77 are made based on similarity to previous work on KcsA [14, 82].

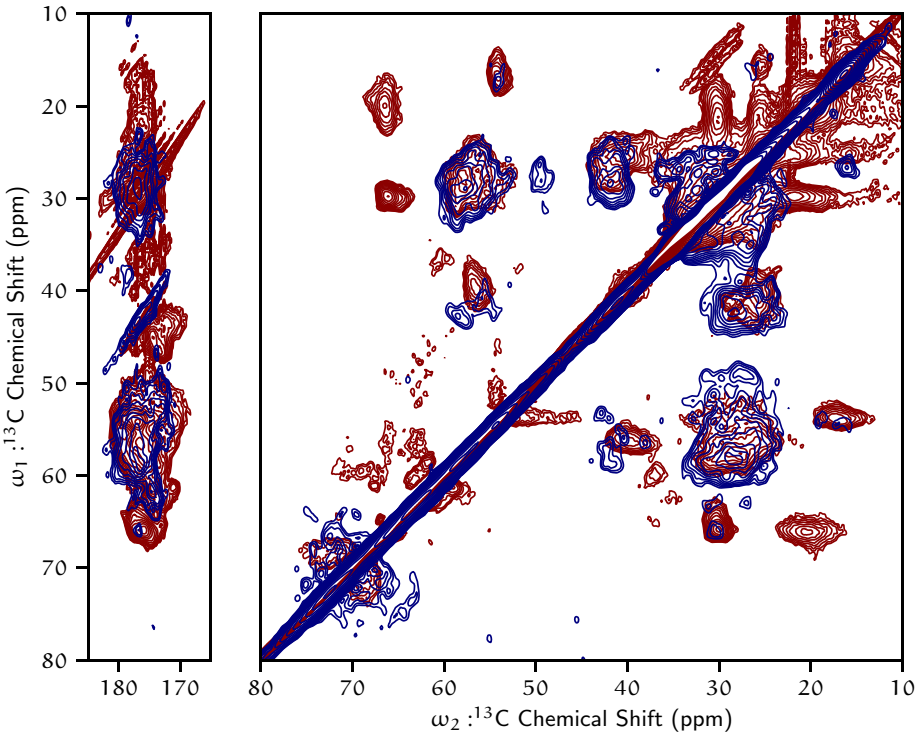


FIGURE 4.8: $^{13}$C-$^{13}$C CP-MAS spectrum (20 ms DARR) of U-$^{13}$C,$^{15}$N-KcsA at 11 kHz with 10 mM AMUPol (red) and aliphatic unlabeled KcsA at 13.3 kHz MAS (blue) with 12 mM AMUPol. Both samples in 50 mM KCl, 50 mM tris, pH 7.25 and at 105 K and collected using 3.2 mm probe, 20 ms DARR period, and 2 ms recycle delay. Uniformly labeled sample and spectra prepared and collected by Rivkah Ragowski.

unlabeled sample has a number of sharp peaks that likely correspond to individual residues. Tryptophan has several resonances that are distinct from phenylalanine, however, all of phenylalanine's resonances are near enough in chemical shift to tryptophan's that they cannot be resolved (if present) in this low temperature spectrum. Valine, though supplemented in natural abundance is present, identifiable by both side chain shifts and also the V76 CO-$\tau$ shift which has previously been assigned by the McDermott Group [15]. By previous assignment, we can also infer the presence of labeled glycines, possibly G79 and G77, CO-C  correlations. These three resonances

(CO-C$\alpha$ of V76, G77, and G79) cannot be definitely confirmed using $^{13}$C-$^{13}$C 2D experiment.

In a study using a similar aliphatic unlabeling scheme of the ABC transporter BmrA, Lacabanne, Meier, and Böckmann [44] found near complete (>90 %) attenuation of C$\gamma$, C$\delta$ of Val and Ile, large attenuation (>75 %) of C$\beta$ of Ala, Val, Ile, and good suppression of (>50 %) C$\alpha$ positions of Ala, Val, Ile. The results of this labeling scheme are in good agreement with those previous observations.

The aliphatic unlabeling successfully improved the resolution of the low temperature spectra by reducing the number of resonances. The scheme was designed to have a $^{13}$C and $^{15}$N bias on sequential amino acid pairs in the termini. Specifically, by having many sequentially labeled pairs in the termini, solid-state backbone experiments would yield previously unassigned resonances in that region. Furthermore, the low-temperatures of DNP reduce conformational dynamics which we suspected to be a major limiting factor regarding the feasibility of CP-MAS on the termini. Finally, the potential DNP enhancement would allow for rapid collection of this data, allowing for the collection of high-dimensional spectra.

The weak and unexpectedly broad resonances from this sample, however, rules out the aliphatic unlabeled sample as a candidate for a 3D spectrum. The double double-CP experiment to selectively transfer from $^{15}$N to either $^{13}$CO ($e^- \xrightarrow{\mu} {}^1H \xrightarrow{CP} {}^{15}N \xrightarrow{CP} {}^{13}C_o$). The $^{13}$C-detected NCO experiment was collected successfully (Figure 4.9), revealing no resolution of individual sites. The experiment required 5 h to

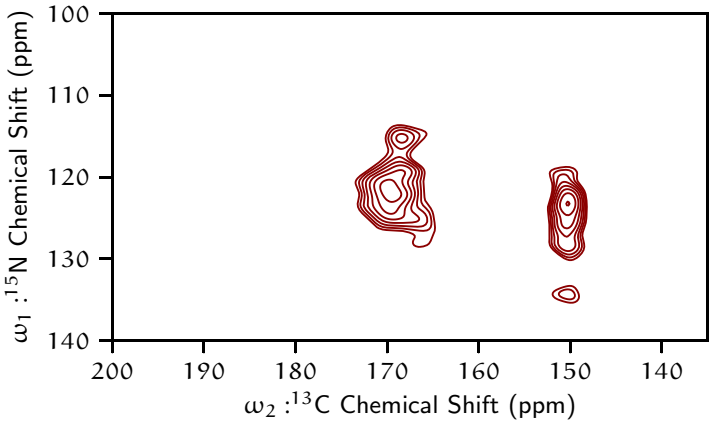


FIGURE 4.9: Selective $^{15}$N-$^{13}$CO double-CP spectrum of aliphatic unlabeled KcsA at 13 kHz MAS. Spectrum leaves N-CO sites completely unresolved, and also shows correlation of side change amines to side chain carbons ( 150 ppm).

achieve a signal-to-noise of 5. A conservative estimate of the time required a 3D data set is 5 days. Also, there would be no guarantee that even with the addition of an extra dimension that the spectrum would be well resolved by site. Considering both the demand for the instrument and the cost to operate the system, the signal-to-noise generated by this sample did not justify the collection of a larger data set.

### 4.3.2 *Lipids in Spectra*

As shown in Chapter 2, the head group and the acyl chain of the lipids are well resolved by HR-MAS, and have much longer relaxation times than than KcsA protein resonances, suggesting that the lipids have much more motional freedom. CP-MAS studies of KcsA in proteoliposomes have observed the resonances which are putatively assigned as arising from the PG head group or glycerol backbone [55, 81]. In the McDermott Group data, those resonances from previous studies are rarely observed.

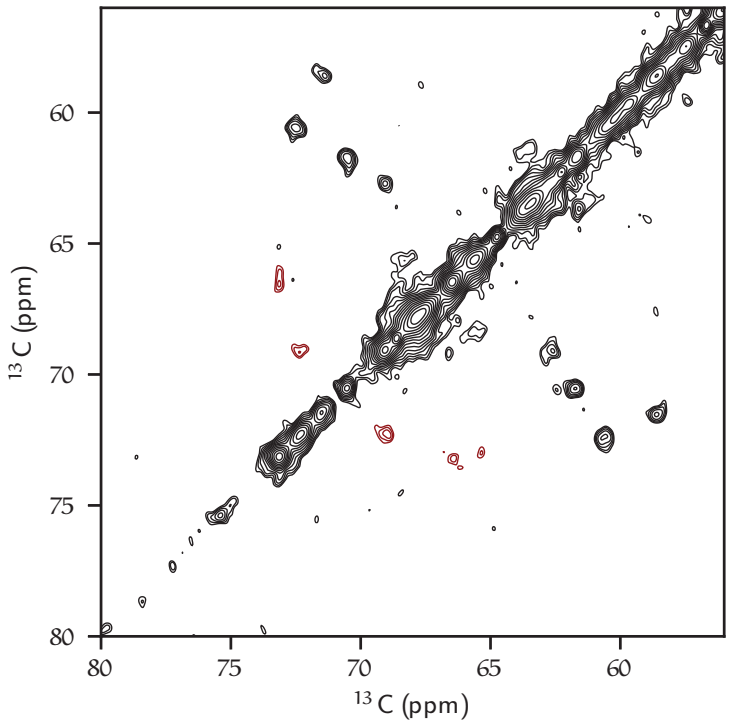


FIGURE 4.10: $^{13}$C-$^{13}$C CP-MAS spectrum at 260 K (50 ms DARR) of KcsA in DOPE lipids pH 4.0, 100mM KcsA with putative lipid resonances highlighted in red. Spectrum collected by Dongyu Zhang from the McDermott group

Occasionally such as in Figure 4.10, two or three resonances are observed which are unlikely from protein based on chemical shift and are in the region expected for a lipid glycerol backbone or PG head group. However, these chemical shifts do not precisely agree with the values found in the HR-MAS data. Also there is not a complete spin system, where, say the PG-β carbon is seen to correlate to both the PG-α and PG-γ carbons, so the resonances cannot be positively assigned. It is possible that the resonances observed in Figure 4.10 are in fact bound PG where as the HR-MAS detected PG that is in the bulk lipid, but this conclusion is far from certain.

Whereas the DARR spectrum of KcsA in proteoliposomes at 260 K shows an incomplete spin system for the headgroup and no identifiable signal of the lipid-acyl chain,

DNP-enhanced spectrum resolves an extensive network of lipid signals. Using the assignments made of lipids in Chapter 2 ( Table 3.2), we can identify both headgroup and acyl chain resonances. The very low temperature of this experiment is expected to freeze-out the conformational dynamics which would limit lipid signals by CP-MAS at 250 K. The only lipid headgroup signals arise correspond to phosphoglycerol which is not present in the exogenous lipid mixture, but rather from lipids co-purifying with KcsA [76], Chapter 2. The strong signal from the in the CP-MAS $^{13}C$-$^{13}C$ experiment supports the conclusions in Chapter 2 that the lipids are isotopically enriched and the absence resonances from exogenous lipids (phosphoethanolamine and phosphoserine) further supports this conclusion. These lipid assignments are labeled on the Figure 4.7 and provided in the peak list at Table 4.5.

### 4.3.3 *Comparison to a Standard*

It is difficult to definitively diagnose why DNP enhancement is low for a particular sample. To paint a more detailed picture of what is occurring in the rotor during a DNP experiment, an exogenous standard was added into the buffer of the sample as a reference compound for enhancements. $^{15}N$-enriched glycine was determined to suit experimental needs well. As a free amino acid, glycine readily dissolves into a host of buffers and has a distinctive $^{15}N$ chemical shift (32 ppm at neutral pH) that does not overlap with protein amide resonances in the 1D $^{15}N$ spectrum, even under DNP conditions. Further the compound is inexpensive relative to other isotopically

enriched amino acids. The ready enhancement of a small dissolved compound readily confirms that DNP is occurring in the rotor at the time of an experiment and can serve as a more direct comparison of enhancement quality across samples. Table 4.3 summarizes a set of experiments in which KcsA samples were compared to a 20 mM $^{15}$N-glycine standard.

The utility of using an internal standard is demonstrated by its incorporation into several unusual preparations of KcsA: KcsA in Zwitterionic lipids, a sample of KcsA in lipid nanodisks, a sample of KcsA in detergent, and a sample of aggregated, lipid-free KcsA.

#### 4.3.3.1 *Zwitterionic Lipids*

Lipid bilayer order and packing vary considerably by headgroup. The phospho-ethanolamine (PE) headgroup is a zwitterion at neutral pH, and its primary amine can coordinate with neighboring lipids [70], creating a tight packing-order and raising the melting temperature of pure PE bilayers compared to many other lipid headgroups. Previous work indicates that PE headgroups provide better order and superior cryoprotection compared to PC membranes [47]. So KcsA was embedded into pure DOPE membranes for investigation, finding a particularly poor enhancement(4.7 at CO), yet the glycine in solution enhanced well (71), demonstrating the value of the internal standard and the poor performance of enhancing KcsA under these conditions. After these measurements were made, Salnikov et al. [66] demonstrated that PE

is generally poor performer in terms of DNP enhancement. This demonstrated that a soluble compound does enhance well, but not the KcsA in liposomes.

#### 4.3.3.2 *KcsA in Detergent*

As an alternative to lipids, KcsA tetramers were solubilized in 10 mM decyl-β-maltopyranoside (DM), a nonionic detergent at protein concentration of $10\,\mathrm{mg\,mL^{-1}}$. Following combination with equal volume cryoprotectant, the DNP-enhanced spectra, finding the largest enhancement reported to date of KcsA of 54. The glycine standard was especially high compared to other trials at 84. The $^{1}$H DNP buildup time was an order of magnitude larger than other samples of KcsA (5.3 s versus ≈0.5 s), and the glycine standard had a similar value that was also much longer than seen in other trials.

#### 4.3.3.3 *Precipitated KcsA*

Noting that reports suggest good enhancement for some sedimented proteins, and suspecting that lipids might be responsible for the poor DNP enhancements KcsA in detergent was precipitated out of solution by a ten-fold dilution with detergent-free buffer, pelleted by centrifuge and washed. The enhancement was of similar order to the lipid samples at 5 for CO and with a good enhancement of the glycine standard at 56.

#### 4.3.3.4 *KcsA in SMA nanodisks*

The measurements above demonstrate soluble KcsA experienced good DNP enhancement and KcsA in liposomes. So, KcsA in soluble nanodisks was selected as a candidate target. A previous report showed that KcsA can be incorporated into steric maleic anhydride (SMA) nanodisks [25] using the SMALPS [43, 48] system. Specifically, *E. coli* cells overexpressing a membrane protein (KcsA in this case) are lysed and than incubated with SMA polymer which acts to surround the overexpressed protein with a section of the *E. coli* membrane to create a circular nanodisk. Dongyu "Allison" Zhang from the McDermott Group prepared wild-type, N-terminally His-tagged U-$^{13}$C,$^{15}$N-KcsA is expressed in uniformly enriched $^{13}$C, $^{15}$N M9 minimal media. The cells are lysed by French pressure cell, solubilized in detergent and then incubated in the presence of steric maleic anhydride polymer (SMA) [68]. This procedure encapsulates membrane proteins in native lipid nanodisks. The nanodisks are then purified by Ni-affinity chromotography. A typical KcsA proteoliposome sample is a viscous, white, opaque colloidal suspension. The SMA KcsA sample is viscous, yellow, transparent solution when mixed with cryoprotection.

The enhancement of SMA KcsA was typical of the other preperations at near 10, very curiously, the glycine standard had a similar enhancement (11), demonstrating that the sample is poorly optimized. The short buildup times of all of the species suggests that nuclear signal quenching from an over abundance of radical may be occurring [23].

The sample was incubated at −80 °C for 3 months and measured again, finding a similar measurements.

Radical concentration was doubled with the addition of buffer-cryoprotectant containing 200 mM AMUPol to test if radical concentration was too low, and found enhancement improvements on all species of less than 10 %. Again, the very short buildup times suggest that nuclear quenching by paramagnetic resonance with the radical may be occurring and that the radical concentration was in fact much too high then the optimum.

### 4.3.4 *Selective Labeling the N-terminus*

Given that aliphatic labeling failed to produce a sample suitable for the 3D correlations, a selective labeling approach was made as an alternative. $^{13}$CO-Met/$^{15}$N-Leu KcsA was expressed which is expected to give only two labeled N-CO pairs at M4-L5 and M154-L155, in the N- and C-termini, respectively. Having only two sites labeled has the advantage that in the N-CO plane, there would only be two peaks and the linewidths of individual sites could be determined. This labeling scheme was chosen as one of the few unique CO-N sparse pairs in KcsA, and that those residues are located at the end of their respective metabolic pathways [44], which decreases the likelihood of label scrambling and complicating data analysis. The $^{15}$N and $^{13}$C CP-MAS 1D spectra (Figure 4.11) yield expected patterns. As there are only 4 methionine residues in KcsA, the 1D $^{13}$C CP-MAS spectrum has weak intensity and resembles

a natural abundance protein sample. The 1D $^{15}$N CP-MAS spectrum yields a single amide peak that is sharper than a fully labeled protein, but given there are 24 leucine residues in KcsA and given the dispersion of leucine $^{15}$N shifts previously published for KcsA ([82]), there is no expectation of a sharp peak in the 1D $^{15}$N. The overall DNP performance of the sample was worse than typical with an enhancement of 24 on $^{15}$N-glycine standard. The enhancements to the protein were 2.3 and 1.9 on $^{13}$CO and amide $^{15}$N, respectively. The $^{13}$C-$^{13}$C spectrum reveals a diagonal and single set of cross peaks in the CO-C$\alpha$ region (Figure 4.12), which would be expected from a sample that only contains a $^{13}$CO enriched protein. Previous work in the McDermott group (unpublished) has assigned Met C$\alpha$-CO pairs at M96 59.6 ppm–177 ppm, and M154 has been assigned in detergent micelles by solution NMR as 57.7 ppm–177.9 ppm [21]. The peak occurring at 177 ppm–67.5 ppm is far from the typical range of methionine [30].

The selective double-cross polarization to CO (Figure 4.11), correlating $^{15}$N-$^{13}$C, shows a single very broad peak in the carbonyl region to amide region. The linewidth (643 ppm in the $^{13}$C dimension), is exceptionally broad even by DNP standards As reported in a previous chapter (Chapter 2), the C-terminus at neutral pH, where this spectrum was collected, is expected to be relatively rigid, which would then be expected to give rise to a sharp peak, at least relative to low pH. The N-terminus' conformational behavior is not well understood. These data suggest that both the termini are highly heterogeneous, likely sampling a large conformational space, and thus giving rise to the broad signal of the N-CO experiment. Previous work has shown that at

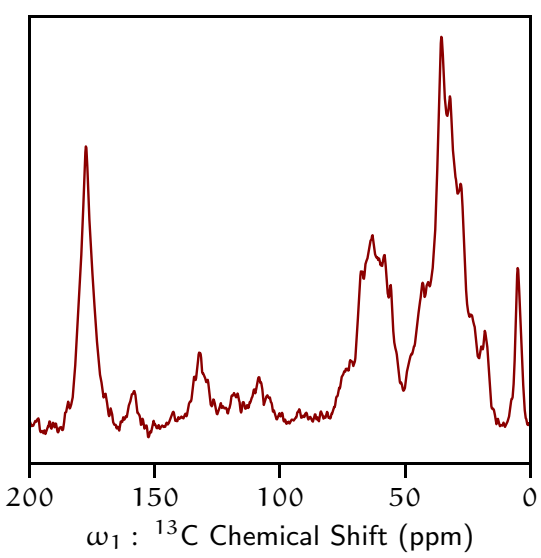


(A) $^{13}$C CP-MAS spectrum

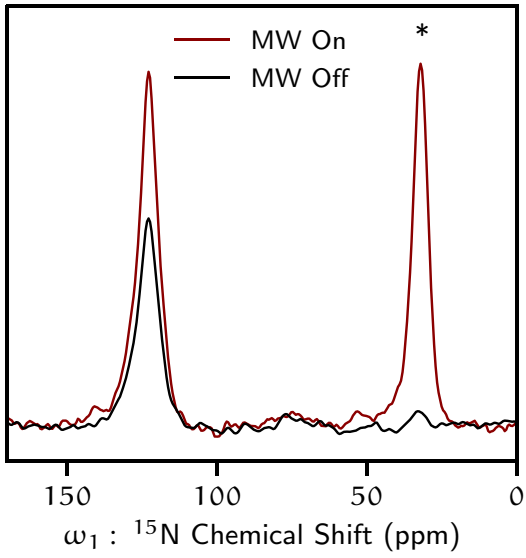


(B) $^{15}$N CP-MAS spectrum. '*' indicates internal 20 mM $^{15}$N-glycine standard

FIGURE 4.11: CP-MAS of Met-$^{13}$CO/Leu-$^{15}$N KcsA in 9 : 1 DOPE-DOPS liposomes by DNP enhanced NMR. 12.5 kHz MAS, 105 K, 15 mM AMUpol.

low temperatures an ensemble of proteins can assume multiple low energy conformations [52], and conformational diversity in solid-state NMR leads to in-homogenous line-broadening [56]. These data suggest that KcsA's termini under these conditions has a highly heterogeneous conformation.

### 4.3.5 *Unilamellar Liposomes*

Liposomes formed by hydrating lipid dried lipid films lead to multilamellar vesicles (MLVs) [59], and repeated freeze-thaw cycles lead to more homogeous, unilamellar proteoliposomes [54, 75]. A potential reason that KcsA fails to enhance well is that the

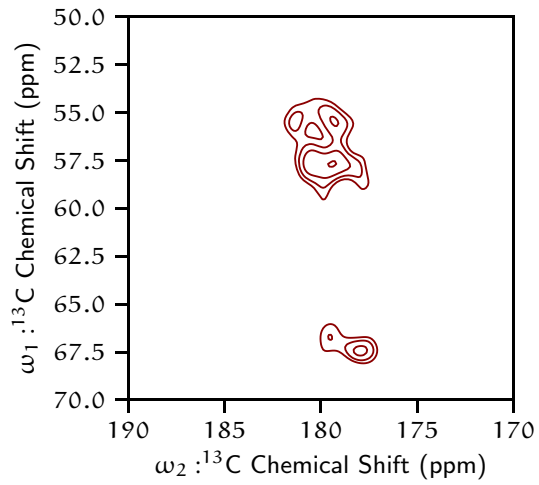


FIGURE 4.12: $^{13}$C-$^{13}$C (The cross peaks from 10 ms DARR) spectrum demonstrating Met CO labeling. Met-$^{13}$CO/Leu-$^{15}$N KcsA in 9 : 1 DOPE-DOPS liposomes by DNP enhanced NMR. 12.5 kHz MAS, 105 K, 15 mM AMUPol.

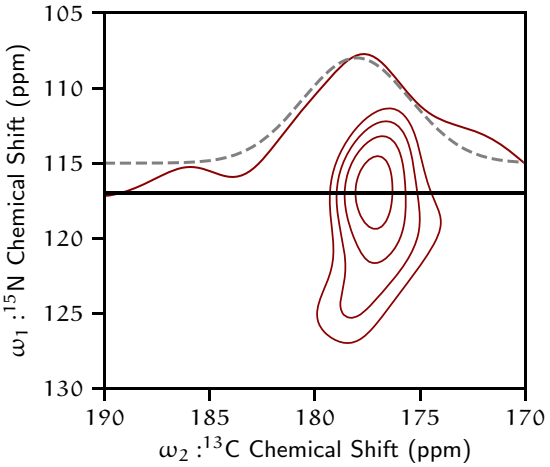


FIGURE 4.13: $^{13}$C-$^{15}$N double CP showing correlations of Met-CO to Leu-N. Met-$^{13}$CO/Leu-$^{15}$N KcsA in 9 : 1 DOPE-DOPS liposomes by DNP enhanced NMR. 12.5 kHz MAS, 105 K, 15 mM AMUPol. Slice of data at black line displayed and peak modeled with Gaussian function (FWHM = 4.26 ppm = 643 Hz)

polarizing agent can not access inner layers of MLVs, or only a single side of the outer most layer of the proteoliposomes has access to radicals.

Cryo-electron microscopy was conducted on aliquots of KcsA proteoliposomes before and after 25 rounds of freeze-thaw cycles in liquid nitrogen and 30° water bath (Figure 4.14), confirming that KcsA liposomes before treatment have an MLV structure, and following freeze-thaw cycles, principally large MLV structures are converted into relatively uniform ULV structures ( Figure 4.14 A an B). However, there exist in the samples, before and after, a population of aggregated liposomes that have been described previously as oligomeric liposomes [60]. These images do not provide enough resolution to distinguish where the protein is located.

Repeated rounds of freeze-thaw cycles on liposomes also efficiently encapsulate both small molecules [57]. In an attempt to better incorporate the radical into the sample AMUPol was added to the proteoliposomes in excess buffer to achieve 30 mM concentration this solution was subjected to 25 freeze-thaw cycles between liquid nitrogen and a 30° water bath. The solution was then pelleted by centrifuge and added to cryoprotectant as usual.

These manipulations produced no benefit in terms of DNP-enhancement, in fact, showing a net decrease of both enhancement and of buildup time.

Figure 4.18 shows the nitrogen enhancements from preparations D - E from Table 4.3. The amide region is located at about 130 ppm, side-chain nitrogen (e.g. arginine) at about 85 ppm, exogenous DL-proline at 65 ppm and free glycine at 42 ppm.

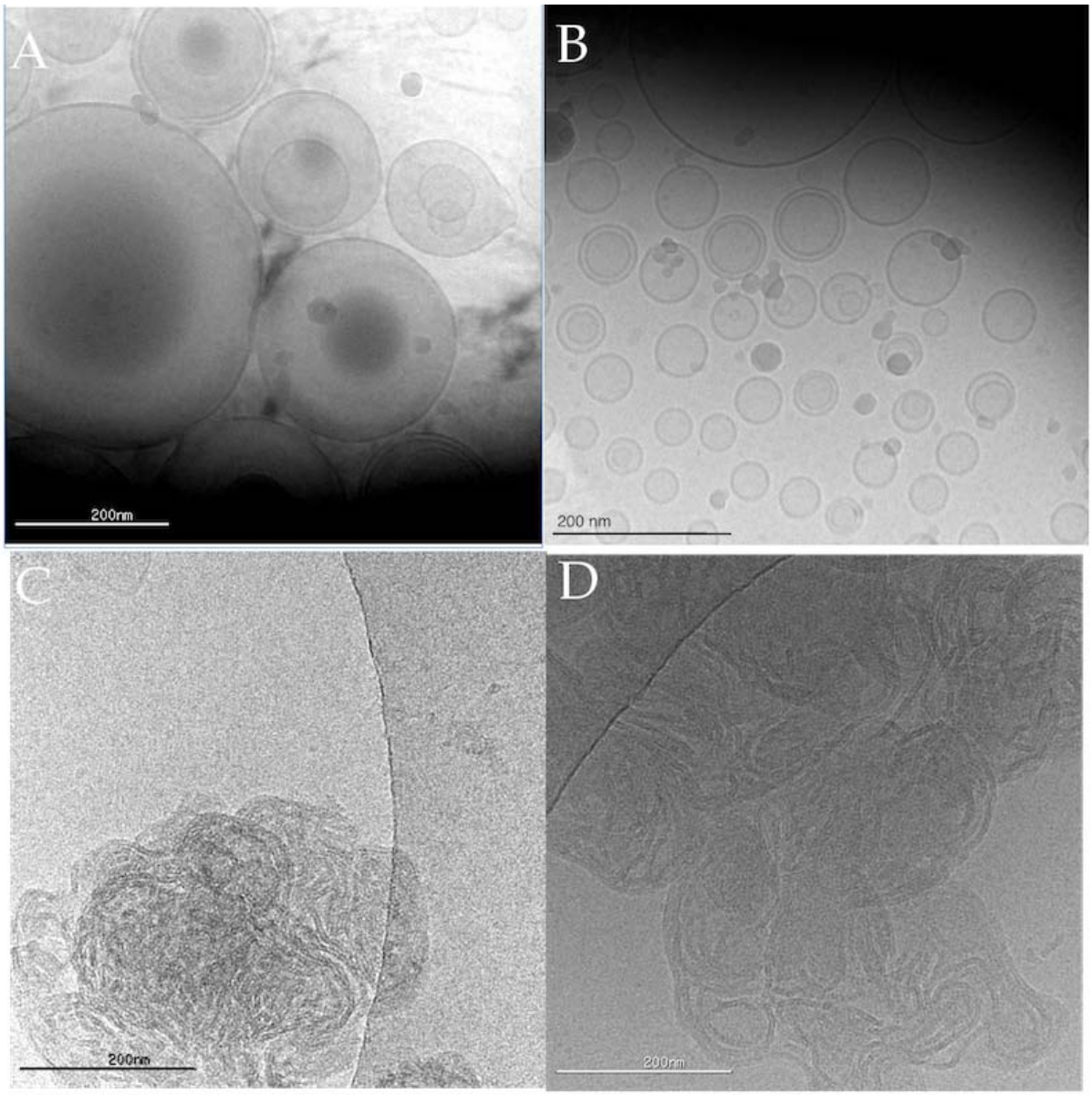


FIGURE 4.14: Cryo-electron micrographs of KcsA proteoliposomes before (A and C) and after (B and D) 25 rounds of freeze thaw cycles showing transition of principally, large MLVs to more uniform ULVs with some oligemeric vesicles in both sets of samples.

| | Labelling | Lipids / Prep. / Exp. | MAS (kHz) | Probe (mm) | AMUPOL (mM) | Protein (mg) | Protein $^{13}$CO | | | Protein amide $^{15}$N | | | $^{15}$N Reference | |
|---|---|---|---|---|---|---|---|---|---|---|---|---|---|---|
| | | | | | | | $\epsilon$ | $\tau$ | S/N | $\epsilon$ | $\tau$ | S/N | $\epsilon$ | $\tau$ |
| A | Aliph. Unlabel | DOPE, DOPS | 13 | 1.9 | 12 | 1.7 | 9.2 | 1.5 | 56 | | | | | |
| B | Aliph. Unlabel | DOPE, DOPS, lyoph. | 13 | 1.9 | 12 | 1.7 | 8.7 | 1.4 | 25 | | | | | |
| C | Aliph. Unlabel | DOPE, DOPS, 25X F/T | 13 | 1.9 | 12 | 1.7 | 6.8 | 1.0 | 33 | | | | | |
| D | Aliph. Unlabel | DOPE | 11 | 3.2 | 12 | 4.6 | 4.7 | 0.72 | 51 | 4.4 | 0.62 | 35 | 71 | 1.7 |
| E | $^{13}$CO-M,$^{15}$N-L | DOPE, DOPS | 11 | 3.2 | 10 | 5.1 | 2.3 | 0.41 | 14 | 1.9 | 0.45 | 42 | 28 | 1.3 |
| F i | U-$^{1}$H, $^{13}$C,$^{15}$N | *E. coli* (SMALPS) | 11 | 3.2 | 12 | 4.4 | 11 | 0.25 | 92 | 11 | 0.31 | 145 | 12 | 0.39 |
| F ii | | after 3 months at −80 °C | 11 | 3.2 | 12 | 4.4 | 12 | 0.31 | 97 | 13 | 0.34 | 187 | 16 | 0.33 |
| G i | U-$^{1}$H, $^{13}$C,$^{15}$N | *E. coli* (SMALPS) | 11 | 3.2 | 23 | 4.4 | 10 | 0.40 | 81 | 14 | 0.40 | 215 | 11 | 0.47 |
| G ii | | fast freeze | 11 | 3.2 | 23 | 4.4 | 13 | 0.52 | 85 | 14 | | 199 | 15 | |
| G iii | | fast freeze | 11 | 3.2 | 23 | 4.4 | 14 | | 88 | 15 | | 209 | 18 | |
| H | U-$^{1}$H, $^{13}$C,$^{15}$N | None | 11 | 3.2 | 18 | 1.2 | 5.7 | 1.7 | 33 | 9.1 | 1.3 | 12 | 56 | 1.3 |
| I | U-$^{1}$H, $^{13}$C,$^{15}$N | DM detergent | 11 | 3.2 | 18 | 0.35 | 69 | 4.9 | 240 | 54 | 5.3 | 99 | 84 | 5.7 |
| J i | F-$^{2}$H,U-$^{13}$C,$^{15}$N | $^{2}$H-DOPE, $^{1}$H-DOPG | 11 | 3.2 | 12 | 3.9 | 16 | 0.49 | 54 | 7.6 | 0.37 | 40.0 | 52 | 0.81 |
| J ii | | Direct polarization (DP), R.D. = 25 s, 64 scans | | | | | 15 | | 93 | | | | | |
| J iii | | DP, R.D. = 2 s, 64 scans | | | | | | | 17 | | | | | |
| J iv | | DP + flip-back, R.D. = 2 s, 64 scans | | | | | | | 32 | | | | | |
| J v | | 38°-DP, R.D. = 2 s, 64 scans | | | | | | | 57 | | | | | |

TABLE 4.3: DNP Enhancements ($\epsilon$) and buildup time constant ($\tau$ in seconds) of various samples of KcsA. All measurements were collected at the 105–109 K stator temperature, with a 2 s recycle delay (R.D., unless specified), and 64 scans (unless specified). Buffer was 50 mM KCl, 50 mM Tris, pH 7.25. Samples were prepared as 50 % wet pellet and 50 % cryoprotectant consisting of 3 : 1 U-$^{2}$H,$^{12}$C-glycerol–$D_2O$ (by mass) containing appropriate amount of AMUPol to reach total concentration specified by total sample volume. Sample 'B' is sample 'A' lyophilized to remove 30 % of total sample mass. Samples 'H' and 'I' were combined with cryoprotectants as solutions. All experiments had high-power proton decoupling applied during acquisition and had 100 Hz exponential line broadening apodization applied to the FID. All measurements were made using individually optimized CP-MAS experiment except J ii–J v which used direct polarization (one-pulse). When used, 20 mM $^{15}$N-glycine was dissolved into the buffer an internal reference standard.

The exogenous standard proves to be a useful diagnostic tool. Specifically from Samples D and E, we can clearly see that while the protein peaks are poorly enhanced, the standard is well enhanced. These results reveal that, at least for the environment occupied by the amino acid standards, there is an adequate combination of radical, protons and cryoprotectant.

### 4.3.6 *Fractional Deuteration*

Deuteration of proteins for analysis by DNP-enhanced NMR has previously been explored [4, 5]. In proton-detected, solution-NMR of macromolecules, deuteration is a matter of course. Since proton-proton dipolar couplings are on the order of 100 kHz, any molecules tumbling near or below that rate will have broadened proton spectra. Diluting the protons with deuteron can greatly diminish these effects, leading to much sharper spectra. Heteronuclear experiments, such as nitrogen and carbon, can be made much sharper with perdeuterated molecules. However, the absence of protons robs the spectroscopist of CP- and DNP-based tools to enhance signal.

In a previous study Chapter 2, I characterized a preparation to fractionally deuterate KcsA. In that sample the H-C$\alpha$ positions are principally deuterated, but the side chains remain fractionally protonated. Using this procedure was used to express fractionally deuterated KcsA and which was embedded in 3 : 1 U-$^{2}$H-DOPE:protonated-DOPG. This particular ratio of lipid was chosen to provide a proton bath while reducing the over all proton content of the lipid membrane in an aim to better target

polarization transfer to protein. It is also a commonly used mixture of lipids (in fully protonated form) in electrophysiology studies of KcsA.

The $^{13}C$-$^{13}C$ (DARR) spectrum of fractionally deuterated KcsA was found to give very weak cross peak signals compared to other samples though a similar 1D-CP MAS spectrum (Figure 4.15, Figure 4.16). The dipolar assisted rotational resonance mixing sequence (DARR) relies on $^{1}H$-$^{1}H$ dipolar couplings for efficient mixing.

Deuterated proteins have a vastly attenuated spin bath of $^{1}H$ on which to draw polarization. Observing that the DARR transfer had poor efficiency, as evidenced by a strong diaganol and week cross peaks, direct polarization was investigated as an alternative. Carbon $T_1$s were measured with a a 1D inversion recovery experiment and found to be approximately 5 s. Table 4.3 rows Ji–Jv compare direct polarization versus cross polarization. Per scan, direct polarization out performed cross polarization when the recycle delay was long (25 s, i.e. $\approx 3.25 \times T_1$), but performs much worse when the recycle delay of the direct polarization experiment was left that of the CP-MAS experiment of 2 s. By using an Ernst-angle pulse, whereby the $^{13}C$ spin is not completely nutated into the the X–Y plane and thus relaxes back to equilibrium sooner than a 90°-pulse, with an optimal flip-angle ($\theta$) of $\theta = arccos(exp(\frac{R.D.}{T_1}))$ [28]. Using a 2 s recycle delay, a 38° was used, achieving the same total time of of the CP-MAS experiment and a very similar signal-to-noise.

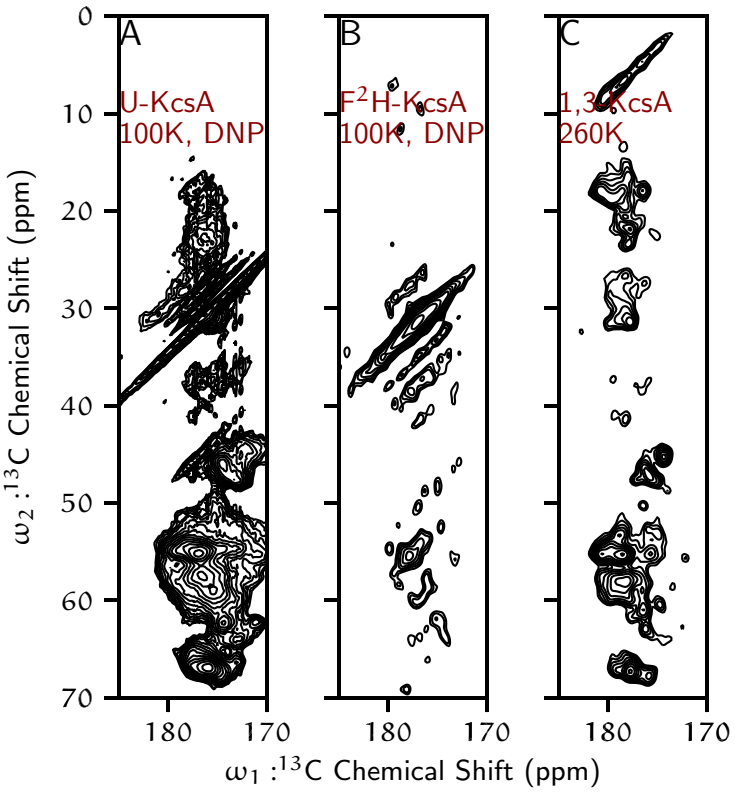


FIGURE 4.15: Carbonyl region of CP-MAS $^{13}$C-$^{13}$C (20 ms DARR) of A: U-$^{1}$H,$^{13}$C,$^{15}$N-KcsA with DNP at 105 K, 6 h acquisition, 13 kHz MAS; B: F-$^{2}$H,U-$^{13}$C,$^{15}$N-KcsA with DNP at 105 K, 13 kHz, 6 h acquisition; C: 1,3-$^{13}$C-glycerol, U-$^{15}$N-KcsA, 265 K, 11 kHz MAS, 14 h acquisition. First contours set to 3 standard deviation of the spectral noise, subsequent contours multiplied by a factor of 1.3, with 24 contours plotted. All spectra collected in 3.2 mm probe on the same 600 MHz system. Uniformly labeled sample and spectra prepared and collected by Rivkah Ragowski. Glycerol-labeled sample and spectra prepared and collected by Dongyu "Allison" Zhang.

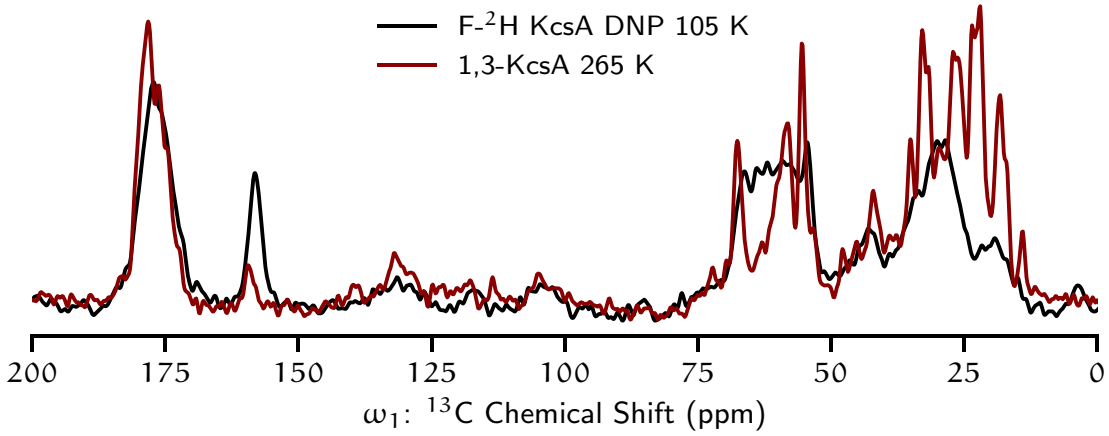


FIGURE 4.16: First point of $^{13}$C-$^{13}$C experiment from Figure 4.15 of F-$^{2}$H,U-$^{13}$C,$^{15}$N-KcsA DNP-enhanced at 105 K with 8 scans (black), and 1,3-glycerol labeled KcsA at 265 K with 16 scans (red). Spectra scaled to equal noise.

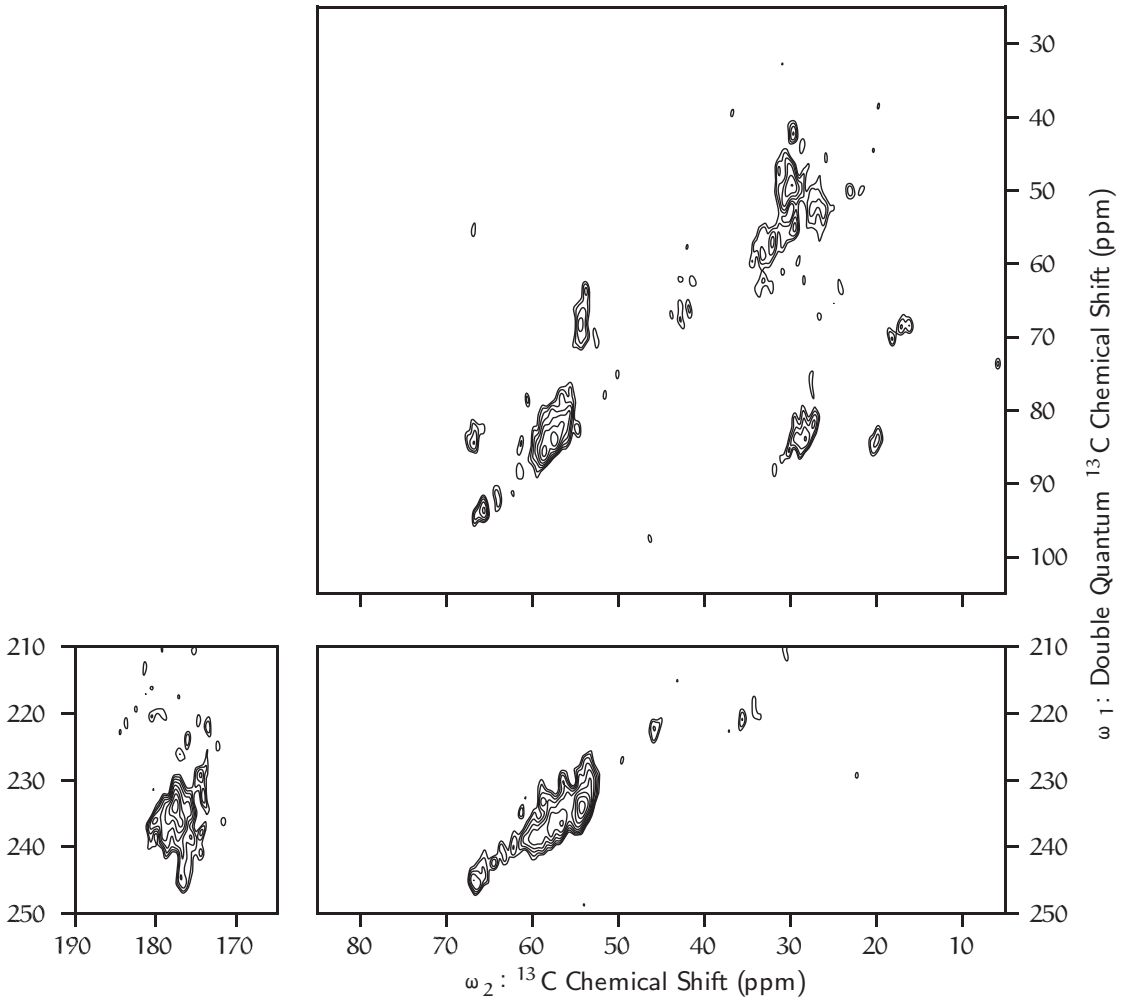


FIGURE 4.17: Two-dimensional $^{13}C$ refocused dipolar-INADEQUATE spectrum of F-$^{2}H$,U-$^{13}C$,U-$^{15}N$-KcsA with DNP enhancement at 105 K and 13 kHz MAS, $^{1}H$-$^{13}C$ CP excitation and post-$C_5$ dipolar recoupling. 4 h acquisition. First contour plotted at 4 sigma of the noise and subsequent multiplied by factor of 1.3. Double quantum correlations (y-axis) appear at the sum of the two correlated shifts.

### 4.3.7 *Fast Freezing*

The DNP system used in these studies uses nitrogen gas at 90 K as gas flow for magic angle spinning. Nitrogen gas is used to 'float' the rotor, suspending it off the stator, to drive the magic angle spinning. A separate flow of nitrogen has an in-line heater to vary the sample temperature. Sample freezing is performed by inserting a room temperature MAS rotor into the probe with gas flows near 100 K. As an alternative, the rotor was inserted into a block of aluminum with a custom milled hole accommodating the rotor with a 0.5 mm tolerance sitting in a bath of liquid nitrogen (rows G ii and G iii in Table 4.3), leading to no significant difference in enhancement. This experiment does demonstrate that for this system, measurements of enhancement and signal to noise are generally reproducible even when varying freezing rates.

## 4.4 DISCUSSION

Membrane proteins are appealing candidates for enhancement by DNP, but their potential as targets has yet to be realized. The data presented in these pages shows that mere sample preparation is not the major barrier, and reiterates previous calls for systematic investigation of the the factors influencing enhancement of membrane proteins.

### 4.4.1 *Radical Concentration*

There is considerable range of radical concentrations used in DNP experiments. TOTAPol alone has been reported as having sample-dependent optimum concentrations at 5–10 mM [63], 25 mM[50], 60 mM[53]. The coarse-grained titration of radical versus polarization buildup and signal enhancement (Figure 4.6) showed only modest effects within the range of 5–40 mM. However, Ravera et al. [63] finds that with sedimented proteins, the best overall signal is achieved with very low concentrations of radical <5 mM and presents data that supports other finding from sedimented protein that TOTAPol may be preferentially binding to protein [64]. It is very possible then that all of the measurements conducted in this study were in entirely the wrong regime.

With regard to concentration, KcsA dissolved into detergent micelles achieves an excellent enhancement, showing that that there is nothing intrinsic to the protein that prohibits signal enhancement by DNP. There are three key differences in the detergent experiment compared to the lipid-embedded experiments. The first is that KcsA is in a micelle environment which effects its accessibility to solvent, the radius of the particles into which it is embedded (e.g. micelles versus liposomes), the chemical composition of the detergent versus lipids, etc. Second, the concentration of the KcsA is an order of magnitude smaller than in the liposome studies. Third a solution of KcsA was combined with cryoprotectant, whereas for all of the other experiments a wet proteoliposome pellet was added to cryoprotectant. In all of the experiments described in Table 4.3 the concentration of the radical is determined by comparison to the total

volume of the rotor, which was essentially full for all experiments. However, the volume of actual liquid varied considerably as the lipids in the pelleted samples occupy a high percentage of volume, which effectively increases the concentration of the radical. A future control experiment would be to use examine a series of protoliposomes a various concentrations suspended into solution.

The transfer of electron polarization to nuclear polarization requires a buildup time and the rate of the buildup is dependent on the concentration and source of unpaired electrons, the concentration of the nuclei, the distance between the electrons and the target nuclei, magnetic field strength, microwave field strength and frequency, polarization pathway, and a number of more poorly understood factors [73]. Some examples of the data and buildup fits generated from this pulse sequence and its analysis are displayed in Figure 4.19.

Considering both the DNP signal enhancements as well as the polarization buildup times, it is clear that the dissolved glycine standard is in a different chemical environment than the protein for the proteoliposome samples. The glycine generally much longer buildup time, and much better enhancement, with a few notable exceptions.

In the case of the soluble naondisks and the KcsA in soluble micelles, we see that protein enhancement and buildup times reflect similar values to soluble glycine. KcsA in micelles is limited to low concentration (KcsA precipitates at high concetration). The nanodisk sample was soluble and at high concentration. The similarly poor per-

formance of all species in the rotor shows the system was not optimized. These experiments justify further efforts to optimizing KcsA in nanodisks.

In the studies of SMA nanodisks the lipid protein concentration is similar to what is seen in liposomes experiments, that is to say, the SMA nanodisks occupy most of the volume that is not occupied by cryoprotectant. The SMA nanodisks disperse into the cryoprotected solution without any visible particles, resulting in a clear, orange solution (AMUPol is orange when dissolved in an aqueous medium and the SMA nanodisk pellet was yellow). The liposome samples are opaque off-white and very viscous. The low enhancements and short buildup times of the SMA sample again suggest that the radical concentration was no optimized. After 3 months in the freezer, the signal enhancement when measured again was higher and the buildup time shorter, and this observation could be explained if the radical were quenched to a small extent in that intervening time. A small amount of cryoprotectant containing a high concentration of AMUPol was added to the sample, roughly doubling the total radical in the rotor, which only modestly increased both enhancement and buildup time. This very small effect might have been from the slight change to the overall cryoprotection affinity rather than from the radical concentration. In fact, it has been shown that as radical concentrations increase beyond the optimum, signal enhancement decreases to a exponentially [45], so doubling the concentration might not make a major difference if the beginning concentration was already far higher than the optimum.

The very short buildup times of KcsA might be an indication of paramagnetic signal quenching [23] in the case that that the radical is binding directly to the protein.

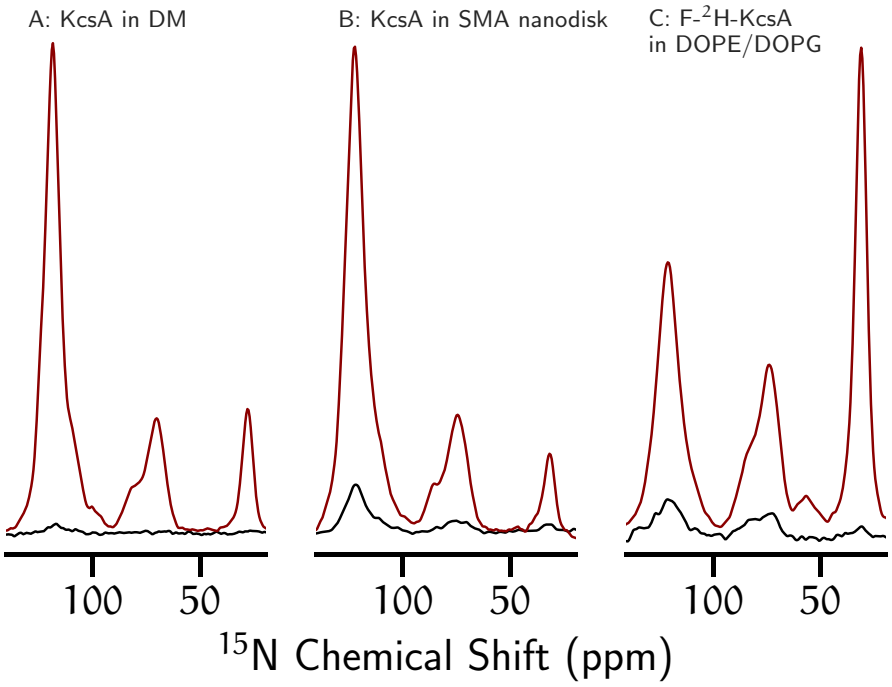


FIGURE 4.18: Examples to DNP enhancements to $^{15}$N CP-MAS experiment of various preparations of two KcsA preparations with microwaves off (black) and microwaves on (red). AM ' * ' indicates internal reference 20 mM $^{15}$N-glycine. 12 mM AMUPol, 11 kHz MAS, 105 K.

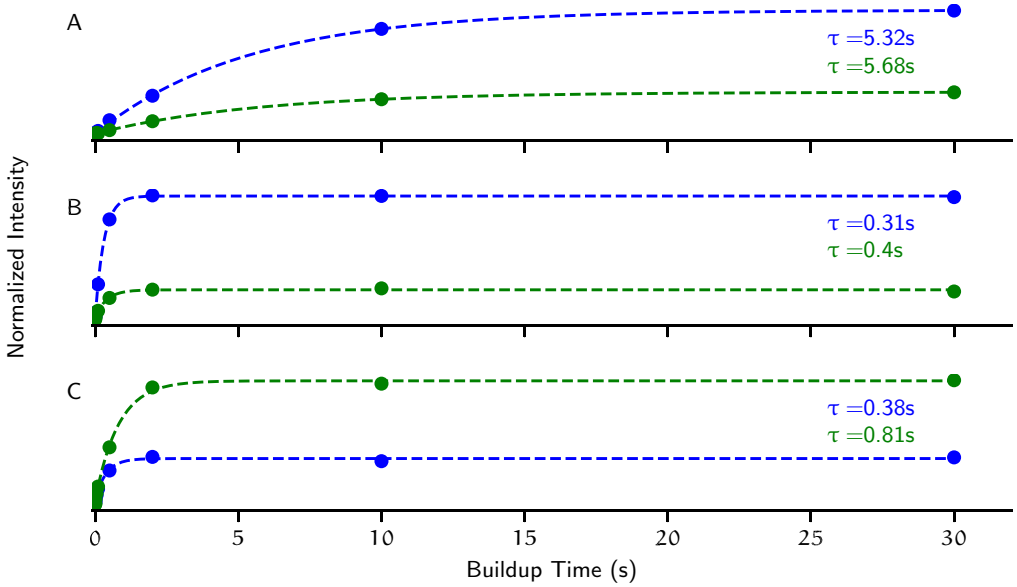


FIGURE 4.19: Buildup peak intensities (points) and fits of Equation 4.4 (traces) of KcsA amide region (blue) and $^{15}$N-glycine standard (green) for KcsA in DM (A), KcsA in SMA nanodisks (B), and F-$^{2}$H-KcsA in DOPE/DOPG (C). 12 mM AMUPol, 11 kHz MAS, 105 K

However, consider there appears to be individual sites resolved in the $^{13}C$-$^{13}C$ spectra of aliphatically unlabeled samples, this is unlikely to be the case as the paramagnetic quenching also leads to line broadening. Fast buildup times are not necessarily indicative of paramagnetic quenching. Dissolved glycine in solution, for example, that both $^{1}H$ DNP buildup times and $^{13}C$ DNP enhancements are roughly proportional to the the amount of glassing agent (the carbohydrate trehalose in this case), ranging from 1 s and $\epsilon = 7$ at 0 M trehalose and 36 s and $\epsilon = 13$ at 4 M trehalose [29].

### 4.4.2 *Fractional Deuteration*

For radical polarizing agents in aqueous systems high levels of deuteration are required for efficient enhancement [73], specifically by directing polarization to the target analytes rather than diluting it to the bulk solvent. Studies of membrane proteins in lipids have shown that a deuterated lipid background leads to somewhat improved enhancement but decreased $^{1}H$-$^{13}C$ cross polarization performance, essentially negating the effects of using deuterated lipids (which are rather expensive by the way) [50]. This experiment is the first time, of which we are aware, that a fractionally deuterated protein has been investigated. Overall enhancement performance using $^{1}H$-$^{13}C$ CP is improved compared to other samples. More interestingly, the direct $^{13}C$ enhancement is of similar order to the CP-mediated (also called indirect) enhancement. Although theoretically, since the the electron-to-$^{13}C$ gyromagnetic ratio is much larger than that for electron-to-$^{1}H$, $^{13}C$ enhancements have potential for larger DNP enhancements.

The SH3 domain of the protein $\alpha$-spectrin (SH3) is a commonly used model peptide. In perdeuterated SH3, for example, the direct $^{13}C$ enhancement is five-fold better than that of CP-mediated enhancement. For protonated SH3, $^{13}C$ enhancement and CP-mediated enhancement of was on a similar order [3, 5]

DNP enhancement for direct $^{13}C$ excitation for this particular spectrometer could likely be further optimized. These experiments were on a setup optimized empirically for $^{1}H$ enhancements of a model compound by sweeping the magnetic field. The DNP system at the NYSBC is equipped with a $B_0$ sweep-coil which allows it to shift magnetic field. The $B_0$, however, is cumbersome to adjust and requires re-shimming of the magnet and interferes with other demands on the instrument. $^{1}H$ enhancements tend to be best on the high-field end of the ESR spectrum, whereas $^{13}C$ DNP occurs better at the low-field side of the ESR spectrum [22]. With the large signal enhancement demonstrated in this sample on $^{13}C$, such an undertaking could be valuable as the enhancements can be more than two-fold greater when sweeping the magnet from the $^{1}H$ optimum to the $^{13}C$ optimum, and this is justified for future experiments.

The cross-polarization magic angle spinning (CP-MAS) forms the basis of the majority of solid-state experiments because it enhances the polarization of heteronuclei (e.g. $^{13}C$ and $^{15}N$) by transferring polarization from $^{1}H$ and it can decrease the recycle delay need for an experiment. CP-MAS transfers polarization from nuclei of a higher gyromagnetic proton to nuclei of lower gyromagnetic ratio, such as from $^{1}H$ to $^{13}C$. From Equation 4.1, $\Delta E = -\hbar B_0 \gamma$, where $B_0$ and $\gamma$ are the magnetic field and the gyromagnetic ratio of a nucleus, respectively. Thinking in thermodynamic terms,

two groups of different nuclides in the same magnetic field will be described by different amounts of polarization, with the group having a higher gyromagnetic ratio experiencing greater polarization. The strong, persistent, dipolar coupling between nuclei in solid-state samples can be exploited to transfer magnetization by applying a resonant magnetic field ($B_1$ to each such sets of spins such that that $\gamma_I B_{1I} = \gamma_S B_{1S}$, which is known as the Hartmann-Hahn matching condition leading to a maximum enhacementment of $\frac{1\gamma_I}{2\gamma_S}$ [35]. So in the case of $^1$H-$^{13}$C cross-polarization experiment, $\frac{26.8 rad T^{-1} s^{-1}}{2 \cdot 6.73 \cdot rad \cdot T^{-1} s^{-1}} \approx 2$ when compared with direct polarization (90°-pulse) of $^{13}$C. The greater benefit to signal-to-noise, is from enhanced relaxation characteristics. In the direct polarization experiment, the $^{13}$C atom must be allowed to return, at least in part, to equilibrium, the process of spin-lattice or $T_1$ relaxation, before the experiment can be repeated and signal averaged. The CP-MAS experiment, however, relies on $^1$H polarization, and therefore is dependent instead on the relaxation of $^1$H in the sample. Generally, $^1$H $T_1$ values are 5–20 times faster than that of $^{13}$C values in a given sample. Thus, CP-MAS is the typical choice of experiment for $^{13}$C observation in solids.

Figure 4.15 compares the carbonyl region of three spectra collected on the same magnet comparing the difference in spectra quality of a uniformly labeled and fractionally deuterated KcsA DNP-enhanced DARR spectra at low temperature to a non DNP-enhanced spectrum of glycerol-labeled KcsA, a metabolic isotope enrichment scheme that gives a characteristic labeling pattern for each amino acid. Figure 4.16 directly below shows the first point of the 2D experiment for the fractionally deuterated sample with DNP enhancement at low compared to the glycerol labeled sample at

265 K. The DNP enhanced spectrum has better signal to noise in the carbonyl region even though it only has the half the number of scans. Yet interestingly, the carbonyl region of the 2D spectrum has much better signal-to-noise for the non enhanced spectrum at higher temperature. The dipolar assisted resonance recoupling (DARR) experiment [74] is an absolute workhorse in solid-state NMR providing proton-assisted $^{13}C$-$^{13}C$ mixing. Although it is known that the normally very efficient DARR sequence provides very poor mixing in the absence of protons, such a for perdeuterated proteins [38], it is unclear what the performance would be like in a fractional deuteration scheme. As Figure 4.15 shows, the DARR mixing scheme is less than satisfactory under fractional deuteration.

The single-quantum (SQ) to double-quantum (DQ) INDADEQUATE [9, 36] has no diagonal, so it therefore allowed for direct optimization on the cross-peak signal, thus avoiding the disappointing results of the DARR spectrum. Past work in McDermott group has shown that several other homonuclear mixing schemes perform better than DARR for perdeuterated proteins [38]. And the POST-C5 was found to work well in 1D testing of the INADEQUATE program. The performance of this scheme is remarkably good Figure 4.17, providing a spectrum with relatively narrow lines, though not site resolved in only a few hours. $^{13}C$ enriched model compounds tend to require 8–16 h of signal averaging, and protein samples that frequently require 24 h or more [51]. Future experiments should systematically examine the spectral quality difference by different mixing scheme on fractionally deuterated proteins at DNP conditions.

## 4.5 CONCLUSION

This work demonstrates that there is hope for examination of KcsA by DNP, but the way forward will not be easy. KcsA dissolved into solution can achieve high enhancement. There is promise that other soluble KcsA systems. The addition of an internal diagnostic standards, $^{15}$N-glycine was a major benefit to these studies,. It demonstrated, for example that the nanodisk system is not optimizes, and urges more work in that direction.

Finally, the low temperatures of DNP did allow the capture of previously unrecorded signals by CP-MAS namely of inter-residue correlations in the termini and the entire lipid spin system.

## 4.6 MATERIALS AND METHODS

## 4.7 DNP-ENHANCED NMR

DNP-enhanced NMR was conducted on a Bruker Avance III DNP commercial spectrometer (on the first commercial unit to ever be install, specifically) with a $^{1}$H $B_0$ of 600.3 MHz field equipped with a 1.9 mm HNC DNP probe or 3.2 mm HNC DNP probe, as specified in the text, and a 395 GHz gyrotron. Room temperature measurements were made on a 3.2 mm HCN e-free probe.

For the 1.9 mm probe, typical 90° pulse lengths were 1.9 µs, 5 µs, 10 µs for $^{1}$H, $^{13}$C, and $^{15}$N, respectively. For the 3.2 mm probes (at room temperature or low temperature), typical 90° pulse lengths were 2.25 µs, 4 µs, 11 µs for $^{1}$H, $^{13}$C, and $^{15}$N, respectively. High-power $^{1}$H decoupling fields were typically 95 kHz.

Low temperature shimming was performed using DEMA as described in [31].

Magic angle spinning, bearing, and drive flows are all run using $N_2$ gas at ~80 K with flows adjusted to system recommendations. Set temperature, measured at the MAS stator was 100 K, and the measured temperature was allowed to stabilize to below 107 K before measurements were taken, typically 105 K was achieved.

DNP buildup using cross polarization experiment was written by Ivan Sergeyev [71] Figure C.7. Each time point was collected with 2048 points over 16 ms with SPINAL64 decoupling during acquisition. Typically 12–20 delay points were collected ranging between 1 ms and 30 s. 64 scans were typically collected per buildup point. 100 Hz of exponential line broadening was applied to the FID.

Dipolar assisted rotational resonance (DARR) [74] Figure C.8 experiments were collected using NYSBC standard pulse sequences. The data was collected with 2560 complex points over 20 ms and 400–600 complex points over 6 ms in the direct and indirect dimensions, respectively. SPINAL64 decoupling was used during acquisition. Lorentzian-to-Gaussian apodization was applied, adjusted empirically, with between 20–70 Hz broadening and Gaussian shift between $0.1 - 0.01 \times \pi$.

The $^{13}$C-resolved CP-INADEQUATE [9, 36] Figure C.9 was collected using a sequence kindly provided by Keith Fritzsching. The data was collected with 2048 complex points over 22.5 ms and 180 complex points over 12 ms in the direct and indirect dimensions, respectively. The $^{13}$C carrier radio frequency was set to 110 ppm with a sweep width of 110 ppm, resulting in the aliasing of resonances correlated to carbonyl sites and those correlated to aliphatic sites, thus requiring the spectra to be reconstructed region-wise. 10 post-C5 cycles were applied for re-conversion. TPPM15 and SPINAL64 decoupling were used during post-C5 recouping and acquisition, respectively. 32 scans were acquired for each transient.

### 4.7.1 *DNP Sample Preparation*

AMUPol (Cortecnect) was dissolved in U-$^{2}$H,$^{12}$C-glycerol to create a 200 mM stock solution. $^{15}$N-glycine (Cambridge) was dissolved in $D_2O$ (Cambridge) to create a 300 mM stock solution.

Unless otherwise noted, samples were combined in a 1 : 1 mass ratio with cryoprotectant solution. The cryoprotectant solution was composed of U-$^{2}$H,$^{12}$C-glycerol $D_2O$ (both from Cambridge Isotopes) in a 3 : 1 ratio by mass. Appropriate amounts of AMUPol and glycine stock solutions were used to create cryoprotectant to yield concentrations specified. The concentrations specified are with respect to total rotor volume. After mixing, samples were stirred with a flame-sealed gel-loading pipette tip to homogenize and centrifuged through a pipette tip into MAS rotors.

Experiments performed in a 1.9 mm probe were conducted using sapphire rotors with zirconia drive tips. Experiments performed in a 3.2 mm probe were performed in zirconia rotors with zirconia drive tips.

### 4.7.2 *AMUpol Titration*

The 7.5 mg of reversed labeled KcsA in 9:1 DOPE-DOPS (LPR = 1) pellet was collected by centrifuge at 20 000 RCF for 30 min and subjected to 5 cycles of freeze thaw cycles in liquid $N_2$ and a water bath at 25 °C, and excess buffer was removed at the end of this procedure. The sample was then mixed with equal volume of 3 : 1 U-$^{2}$H,$^{12}$C-glycerol-$D_2O$ cryoprotectant containing 10 mM AMUPol and the sample packed into a 1.9 mm zirconia DNP rotor by centrifugation. NMR spectra of the sample were collected with microwaves on and off, re-tuning the probe between trials. The sample was then unpacked by centrifuge and aliquots of 3 : 1 U-$^{2}$H,$^{12}$C-glycerol-$D_2O$ containing 200 mM AMUPol were added such that the desired concentration of radical was achieved per total rotor volume. The sample was subsequently stirred with a flame sealed gel-loading pipette tip until visibly homogenous and then repacked by centrifugation. Buildup curves were collected by using the sequence described in Figure 4.4 using buildup time points of 0.1000, 0.5000, 1.000, 10.00, 100.0, 500.0, 1000.0, 2000.0, 3000.0, 4000.0 and 6000.0 ms and fit using a monoexponential buildup function.

### 4.7.3 *Proteoliposomes Preparation*

U-$^{1}$H,$^{13}$C,$^{15}$N-KcsA was expressed, purified, and reconstituted as described in a previous chapter Section 2.6.1.

### 4.7.4 *'Alternative' KcsA Preparations*

For detergent solubilized KcsA experiments. The protein was expressed and purified by FPLC as described in Appendix A containing a final buffer of 10 mM β-D-decyl-maltopyranoside non-ionic detergent (Anatrace), 50 mM Tris, and 50 mM KCl. The sample was concentrated using a centrigual concentration device with a 50 MWCO membrane (Amicon). A concentrator with buffer only was used run in parallel and used a reference for UV-VIS determination of protein concentration. Protein was concentrated to approximately 10 mg mL$^{-1}$, and this solution was immediately combine with cryoprotection solution.

Aggregated KcsA was prepared from an aliquot of the solution from the detergent sample described directly above before concentration and was precipitated out of solution by 20× dilution with buffer without detergent, leading to visible precipitation. The precipitated protein was then centrifuged to pellet at maximum speed on a bench top centrifuge, the solution was removed by pipette and fresh, no detergent buffer was added, and this was repeated two more times to remove excess detergent. The pellet was suspended into 15 µL of buffer and combined in equal mass with cryoprotectant.

KcsA for SMA nanodisks was expressed by Dongyu "Allison" Zhang in the McDermott group who provided the cells to Youzhong Guo, Assistant Professor of Medicinal Chemistry of Virginia Commonwealth University, who incorporated the KcsA into SMA nanodisks and purified them by His-affinity chromotography, and returned them as a frozen solution. The purity of the sample was verified by SDS-PAGE gel finding a single band corresponding to the KcsA tetramer molecular weight.

### 4.7.5 *Electron Microscopy*

Samples were diluted to approximately $50\,\mathrm{mg\,mL^{-1}}$ with buffer and shaken vigorously by hand. Samples were plunged freezed in liquid ethane at $-173\,^{\circ}\mathrm{C}$ was performed using a CP3 Cryoplunge (Gatan) using 3 µL of sample incubated for 30 second and blotted for 0.5 s on Quantifoil R 1.2/1.3 grids (Electron Microscopy Sciences) that had been glow discharged (Gatan Solarus 950) for 45 s at $50\,W$ using $O_2$ and $H_2$ gases.

Cryo-electron micrographs were collected using a Tecnai F20 Twin transmission electron microscope operating at $120\,\mathrm{keV}$ defocused to $-3.00\,\mu\mathrm{m}$ detected using a Tietz F416 charged-coupled-device camera. Micrographs presented in images from Figure 4.14 were collected with a calibrated magnification of $\times 49\,000$ (3.44 Å per pixel) with a dosage of 30.40 $e^-$ per $Å^2$.

### 4.7.6 *Cryo-Protection*

Unless noted otherwise, DNP cryoprotection was provided by using 3 : 1 (w/w) U-$^{2}H$,$^{12}C$-glycerol–$D_2O$ (Cambridge) typically added in an equal volume to the sample.

### 4.7.7 *'Aliphatic Unlabeled' KcsA Protein Expression*

Using the work of Lacabanne, Meier, and Böckmann [44] which reviews which amino acids in BL21 *E. coli* cells can be unlabeled, an unlabeling strategy was developed that would principally unlabel aliphatic residues of KcsA through a combination of direct supplementation of natural abundance amino acids and through secondary metabolic products from supplied natural abundance amino acids. This labeling scheme was designed to provide many $^{15}N$-amide and $^{13}C$-carbonyl of adjacent residues in the termini but would leave have very few adjcent pairs labeled in the transmembrane domain.

To produce the unlabeled sample, KcsA was grown as described above with the following changes. Following growth of BL21(DE3) cells containing a KcsA plasmid in 1 L of LB to an $OD_{600} = 0.5$, the cells were pelleted by centrifuge and resuspended in 1 L M9 containing the ingredients described in Section A.6. This was allowed to grow to an $OD_{600} = 0.8$ and then induced with aTC at 35 °C, 300 RPM shaking for 3 h and then harvested by centrifuge and stored at −80 °C.

| | U-KcsA | Rev-KcsA |
|---|---|---|
| Pulse seq. | PDSDdarr.ivs | PDSDdarr.ivs |
| Scans | 32 | 16 |
| MAS (kHz) | 11 | 13.3 |
| R.D. (s) | 2 | 290° (us),4,3.2 |
| decoup. (us) | 4.4 | 2.8 |
| CP (us) | 550 | 600 |
| Operator | Rivkah Ragowski | Gary Howarth |

Table 4.4: Key NMR paramaters used to collect DNP-enhanced spectra of KcsA displayed in Figure 4.8.

### 4.7.8 *NMR Parameters Used to Compare U- and Reverse-Labeled KcsA*

## 4.8 acknowledgments

Several spectra are displayed as points of comparison for original data collected for this chapter. The author is grateful to Rivkah Rogawski and Dongyu (Allison) Zhang for permission and for providing the data related to U-$^{13}$C,$^{15}$N-KcsA DNP data, and 1,3-$^{13}$C-glycerol-KcsA data, respectively.

The aluminum block used for fast-freezing experiments was imagine, designed, and commissioned by Keith Fritzsching. The author is grateful to use it and for Dr. Fritzching's guidance throughout all of the experiments in this chapter.

TABLE 4.5: Peak assignments with peaks heights, volumes, and linewidths (as measured by parabolic fit) for aliphatic unlabeled KcsA by DNP-enhanced DARR.

| $\omega_2$ (ppm) | $\omega_1$ (ppm) | Height (A.U.) | Volume (A.U) | FWHM $\omega_2$ (Hz) | FWHM $\omega_1$ (Hz) | Resonance |
|---|---|---|---|---|---|---|
| 17.0 | 27.4 | 399000 | 3.49e+06 | 256.7 | 276.2 | $(\omega)$–$(\omega-1)$ |
| 20.1 | 55.0 | 196000 | 1.70e+06 | 663.7 | 306.4 | A? C$\beta$–C$\alpha$ |
| 31.3 | 66.8 | 219000 | 1.93e+06 | 332.8 | 323.5 | V? $\beta$–$\alpha$ |
| 55.0 | 18.1 | 217000 | 1.90e+06 | 221.0 | 348.4 | M–$\alpha-\epsilon$ |
| 55.5 | 133.9 | 150000 | 1.31e+06 | 159.2 | 255.6 | H–$\alpha-\gamma$ |
| 56.8 | 41.5 | 230000 | 2.03e+06 | 325.7 | 471.2 | Arg-$\alpha-\delta$-coil |
| 57.7 | 134.6 | 153000 | 1.31e+06 | 252.2 | 288.1 | H–$\alpha-\gamma$ |
| 58.6 | 44.0 | 275000 | 2.40e+06 | 321.6 | 428.2 | Arg-$\alpha-\delta$-helix |
| 70.5 | 64.9 | 189000 | 1.64e+06 | 188.1 | 223.4 | (PG-$\alpha$)–(PG-$\beta$) |
| 73.3 | 67.3 | 312000 | 2.76e+06 | 1306.4 | 467.3 | G2–G1/G2 |
| 123.4 | 113.4 | 332000 | 2.93e+06 | 613.7 | 356.3 | W–CN-$\zeta$ |
| 127.2 | 119.7 | 218000 | 1.93e+06 | 732.5 | 629.1 | W-$\delta-\epsilon$-helix |
| 130.1 | 121.3 | 350000 | 3.11e+06 | 343.2 | 782.1 | W-$\delta-\epsilon$-coil |
| 130.4 | 27.4 | 210000 | 1.82e+06 | 209.0 | 258.8 | (=C)–($\omega$-1) |
| 131.1 | 31.5 | 160000 | 1.40e+06 | 334.9 | 314.3 | (=C)–($CH_2$) |
| 131.6 | 35.4 | 216000 | 1.86e+06 | 166.7 | 244.3 | (=C)–($\omega$-2) |
| 138.4 | 113.2 | 273000 | 2.37e+06 | 234.5 | 466.6 | W-$\epsilon-\beta$ |
| 138.4 | 123.4 | 348000 | 3.05e+06 | 205.3 | 878.9 | W-$\epsilon$–CN |
| 138.4 | 121.4 | 306000 | 2.68e+06 | 268.6 | 905.5 | H–$\epsilon-\delta$ |
| 138.7 | 119.5 | 345000 | 3.01e+06 | 308.2 | 895.7 | W-$\epsilon1-\epsilon2$ |
| 158.7 | 43.7 | 226000 | 2.00e+06 | 296.4 | 574.8 | Arg-$\zeta-\delta$ |
| 172.7 | 48.9 | 166000 | 1.41e+06 | 523.0 | 1496.9 | G? |
| 174.7 | 47.5 | 206000 | 1.80e+06 | 145.6 | 331.9 | G? |
| 177.6 | 66.7 | 229000 | 1.98e+06 | 238.3 | 226.1 | V? CO–$\alpha$ |
| 183.9 | 38.2 | 172000 | 1.48e+06 | 252.8 | 265.7 | E51 (CO–$\gamma$) |

Table 4.6: Peaks from INADEQUATE experiment of F-$^2$H-KcsA.

| $\omega_2$ (ppm) | $\omega_1$ (ppm) | Height (A.U) | Volume (A.U.) | FWHM $\omega_2$ (Hz) | FWHM $\omega_1$ (Hz) |
|---|---|---|---|---|---|
| 16.2 | 68.5 | 199291 | 1.8e+06 | 423.3 | 442.1 |
| 17.2 | 68.6 | 202863 | 1.8e+06 | 559.2 | 528.4 |
| 18.2 | 70.2 | 201771 | 1.8e+06 | 190.1 | 458.9 |
| 20.0 | 84.1 | 209208 | 1.9e+06 | 293.2 | 661.7 |
| 23.1 | 50.1 | 187337 | 1.7e+06 | 431.5 | 470.8 |
| 26.2 | 52.8 | 223024 | 2.0e+06 | 554.0 | 1038.7 |
| 26.6 | 52.0 | 207071 | 1.9e+06 | 1082.3 | 1685.4 |
| 27.4 | 81.8 | 248244 | 2.2e+06 | 494.3 | 1009.8 |
| 27.5 | 52.5 | 219807 | 2.0e+06 | 564.0 | 997.5 |
| 28.3 | 83.9 | 289804 | 2.6e+06 | 422.2 | 845.3 |
| 29.3 | 83.9 | 266992 | 2.4e+06 | 439.7 | 803.9 |
| 29.6 | 55.1 | 254413 | 2.3e+06 | 739.2 | 1611.8 |
| 29.7 | 42.3 | 241210 | 2.1e+06 | 193.5 | 524.0 |
| 29.9 | 49.3 | 344330 | 3.1e+06 | 471.1 | 810.1 |
| 30.1 | 85.0 | 198287 | 1.8e+06 | 473.5 | 824.3 |
| 30.2 | 85.5 | 202502 | 1.8e+06 | 575.4 | 741.9 |
| 30.6 | 204.7 | 195207 | 1.7e+06 | 194.4 | 892.4 |
| 30.7 | 55.9 | 197093 | 1.8e+06 | 953.9 | 2293.7 |
| 31.4 | 47.3 | 206628 | 1.8e+06 | 656.7 | 2274.4 |
| 32.1 | 57.0 | 254689 | 2.3e+06 | 691.7 | 767.3 |
| 33.3 | 56.1 | 197625 | 1.8e+06 | 953.1 | 1510.2 |
| 33.3 | 58.8 | 221644 | 2.0e+06 | 592.5 | 1435.0 |
| 35.7 | 217.1 | 199625 | 1.8e+06 | 187.9 | 625.2 |
| 45.9 | 218.4 | 200585 | 1.8e+06 | 267.2 | 635.7 |
| 53.8 | 63.8 | 210573 | 1.9e+06 | 170.6 | 1408.4 |
| 54.3 | 230.3 | 656691 | 5.9e+06 | 328.5 | 832.1 |
| 54.5 | 68.3 | 262610 | 2.3e+06 | 226.0 | 1063.2 |
| 54.8 | 82.5 | 190193 | 1.7e+06 | 909.1 | 990.3 |
| 55.9 | 80.8 | 302082 | 2.7e+06 | 613.8 | 1221.3 |
| 56.5 | 226.4 | 239839 | 2.1e+06 | 223.4 | 1654.9 |
| 56.6 | 78.5 | 216823 | 1.9e+06 | 460.4 | 1403.8 |

Continued on next page

| $\omega_2$ (ppm) | $\omega_1$ (ppm) | Height | Volume | FWHM $\omega_2$ (Hz) | FWHM $\omega_1$ (Hz) |
|---|---|---|---|---|---|
| 56.6 | 232.6 | 419878 | 3.8e+06 | 830.0 | 1077.3 |
| 57.5 | 84.0 | 469047 | 4.2e+06 | 521.8 | 899.8 |
| 57.9 | 233.7 | 376788 | 3.4e+06 | 736.1 | 1165.8 |
| 58.7 | 85.6 | 443098 | 4.0e+06 | 413.3 | 987.3 |
| 58.9 | 229.4 | 255461 | 2.3e+06 | 1030.3 | 1732.8 |
| 59.1 | 234.3 | 340138 | 3.0e+06 | 775.7 | 825.1 |
| 59.3 | 118.6 | 187532 | 1.7e+06 | 166.7 | 567.0 |
| 59.9 | 159.1 | 189782 | 1.7e+06 | 262.8 | 415.8 |
| 59.9 | 234.8 | 329955 | 3.0e+06 | 776.3 | 982.3 |
| 60.5 | 163.8 | 182271 | 1.6e+06 | 176.8 | 426.6 |
| 61.4 | 231.0 | 192470 | 1.7e+06 | 140.0 | 476.6 |
| 61.5 | 123.6 | 195511 | 1.7e+06 | 160.4 | 1633.8 |
| 62.0 | 120.1 | 249602 | 2.2e+06 | 308.1 | 1181.8 |
| 62.3 | 236.2 | 200825 | 1.8e+06 | 1023.4 | 834.7 |
| 64.0 | 92.3 | 181792 | 1.6e+06 | 195.9 | 751.3 |
| 64.5 | 238.5 | 224708 | 2.0e+06 | 631.9 | 383.8 |
| 65.7 | 93.7 | 296237 | 2.6e+06 | 253.2 | 539.9 |
| 65.7 | 240.6 | 207878 | 1.9e+06 | 407.0 | 967.2 |
| 66.0 | 131.1 | 434644 | 3.9e+06 | 527.1 | 574.9 |
| 66.7 | 241.5 | 283365 | 2.5e+06 | 339.0 | 695.8 |
| 66.8 | 130.9 | 418974 | 3.7e+06 | 546.5 | 732.1 |
| 66.9 | 241.2 | 286008 | 2.5e+06 | 359.2 | 618.5 |
| 66.9 | 84.5 | 240376 | 2.1e+06 | 238.9 | 727.2 |
| 68.0 | 126.2 | 194560 | 1.7e+06 | 636.7 | 1446.4 |
| 69.5 | 127.8 | 197872 | 1.7e+06 | 818.1 | 565.0 |
| 174.2 | 228.6 | 227730 | 2.0e+06 | 157.8 | 1126.4 |
| 174.5 | 225.4 | 247061 | 2.2e+06 | 276.6 | 897.0 |
| 175.7 | 234.7 | 242918 | 2.2e+06 | 1055.3 | 2195.8 |
| 176.0 | 230.5 | 321660 | 2.9e+06 | 736.9 | 2146.7 |
| 176.9 | 240.7 | 240793 | 2.2e+06 | 313.0 | 2694.8 |
| 176.9 | 232.6 | 432826 | 3.9e+06 | 737.8 | 2277.9 |
| 177.6 | 230.1 | 551820 | 4.9e+06 | 507.7 | 1237.0 |
| 179.0 | 233.9 | 336370 | 3.0e+06 | 679.1 | 1256.2 |
| 180.2 | 232.3 | 300951 | 2.7e+06 | 864.4 | 523.7 |

[1] A. Abragam, A. Landesman, and J. Winter. "Effet Overhauser dans les charbons et graphites." In: *Comptes rendus hebdomadaires des séances de l'Académie des sciences* 247 (1958), p. 1852.

[2] A. Abragam and W. G. Proctor. "Une nouvelle méthode de polarisation dynamique des noyaux atomiques dans les solides." In: *Comptes rendus hebdomadaires des séances de l'Académie des sciences* 246 (1958).

[3] Ü. Akbey, A. H. Linden, and H. Oschkinat. "High-Temperature Dynamic Nuclear Polarization Enhanced Magic-Angle-Spinning NMR." In: *Applied Magnetic Resonance* 43.1-2 (2012), pp. 81–90. DOI: 10.1007/s00723-012-0357-2.

[4] Ü. Akbey and H. Oschkinat. "Structural biology applications of solid state MAS DNP NMR." In: *Journal of Magnetic Resonance* 269 (2016), pp. 213–224. DOI: 10.1016/j.jmr.2016.04.003.

[5] Ü. Akbey et al. "Dynamic Nuclear Polarization of Deuterated Proteins." In: *Angewandte Chemie International Edition* 49.42 (Oct. 2010), pp. 7803–7806. DOI: 10.1002/anie.201002044.

[6] J. T. Arnold, S. S. Dharmatti, and M. E. Packard. *Chemical effects on nuclear induction signals from organic compounds*. 1951. DOI: 10.1063/1.1748264.

[7] V. S. Bajaj, P. C. Van Der Wel, and R. G. Griffin. "Observation of a low-temperature, dynamically driven structural transition in a polypeptide by solid-state NMR spectroscopy." In: *Journal of the American Chemical Society* 131.1 (2009), pp. 118–128. DOI: 10.1021/ja8045926.

[8] V. S. Bajaj, M. L. Mak-Jurkauskas, M. Belenky, J. Herzfeld, and R. G. Griffin. "Functional and shunt states of bacteriorhodopsin resolved by 250 GHz dynamic nuclear polarization-enhanced solid-state NMR." In: *Proceedings of the National Academy of Sciences* 106.23 (June 2009), pp. 9244–9249. DOI: 10.1073/pnas.0900908106.

[9] A. Bax, R. Freeman, and S. P. Kempsell. "Natural Abundance 13C-13C Coupling Observed via Double-Quantum Coherence." In: *Journal of the American Chemical Society* 102.14 (1980), pp. 4849–4851. DOI: 10.1021/ja00534a056.

[10] L. R. Becerra et al. "A Spectrometer for Dynamic Nuclear Polarization and Electron Paramagnetic Resonance at High Frequencies." In: *Journal of Magnetic Resonance, Series A* (1995). DOI: 10.1006/jmra.1995.9975.

[11] L. R. Becerra, G. J. Gerfen, R. J. Temkin, D. J. Singel, and R. G. Griffin. "Dynamic nuclear polarization with a cyclotron resonance maser at 5 T." In: *Physical Review Letters* (1993). DOI: 10.1103/PhysRevLett.71.3561.

[12] H. Beljers, L. van der Kint, and J. van Wieringen. "Overhauser Effect in a Free Radical." In: *Physical Review* 95.6 (1954), p. 95.

[13] P. Bellstedt et al. "Resonance assignment for a particularly challenging protein based on systematic unlabeling of amino acids to complement incomplete NMR data sets." In: *Journal of Biomolecular NMR* 57.1 (Sept. 2013), pp. 65–72. DOI: 10.1007/s10858-013-9768-0.

[14] M. P. Bhate and A. E. McDermott. "Protonation state of E71 in KcsA and its role for channel collapse and inactivation." In: *Proceedings of the National Academy of Sciences of the United States of America* 109.38 (Sept. 2012), pp. 15265–70. DOI: 10.1073/pnas.1211900109.

[15] M. P. Bhate, B. J. Wylie, L. Tian, and A. E. McDermott. "Conformational dynamics in the selectivity filter of KcsA in response to potassium ion concentration." In: *Journal of molecular biology* 401.2 (Aug. 2010), pp. 155–66. DOI: 10.1016/j.jmb.2010.06.031.

[16] F. Bloch. "Dynamical Theory of Nuclear Induction. II." In: *Physical Review* 102.1 (Apr. 1956), pp. 104–135. DOI: 10.1103/PhysRev.102.104.

[17] F. Bloch, W. W. Hansen, and M. Packard. *Nuclear induction*. 1946. DOI: 10.1103/PhysRev.69.127.

[18] C. E. Bronnimann and G. E. Maciel. "13C NMR study of methanol in HY zeolite." In: *Journal of the American Chemical Society* 108.23 (1986), pp. 7154–7159. DOI: 10.1021/ja00283a003.

[19] T. R. Carver and C. P. Slichter. "Polarization of Nuclear Spins in Metals." In: *Physical Review* 92.1 (Oct. 1953), pp. 212–213. DOI: 10.1103/PhysRev.92.212.2.

[20] T. R. Carver and C. P. Slichter. "Experimental verification of the overhauser nuclear polarization effect." In: *Physical Review* 102.4 (1956), pp. 975–980. DOI: 10.1103/PhysRev.102.975.

[21] J. H. Chill, J. M. Louis, F. Delaglio, and A. Bax. "Local and global structure of the monomeric subunit of the potassium channel KcsA probed by NMR." In: *Biochimica et Biophysica Acta - Biomembranes* 1768.12 (2007), pp. 3260–3270. DOI: 10.1016/j.bbamem.2007.08.006.

[22] B. Corzilius. "Theory of solid effect and cross effect dynamic nuclear polarization with half-integer high-spin metal polarizing agents in rotating solids." In: *Physical Chemistry Chemical Physics* 18.39 (2016), pp. 27190–27204. DOI: 10.1039/c6cp04621e.

[23] B. Corzilius, L. B. Andreas, A. A. Smith, Q. Z. Ni, and R. G. Griffin. "Paramagnet induced signal quenching in MAS-DNP experiments in frozen homogeneous solutions." In: *Journal of Magnetic Resonance* (2014). DOI: 10.1016/j.jmr.2013.11.013.

[24] W. C. Dickinson. "Hartree computation of the internal diamagnetic field for atoms." In: *Physical Review* (1950). DOI: 10.1103/PhysRev.80.563.

[25] J. M. Dörr et al. "Detergent-free isolation, characterization, and functional reconstitution of a tetrameric K+ channel: the power of native nanodiscs." In: *Proceedings of the National Academy of Sciences of the United States of America* 111.52 (Dec. 2014), pp. 18607–12. DOI: 10.1073/pnas.1416205112.

[26] W. Doster. "The protein-solvent glass transition." In: *Biochimica et Biophysica Acta - Proteins and Proteomics* 1804.1 (2010), pp. 3–14. DOI: 10.1016/j.bbapap.2009.06.019.

[27] W. Doster, S. Cusack, and W. Petry. "Dynamical transition of myoglobin revealed by inelastic neutron scattering." In: *Nature* 337.6209 (Feb. 1989), pp. 754–756. DOI: 10.1038/337754a0.

[28] R. R. Ernst and W. A. Anderson. "Application of Fourier Transform Spectroscopy to Magnetic Resonance." In: *Review of Scientific Instruments* 37.1 (Jan. 1966), pp. 93–102. DOI: 10.1063/1.1719961.

[29] C. Fernández-de-Alba et al. "Matrix-Free DNP-Enhanced NMR Spectroscopy of Liposomes Using a Lipid-Anchored Biradical." In: *Chemistry - A European Journal* 21.12 (Mar. 2015), pp. 4512–4517. DOI: 10.1002/chem.201404588.

[30] K. J. Fritzsching, M. Hong, and K. Schmidt-Rohr. "Conformationally selective multidimensional chemical shift ranges in proteins from a PACSY database purged using intrinsic quality criteria." In: *Journal of Biomolecular NMR* 64.2 (Feb. 2016), pp. 115–130. DOI: 10.1007/s10858-016-0013-5.

[31] K. J. Fritzsching, B. Itin, and A. E. McDermott. "N,N-Diethylmethylamine as lineshape standard for NMR above 130 K." In: *Journal of Magnetic Resonance* 287 (Feb. 2018), pp. 110–112. DOI: 10.1016/J.JMR.2017.12.021.

[32] T. W. Griswold, A. F. Kip, and C. Kittel. "Microwave spin resonance absorption by conduction electrons in metallic sodium." In: *Physical Review* 88.4 (1952), pp. 951–952. DOI: 10.1103/PhysRev.88.951.

[33] H. S. Gutowsky, D. W. McCall, and C. P. Slichter. *Coupling among nuclear magnetic dipoles in molecules*. 1951. DOI: 10.1103/PhysRev.84.589.2.

[34] D. A. Hall et al. "Polarization-enhanced NMR spectroscopy of biomolecules in frozen solution." In: *Science* (1997). DOI: 10.1126/science.276.5314.930.

[35] S. R. Hartmann and E. L. Hahn. "Nuclear double resonance in the rotating frame." In: *Physical Review* 128.5 (1962), pp. 2042–2053. DOI: 10.1103/PhysRev.128.2042.

[36] M. Hong. "Solid-State Dipolar INADEQUATE NMR Spectroscopy with a Large Double-Quantum Spectral Width." In: *Journal of Magnetic Resonance* 136.1 (1999), pp. 86–91. DOI: 10.1006/jmre.1998.1631.

[37] K. N. Hu, V. S. Bajaj, M. Rosay, and R. G. Griffin. "High-frequency dynamic nuclear polarization using mixtures of TEMPO and trityl radicals." In: *Journal of Chemical Physics* 126.4 (2007). DOI: 10.1063/1.2429658.

[38] K. Y. Huang, A. B. Siemer, and A. E. McDermott. "Homonuclear mixing sequences for perdeuterated proteins." In: *Journal of Magnetic Resonance* 208.1 (2011), pp. 122–127. DOI: 10.1016/j.jmr.2010.10.015.

[39] T. Idehara et al. "The Development of 460 GHz gyrotrons for 700 MHz DNP-NMR spectroscopy." In: *Journal of Infrared, Millimeter, and Terahertz Waves* 36.7 (2015), pp. 613–627. DOI: 10.1007/s10762-015-0150-z.

[40] B. Itin and I. V. Sergeyev. "Strategies for Efficient Sample Preparation for Dynamic Nuclear Polarization Solid-State NMR of Biological Macromolecules." In: *Protein NMR: Methods and Protocols, Methods in Molecular Biology, vol 1688*. Ed. by R. Ghose. Humana Press, New York, NY, 2018, pp. 133–154. DOI: 10.1007/978-1-4939-7386-6_7.

[41] C. P. Jaroniec. "Solid-state nuclear magnetic resonance structural studies of proteins using paramagnetic probes." In: *Solid State Nuclear Magnetic Resonance* 43-44 (May 2012), pp. 1–13. DOI: 10.1016/j.ssnmr.2012.02.007.

[42] M. Kaplan et al. "Probing a cell-embedded megadalton protein complex by DNP-supported solid-state NMR." In: *Nature Methods* 12.7 (July 2015), pp. 649–652. DOI: 10.1038/nmeth.3406.

[43] T. J. Knowles et al. "Membrane Proteins Solubilized Intact in Lipid Containing Nanoparticles Bounded by Styrene Maleic Acid Copolymer." In: *Journal of the American Chemical Society* 131.22 (June 2009), pp. 7484–7485. DOI: 10.1021/ja810046q.

[44] D. Lacabanne, B. H. Meier, and A. Böckmann. "Selective labeling and unlabeling strategies in protein solid-state NMR spectroscopy." In: *Journal of Biomolecular NMR* (Dec. 2017), pp. 1–10. DOI: 10.1007/s10858-017-0156-z.

[45] S. Lange et al. "The effect of biradical concentration on the performance of DNP-MAS-NMR." In: *Journal of magnetic resonance (San Diego, Calif. : 1997)* 216 (Mar. 2012), pp. 209–12. DOI: 10.1016/j.jmr.2012.01.002.

[46] D. Le et al. "Optimizing sample preparation methods for dynamic nuclear polarization solid-state NMR of synthetic polymers." In: *Macromolecules* (2014). DOI: 10.1021/ma500788n.

[47] M. Lee and M. Hong. "Cryoprotection of lipid membranes for high-resolution solid-state NMR studies of membrane peptides and proteins at low temperature." In: *Journal of Biomolecular NMR* 59.4 (Aug. 2014), pp. 263–277. DOI: 10.1007/s10858-014-9845-z.

[48] S. C. Lee et al. "A method for detergent-free isolation of membrane proteins in their local lipid environment." In: *Nature Protocols* (2016). DOI: 10.1038/nprot.2016.070.

[49] M. Lelli et al. "Hydrophobic radicals embedded in neutral surfactants for dynamic nuclear polarization of aqueous environments at 9.4 Tesla." In: *Chem. Commun.* 50.71 (Aug. 2014), pp. 10198–10201. DOI: 10.1039/C4CC02152E.

[50] S. Y. Liao, M. Lee, T. Wang, I. V. Sergeyev, and M. Hong. "Efficient DNP NMR of membrane proteins: sample preparation protocols, sensitivity, and radical location." In: *Journal of Biomolecular NMR* 64.3 (Mar. 2016), pp. 223–237. DOI: 10.1007/s10858-016-0023-3.

[51] S. Y. Liao, K. J. Fritzsching, and M. Hong. "Conformational analysis of the full-length M2 protein of the influenza A virus using solid-state NMR." In: *Protein Science* 22.11 (Nov. 2013), pp. 1623–1638. DOI: 10.1002/pro.2368.

[52] A. H. Linden et al. "Cryogenic temperature effects and resolution upon slow cooling of protein preparations in solid state NMR." In: *Journal of Biomolecular NMR* 51.3 (2011), pp. 283–292. DOI: 10.1007/s10858-011-9535-z.

[53] A. H. Linden et al. "Neurotoxin II Bound to Acetylcholine Receptors in Native Membranes Studied by Dynamic Nuclear Polarization NMR." In: *Journal of the American Chemical Society* 133.48 (Dec. 2011), pp. 19266–19269. DOI: 10.1021/ja206999c.

[54] R. C. MacDonald, F. D. Jones, and R. Qui. "Fragmentation into small vesicles of dioleoylphosphatidylcholine bilayers during freezing and thawing." In: *Biochimica et Biophysica Acta (BBA) - Biomembranes* 1191.2 (May 1994), pp. 362–370. DOI: 10.1016/0005-2736(94)90187-2.

[55] D. Mance et al. "An Efficient Labelling Approach to Harness Backbone and Side-Chain Protons in 1 H-Detected Solid-State NMR Spectroscopy." In: *Angewandte Chemie* 127.52 (Dec. 2015), pp. 16025–16029. DOI: 10.1002/ange.201509170.

[56] M. M. Maricq and J. S. Waugh. "NMR in rotating solids." In: *The Journal of Chemical Physics* (1979). DOI: 10.1063/1.437915.

[57] L. D. Mayer, M. J. Hope, P. R. Cullis, and A. S. Janoff. "Solute distributions and trapping efficiencies observed in freeze-thawed multilamellar vesicles." In: *BBA - Biomembranes* (1985). DOI: 10.1016/0005-2736(85)90084-7.

[58] A. W. Overhauser. "Polarization of Nuclei in Metals." In: *Physical Review* 92.2 (Oct. 1953), pp. 411–415. DOI: 10.1103/PhysRev.92.411.

[59] Y. P. Patil and S. Jadhav. "Novel methods for liposome preparation." In: *Chemistry and physics of lipids* 177 (Jan. 2014), pp. 8–18. DOI: 10.1016/j.chemphyslip.2013.10.011.

[60] B. Pozo Navas et al. "Composition dependence of vesicle morphology and mixing properties in a bacterial model membrane system." In: *Biochimica et Biophysica Acta - Biomembranes* 1716.1 (2005), pp. 40–48. DOI: 10.1016/j.bbamem.2005.08.003.

[61] W. G. Proctor and F. C. Yu. "On the nuclear magnetic moments of several stable isotopes." In: *Physical Review* (1951). DOI: 10.1103/PhysRev.81.20.

[62] E. M. Purcell, H. C. Torrey, and R. V. Pound. *Resonance absorption by nuclear magnetic moments in a solid*. 1946. DOI: 10.1103/PhysRev.69.37.

[63] E. Ravera et al. "DNP-Enhanced MAS NMR of Bovine Serum Albumin Sediments and Solutions." In: *The Journal of Physical Chemistry B* 118.11 (Mar. 2014), pp. 2957–2965. DOI: 10.1021/jp500016f.

[64] E. Ravera et al. "Dynamic nuclear polarization of sedimented solutes." In: *Journal of the American Chemical Society* 135.5 (2013), pp. 1641–1644. DOI: 10.1021/ja312553b.

[65] V. Royden. *Measurement of the Spin and gyromagnetic ratio of C13 by the collapse of Spin-Spin Splitting*. 1954. DOI: 10.1103/PhysRev.96.543.

[66] E. S. Salnikov et al. "Dynamic Nuclear Polarization/Solid-State NMR Spectroscopy of Membrane Polypeptides: Free-Radical Optimization for Matrix-Free Lipid Bilayer Samples." In: *ChemPhysChem* 18.15 (Aug. 2017), pp. 2103–2113. DOI: 10.1002/cphc.201700389.

[67] C. Sauvée et al. "Highly Efficient, Water-Soluble Polarizing Agents for Dynamic Nuclear Polarization at High Frequency." In: *Angewandte Chemie* 125.41 (Oct. 2013), pp. 11058–11061. DOI: 10.1002/ange.201304657.

[68] S. Scheidelaar et al. "Molecular model for the solubilization of membranes into nanodisks by styrene maleic Acid copolymers." In: *Biophysical journal* 108.2 (Jan. 2015), pp. 279–90. DOI: 10.1016/j.bpj.2014.11.3464.

[69] A. Schulte et al. "Glassy Behavior of a Protein." In: *Physical Review Letters* 62.16 (1989), pp. 1–4.

[70] J. Seelig and A. Seelig. "Lipid conformation in model membranes and biological membranes." In: *Quarterly Reviews of Biophysics* 13.01 (Feb. 1980), p. 19. DOI: 10.1017/S0033583500000305.

[71] I. V. Sergeyev, B. Itin, R. Rogawski, L. A. Day, and A. E. McDermott. "Efficient assignment and NMR analysis of an intact virus using sequential side-chain correlations and DNP sensitization." In: *Proceedings of the National Academy of Sciences* 114.20 (2017), pp. 5171–5176. DOI: 10.1073/pnas.1701484114.

[72] A. B. Siemer, K. Y. Huang, and A. E. McDermott. "Protein Linewidth and Solvent Dynamics in Frozen Solution NMR." In: *PLoS ONE* 7.10 (2012). DOI: 10.1371/journal.pone.0047242.

[73] A. A. Smith, B. Corzilius, A. B. Barnes, T. Maly, and R. G. Griffin. "Solid effect dynamic nuclear polarization and polarization pathways." In: *Journal of Chemical Physics* 136.1 (2012). DOI: 10.1063/1.3670019.

[74] K. Takegoshi, S. Nakamura, and T. Terao. "13C–1H dipolar-assisted rotational resonance in magic-angle spinning NMR." In: *Chemical Physics Letters* 344.5-6 (Aug. 2001), pp. 631–637. DOI: 10.1016/S0009-2614(01)00791-6.

[75] M. Traïkia, D. E. Warschawski, M. Recouvreur, J. Cartaud, and P. F. Devaux. "Formation of unilamellar vesicles by repetitive freeze-thaw cycles: characterization by electron microscopy and 31 P-nuclear magnetic resonance." In: *European Biophysics Journal* 29.3 (June 2000), pp. 184–195. DOI: 10.1007/s002490000077.

[76] F. I. Valiyaveetil, Y. Zhou, and R. MacKinnon. "Lipids in the structure, folding, and function of the KcsA K+ channel." In: *Biochemistry* 41.35 (2002), pp. 10771–10777. DOI: 10.1021/bi026215y.

[77] E. A. Van Der Cruijsen et al. "Biomolecular DNP-Supported NMR Spectroscopy using Site-Directed Spin Labeling." In: *Chemistry - A European Journal* 21.37 (2015), pp. 12971–12977. DOI: 10.1002/chem.201501376.

[78] R. Verardi, N. J. Traaseth, L. R. Masterson, V. V. Vostrikov, and G. Veglia. "Isotope Labeling for Solution and Solid-State NMR Spectroscopy of Membrane Proteins." In: Springer, Dordrecht, 2012, pp. 35–62. DOI: 10.1007/978-94-007-4954-2_3.

[79] K. M. Visscher et al. "Supramolecular Organization and Functional Implications of K + Channel Clusters in Membranes." In: *Angewandte Chemie - International Edition* 56.43 (2017), pp. 13222–13227. DOI: 10.1002/anie.201705723.

[80] A. J. Wand and A. L. Lee. "Microscopic origins of entropy, heat capacity and the glass transition in proteins." In: *Nature* 411.6836 (2001), pp. 501–4. DOI: 11373686.

[81] M. Weingarth et al. "Structural determinants of specific lipid binding to potassium channels." In: *Journal of the American Chemical Society* 135.10 (2013), pp. 3983–3988. DOI: 10.1021/ja3119114.

[82] B. J. Wylie, M. P. Bhate, and A. E. McDermott. "Transmembrane allosteric coupling of the gates in a potassium channel." In: *Proceedings of the National Academy of Sciences of the United States of America* 111.1 (Jan. 2014), pp. 185–90. DOI: 10.1073/pnas.1319577110.

# FUTURE DIRECTIONS 5

Where to go from here?

The purpose of these studies was to capture more information about the little charted termini of KcsA. The cytosolic regions of KcsA are interesting in their own right. Moreover, capturing information from mobile portions of membrane proteins is a general problem. We have very little information on *any* extracellular region of any membrane protein when embedded into a membrane. How are we going to change that?

## 5.1 EXTENDING THE CURRENT STUDIES

Chapter 2 showed genuine progress with respect to detecting the C-terminus of KcsA and the effort was largely frustrated by the presence of fast $T_2$ relaxation. Fractional deuteration of KcsA saw huge leaps forward when compared to fully protonated KcsA. There is every reason to expect that perdeuterated and back-aminated KcsA would have even more gains. In fact, back-exchanging per deuterated KcsA also has the advantage that the amide in the transmembrane domain does not exchange in KcsA [2], thus selectively labeling the termini. There are several reports of the use of

perdeuterated KcsA [2, 9, 10], yet many repeated attempts in the McDermott group, including by significantly more competent biochemist than this author, have failed to yield any significant quantity of deuterated KcsA. It seems than instead of an all-out assault on in the laboratory and the associated, time, money, and tears required, a collaboration is required. It is easy for advances in spectroscopy to be derailed by problems with the biochemistry.

The problem with assigning any of the resonances in the 3D backbone experiment is connecting the various C$\alpha$ resonances to its respective C$\beta$ resonance, yet protons at that site severely decrease the $T_2$ and with it the signal also vanishes. Perdeuteration might even allow for collection of canonical backbone experiments from solution spectroscopy. Perdeuterated KcsA in nanodisks was unable to accomplish this in traditional solution spectroscopy [7]. Yet, even with fractional deuteration, HR-MAS shows real promise for use in taking the next step to making sequential assignments of the terminus.

Even the current advances made in these pages can provide real utility, and can applied to questions of the biology of KcsA. For example, using the C-terminal conformational markers specified in the Chapter 2, and with the markers identified in previous work [11, 12] one can now ask if there is an allosteric connection between the selectivity filter, the outer gate, and the C-terminus.

For example, by depleting $K^+$ while in low pH, KcsA's selectivity filter collapses. Does this then mean the C-terminus transitions from low mobility to high mobility?

### 5.1.1 *Dynamic Nuclear Polarization*

Dynamic nuclear polarization NMR is not for the faint of heart. The technique has incredible potential, but it carries many caveats. DNP has only shown limited utility in *de novo* assignment, and as the the challenges posed by cryogenic temperature (e.g. changes in chemical shifts and increased linewidths), demand that those assignments rely on 4- or even 5D spectra (see Sergeyev et al. [8]). To justify the instrument time, the extra preparation, and the added expense of DNP-enhanced NMR, the enhancements must significantly accelerate experiments. The data presented in Chapter 4 provided such poor resolution (i.e. no resolution) in the the N-CO double cross polarization experiment, it is possible that a 3D experiment would not provide any significant amount of single site resolution. It is not even clear if the the DNP system could operate continuously for the period required. Also, if we identify these missing resonances by DNP, we must go back to the DNP system to ask any questions of this domain, in which case they ought to be some really good questions.

In this particular instance, the extreme low temperatures of the system were used in an attempt to trap the highly mobile portions of KcsA. Yet there must be enough enhancements by DNP to offset the decrease in resolution caused by the same low temperatures. However, the mobile portions are important, in part, *because they are mobile*. The dynamics of these regions makes them hard to study but are essential to their function. Crystallography has provided beautiful structures of trapped conformations. The advantage of NMR is that the technique can examine dynamic systems

in all their dynamic glory, drawing conclusions from those dynamics. Yet the application of DNP to study mobile portions of a protein mitigates the advantages of NMR and exacerbates the short-comings that other techniques share.

## 5.2 FAST(ER) MAS

As was demonstrated in Chapter 2, $^{1}$H-detected magic angle spinning NMR provides an avenue to examine the mobile regions of KcsA. Over the past ten years advances in magic angle spinning technology have allowed for experiments to be routinely conducted at 60 kHz MAS and as high as 120 kHz, allowing for proton detection of highly anisotropic systems.

Highly deuterated proteins that are have partially $^{1}$H back-exchange on the amide show good resolution at 40 kHz and similar resolution can be achieved on fully back-exchanged proteins at 60 kHz MAS [6]. Yet despite these advances, mobile regions continue to be difficult. A study of the beta-barrel protein OmpX in membranes at 60 and 120 kHz failed to resolve the resonances in the loop region [4].

Very little work has been published on how fast MAS might be applied to mobile regions. At the rotor wall of a 0.8 mm rotor spinning at 100 kHz the relative centrifugal force is $1.1 \cdot 10^{7} \times g$. It has been noted that these extreme forces do not appear to deteriorate ubiquitin [1] over a period of a week or more. However, it remains an open question if these forces might trap highly mobile regions of a protein into specific

conformations, potentially many different conformations, leading to the inability to be resolved by CP-based or J-based methods.

Although usually ignored in solid-state NMR, J-couplings between atoms in a protein are always present. As discussed at length in Chapter 2, the sites of interest must have at least have $T_2$ relaxation values of 10s of milliseconds in order to transfer polarization efficiently. Even at 100 kHz of spinning relaxation is still very fast. Simulations estimate that 300 kHz of mechanical spinning would be required to used J-based methods to resolve all the sites of a very rigid protein [13].

In order to properly evaluate whether fast magic angle spinning can provide more information, a systematic study must investigate the effects of centrifugal forces on mobile regions. Since residues of the C-terminus are well resolved in the studies described in Chapter 2, KcsA would make an excellent model system for such a study. Specifically, using the $^{1}$H-$^{15}$N HSQC of KcsA at increasing speeds of a fast MAS probe, a spectroscopist could track the linewidths and relaxation behavior through a series and verify to what degree signal is attenuated or improved as spinning reaches high rates. In all likelihood there is a regime in which resolution is best enhanced and conformation is not distorted. Identifying this regime and applying judicious detueration would appear to be the most promising way forward in developing methods of resolving highly mobile portions of membrane proteins.

Cryo-electron microscopy is another area that has proven its merit in determining the structure of membrane proteins, and some success in resolving the mobile portion of ion channels in particular. The structure of the transient receptor potential channel TRPV1 was solved by cryo-electron microscopy at 3.4 Å resolution, resolving some side chains [5]. That channel has a substantial cytoplasmic region, and the microscopy go the channel in liposomes resolved the cytoplasmic regions nearest the transmembrane domain, but did not resolve the more distal N-terminus. TRPV2 has demonstrated more completeness in the termini and loop regions, yet, the resolution of that structure is weak in those regions and a failure to refine the most mobile regions [16].

KcsA has approximately 60 cytosolic residues, and, as shown in these pages, has proven to be a challenge to solve when the channel is in a membrane. Sixty residues is cute in comparison to many channels, such as the ryanodine receptors, whose cytoplasmic domains can exceed 4500 residues. In these massive proteins, cry-electron microscopy shows outstanding promise, with the technique demonstrating the ability to resolve structures an order of magnitude larger than NMR is able to handle [15]. Yet these massive domains are relatively immobile and many of the mobile details are lost [14]. Cryo-electron microscopy relies on relatively ordered structures.

A multi-technique integrated approach seems especially promoting. For example, Gauto et al. [3], has shown the ability to combine structural information from CP-MAS

NMR with the EM structural data to refine the 468 kDa dodecameric aminopeptidase TET2 protein to below 1 Å much improving on what NMR or electron microscopy could accomplish alone.

[1] V. Agarwal et al. "De novo 3D structure determination from sub-milligram protein samples by solid-state 100 kHz MAS NMR spectroscopy." In: *Angewandte Chemie (International ed. in English)* 53.45 (Nov. 2014), pp. 12253–6. DOI: 10.1002/anie.201405730.

[2] J. H. Chill, J. M. Louis, C. Miller, and A. Bax. "NMR study of the tetrameric KcsA potassium channel in detergent micelles." In: *Protein science : a publication of the Protein Society* 15.4 (Apr. 2006), pp. 684–98. DOI: 10.1110/ps.051954706.

[3] D. F. Gauto et al. "Integrated NMR and cryo-EM atomic-resolution structure determination of a half-megadalton enzyme complex." In: *Nature Communications* 10.1 (2019), pp. 1–12. DOI: 10.1038/s41467-019-10490-9.

[4] N. A. Lakomek et al. "Proton-detected NMR spectroscopy of nanodisc-embedded membrane proteins: MAS solid-state vs solution-state methods." In: *Journal of Physical Chemistry B* 121.32 (2017), pp. 7671–7680. DOI: 10.1021/acs.jpcb.7b06944.

[5] M. Liao, E. Cao, D. Julius, and Y. Cheng. "Structure of the TRPV1 ion channel determined by electron cryo-microscopy." en. In: *Nature* 504.7478 (Dec. 2013), pp. 107–12. DOI: 10.1038/nature12822.

[6] A. J. Nieuwkoop et al. "Sensitivity and resolution of proton detected spectra of a deuterated protein at 40 and 60 kHz magic-angle-spinning." In: *Journal of Biomolecular NMR* 61.2 (2015), pp. 161–171. DOI: 10.1007/s10858-015-9904-0.

[7] A. Qasim et al. "Investigation of a KcsA Cytoplasmic pH Gate in Lipoprotein Nanodiscs." In: *ChemBioChem* 20.6 (Mar. 2019), pp. 813–821. DOI: 10.1002/cbic.201800627.

[8] I. V. Sergeyev, B. Itin, R. Rogawski, L. A. Day, and A. E. McDermott. "Efficient assignment and NMR analysis of an intact virus using sequential side-chain correlations and DNP sensitization." In: *Proceedings of the National Academy of Sciences* 114.20 (2017), pp. 5171–5176. DOI: 10.1073/pnas.1701484114.

[9] K. Takeuchi, H. Takahashi, S. Kawano, and I. Shimada. "Identification and characterization of the slowly exchanging pH-dependent conformational rearrangement in KcsA." en. In: *The Journal of biological chemistry* 282.20 (May 2007), pp. 15179–86. DOI: 10.1074/jbc.M608264200.

[10] M. Weingarth et al. "Quantitative Analysis of the Water Occupancy around the Selectivity Filter of a K + Channel in Different Gating Modes." In: *Journal of the American Chemical Society* 136.5 (Feb. 2014), pp. 2000–2007. DOI: 10.1021/ja411450y.

[11] B. J. Wylie, M. P. Bhate, and A. E. McDermott. "Transmembrane allosteric coupling of the gates in a potassium channel." In: *Proceedings of the National Academy of Sciences of the United States of America* 111.1 (Jan. 2014), pp. 185–90. DOI: 10.1073/pnas.1319577110.

[12] Y. Xu, M. P. Bhate, and A. E. McDermott. "Transmembrane allosteric energetics characterization for strong coupling between proton and potassium ion binding in the KcsA channel." In: *Proceedings of the National Academy of Sciences of the United States of America* 114.33 (Aug. 2017), pp. 8788–8793. DOI: 10.1073/pnas.1701330114.

[13] K. Xue et al. "Magic-Angle Spinning Frequencies beyond 300 kHz Are Necessary to Yield Maximum Sensitivity in Selectively Methyl Protonated Protein Samples in Solid-State NMR." In: *Journal of Physical Chemistry C* 122.28 (2018), pp. 16437–16442. DOI: 10.1021/acs.jpcc.8b05600.

[14] Z. Yuchi and F. Van Petegem. "Ryanodine receptors under the magnifying lens: Insights and limitations of cryo-electron microscopy and X-ray crystallography studies." In: *Cell Calcium* 59.5 (2016), pp. 209–227. DOI: 10.1016/j.ceca.2016.04.003.

[15] R. Zalk et al. "Structure of a mammalian ryanodine receptor." In: *Nature* 517.7532 (2015), pp. 44–49. DOI: 10.1038/nature13950.

[16] L. Zubcevic et al. "Cryo-electron microscopy structure of the TRPV2 ion channel." In: *Nature Structural & Molecular Biology* 23.2 (Feb. 2016), pp. 180–186. DOI: 10.1038/nsmb.3159.

# Part II

# APPENDICES

# BACTERIAL CONSTRUCTS AND PREPARATIONS

## A.1 KCSA CONSTRUCT

Heginbotham, Odessey, and Miller first report discovering a gene in *Streptomyces lividans* they believed to be a potassium channel and confirmed this was the case using a synthetic construct [4].

The wild type KcsA channel is a 160 residue, 17.5 kDa peptide that forms a homotetrameric, inward rectifying, pH-gated potassium channel.

LISTING A.1: Amino acid sequence of single wild type KcsA subunit

```
  1  MPPML SGLLA RLVKL LLGRH GSALH WRAAG AATVL LVIVL LAGSY LAVLA
 51  ERGAP GAQLI TYPRA LWWSV ETATT VGYGD LYPVT LWGRL VAVVV MVAGI
101  TSFGL VTAAL ATWFV GREQE RRGHF VRHSE KAAEE AYTRT TRALH ERFDR
151  LERML DDNRR
```

LISTING A.2: DNA sequence of $His_6$-KcsA gene used throughout this thesis (unless noted otherwise)

```
  1  ATGCA TCATC ATCAT CATCA TCCGC CAATG TTGTC CGGTC TGCTT GCTCG
 51  TCTGG TTAAG TTGCT TCTGG GCCGT CACGG TTCTG CGCTG CACTG GCGTG
101  CTGCA GGCGC TGCCA CCGTC CTTCT GGTGA TCGTA CTGCT TGCTG GTTCC
151  TACTT GGCGG TTCTG GCTGA ACGGG GCGCA CCTGG TGCTC AGCTT ATTAC
201  TTATC CTCGT GCCTT GTGGT GGTCT GTCGA GACCG CTACT ACCGT GGGTT
251  ACGGC GACTT GTATC CGGTG ACCCT TTGGG GTCGT CTGGT AGCGG TTGTC
301  GTTAT GGTGG CTGGC ATCAC CTCCT TCGGT CTGGT AACTG CTGCC CTTGC
351  TACTT GGTTT GTAGG CCGCG AACAA GAGCG TCGTG GTCAT TTCGT TCGTC
401  ACTCT GAAAA AGCGG CTGAG GAGGC ATACA CCCGT ACTAC CCGTG CTCTG
451  CACGA GCGCT TTGAC CGTCT GGAAC GTATG CTTGA CGATA ACCGT CGT
```

## A.2 KCSA PROTEIN EXPRESSION

KcsA was expressed as a N-terminal $His_6$ fusion protein cloned onto a PASK90 plasmid and over expressed in *Escherichia coli* using established protocols developed by Manasi Bhate in our group[2].

Typically, KcsA gene Listing A.2 on a PASK90 plasmid, which confers ampicillin resistance, was transformed into chemically competent cells by heat shock at 42 °C, and plated onto Luria broth (LB) agar plates augmented with 100 mg $L^{-1}$ carbenicillin plates overnight at 37 °C. Individual colonies were picked and used to inoculate several precultures of 5 mL of carbenicillin LB media and grown to an $OD_{600} \approx 1$. Four 1 L LB cultures were inoculated using one preculture each and allowed to grow at 37 °C and 250 RPM of shaking to $OD_{600}=0.9$, at which point the cultures were harvested by centrifugation at $4 \times 10^3$ RCF for 10 min. The cells were then resuspended in 1 L M9 minimal media (see Section A.3.1.2 for complete recipe) whose sole source of carbon was U-$^{13}$C glucose and nitrogen $^{15}$N ammonium chloride. The cells were incubated for 60 min at 37 °C and 250 RPM of shaking. The culture temperature was lowered to 25 °C and shaking rate increased to 300 RPM. Protein expression was then initiated by the addition of 1 µg $L^{-1}$ anhydrotetracyclin (aTC), a synthetic lactose mimic, and the culture allowed to express overnight. Cells were then harvested by centrifugation at $4 \times 10^3$ RCF for 30 min and frozen at −80 °C until further processed.

## A.3 FRACTIONALLY DEUTERATED KCSA PROTEIN EXPRESSION

Two fractional deuteration protocols were employed, the first was used without major modification from [5] which in turn was an adaptation from [6].

Briefly, KcsA culture was prepared as described above using Bl21(DE3) *E. coli* cells (New England Biolabs). Cells were grown at 35 °C, 250 RPM shaking, in 1 L of LB selection medium (using carbenicillin) to an $OD_{600} = 0.8$ and were collected by centrifugation. The cell pellet was rinsed in approximately 50 mL of $D_2O$. The cells were then suspended in 500 mL of M9 media solution described below Section A.3.1.2 with the exception that instead of using deionized water to prepare the M9 minimal media, 98 % $D_2O$ (Cambridge) was used. The media, as shown below, was supplemented with 3 g U-$^{13}$C-glucose and $^{15}$N-ammonia 1 g. This culture was allowed to grow for 1 h, then the temperature lowered to 25 °C and shaking increased to 300 RPM, and induced with aTC. The cells were allowed to express for 10 h and harvested by centrifuge, stored at −80 °C and purified as described in this appendix.

### A.3.1 *Minimal Media Recipes*

#### A.3.1.1 *R2 YE Media*

Modified from Shepherd et al. [7].

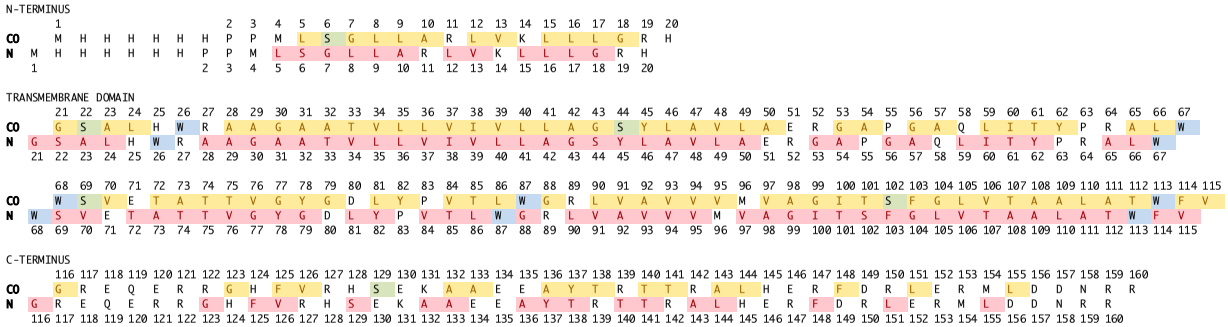


FIGURE A.1: KcsA sequence showing expected labeling scheme for both amide-nitrogen and amide-carbonyl, with color indicating near natural abundance label. The CO series is offset to better demonstrate anticipated CO–N inter-residue correlations expected on an N-CO correlation spectrum. Ser and Trp residues are expected to have less than complete reverse labeling as they are down stream metabolic products and not specifically unlabeled

Part A and B are combined, adjusted to pH 7.2, diluted to 1 L and sterile filtered.

**Part A:**

Diluted to 0.8 L with deionized water, autoclaved.

- Sucrose: 103 g
- $K_2SO_4$: 0.25 g
- $MgCl_2 \cdot 6\,H_2O$: 10.12 g
- Glucose: 10 g
- Casamino acids: 0.1 g
- Yeast extract: 5 g

**Part B:**

Combined, sterile filtered, and added ascetically to added to Part A.

- Trace Solution: 2 mL
- TES buffer 5.75 g in 100 mL
- $KH_2PO_4$ 50 mg in 10 mL
- $CaCl_2 \cdot 2\,H_2O$ 3 g in 80 mL
- L-proline 3 g in 15 mL
- NaOH (1 N): 5 mL
- Yeast extract 5 g in 50 mL
- Thiostrepton 50 mg in 1 mg

**Trace Element Solution**:

Diluted to 1 L with deionized water, sterile filtered.

- $ZnCl_2$: 40 mg
- $FeCl_3 \cdot 6\,H_2O$: 200 mg
- $CuCl_2 \cdot 2\,H_2O$: 10 mg
- $MnCl_2 \cdot 4\,H_2O$: 10 mg

- $Na_2B_4O_7 \cdot 10\,H_2O$: 10 mg
- $(NH_4)_6Mo_7O_{24} \cdot 4\,H_2O$ 10 mg

#### A.3.1.2 $^{13}C$, $^{15}N$ *M9 Minimal Media:*

Adapted from Bhate et al. [1].

**M9**:

Combined, adjusted to pH 7.2, diluted to 1 L in deionized water, and sterile-filtered.

- 10X M9 salts: 100 mL
- Solution C: 20 mL
- Vitamin solution: 500 µL
- Gibco 100X MEM vitamin solution: 10 mL
- $MgSO_4$ (1 M): 2 mL
- $CaCl_2$ (1 M): 100 µL
- Carbenicillin: 100 mg
- U-$^{13}C$ glucose: 3 g
- $^{15}N$ ammonium chloride: 1.0 g
- L-Proline (when using JM-83 cell line) 1 g

**M9 Salts (10X)**

Diluted to 1 L deionized water and sterile-filtered.

- $Na_2HPO_4 \cdot 7\,H_2O$: 128 g
- $KH_2PO_4$: 30 g
- NaCl: 5 g

**Solution C**

Adjusted to pH 6.5, diluted to 1 L, sterile-filtered, stored in the dark at 4 °C.

- Metal 44: 50 mL
- KOH: 7.3 g

- Nitrilotriacetic acid: 10 g
- $MgCl_2 \cdot 6\,H_2O$: 24 g
- $CaCl_2 \cdot 2\,H_2O$: 3.5 g

**Metal 44 solution**

Diluted to 100 mL, sterile-filtered, stored in the dark at 4 °C.

- $K_2EDTA \cdot 2\,H_2O$: 0.35 g
- $ZnCl_2$: 0.5 g
- $FeCl_2 \cdot 4\,H_2O$: 0.5 g
- $MnCl_2 \cdot 4\,H_2O$: 0.2 g
- $(NH_4)_6Mo_7O_{24} \cdot 6\,H_2O$: 19 mg
- $CuCl_2 \cdot 2\,H_2O$: 16 mg
- $Co(NO_3)_2 \cdot 6\,H_2O$: 25 mg
- $H_3BO_3$: 12 mg

**Vitamin stock:**

Diluted to 50 mL, stored in the dark at 4 °C.

- Nicotinic acid: 0.5 g
- 4-aminobenzoic acid 50 mg
- Biotin: 5 mg

### A.3.1.3 *Aliphatic Reverse Labeling*

The typical $^{13}C$, $^{15}N$ M9 media above is supplemented with the 1 g each of the following, natural-abundance L-amino acids:

- Alanine
- Glycine
- Isoleucine
- Leucine
- Phenylalanine

- Threonine
- Tyrosine
- Valine

#### A.3.1.4 *Methionine, leucine specific labeling:*

The typical $^{13}C$, $^{15}N$ M9 media above has natural-abundance glucose and ammonium chloride instead of enriched compounds. The media is supplemented with 200 mg $^{15}N$-L-leucine and 1 g $^{13}CO$-L-methionine, 200 mg of natural abundance L-cysteine, 1 g each of the following natural abundance L-amino acids:

- Arginine
- Aspartamine
- Aspartate
- Glutamine
- Glutamate
- Glycine
- Histadine
- Lysine
- Phenylalanine
- Proline
- Serine
- Threonine
- Tryptophan
- Tyrosine

2 g each of the following natural abundance L-amino acids:

- Alanine
- Isoleucine
- Valine

## A.4 KCSA PURIFICATION

Frozen cells were resuspended in 50 mM tris base, 150 mM potassium chloride, 2 mM **DM!** (DM!), pH 7.5, using ≈5 mL $g^{-1}$ of cell pellet. The cells were then lysed by passage through a French Pressure cell operating at 10 000–20 000 PSI three to four times. Protease inhibitor cocktail and 10 % DM per cell pellet mass was added to the lysate and was incubated overnight at 4 °C while rocking. The lysate was then centrifuged at $2.5 \times 10^5$ RPM and the resulting pellet, lipids and other cell debris, was discarded. The crude lysate was sterile filtered and purified by Ni-NTA chromatography using buffer consisting of 50 mM tris base, 300 mM potassium chloride, 5 mM DM, pH 7.5 as equilibrium buffer, with 40 mM imidizole in the wash buffer and 300 mM in the elution buffer. The presence and purity of the resulting KcsA was determined by SDS-PAGE which a characteristic band for the properly folded tetramer appearing at 70 kDa. The concentration of the protein was determined by UV-Vis spectroscopy at 280 nm the calculated[3] extinction coefficient of 33 570 $M^{-1}$ $cm^{-1}$. Imidazole was removed by spin-concentrator (Amicon) or Sephadex G-25 desalting column. The purified, concentrated, KcsA was stored at 4 °C and reconstituted with lipids within a matter of hours.

### A.4.1 *Reconstitution of KcsA into Liposomes*

Proteoliposomes throughout this thesis were prepared by hydrating thin lipid films with KcsA detergent solution and then dialyzed to remove detergent and achieve final desired buffer.

Lipids were were generally obtained as a chloroform solution (Avanti), dried as a thin film over nitrogen gas, resolubilized in n-hexane, dried again over nitrogen gas and solubilized by bath sonication in 10 mM DM, 50 mM Tris, 100 mM KCl, pH 7.5. This yields a hydrated suspension of multilamellar liposomes.

Liposomes were then with KcsA in 2–10 mM DM and buffer described above. This solution was then diluted to 2 mM DM with additional buffer and dialyzed in 30 kDa MWCO tubing (Spectum) with three exchanges of 4 L of buffer at 8–16 h intervals at room temperature. Proteoliposomes were harvested by centrifugation at 5700 g for 30 min.

### A.5.1 *R2 YE Media*

Modified from Shepherd et al. [7].

Part A and B are combined, adjusted to pH 7.2, diluted to 1 L and sterile filtered.

**Part A:**

Diluted to 0.8 L with deionized water, autoclaved.

- Sucrose: 103 g
- $K_2SO_4$: 0.25 g
- $MgCl_2 \cdot 6\,H_2O$: 10.12 g
- Glucose: 10 g
- Casamino acids: 0.1 g
- Yeast extract: 5 g

**Part B:**

Combined, sterile filtered, and added ascetically to added to Part A.

- Trace Solution: 2 mL
- TES buffer 5.75 g in 100 mL
- $KH_2PO_4$ 50 mg in 10 mL
- $CaCl_2 \cdot 2\,H_2O$ 3 g in 80 mL
- L-proline 3 g in 15 mL
- NaOH (1 N): 5 mL
- Yeast extract 5 g in 50 mL
- Thiostrepton 50 mg in 1 mg

**Trace Element Solution**:

Diluted to 1 L with deionized water, sterile filtered.

- $ZnCl_2$: 40 mg
- $FeCl_3 \cdot 6\,H_2O$: 200 mg
- $CuCl_2 \cdot 2\,H_2O$: 10 mg
- $MnCl_2 \cdot 4\,H_2O$: 10 mg
- $Na_2B_4O_7 \cdot 10\,H_2O$: 10 mg
- $(NH_4)_6Mo_7O_{24} \cdot 4\,H_2O$ 10 mg

### A.5.2 $^{13}C$, $^{15}N$ *M9 Minimal Media:*

Adapted from Bhate et al. [1].

**M9**:

Combined, adjusted to pH 7.2, diluted to 1 L in deionized water, and sterile-filtered.

- 10X M9 salts: 100 mL
- Solution C: 20 mL
- Vitamin solution: 500 µL
- Gibco 100X MEM vitamin solution: 10 mL
- $MgSO_4$ (1 M): 2 mL
- $CaCl_2$ (1 M): 100 µL
- Carbenicillin: 100 mg
- U-$^{13}C$ glucose: 3 g
- $^{15}N$ ammonium chloride: 1.0 g
- L-Proline (when using JM-83 cell line) 1 g

**M9 Salts (10X)**

Diluted to 1 L deionized water and sterile-filtered.

- $Na_2HPO_4 \cdot 7\,H_2O$: 128 g
- $KH_2PO_4$: 30 g
- NaCl: 5 g

**Solution C**

Adjusted to pH 6.5, diluted to 1 L, sterile-filtered, stored in the dark at 4 °C.

- Metal 44: 50 mL
- KOH: 7.3 g
- Nitrilotriacetic acid: 10 g
- $MgCl_2 \cdot 6\,H_2O$: 24 g
- $CaCl_2 \cdot 2\,H_2O$: 3.5 g

**Metal 44 solution**

Diluted to 100 mL, sterile-filtered, stored in the dark at 4 °C.

- $K_2EDTA \cdot 2\,H_2O$: 0.35 g
- $ZnCl_2$: 0.5 g
- $FeCl_2 \cdot 4\,H_2O$: 0.5 g
- $MnCl_2 \cdot 4\,H_2O$: 0.2 g
- $(NH_4)_6Mo_7O_{24} \cdot 6\,H_2O$: 19 mg
- $CuCl_2 \cdot 2\,H_2O$: 16 mg
- $Co(NO_3)_2 \cdot 6\,H_2O$: 25 mg
- $H_3BO_3$: 12 mg

**Vitamin stock:**

Diluted to 50 mL, stored in the dark at 4 °C.

- Nicotinic acid: 0.5 g
- 4-aminobenzoic acid 50 mg
- Biotin: 5 mg

## A.6 ALIPHATIC UNLABELING LABELING

The typical $^{13}C$, $^{15}N$ M9 media above is supplemented with the 1 g each of the following, natural-abundance L-amino acids:

- Alanine

- Glycine
- Isoleucine
- Leucine
- Phenylalanine
- Threonine
- Tyrosine
- Valine

### A.6.1 *Methionine, Leucine Specific Labeling:*

The typical $^{13}C$, $^{15}N$ M9 media above has natural-abundance glucose and ammonium chloride instead of enriched compounds. The media is supplemented with 200 mg $^{15}N$-L-leucine and 1 g $^{13}CO$-L-methionine, 200 mg of natural abundance L-cysteine, 1 g each of the following natural abundance L-amino acids:

- Arginine
- Aspartamine
- Aspartate
- Glutamine
- Glutamate
- Glycine
- Histadine
- Lysine
- Phenylalanine
- Proline
- Serine
- Threonine
- Tryptophan
- Tyrosine

2 g each of the following natural abundance L-amino acids:

- Alanine
- Isoleucine
- Valine

[1] M. P. Bhate et al. "Preparation of uniformly isotope labeled KcsA for solid state NMR: Expression, purification, reconstitution into liposomes and functional assay." In: *Protein Expression and Purification* (2013). DOI: 10.1016/j.pep.2013.07.013.

[2] M. P. Bhate and A. E. McDermott. "Protonation state of E71 in KcsA and its role for channel collapse and inactivation." In: *Proceedings of the National Academy of Sciences of the United States of America* 109.38 (Sept. 2012), pp. 15265–70. DOI: 10.1073/pnas.1211900109.

[3] S. C. Gill and P. H. von Hippel. *Calculation of protein extinction coefficients from amino acid sequence data.* 1989. DOI: 10.1016/0003-2697(89)90602-7.

[4] L. Heginbotham, E. Odessey, and C. Miller. "Tetrameric stoichiometry of a prokaryotic K+ channel." In: *Biochemistry* 36.33 (Aug. 1997), pp. 10335–42. DOI: 10.1021/bi970988i.

[5] D. Mance et al. "An Efficient Labelling Approach to Harness Backbone and Side-Chain Protons in 1 H-Detected Solid-State NMR Spectroscopy." In: *Angewandte Chemie* 127.52 (Dec. 2015), pp. 16025–16029. DOI: 10.1002/ange.201509170.

[6] A. Shekhtman, R. Ghose, M. Goger, and D. Cowburn. "NMR structure determination and investigation using a reduced proton (REDPRO) labeling strategy for proteins." In: *FEBS Letters* 524.1-3 (July 2002), pp. 177–182. DOI: 10.1016/S0014-5793(02)03051-X.

[7] M. D. Shepherd, M. K. Kharel, M. A. Bosserman, and J. Rohr. "Laboratory Maintenance of Streptomyces Species." In: *Current Protocols in Microbiology*. SUPP.18. Hoboken, NJ, USA: John Wiley & Sons, Inc., Aug. 2010, pp. 1–8. DOI: 10.1002/9780471729259.mc10e01s18.

# B

# MASS SPECTROMETRY OF KCSA-Δ126

Shotgun proteomics were completed by the Columbia University Herbert Irving Comprehensive Cancer Center Mass Spectrometry Proteomics Shared Resource.

## B.1 METHODS

N-terminal His-tagged KcsA was expressed and purified as described in Appendix A. To cleave the C-terminus, 1 mg mL$^{-1}$ KcsA in 5 mM decyl-β-maltopyranoside (Anatrace) detergent (DM) was incubated with 20 µg mL$^{-1}$ of bovine α-chymotrypsin (Sigma) for 3 h at 35 °C. KcsA was isolated using His-Select nickle-affinity gel (Fisher) by gravity column, washing with five volumes of buffer 35 mM imidazole and eluting with two volumes of buffer containing 300 mM imidazole. An aliquot of the full-length construct and the post-reaction purified KcsA were analyzed by SDS-PAGE using a 4–12 % Bis-Tris mini gel (Thermo Fisher) at 200 V until the 5 kDa pre-stained band of the the protein ladder (Fisher) reached the bottom of the gel (35 min) (Figure 2.5a). The gel was then stained with PageBlue (Thermo Fisher) coomassie brilliant blue according to manufacturer direction. Individual bands were then cut from the gel and placed into new centriguge tubes and delivered within two hours, on ice, to the proteomics core.

In-gel trypsin digest was conducted by the core according to standard protocols. The two samples were subjected liquid chromatography using an Eksigent

nanoLC-Ultra 2D HPLC system and tandem mass spectrometry-mass spectrometry was conducted using a QE HF mass spectrometer. The spectra were then analyzed with Scaffold 4.8.6 proteome software (Portland, Oregon) and compared against the full-length, wild-type KcsA sequence (Listing A.2) using an 80 % peptide probability cut-off.

## B.2 RESULTS

## B.3 REPORT FROM SCAFFOLD

```
Experiment: KcsA-FL v. KcsA-Delta-C
        Database Set: 1 Database
                Database Name: GH699.Fasta
                        Number of Proteins: 2
                Does database contain common contaminants?: Yes
        Search Engine Set: 1 Search Engine
                Search Engine: Sequest (XCorr Only)
                        Version: IseNode in Proteome Discoverer 2.2.0.388

                        Samples: All Samples
                        Fragment Tolerance: 0.60 Da (Monoisotopic)
                        Parent Tolerance: 10.0 PPM (Monoisotopic)
                        Fixed Modifications: +57 on C (Carbamidomethyl)
                        Variable Modifications: +16 on M (Oxidation), +42 on
                             n (Acetyl)
                        Database: GH699.Fasta (unknown version, 2 entries)

                        Digestion Enzyme: Trypsin
                        Max Missed Cleavages: 2
                        Probability Model:
                                LFDR Model, No Classifier [all charge states
                                   ]
        Scaffold: Version: Scaffold 4.8.6
                Peptide Thresholds: 80.0-percent minimum
```

| Sample | Peptide start index | Peptide stop index | Protein ID probability | unique peptide count | unique spectrum count | spectrum count | Percentage of total spectra | Peptide sequence | ID probability | +2H spectra | +3H spectra | +4H spectra | Calculated Mass (AMU) | Median Retention Time | Total TIC |
|---|---|---|---|---|---|---|---|---|---|---|---|---|---|---|---|
| ΔC | 1 | 17 | 1 | 3 | 10 | 218 | 0.0108 | MHHHHHHPPMLSGLLAR | 0.997 | 0 | 12 | 100 | 2024 | 3068.4 | 2.54E+07 |
| FL | 1 | 17 | 1 | 7 | 18 | 369 | 0.0178 | MHHHHHHPPMLSGLLAR | 0.997 | 0 | 22 | 131 | 2024 | 3102.95 | 5.18E+07 |
| ΔC | 26 | 33 | 1 | 3 | 10 | 218 | 0.0108 | HGSALHWR | 0.99 | 24 | 0 | 0 | 963.4907 | 1792.42 | 3165370 |
| FL | 26 | 33 | 1 | 7 | 18 | 369 | 0.0178 | HGSALHWR | 0.99 | 19 | 0 | 0 | 963.4907 | 2117.95 | 2500050 |
| ΔC | 59 | 70 | 1 | 3 | 10 | 218 | 0.0108 | GAPGAQLITYPR | 0.997 | 78 | 2 | 0 | 1243.68 | 4203.09 | 3.01E+08 |
| FL | 59 | 70 | 1 | 7 | 18 | 369 | 0.0178 | GAPGAQLITYPR | 0.997 | 69 | 1 | 0 | 1243.68 | 4385.85 | 6.33E+07 |
| FL | 134 | 145 | 1 | 7 | 18 | 369 | 0.0178 | HSEKAAEEAYTR | 0.997 | 1 | 1 | 0 | 1391.65 | 1204.2 | 785567 |
| FL | 138 | 145 | 1 | 7 | 18 | 369 | 0.0178 | AAEEAYTR | 0.99 | 85 | 0 | 0 | 910.4264 | 4090.02 | 1.71E+07 |
| FL | 160 | 166 | 1 | 7 | 18 | 369 | 0.0178 | MLDDNRR | 0.9 | 19 | 0 | 0 | 919.4415 | 1291.94 | 1.10E+08 |

TABLE B.1: Peptide mass spectrometry

Peptide matches from HPLC-MS/MS

Protein Thresholds: 90.0-percent minimum and 1 peptide minimum

DATABASE SEARCHING-- Tandem mass spectra were extracted and charge state deconvoluted by [unknown] version [unknown]. Deisotoping was not performed. All MS/MS samples were analyzed using Sequest (XCorr Only) ( Thermo Fisher Scientific, San Jose, CA, USA; version IseNode in Proteome Discoverer 2.2.0.388). Sequest (XCorr Only) was set up to search GH699. Fasta (unknown version, 2 entries) assuming the digestion enzyme trypsin. Sequest (XCorr Only) was searched with a fragment ion mass tolerance of 0.60 Da and a parent ion tolerance of 10.0 PPM. Carbamidomethyl of cysteine was specified in Sequest (XCorr Only) as a fixed modification. Oxidation of methionine and acetyl of the n-terminus were specified in Sequest (XCorr Only) as variable modifications.

CRITERIA FOR PROTEIN IDENTIFICATION-- Scaffold (version Scaffold 4.8.6, Proteome Software Inc., Portland, OR) was used to validate MS/MS based peptide and protein identifications. Peptide identifications were accepted if they could be established at greater than 80.0-percent probability by the Scaffold Local FDR algorithm. Protein identifications were accepted if they could be established at greater than 90.0-percent probability and contained at least 1 identified peptide. Protein probabilities were assigned by the Protein Prophet algorithm (Nesvizhskii , Al et al Anal. Chem. 2003;75(17):4646-58). Proteins that contained similar peptides and could not be differentiated based on MS/MS analysis alone were grouped to satisfy the principles of parsimony.

# PULSE SEQUENCES

# C

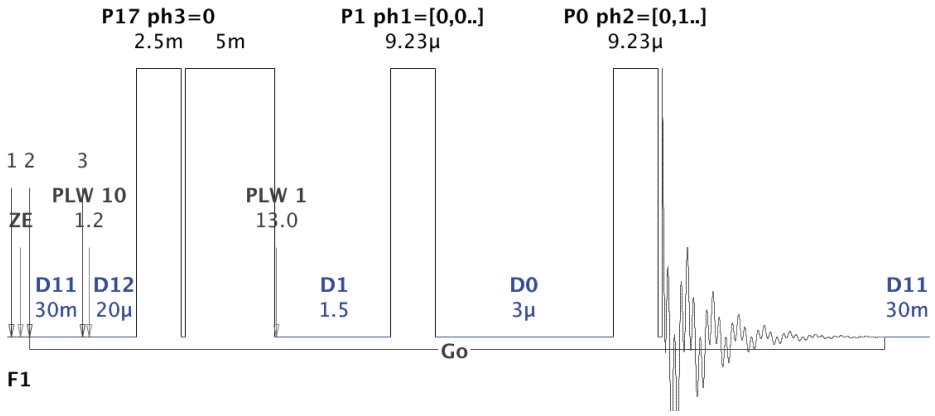


FIGURE C.1: Gradient selected, echo/anti-echo COSY. Bruker Avance II cosyppqf pulse sequence. ph1= x x x x y y y y -x -x -x -x -y -y -y -y, ph2= x y -x -y, ph3= x, ph4=1, ph31= x -x x -x -y y -y y -x x -x x y -y y -y

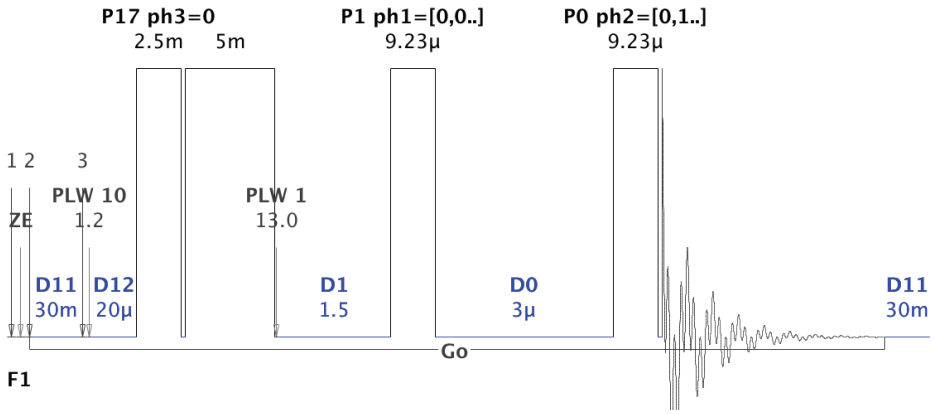


FIGURE C.2: Gradient selected, echo/anti-echo TOCSY-COSY. Bruker Avance II cosyppqf pulse sequence. ph1= x x x x y y y y -x -x -x -x -y -y -y -y, ph2= x y -x -y, ph3= x, ph4=1, ph31= x -x x -x -y y -y y -x x -x x y -y y -y

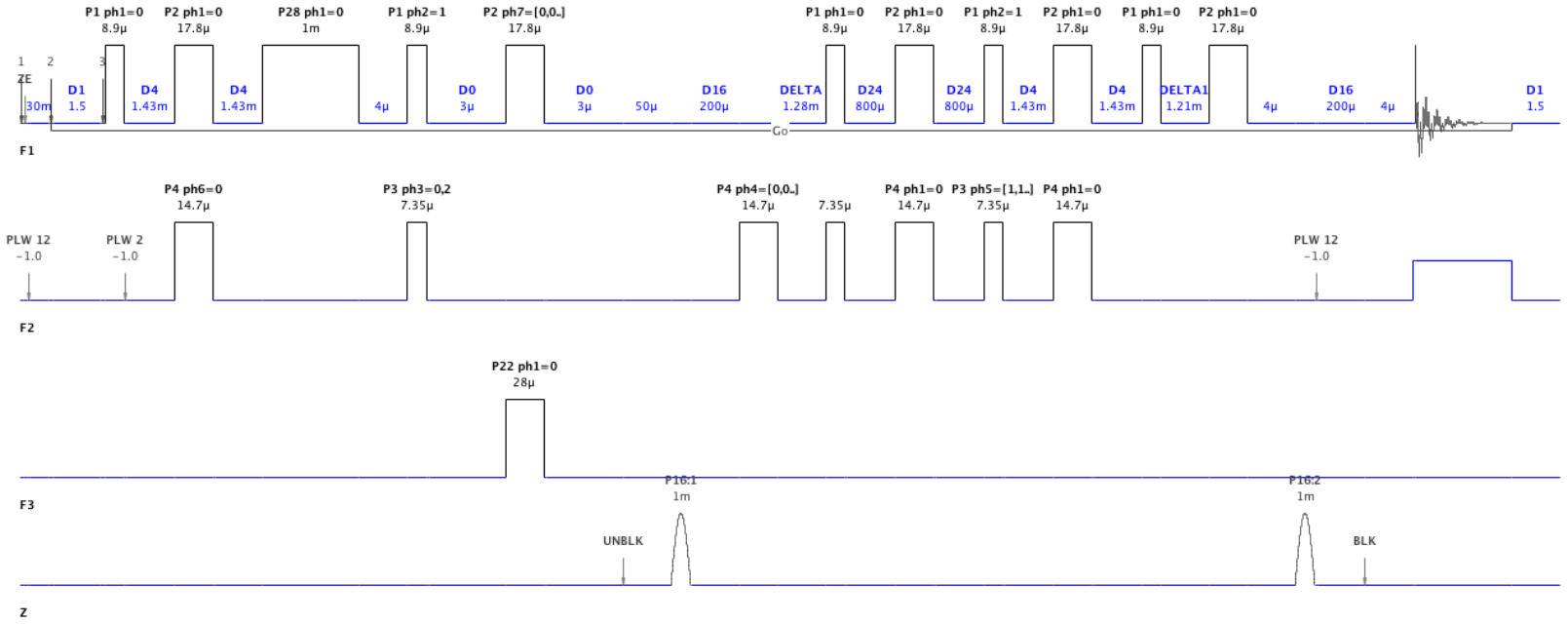


FIGURE C.3: Gradient selected, echo/anti-echo, sensitivity-enhanced HSQC. Bruker Avance II hsqcetgpsi pulse sequence. ph1 = ph6 = x, ph2 = y ph3 = x -x, ph4 = y y -y -y, ph5 = y y -y -y, ph7= x x -x -x ph9 = -y, ph31 = x -x -x x

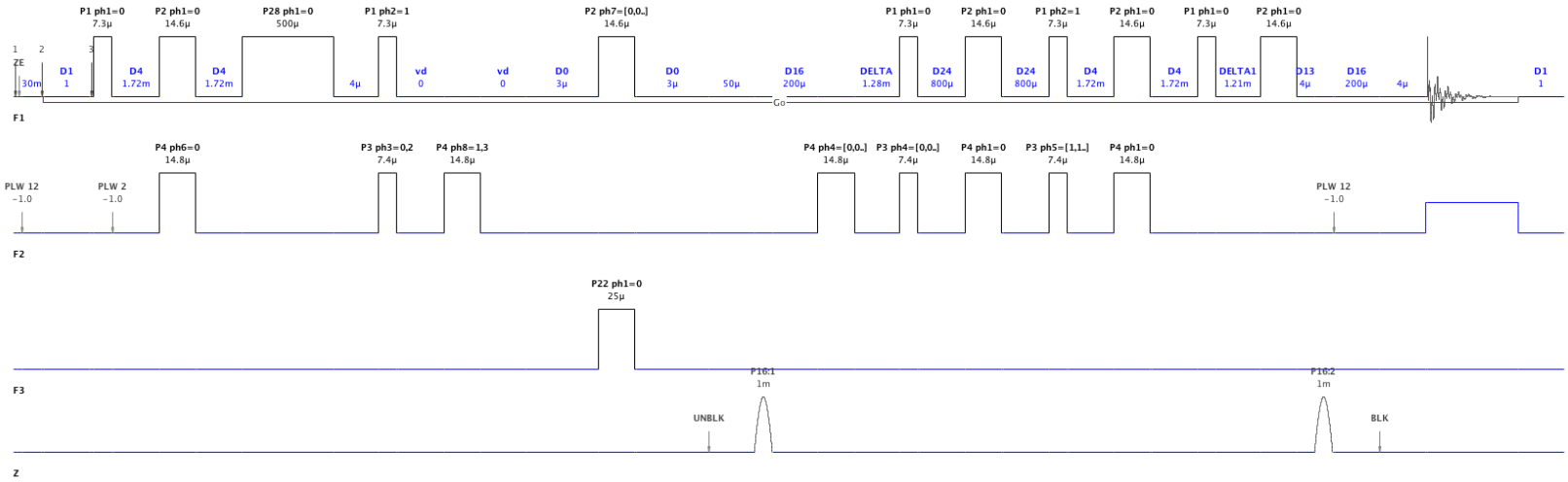


FIGURE C.4: Gradient selected, echo/anti-echo, sensitivity-enhanced, pseudo 3D T2-filtered, HSQC. ph1 = ph6 = x, ph2 = y, ph3 = x -x, ph4 = ph7 = x x -x -x, ph5 = y y -y -y, ph8 = y -y, ph31 = x -x -x x

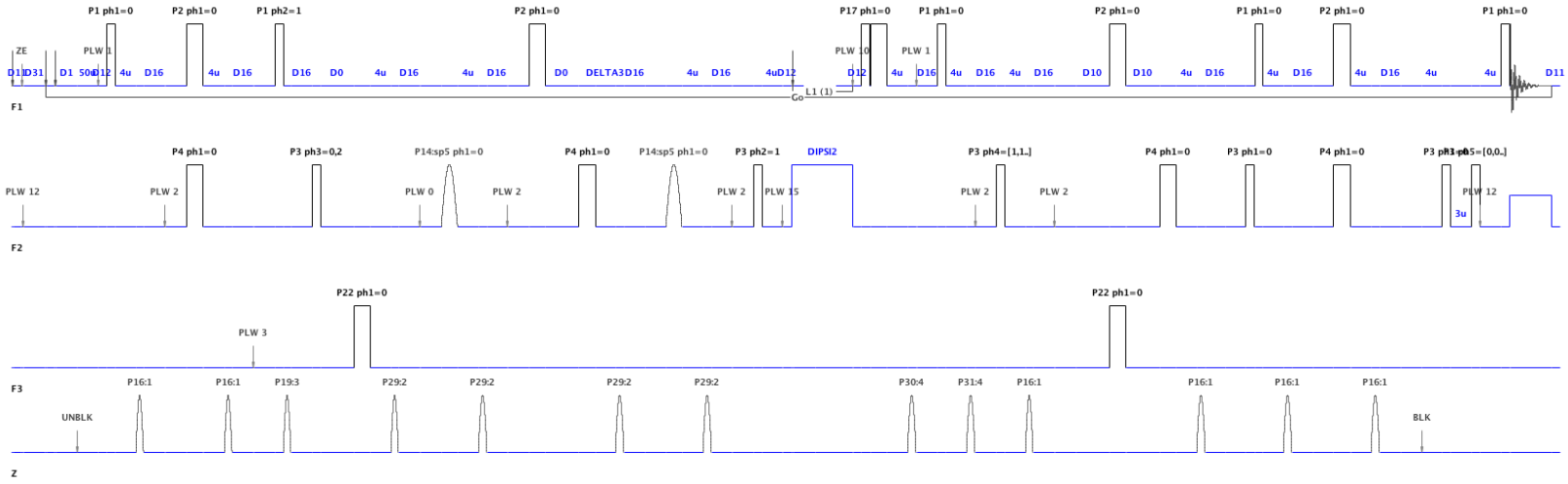


FIGURE C.5: Gradient selected, echo/anti-echo 3D hCCH-TOCSY. Bruker Avance II hcchdigp3d2 pulse sequence. ph1 = x, ph2 = ph7 = y, ph3 = x -x, ph4 = y y -y -y, ph5 = x x x x -x -x -x -x, ph9 = -y, ph31 = x -x -x x

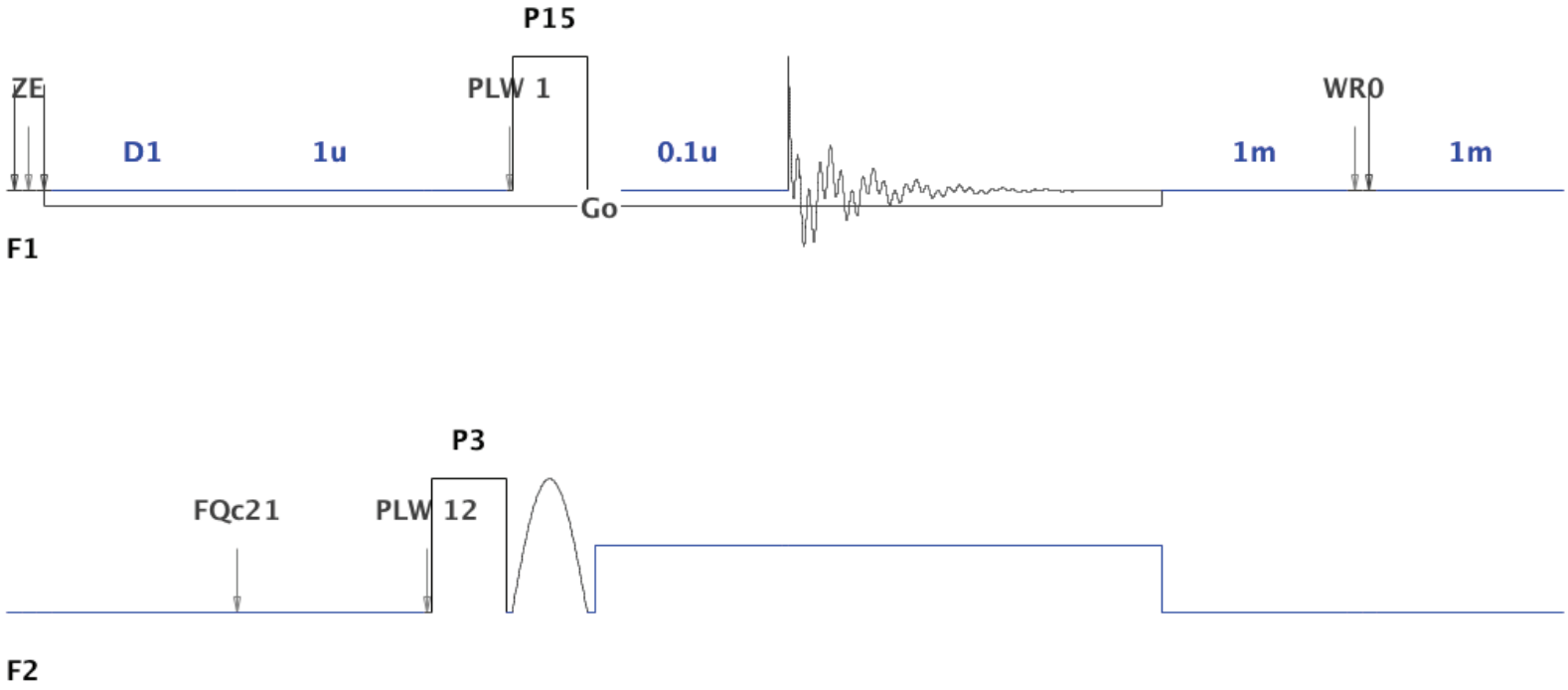


FIGURE C.6: Cross polarization magic angle spinning pulse sequence. Pulse phase cycle: p3 = x -x p15 = x x -x -x y y -y -y, aq = x -x -x x y -y -y y

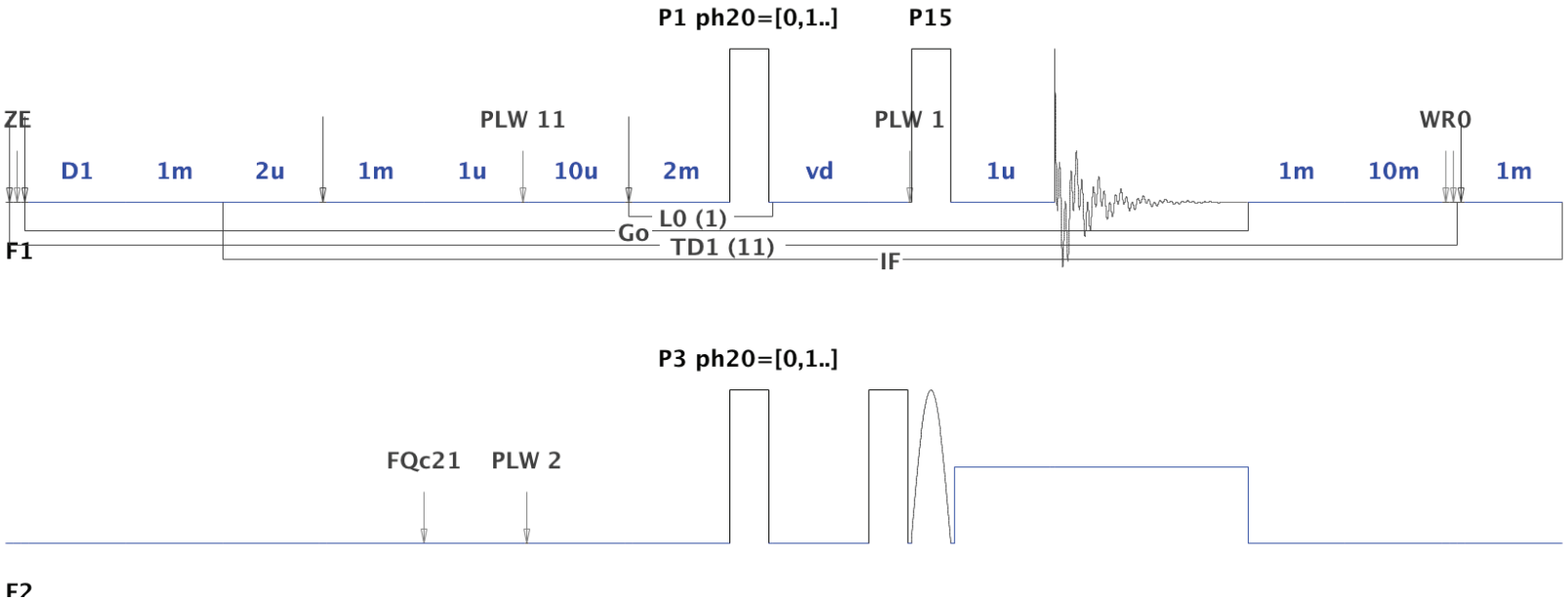


FIGURE C.7: Cross polarization magic angle spinning build-up pseudo-2D pulse sequence. Pulse phase cycle: ph20 = x y x y x y x y, p15 = x x -x -x y y -y -y, aq = x -x -x x y -y -y y

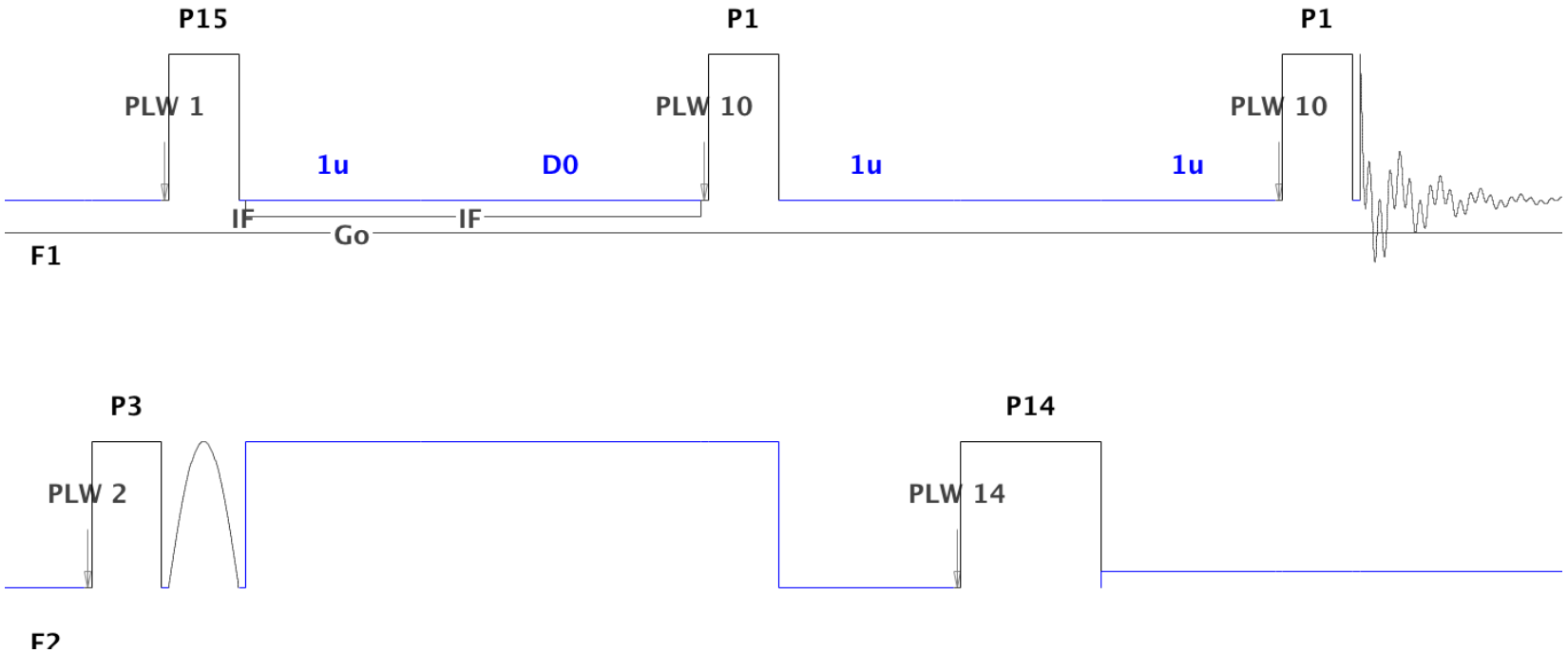


FIGURE C.8: Dipolar assisted rotational resonance (DARR) 2D sequence. Phase cycle: p1:y p1:x -x; p15-C: y; p15-H: x; p1(final): x x -x -x; acquisition: x -x -x x

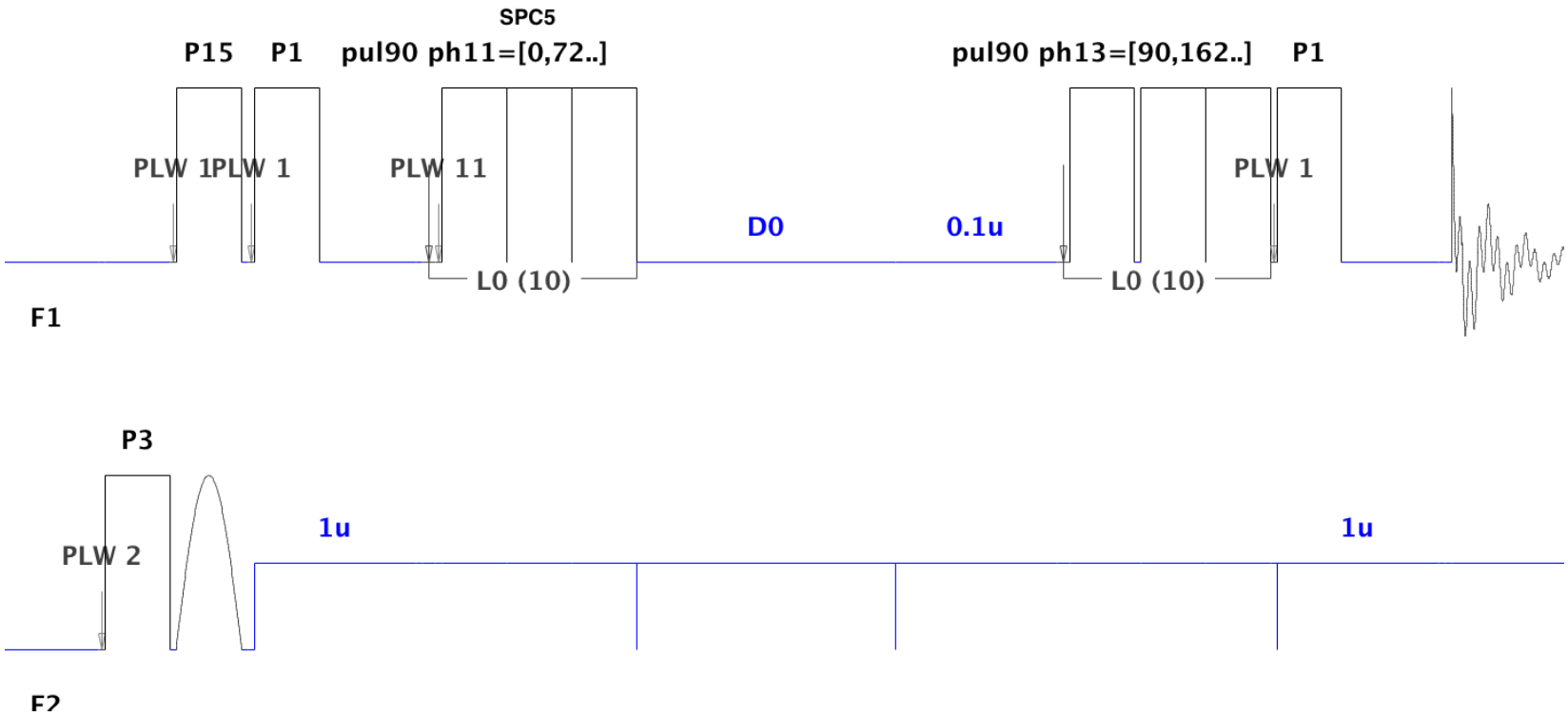


FIGURE C.9: Dipolar INADEQUATE

$^{13}$C refocused dipolar INADEQUATE with post-C5 mixing, 2D sequence. Phase cycle (specified in degrees where x = 0°): ph1 = 90*16 270*16; ph2= 0; ph4= 270*16 90*16; ph5= 90 180 270 0 180 270 0 90 270 0 90 180 0 90 180 270; ph10=0; ph11= 0 72 144 216 288 180 252 324 36 108; ph12= 180 252 324 36 108 0 72 144 216 288; ph13= 90 162 234 306 18 270 342 54 126 198; ph14= 270 342 54 126 198 90 162 234 306 18; ph31 = 270 90 0 270 270 180 90 0 0 270 180 90 90 0 270 180

# SUPPLEMENTARY SPECTRA AND PEAK LISTS

# D

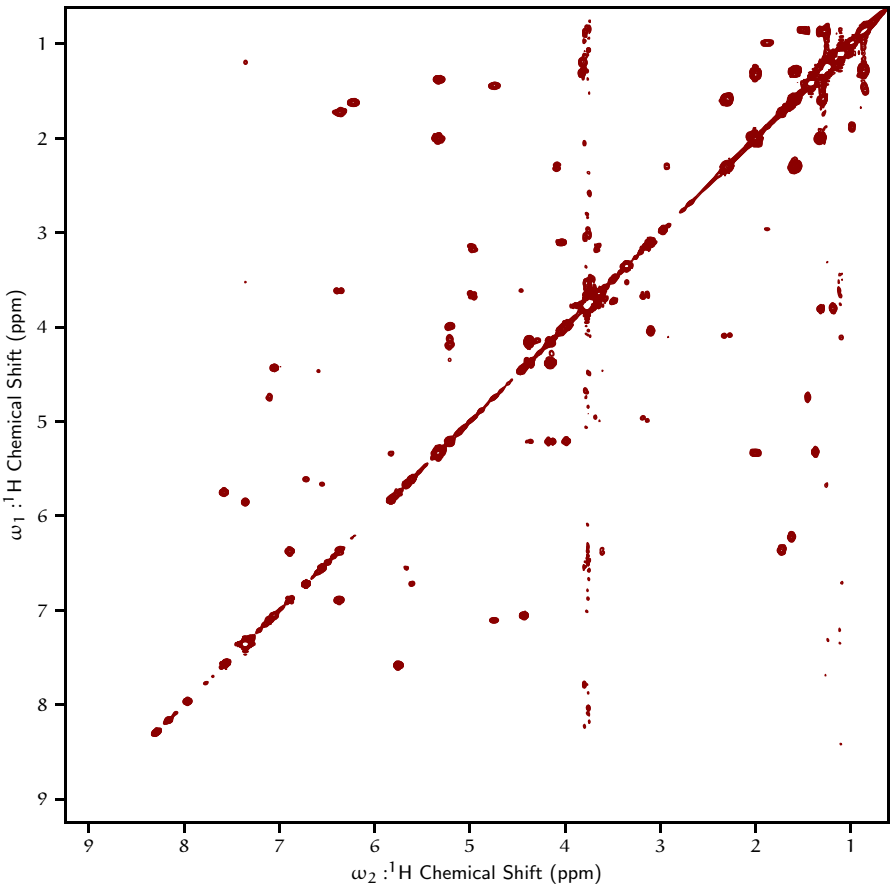


FIGURE D.1: $^1$H–$^1$H COSY spectrum of *S. lividans* total lipid extract in 2 : 1 $CDCl_3$ – MeOD at 300 K. See Chapter 3. Pulse sequence: cosyppqf

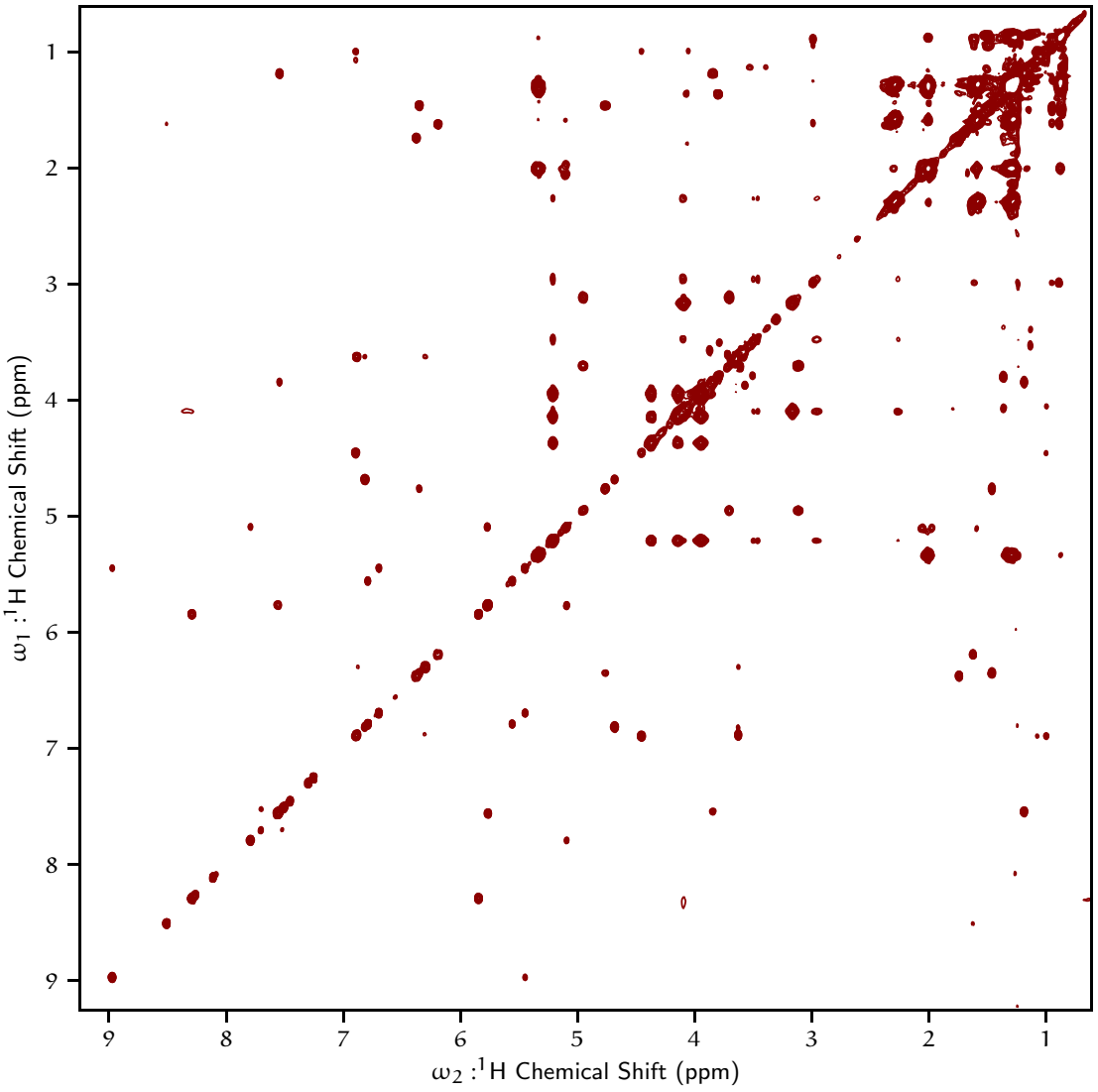


FIGURE D.2: $^1$H–$^1$H TOCSY-COSY spectrum of *S. lividans* total lipid extract in 2 : 1 $CDCl_3$ – MeOD at 300 K. See Chapter 3. Pulse sequence: dipsi2gpphzs

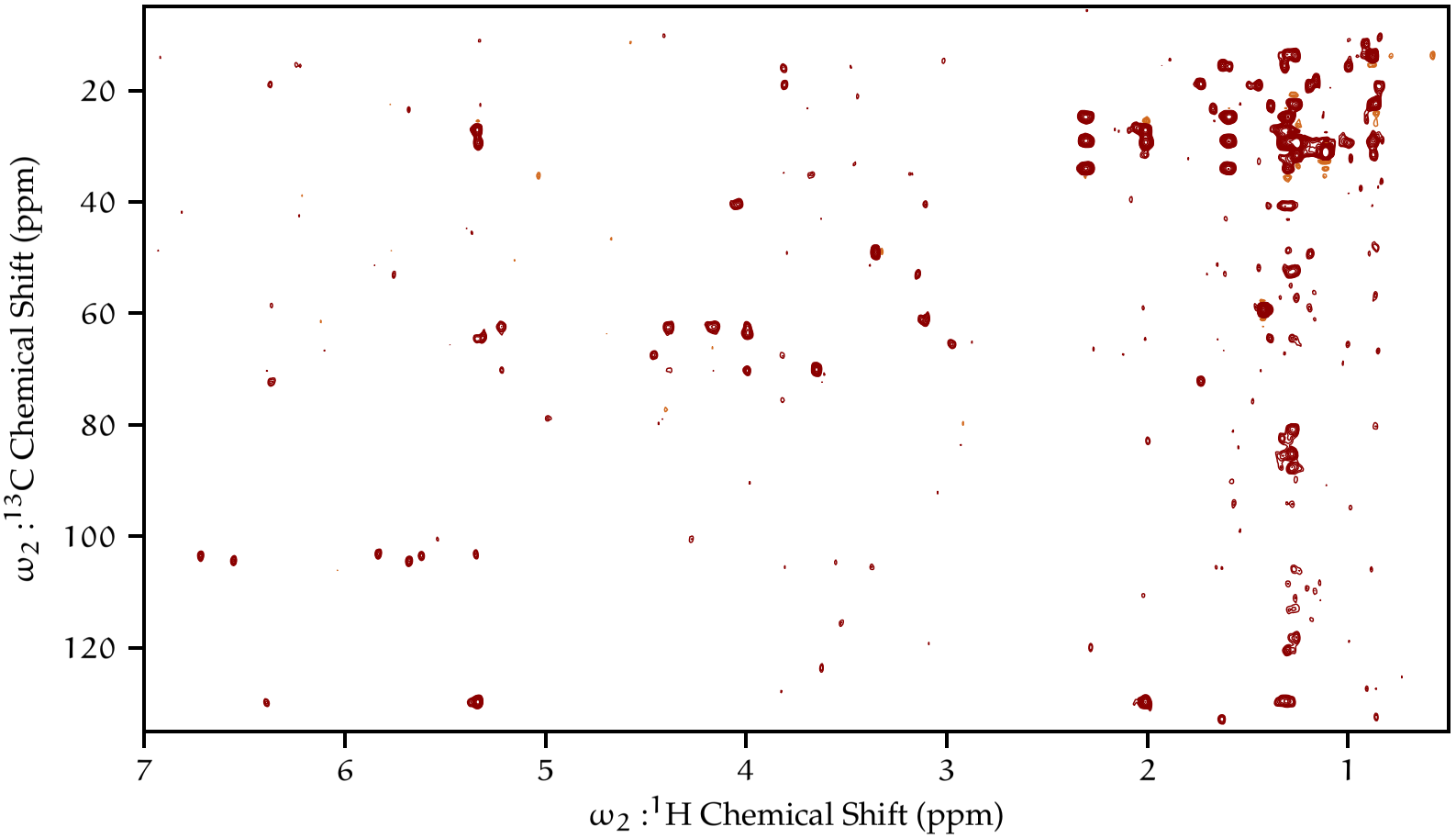


FIGURE D.3: $^{1}$H–$^{13}$C TOCSY-HSQC spectrum of *S. lividans* total lipid extract in 2 : 1 $CDCl_3$–MeOD at 300 K. See Chapter 3. Pulse sequence: hsqcdietgpsisp

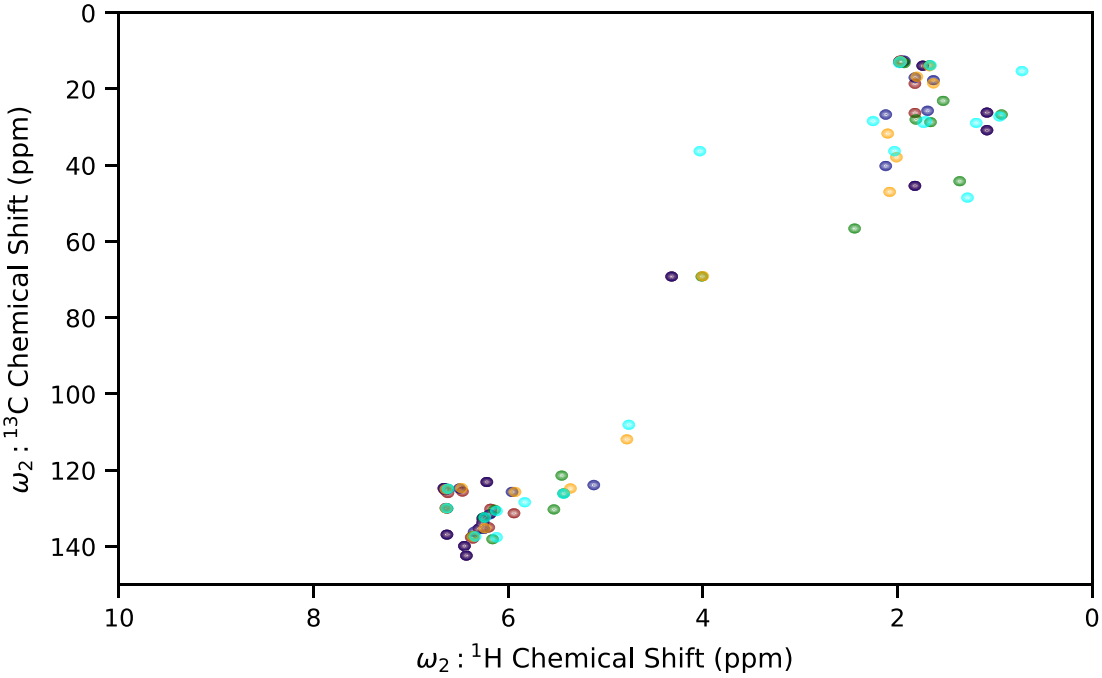


FIGURE D.4: Simulated $^{1}$H–$^{13}$C HSQC of various carotenoids: (3R)-3-Hydroxy-4-ketotorulene(red) [2], (3R)-3-Hydroxy-4-keto- -carotene [2], decaprenoxanthin (green) [1], flavuxanthin (orange)[1], sarcinaxanthin(cyan) [1]. Peaks simulated with uniform intensity with Gaussian lineshapes with 25 Hz FWHM linewidths using frequencies measured and reported in cited references.

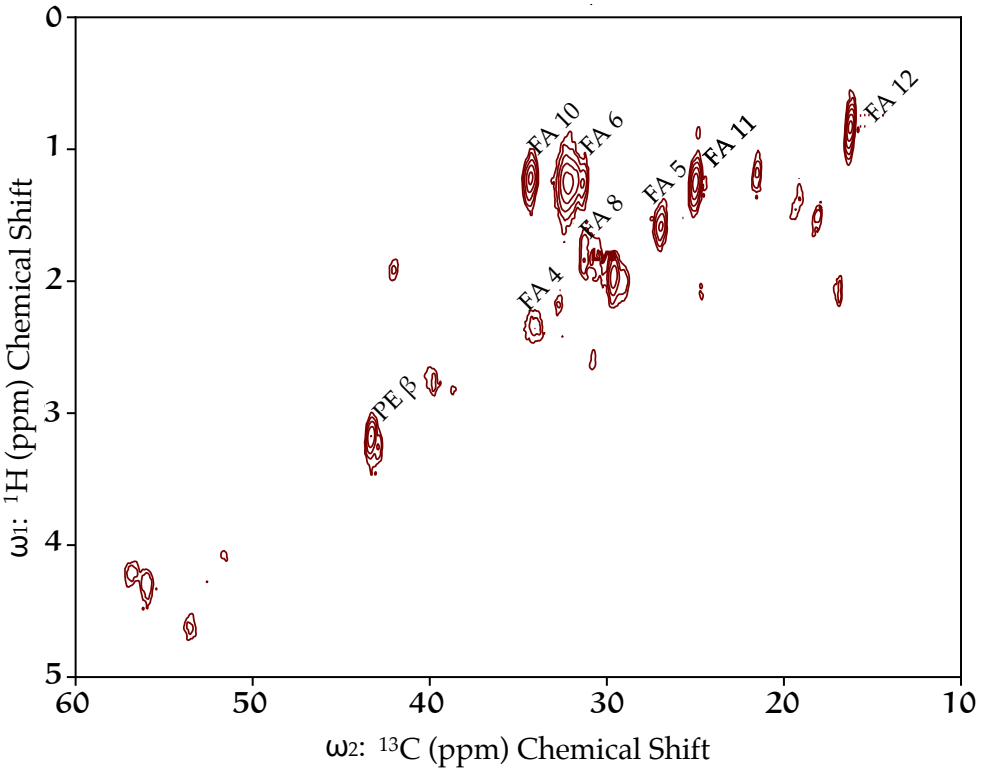


FIGURE D.5: J-resolved heteronuclear correlation spectrum of KcsA in proteoliposomes. 9 : 1 DOPE-DOPS. 17.4 kHz MAS, 295K.

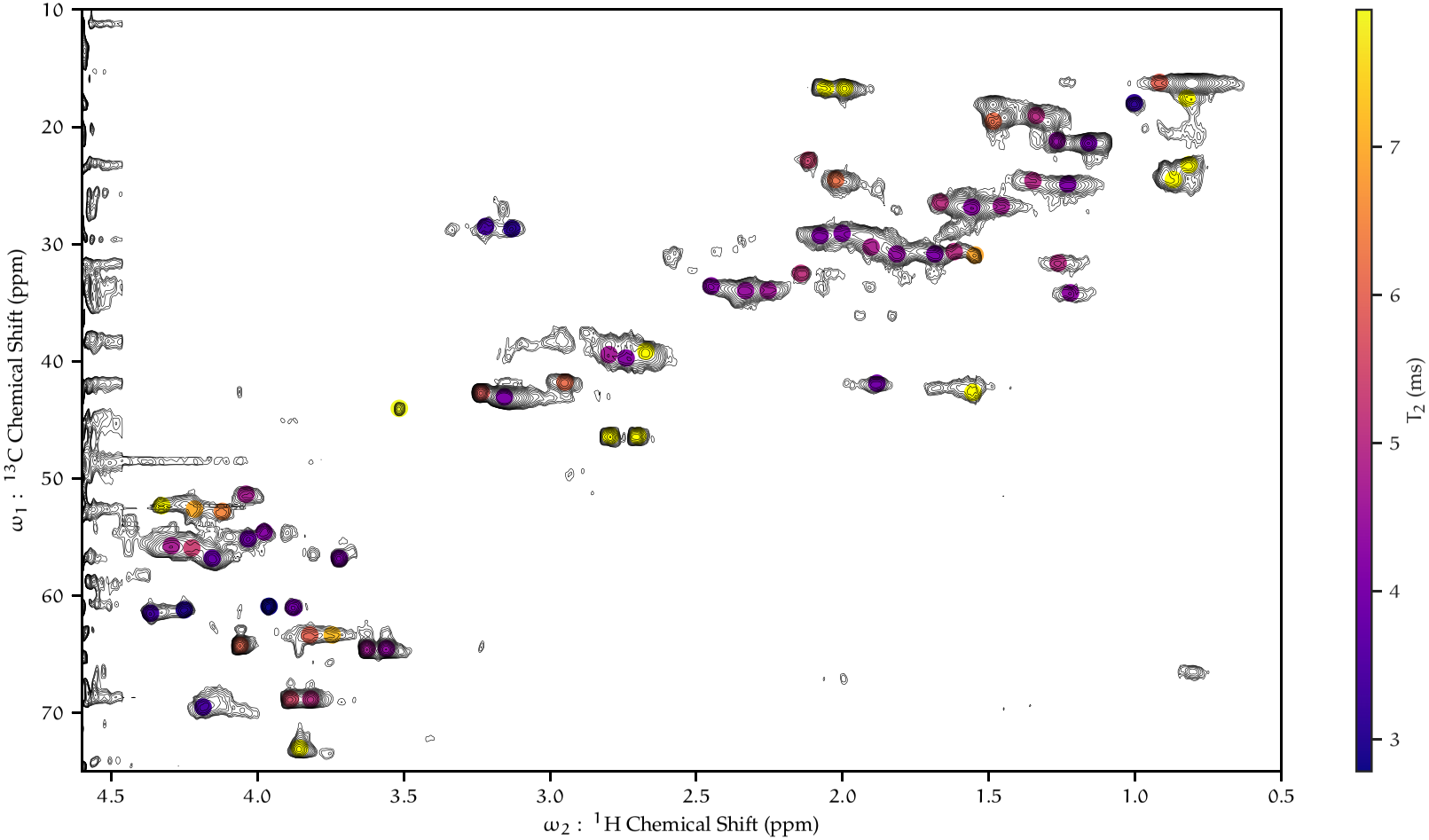


FIGURE D.6: $^{1}$H-$^{13}$C HSQC by HR-MAS of KcsA in proteoliposomes (black) (9 : 1 DOPE-DOPS, pH 4.0, 50 mM $K^+$) with $^{1}$3C $T_2$ overlay by color map. All $T_2$ values of 8–350 ms are shown in yellow. 5 kHz MAS, 308 K.

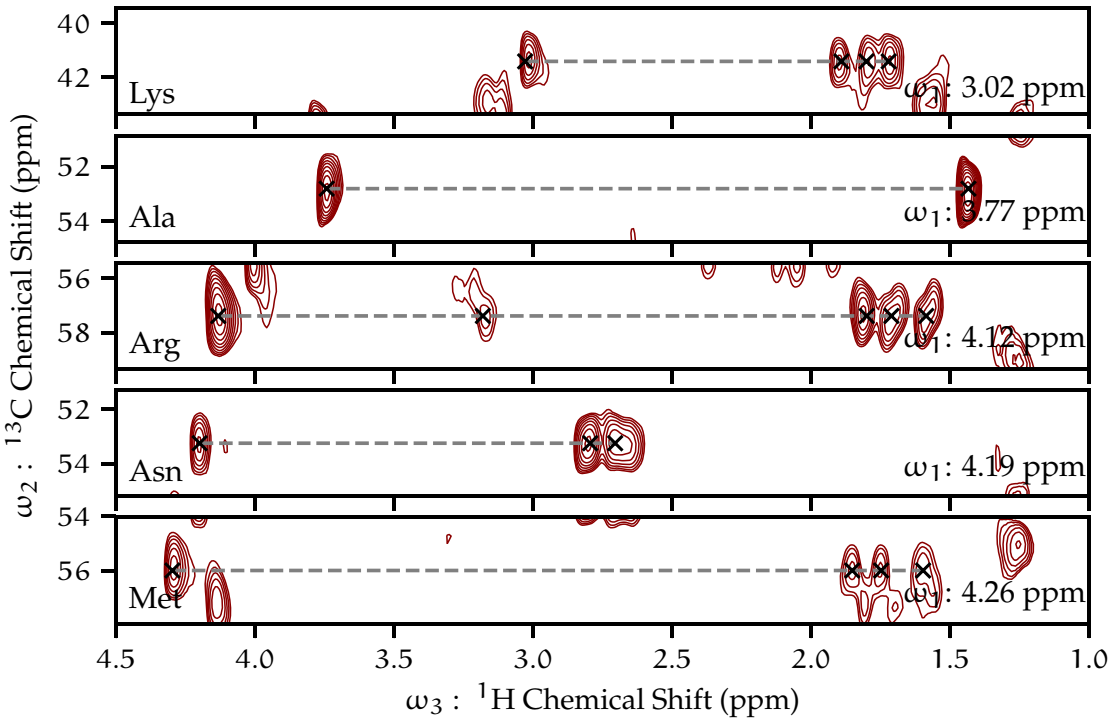


FIGURE D.7: Strip plots of 3D TOCSY experiment. The Z-axis ( $_1$) are $^1$H chemical shifts in ppm. Residue types and spin systems are indicated.

# COLOPHON

This document was typeset using the typographical look-and-feel `classicthesis` developed by André Miede. The style was inspired by Robert Bringhurst's seminal book on typography "*The Elements of Typographic Style*" (2012). `classicthesis` is available for both LaTeX and LyX:

https://bitbucket.org/amiede/classicthesis/

Data representations were rendered with the Python library Matplotlib (Hunter, 2007). Molecular models were rendered using PyMOL (Schrödinger LLC).

R. Bringhurst. *The elements of typographic style*. Hartley & Marks, 2012, p. 398

J. D. Hunter. "Matplotlib: A 2D Graphics Environment." In: *Computing in Science & Engineering* 9.3 (2007), pp. 90–95. DOI: 10.1109/MCSE.2007.55

Schrödinger LLC. "The PyMOL Molecular Graphics System, Version 1.8." Nov. 2015